

## **Design and Processing of Particulate Products**

With this unique and comprehensive text, readers will gain the quantitative tools needed to engineer the particulate processes and products that are ubiquitous in modern life. Covering a series of particle and particulate delivery form design processes, with emphasis on design and operation to control particle attributes, and supported by many worked examples, it is essential reading for students and practitioners. Topics covered include a range of particle design processes such as crystallization and precipitation, granulation, grinding, aerosol processes, and spray drying, as well as forms of delivery such as granules, tablets, dry powders, and aerosols. Readers will learn from real-world examples how the primary particle properties and the structure and properties of the delivery form can lead to high-performance products, ranging from pharmaceuticals, consumer goods and foods, to specialty chemicals, paints, agricultural chemicals, and minerals.

**Jim Litster** is Professor of Chemical and Pharmaceutical Engineering at the University of Sheffield. His research area is Particulate Products and Processes, and he is an international leading expert on wet granulation with over 30 years of experience in the field. In recognition of his contribution to the field, he was elected a Fellow of the Australian Academy of Technological Sciences and Engineering in 2010, was awarded the Thomas Barron Award in Fluid-Particle Systems from the American Institute of Chemical Engineers in 2012, and the Pharmaceutical Discovery, Development and Manufacturing Forum Award from the American Institute of Chemical Engineers in 2015.

## Cambridge Series in Chemical Engineering

### SERIES EDITOR

Arvind Varma, *Purdue University*

### EDITORIAL BOARD

Christopher Bowman, *University of Colorado*

Edward Cussler, *University of Minnesota*

Chaitan Khosla, *Stanford University*

Athanasios Z. Panagiotopoulos, *Princeton University*

Gregory Stephanopoulos, *Massachusetts Institute of Technology*

Jackie Ying, *Institute of Bioengineering and Nanotechnology, Singapore*

### Books in Series

Baldea and Daoutidis, *Dynamics and Nonlinear Control of Integrated Process Systems*

Chau, *Process Control: A First Course with Matlab*

Cussler, *Diffusion: Mass Transfer in Fluid Systems, Third Edition*

Cussler and Moggridge, *Chemical Product Design, Second Edition*

De Pablo and Schieber, *Molecular Engineering Thermodynamics*

Deen, *Introduction to Chemical Engineering Fluid Mechanics*

Denn, *Chemical Engineering: An Introduction*

Denn, *Polymer Melt Processing: Foundations in Fluid Mechanics and Heat Transfer*

Duncan and Reimer, *Chemical Engineering Design and Analysis: An Introduction*

Fan and Zhu, *Principles of Gas-Solid Flows*

Fox, *Computational Models for Turbulent Reacting Flows*

Franses, *Thermodynamics with Chemical Engineering Applications*

Leal, *Advanced Transport Phenomena: Fluid Mechanics and Convective Transport Processes*

Lim and Shin, *Fed-Batch Cultures: Principles and Applications of Semi-Batch Bioreactors*

Marchisio and Fox, *Computational Models for Polydisperse Particulate and Multiphase Systems*

Mewis and Wagner, *Colloidal Suspension Rheology*

Morbidelli, Gavriilidis, and Varma, *Catalyst Design: Optimal Distribution of Catalyst in Pellets, Reactors, and Membranes*

Nicoud, *Chromatographic Processes*

Noble and Terry, *Principles of Chemical Separations with Environmental Applications*

Orbey and Sandler, *Modeling Vapor-Liquid Equilibria: Cubic Equations of State and their Mixing Rules*

Petyluk, *Distillation Theory and its Applications to Optimal Design of Separation Units*

Rao and Nott, *An Introduction to Granular Flow*

Russell, Robinson, and Wagner, *Mass and Heat Transfer: Analysis of Mass Contactors and Heat Exchangers*

Schobert, *Chemistry of Fossil Fuels and Biofuels*

Shell, *Thermodynamics and Statistical Mechanics*

Sirkar, *Separation of Molecules, Macromolecules and Particles: Principles, Phenomena and Processes*

Slattery, *Advanced Transport Phenomena*

Varma, Morbidelli, and Wu, *Parametric Sensitivity in Chemical Systems*

# Design and Processing of Particulate Products

JIM LITSTER

University of Sheffield



**CAMBRIDGE**  
UNIVERSITY PRESS

University Printing House, Cambridge CB2 8BS, United Kingdom

Cambridge University Press is part of the University of Cambridge.

It furthers the University's mission by disseminating knowledge in the pursuit of education, learning and research at the highest international levels of excellence.

[www.cambridge.org](http://www.cambridge.org)

Information on this title: [www.cambridge.org/9781107007376](http://www.cambridge.org/9781107007376)

© Jim Litster 2016

This publication is in copyright. Subject to statutory exception and to the provisions of relevant collective licensing agreements, no reproduction of any part may take place without the written permission of Cambridge University Press.

First published 2016

Printed in the United Kingdom by TJ International Ltd. Padstow Cornwall

*A catalogue record for this publication is available from the British Library*

*Library of Congress Cataloging-in-Publication data*

Names: Litster, Jim, author.

Title: Design and processing of particulate products / Jim Litster.

Description: Cambridge, United Kingdom: Cambridge University Press, 2016. |

Series: Cambridge series in chemical engineering

Identifiers: LCCN 2016025984 | ISBN 9781107007376 (hardback)

Subjects: LCSH: Particles. | Chemical engineering. |

BISAC: TECHNOLOGY & ENGINEERING / Chemical & Biochemical.

Classification: LCC TP156.P3 L58 2016 | DDC 620/.43-dc23

LC record available at <https://lccn.loc.gov/2016025984>

ISBN 978-1-107-00737-6 Hardback

Cambridge University Press has no responsibility for the persistence or accuracy of URLs for external or third-party internet websites referred to in this publication, and does not guarantee that any content on such websites is, or will remain, accurate or appropriate.

## **Design and Processing of Particulate Products**

With this unique and comprehensive text, readers will gain the quantitative tools needed to engineer the particulate processes and products that are ubiquitous in modern life. Covering a series of particle and particulate delivery form design processes, with emphasis on design and operation to control particle attributes, and supported by many worked examples, it is essential reading for students and practitioners. Topics covered include a range of particle design processes such as crystallization and precipitation, granulation, grinding, aerosol processes, and spray drying, as well as forms of delivery such as granules, tablets, dry powders, and aerosols. Readers will learn from real-world examples how the primary particle properties and the structure and properties of the delivery form can lead to high-performance products, ranging from pharmaceuticals, consumer goods and foods, to specialty chemicals, paints, agricultural chemicals, and minerals.

**Jim Litster** is Professor of Chemical and Pharmaceutical Engineering at the University of Sheffield. His research area is Particulate Products and Processes, and he is an international leading expert on wet granulation with over 30 years of experience in the field. In recognition of his contribution to the field, he was elected a Fellow of the Australian Academy of Technological Sciences and Engineering in 2010, was awarded the Thomas Barron Award in Fluid-Particle Systems from the American Institute of Chemical Engineers in 2012, and the Pharmaceutical Discovery, Development and Manufacturing Forum Award from the American Institute of Chemical Engineers in 2015.

## Cambridge Series in Chemical Engineering

### SERIES EDITOR

Arvind Varma, *Purdue University*

### EDITORIAL BOARD

Christopher Bowman, *University of Colorado*

Edward Cussler, *University of Minnesota*

Chaitan Khosla, *Stanford University*

Athanasios Z. Panagiotopoulos, *Princeton University*

Gregory Stephanopoulos, *Massachusetts Institute of Technology*

Jackie Ying, *Institute of Bioengineering and Nanotechnology, Singapore*

### Books in Series

Baldea and Daoutidis, *Dynamics and Nonlinear Control of Integrated Process Systems*

Chau, *Process Control: A First Course with Matlab*

Cussler, *Diffusion: Mass Transfer in Fluid Systems, Third Edition*

Cussler and Moggridge, *Chemical Product Design, Second Edition*

De Pablo and Schieber, *Molecular Engineering Thermodynamics*

Deen, *Introduction to Chemical Engineering Fluid Mechanics*

Denn, *Chemical Engineering: An Introduction*

Denn, *Polymer Melt Processing: Foundations in Fluid Mechanics and Heat Transfer*

Duncan and Reimer, *Chemical Engineering Design and Analysis: An Introduction*

Fan and Zhu, *Principles of Gas-Solid Flows*

Fox, *Computational Models for Turbulent Reacting Flows*

Franses, *Thermodynamics with Chemical Engineering Applications*

Leal, *Advanced Transport Phenomena: Fluid Mechanics and Convective Transport Processes*

Lim and Shin, *Fed-Batch Cultures: Principles and Applications of Semi-Batch Bioreactors*

Marchisio and Fox, *Computational Models for Polydisperse Particulate and Multiphase Systems*

Mewis and Wagner, *Colloidal Suspension Rheology*

Morbidelli, Gavriilidis, and Varma, *Catalyst Design: Optimal Distribution of Catalyst in Pellets, Reactors, and Membranes*

Nicoud, *Chromatographic Processes*

Noble and Terry, *Principles of Chemical Separations with Environmental Applications*

Orbey and Sandler, *Modeling Vapor-Liquid Equilibria: Cubic Equations of State and their Mixing Rules*

Petyluk, *Distillation Theory and its Applications to Optimal Design of Separation Units*

Rao and Nott, *An Introduction to Granular Flow*

Russell, Robinson, and Wagner, *Mass and Heat Transfer: Analysis of Mass Contactors and Heat Exchangers*

Schobert, *Chemistry of Fossil Fuels and Biofuels*

Shell, *Thermodynamics and Statistical Mechanics*

Sirkar, *Separation of Molecules, Macromolecules and Particles: Principles, Phenomena and Processes*

Slattery, *Advanced Transport Phenomena*

Varma, Morbidelli, and Wu, *Parametric Sensitivity in Chemical Systems*

# Design and Processing of Particulate Products

JIM LITSTER

University of Sheffield



**CAMBRIDGE**  
UNIVERSITY PRESS

University Printing House, Cambridge CB2 8BS, United Kingdom

Cambridge University Press is part of the University of Cambridge.

It furthers the University's mission by disseminating knowledge in the pursuit of education, learning and research at the highest international levels of excellence.

[www.cambridge.org](http://www.cambridge.org)

Information on this title: [www.cambridge.org/9781107007376](http://www.cambridge.org/9781107007376)

© Jim Litster 2016

This publication is in copyright. Subject to statutory exception and to the provisions of relevant collective licensing agreements, no reproduction of any part may take place without the written permission of Cambridge University Press.

First published 2016

Printed in the United Kingdom by TJ International Ltd. Padstow Cornwall

*A catalogue record for this publication is available from the British Library*

*Library of Congress Cataloging-in-Publication data*

Names: Litster, Jim, author.

Title: Design and processing of particulate products / Jim Litster.

Description: Cambridge, United Kingdom: Cambridge University Press, 2016. |

Series: Cambridge series in chemical engineering

Identifiers: LCCN 2016025984 | ISBN 9781107007376 (hardback)

Subjects: LCSH: Particles. | Chemical engineering. |

BISAC: TECHNOLOGY & ENGINEERING / Chemical & Biochemical.

Classification: LCC TP156.P3 L58 2016 | DDC 620/.43-dc23

LC record available at <https://lccn.loc.gov/2016025984>

ISBN 978-1-107-00737-6 Hardback

Cambridge University Press has no responsibility for the persistence or accuracy of URLs for external or third-party internet websites referred to in this publication, and does not guarantee that any content on such websites is, or will remain, accurate or appropriate.



## **Design and Processing of Particulate Products**

With this unique and comprehensive text, readers will gain the quantitative tools needed to engineer the particulate processes and products that are ubiquitous in modern life. Covering a series of particle and particulate delivery form design processes, with emphasis on design and operation to control particle attributes, and supported by many worked examples, it is essential reading for students and practitioners. Topics covered include a range of particle design processes such as crystallization and precipitation, granulation, grinding, aerosol processes, and spray drying, as well as forms of delivery such as granules, tablets, dry powders, and aerosols. Readers will learn from real-world examples how the primary particle properties and the structure and properties of the delivery form can lead to high-performance products, ranging from pharmaceuticals, consumer goods and foods, to specialty chemicals, paints, agricultural chemicals, and minerals.

**Jim Litster** is Professor of Chemical and Pharmaceutical Engineering at the University of Sheffield. His research area is Particulate Products and Processes, and he is an international leading expert on wet granulation with over 30 years of experience in the field. In recognition of his contribution to the field, he was elected a Fellow of the Australian Academy of Technological Sciences and Engineering in 2010, was awarded the Thomas Barron Award in Fluid-Particle Systems from the American Institute of Chemical Engineers in 2012, and the Pharmaceutical Discovery, Development and Manufacturing Forum Award from the American Institute of Chemical Engineers in 2015.

## Cambridge Series in Chemical Engineering

### SERIES EDITOR

Arvind Varma, *Purdue University*

### EDITORIAL BOARD

Christopher Bowman, *University of Colorado*

Edward Cussler, *University of Minnesota*

Chaitan Khosla, *Stanford University*

Athanasios Z. Panagiotopoulos, *Princeton University*

Gregory Stephanopoulos, *Massachusetts Institute of Technology*

Jackie Ying, *Institute of Bioengineering and Nanotechnology, Singapore*

### Books in Series

Baldea and Daoutidis, *Dynamics and Nonlinear Control of Integrated Process Systems*

Chau, *Process Control: A First Course with Matlab*

Cussler, *Diffusion: Mass Transfer in Fluid Systems, Third Edition*

Cussler and Moggridge, *Chemical Product Design, Second Edition*

De Pablo and Schieber, *Molecular Engineering Thermodynamics*

Deen, *Introduction to Chemical Engineering Fluid Mechanics*

Denn, *Chemical Engineering: An Introduction*

Denn, *Polymer Melt Processing: Foundations in Fluid Mechanics and Heat Transfer*

Duncan and Reimer, *Chemical Engineering Design and Analysis: An Introduction*

Fan and Zhu, *Principles of Gas-Solid Flows*

Fox, *Computational Models for Turbulent Reacting Flows*

Franses, *Thermodynamics with Chemical Engineering Applications*

Leal, *Advanced Transport Phenomena: Fluid Mechanics and Convective Transport Processes*

Lim and Shin, *Fed-Batch Cultures: Principles and Applications of Semi-Batch Bioreactors*

Marchisio and Fox, *Computational Models for Polydisperse Particulate and Multiphase Systems*

Mewis and Wagner, *Colloidal Suspension Rheology*

Morbidelli, Gavriilidis, and Varma, *Catalyst Design: Optimal Distribution of Catalyst in Pellets, Reactors, and Membranes*

Nicoud, *Chromatographic Processes*

Noble and Terry, *Principles of Chemical Separations with Environmental Applications*

Orbey and Sandler, *Modeling Vapor-Liquid Equilibria: Cubic Equations of State and their Mixing Rules*

Petyluk, *Distillation Theory and its Applications to Optimal Design of Separation Units*

Rao and Nott, *An Introduction to Granular Flow*

Russell, Robinson, and Wagner, *Mass and Heat Transfer: Analysis of Mass Contactors and Heat Exchangers*

Schobert, *Chemistry of Fossil Fuels and Biofuels*

Shell, *Thermodynamics and Statistical Mechanics*

Sirkar, *Separation of Molecules, Macromolecules and Particles: Principles, Phenomena and Processes*

Slattery, *Advanced Transport Phenomena*

Varma, Morbidelli, and Wu, *Parametric Sensitivity in Chemical Systems*

# Design and Processing of Particulate Products

JIM LITSTER

University of Sheffield



**CAMBRIDGE**  
UNIVERSITY PRESS

University Printing House, Cambridge CB2 8BS, United Kingdom

Cambridge University Press is part of the University of Cambridge.

It furthers the University's mission by disseminating knowledge in the pursuit of education, learning and research at the highest international levels of excellence.

[www.cambridge.org](http://www.cambridge.org)

Information on this title: [www.cambridge.org/9781107007376](http://www.cambridge.org/9781107007376)

© Jim Litster 2016

This publication is in copyright. Subject to statutory exception and to the provisions of relevant collective licensing agreements, no reproduction of any part may take place without the written permission of Cambridge University Press.

First published 2016

Printed in the United Kingdom by TJ International Ltd. Padstow Cornwall

*A catalogue record for this publication is available from the British Library*

*Library of Congress Cataloging-in-Publication data*

Names: Litster, Jim, author.

Title: Design and processing of particulate products / Jim Litster.

Description: Cambridge, United Kingdom: Cambridge University Press, 2016. |

Series: Cambridge series in chemical engineering

Identifiers: LCCN 2016025984 | ISBN 9781107007376 (hardback)

Subjects: LCSH: Particles. | Chemical engineering. |

BISAC: TECHNOLOGY & ENGINEERING / Chemical & Biochemical.

Classification: LCC TP156.P3 L58 2016 | DDC 620/.43-dc23

LC record available at <https://lccn.loc.gov/2016025984>

ISBN 978-1-107-00737-6 Hardback

Cambridge University Press has no responsibility for the persistence or accuracy of URLs for external or third-party internet websites referred to in this publication, and does not guarantee that any content on such websites is, or will remain, accurate or appropriate.

## **Design and Processing of Particulate Products**

With this unique and comprehensive text, readers will gain the quantitative tools needed to engineer the particulate processes and products that are ubiquitous in modern life. Covering a series of particle and particulate delivery form design processes, with emphasis on design and operation to control particle attributes, and supported by many worked examples, it is essential reading for students and practitioners. Topics covered include a range of particle design processes such as crystallization and precipitation, granulation, grinding, aerosol processes, and spray drying, as well as forms of delivery such as granules, tablets, dry powders, and aerosols. Readers will learn from real-world examples how the primary particle properties and the structure and properties of the delivery form can lead to high-performance products, ranging from pharmaceuticals, consumer goods and foods, to specialty chemicals, paints, agricultural chemicals, and minerals.

**Jim Litster** is Professor of Chemical and Pharmaceutical Engineering at the University of Sheffield. His research area is Particulate Products and Processes, and he is an international leading expert on wet granulation with over 30 years of experience in the field. In recognition of his contribution to the field, he was elected a Fellow of the Australian Academy of Technological Sciences and Engineering in 2010, was awarded the Thomas Barron Award in Fluid-Particle Systems from the American Institute of Chemical Engineers in 2012, and the Pharmaceutical Discovery, Development and Manufacturing Forum Award from the American Institute of Chemical Engineers in 2015.

## Cambridge Series in Chemical Engineering

### SERIES EDITOR

Arvind Varma, *Purdue University*

### EDITORIAL BOARD

Christopher Bowman, *University of Colorado*

Edward Cussler, *University of Minnesota*

Chaitan Khosla, *Stanford University*

Athanasios Z. Panagiotopoulos, *Princeton University*

Gregory Stephanopoulos, *Massachusetts Institute of Technology*

Jackie Ying, *Institute of Bioengineering and Nanotechnology, Singapore*

### Books in Series

Baldea and Daoutidis, *Dynamics and Nonlinear Control of Integrated Process Systems*

Chau, *Process Control: A First Course with Matlab*

Cussler, *Diffusion: Mass Transfer in Fluid Systems, Third Edition*

Cussler and Moggridge, *Chemical Product Design, Second Edition*

De Pablo and Schieber, *Molecular Engineering Thermodynamics*

Deen, *Introduction to Chemical Engineering Fluid Mechanics*

Denn, *Chemical Engineering: An Introduction*

Denn, *Polymer Melt Processing: Foundations in Fluid Mechanics and Heat Transfer*

Duncan and Reimer, *Chemical Engineering Design and Analysis: An Introduction*

Fan and Zhu, *Principles of Gas-Solid Flows*

Fox, *Computational Models for Turbulent Reacting Flows*

Franses, *Thermodynamics with Chemical Engineering Applications*

Leal, *Advanced Transport Phenomena: Fluid Mechanics and Convective Transport Processes*

Lim and Shin, *Fed-Batch Cultures: Principles and Applications of Semi-Batch Bioreactors*

Marchisio and Fox, *Computational Models for Polydisperse Particulate and Multiphase Systems*

Mewis and Wagner, *Colloidal Suspension Rheology*

Morbideilli, Gavriilidis, and Varma, *Catalyst Design: Optimal Distribution of Catalyst in Pellets, Reactors, and Membranes*

Nicoud, *Chromatographic Processes*

Noble and Terry, *Principles of Chemical Separations with Environmental Applications*

Orbey and Sandler, *Modeling Vapor-Liquid Equilibria: Cubic Equations of State and their Mixing Rules*

Petyluk, *Distillation Theory and its Applications to Optimal Design of Separation Units*

Rao and Nott, *An Introduction to Granular Flow*

Russell, Robinson, and Wagner, *Mass and Heat Transfer: Analysis of Mass Contactors and Heat Exchangers*

Schobert, *Chemistry of Fossil Fuels and Biofuels*

Shell, *Thermodynamics and Statistical Mechanics*

Sirkar, *Separation of Molecules, Macromolecules and Particles: Principles, Phenomena and Processes*

Slattery, *Advanced Transport Phenomena*

Varma, Morbidelli, and Wu, *Parametric Sensitivity in Chemical Systems*

# Design and Processing of Particulate Products

JIM LITSTER

University of Sheffield



**CAMBRIDGE**  
UNIVERSITY PRESS

**CAMBRIDGE**  
UNIVERSITY PRESS

University Printing House, Cambridge CB2 8BS, United Kingdom

Cambridge University Press is part of the University of Cambridge.

It furthers the University's mission by disseminating knowledge in the pursuit of education, learning and research at the highest international levels of excellence.

[www.cambridge.org](http://www.cambridge.org)

Information on this title: [www.cambridge.org/9781107007376](http://www.cambridge.org/9781107007376)

© Jim Litster 2016

This publication is in copyright. Subject to statutory exception and to the provisions of relevant collective licensing agreements, no reproduction of any part may take place without the written permission of Cambridge University Press.

First published 2016

Printed in the United Kingdom by TJ International Ltd. Padstow Cornwall

*A catalogue record for this publication is available from the British Library*

*Library of Congress Cataloging-in-Publication data*

Names: Litster, Jim, author.

Title: Design and processing of particulate products / Jim Litster.

Description: Cambridge, United Kingdom: Cambridge University Press, 2016. |

Series: Cambridge series in chemical engineering

Identifiers: LCCN 2016025984 | ISBN 9781107007376 (hardback)

Subjects: LCSH: Particles. | Chemical engineering. |

BISAC: TECHNOLOGY & ENGINEERING / Chemical & Biochemical.

Classification: LCC TP156.P3 L58 2016 | DDC 620/.43-dc23

LC record available at <https://lccn.loc.gov/2016025984>

ISBN 978-1-107-00737-6 Hardback

Cambridge University Press has no responsibility for the persistence or accuracy of URLs for external or third-party internet websites referred to in this publication, and does not guarantee that any content on such websites is, or will remain, accurate or appropriate.



**To my parents,  
Don and Nola, who taught me to love both learning and learners.**



# Contents

	<i>Contributors</i>	page xii
	<i>Preface</i>	xiii
<b>1</b>	<b>Introduction</b>	1
	1.1 The Joy of Particulate Products	1
	1.2 Process and Product Engineering	4
	1.3 How to Use this Book	6
	1.4 Discussion Questions and Problems	7
<b>2</b>	<b>Particle Characterization and Particle Property Distributions</b>	9
	2.1 Consider a Case Study ...	9
	2.2 Learning Goals	11
	2.3 Defining Properties of a Single Particle	11
	2.3.1 Particle Size	12
	2.3.2 Particle Shape	14
	2.3.3 Particle Density and Porosity	17
	2.4 The Mathematics of Property Distributions for Particle Populations	19
	2.4.1 Basic Definitions	19
	2.4.2 Changing the Way that We Represent the Distributions	23
	2.4.3 Properties of the Frequency and Cumulative Distributions	26
	2.4.4 Some Special Distributions	28
	2.5 Measuring Properties of Populations of Particles	30
	2.5.1 Particle Size	30
	2.5.2 Particle and Powder Density Measurement	31
	2.5.3 Porosity and Pore Size Distribution Measurement	33
	2.6 Another Case Study	36
	2.7 Summary	39
	2.8 Bibliography	39
	2.9 Problems	40
<b>3</b>	<b>The Population Balance</b>	46
	3.1 Consider a Case Study ...	46
	3.2 Learning Goals	48
	3.3 Modeling a Well-mixed Particle Generator	48

3.4	Derivation of the Macroscopic Population Balance	50
3.4.1	Variations on a Theme	51
3.4.2	Moments Form of the Population Balance	53
3.4.3	An Example	54
3.5	Differential Growth Processes	59
3.6	The Birth and Death Terms: Nucleation, Agglomeration, and Breakage	64
3.6.1	Nucleation	64
3.6.2	Agglomeration	65
3.6.3	Breakage	70
3.7	Summary	74
3.8	Bibliography	75
3.9	Problems	76
<b>4</b>	<b>Industrial Crystallization</b>	<b>80</b>
4.1	Consider a Case Study ...	80
4.2	Learning Goals	82
4.3	The Driving Force for Crystallization – Solubility and Supersaturation	83
4.4	Crystallizer Design Choices and Configurations	86
4.5	Crystallization Rate Processes	88
4.5.1	Crystal Growth Kinetics	88
4.5.2	Crystal Nucleation Kinetics	93
4.6	Crystallizer Analysis and Design	98
4.6.1	Batch Crystallizers	98
4.6.2	The MSMPR Continuous Crystallizer	101
4.7	Crystal Engineering	108
4.8	Summary	110
4.9	Bibliography	112
4.10	Problems	113
<b>5</b>	<b>Particle Size Reduction</b>	<b>117</b>
5.1	Consider a Case Study ...	117
5.2	Learning Goals	118
5.3	Breakage Mechanisms and Fracture Mechanics	119
5.4	Population Balance Models	123
5.4.1	Derivation of the Mass–Size Balance for Particle Size Reduction	123
5.4.2	The Breakage Rate Constant and the Breakage Kernel	130
5.4.3	Size Reduction with Classification	136
5.5	Particle Size Reduction Equipment	141
5.5.1	Crushers	141
5.5.2	Impact Mills	142
5.5.3	Tumbling Mills	142
5.5.4	Stirred Media Mills	144

5.5.5	Jet Mills	144
5.5.6	Selection of Particle Size Reduction Equipment	144
5.6	Energy Relationships and Scaling	145
5.6.1	The Bond Work Index	146
5.6.2	Energy–Size Relationships from Single Particle Impacts	147
5.6.3	Semi-mechanistic Approaches for Stirred Media Mills	149
5.6.4	Energy Relationships and the Population Balance	151
5.7	Summary	154
5.8	Bibliography	155
5.9	Problems	156
<b>6</b>	<b>Aerosol Processes</b>	<b>161</b>
6.1	Consider a Case Study ...	161
6.2	Learning Goals	163
6.3	Aerosol Reactor Overview	163
6.4	The Rate Processes of Aerosol Reactors	166
6.4.1	Nucleation	168
6.4.2	Growth	168
6.4.3	Collision-based Agglomeration and Aggregation	169
6.4.4	Coalescence	171
6.4.5	Agglomerate Breakage	172
6.5	The Population Balance for an Aerosol Reactor	176
6.5.1	General Expressions for Each Reactor Zone	176
6.5.2	Moments of the Population Balance	177
6.6	Case Study Revisited	184
6.7	Summary	188
6.8	Bibliography	189
6.9	Problems	190
<b>7</b>	<b>Spray Drying and Spray Cooling</b>	<b>192</b>
7.1	Consider a Case Study ...	192
7.2	Learning Goals	193
7.3	Drop Formation and Atomization	194
7.3.1	Rayleigh Jet Break Up	194
7.3.2	Relaxing the Rayleigh Assumptions	196
7.3.3	Atomization from Nozzles and Rotating Discs	198
7.4	Drop Drying and Solidification and Particle Formation	200
7.4.1	Cooling and Solidification of a Single Melt Drop	200
7.4.2	Evaporation of a Single Drop	202
7.4.3	Drying Drops with Dissolved or Suspended Solids	204
7.5	Particle Morphology from Spray Drying and Spray Cooling	209
7.6	Spray-drier and Spray-cooler Design	213
7.6.1	Spray-cooling Towers (Prill Towers)	213

7.6.2	Spray-drier Design	218
7.6.3	Population Balance Models for Spray Drying and Spray Cooling	221
7.7	Summary	224
7.8	Bibliography	225
7.9	Problems	225
<b>8</b>	<b>Wet Granulation</b>	<b>228</b>
8.1	Consider a Case Study ...	228
8.2	Learning Goals	229
8.3	Overview	230
8.4	Rate Processes and Regime Maps	231
8.4.1	Nucleation	232
8.4.2	Wet Granule Strength and Consolidation	240
8.4.3	Growth by Coalescence or Powder Layering	245
8.4.4	Wet Granule Breakage	251
8.5	The Population Balance for Granulation	252
8.6	Equipment Design and Scaling Rules	258
8.6.1	Tumbling Granulators	258
8.6.2	Mixer Granulators	260
8.6.3	Fluidized Granulators	261
8.6.4	Scaling Rules	265
8.7	Summary	267
8.8	Bibliography	267
8.9	Problems	268
<b>9</b>	<b>Strength, Breakage, and Attrition of Particulate Delivery Forms</b>	<b>273</b>
9.1	Consider a Case Study ...	273
9.2	Learning Goals	274
9.3	Micromechanical Models for Agglomerate Strength	275
9.3.1	The Rumpf Model for Agglomerate Tensile Strength	275
9.3.2	The Kendall Model	277
9.4	Macroscopic Strength of Particles and Particulate Products	282
9.5	Agglomerate Attrition and Breakage	286
9.5.1	A Case Study – Fluid Bed Attrition of Agglomerates	288
9.6	Summary	290
9.7	Bibliography	291
9.8	Problems	292
<b>10</b>	<b>Dispersion, Disintegration, and Dissolution</b>	<b>294</b>
10.1	Consider a Case Study ...	294
10.2	Learning Goals	295
10.3	Overview of Agglomerate Dispersion	295

---

10.4 Dispersion by Gases	300
10.5 Dispersion and Disintegration of Agglomerates and Powders in Liquids	302
10.5.1 Wet Dispersion Kinetics	307
10.6 Agglomerate and Powder Dissolution	309
10.6.1 Single Particle Dissolution	309
10.6.2 Dissolution of a Powder (Multiparticle System)	314
10.7 Summary	318
10.8 Bibliography	319
10.9 Problems	320
<i>Index</i>	323

# Contributors

Bert Diemer (Chapter 6)

Tony Howes (Chapter 7)

Jim Michaels (Chapter 10)

Carl Wassgren (problems 3, 4, 7, 8, 10, 13, 17 and 18 in Chapter 2)



# Preface

Particulate products are ubiquitous and highly valued across a range of industry sectors. Why, then, are they often still designed and operated with little regard to the underlying science, and why is their design and manufacture largely absent from our engineering curricula? Of course, these two questions are strongly related. We don't adequately prepare our engineers and technologists to develop these complex products and design the complex flowsheets that produce them.

The reasons for resistance to change in the modern chemical engineering curricula are complex, but one observation is clear. Where new engineering approaches have been embedded in practice, there are (1) good textbooks to support curriculum development, and (2) good tools for practitioners to use. Very recently, process simulation tools to model flowsheets where new particles are formed and built into structured products have become available. I hope that this book will complement these tools and contribute to the canon for teaching modern, sophisticated programs on engineering particulate products.

Particle technology in general is short on high-quality textbooks. Those that do exist, such as Martin Rhodes' excellent introductory text, have a heavy focus on applying fluid and powder mechanics principles to the storage and flow of powders and their separation from fluids. In this case, the particle properties are a given. To use a fashion analogy, these are "off-the-rack" particles. In contrast, here we focus on how to make particles and particulate delivery forms. We deal in "designer" particles. So this book should complement, rather than compete with, existing texts. The logical extension of this argument is that a modern foundation in particulate products cannot be covered in a single survey course. At Purdue, there are a suite of three core courses. The new Masters program at University of Delaware has four.

The inspiration for the book comes from my involvement over the last 18 years with the International Fine Particle Research Institute (IFPRI). This unique club of companies spanning a range of industry sectors invites academics to address problems in particle technology, especially in particle design, and challenges them to produce science-based solutions that have broad application. I learnt many things from IFPRI, including:

- how to identify important problems worth solving related to particulate products;
- that solving these problems requires a mix of both process and product engineering; and

- underlying science from a wide range of disciplines is necessary to solve the problems.

Much of the engineering science described in this book was directly or indirectly sponsored by IFPRI and many of the case studies that begin each chapter resulted from fascinating conversations with IFPRI company representatives.

There are many people to acknowledge in the writing of this book. First, I wish to thank Jim Michaels, Bert Diemer, and Tony Howes, who each co-authored one of the book chapters. I also want to thank Carl Wassgren for supplying many of the problems in Chapter 2, and more broadly for the many discussions we had about the need for, and scope of, this text. I am grateful to my research group at Purdue, especially Steven Dale, Coco Abbou Oucherif, Nathan J. Davis, Jennifer Lu, and Sudarshan Ganesh, who kindly helped with generating some of the worked examples, graphs, and figures. The content of the book is partly based on courses developed and taught at The University of Queensland, Purdue University, and The University of Delaware, and I want to acknowledge the students and academic staff at those universities for their feedback and patience. Speaking of patience, the publishing team at Cambridge University Press has always been very encouraging and tolerant of my many slipped deadlines. Finally, my thanks to my first mentor in the field, Ted White, who set me off on this fascinating path.

# 1 Introduction

---

## 1.1 The Joy of Particulate Products

Particulate products represent a large proportion of *formulated products*. The performance of these products is a function not only of their composition, but also of their particulate structure, properties, and attributes. There are a remarkable array of such products, including crystals, granules, compacts, pastes, and emulsions. The products appear in industry sectors as diverse as agricultural and specialty chemicals, food, consumer goods, agricultural products, energetic materials, and pharmaceuticals. In fact, 70% of products from these industries are in particulate form. Particle products contribute more than one trillion dollars to the US economy, which is the world's largest manufacturer of these high-value particulate products. They impact positively on people's quality of life all over the world.

Why are particulate products so wildly popular? They have a number of advantages over simple liquid formulations.

1. They reduce transport and handling costs through not having to transport large amounts of solvent, typically water, over large distances.
2. They have improved physical and chemical stability over liquid products. This gives longer shelf life and improves safety for consumers for food and pharmaceutical products, for example.
3. They allow us to design-in complex product performance – e.g., a controlled-release profile for a drug. Sometimes, the performance attributes are apparently in direct competition – e.g., an agricultural chemical granule that is strong to resist attrition during handling, but “instantaneously” breaks down and dissolves when mixed with water.
4. The product can be designed to consist of many components – e.g., a detergent granule or tablet can include surfactant, bleach, enzymes, etc.
5. Consumers like them!

In many cases, the final delivery form for a particulate product is a structure containing smaller, primary particles that is built up over many length scales. Figure 1.1 illustrates this for a pharmaceutical solid oral dosage form – a tablet. The active pharmaceutical ingredient (API) is a molecule, often present as a crystalline particle. Single crystals interact with each other, and aggregate or agglomerate. This helps define how they behave as a bulk powder. The API powder is blended with

**Table 1.1** Some examples of particulate products and their required attributes

Product	Form	Desired attributes
Table sugar	Crystals	<ul style="list-style-type: none"> <li>• White, pleasant appearance</li> <li>• Non-sticky</li> <li>• Flows freely</li> <li>• Resists caking</li> </ul>
Herbicides	Granules	<ul style="list-style-type: none"> <li>• Flows freely</li> <li>• Resists attrition</li> <li>• Non-dusty</li> <li>• Disperses instantaneously in water</li> </ul>
Pharmaceutical oral dosage form	Tablet	<ul style="list-style-type: none"> <li>• Drug content uniformity</li> <li>• Resists attrition, breakage</li> <li>• Has good physical and chemical stability</li> <li>• Dissolves in the GI tract at the required rate</li> </ul>
Paint	Suspension	<ul style="list-style-type: none"> <li>• Opaque to light in visible wavelength region</li> <li>• Complex rheology – sticks on the brush, but easily spreads on the wall</li> <li>• Physically stable – is not a sludge with clear liquor on top when the tin is opened</li> </ul>

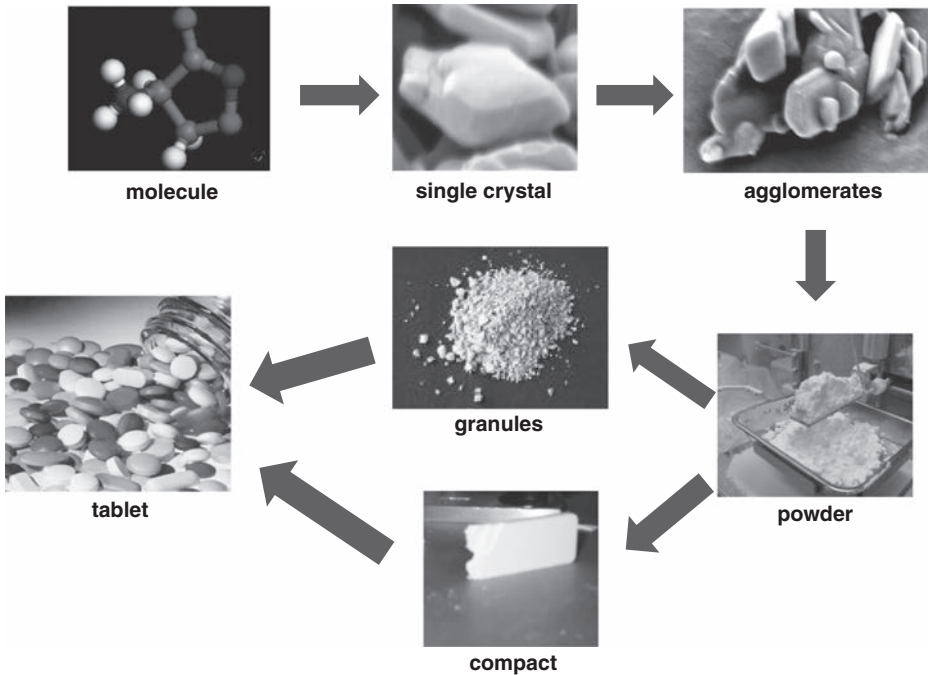


**Figure 1.1** A pharmaceutical tablet is a particulate product built up over many length scales.

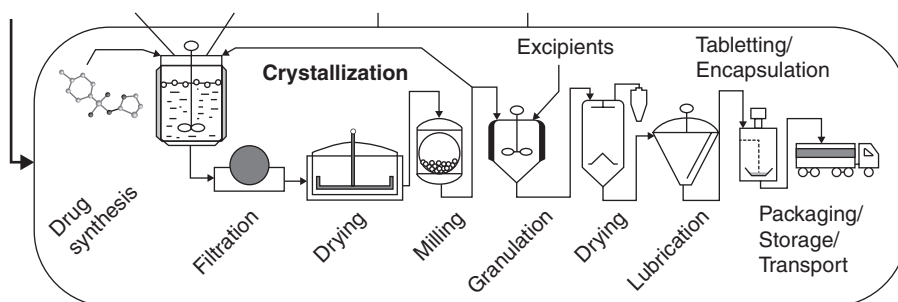


**Figure 1.2** A simplified flowsheet for the manufacture of a pharmaceutical solid oral dosage form.

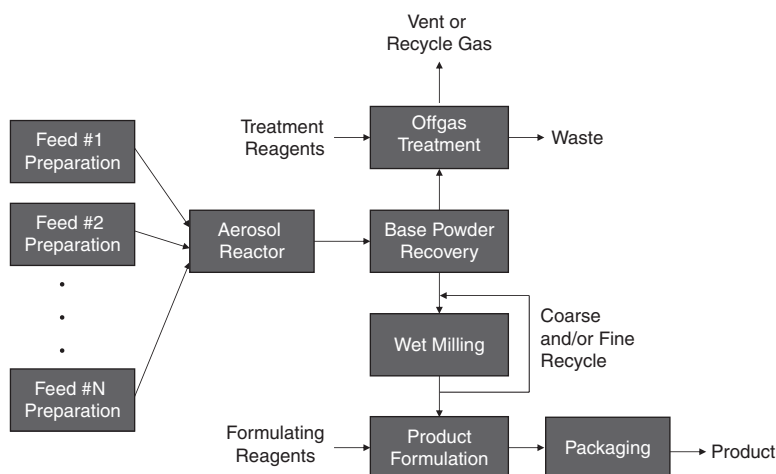


**Figure 1.3** A simplified flowsheet for paint pigment manufacture via an aerosol reactor.

excipients and granulated (wet or dry) to give free-flowing granules suitable for compacting into a tablet. Building such complex products requires complex process flowsheets involving many unit operations (see Figure 1.2).

Figure 1.3 shows the flowsheet for producing a very different particulate product – paint pigments. Here, the submicron primary particles are produced in a flame reactor. They self-agglomerate, which is useful to help separate them from the flowing gas stream. Downstream, they may be granulated into some easy-to-handle particulate form. Ultimately, the agglomerates must be milled and dispersed as a stable, shear-thinning suspension – paint.

Note that many of the unit operations on the flowsheets are processes that create new particles, modify particle properties, or build new particulate delivery forms: crystallization, aerosol reactors, grinding, agglomeration, compaction, and so on. These are the processes of interest in this book. We need to be able to predict the particle properties (size and size distribution, morphology, porosity, and

structure) that result from these processes. We are interested in *made-to-measure designer particles*. Other texts in particle technology deal primarily in *off-the-rack* particles, and how they are processed and handled. The engineer has no control over off-the-rack particles. He or she must simply deal with them. Designer particles offer the opportunity for creativity and synthesis, which we think is much more interesting.

Particulate products are complex, and the physics of particulate materials is not completely understood. For example, the full constitutive behavior of powder flow has not yet been defined in the way Stokes did for fluid mechanics 150 years ago. Furthermore, the discrete nature of particulate materials means that we also must track distributions of particle properties, not just point values. This means that it is rare we can design a product or process completely from first principles. Nevertheless, quantitative engineering tools based on fundamental physics do exist for most processes and they should be used! That is the rationale for this book.

## 1.2 Process and Product Engineering

Typically, chemical engineers are very good at process engineering – designing and optimizing individual unit operations and integrated flowsheets to produce the right production rate of material while minimizing cost and waste. This is a good approach for commodity chemicals produced in large tonnages over a long period of time. However, process engineers have little knowledge of formulation or new product development and the engineering tools are usually designed for processes involving simple fluids rather than particulate materials or complex fluids such as emulsions.

Traditionally, formulators in industries making particulate products have taken a product engineering view. New products are formulated to give the desired product attributes. Manufacture is recipe driven using available off-the-shelf equipment with heuristics used to choose and scale the equipment. This can lead to time-consuming experiments at many scales to get the product to manufacture and often non-optimal processes. This dichotomy between formulators and process engineers is often reinforced in the company structure.

A better way is needed. Optimal engineering development and scale up of a particulate product requires a combination of *both* process and product engineering. This approach is illustrated in Figure 1.4. First, the properties of the formulation must be carefully characterized (product engineering). This characterization step is always essential because the properties of particles and powders are not only a function of their *thermodynamic* state, but also their *particulate* state, which depends on their particle property distributions (especially size) and their processing history. Second, the key operating conditions in the process equipment (velocity, concentration, and stress fields) must be characterized in terms of process parameters that can be controlled: impeller speed, temperature, etc. (process engineering).

For each operation, we need a *process model* that tracks the evolution of the particle properties distributions in the process equipment. Where possible, we use a

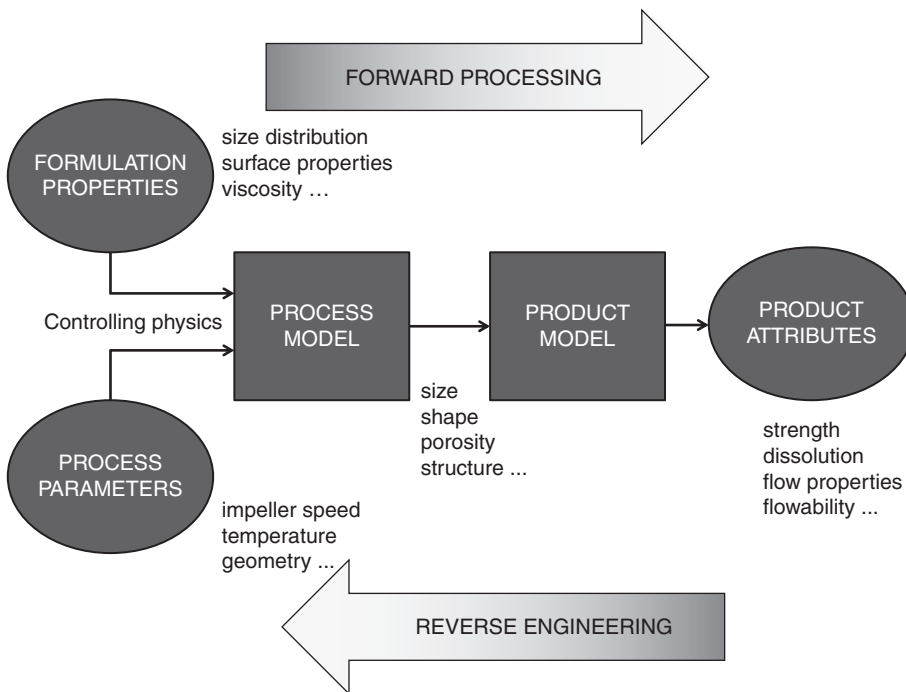


**Figure 1.4** Combining product and process engineering for particulate product design and manufacture.

mathematical tool, the population balance, as the framework for the process model in combination with mass and energy balances. The structure of the model, and the value of the rate constants, are linked to the process parameters and formulation properties through an understanding of the controlling physics and/or chemistry.

We are not finished yet. Typically, our end goal is to know the product attributes such as those described in Table 1.1. For this we need a *product model* which predicts product performance – e.g., dissolution rate – given the particulate product structure and property distribution.

To this point, we have described a combination of product and process engineering for forward development. This approach is generally used to scale up and optimize a new formulation with an existing process or choice of processes. Ideally, in the design phase we should be *reverse engineering* our product. By this I mean that we first define our required product attributes, then work backwards using our product and process models to choose a process and formulation that meets our needs. Reverse engineering is more challenging because there is no single correct solution, but rather a family of possible solutions that can be used.

Note that Figure 1.4 seems to imply our particulate product is made in a single step. As we saw from Figures 1.2 and 1.3, manufacturing a particulate product is a multistep process, so many process models are needed. The more complex the product, the more steps that are required. Broadly speaking, we can divide particulate

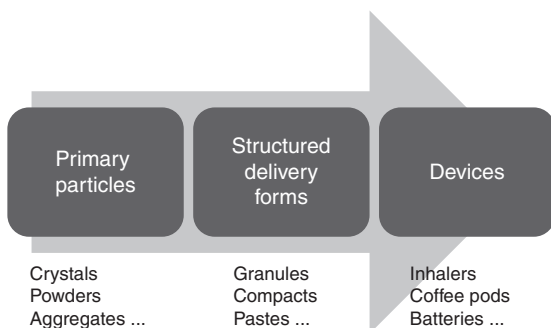


**Figure 1.5** Increasing complexity of particulate products.

products into three categories (Figure 1.5). *Single particles and powders* are the simplest particulate products. Granular sugar is a good example. *Structured products and delivery forms* are often built from single particles and may have several components. For example, a pesticide water-dispersible granule to be reconstituted as a solution or slurry to spray onto crops will consist of the active ingredient combined with a binder, surfactant, and disintegrant into a porous, free-flowing granule. The most complex products are those where the particulate product is combined with a *delivery device*. For example, a dry powder inhalation system to deliver insulin to the lungs consists of (1) agglomerates of the active ingredient attached to lactose carrier particles, and (2) an inhalation device which is designed so the agglomerates break down by impact or shear and are inhaled as primary particles.

In the following chapters, we consider the manufacture of single particles, powders, and structured products in some details, but delivery device design is beyond the scope of the book.

### 1.3 How to Use this Book

The book is organized along the lines of process and product engineering described above (Table 1.2). Chapters 2 and 3 give essential tools for studying any particulate systems: (1) definitions of key properties and tools and for both formulation and product characterization, and (2) the mathematical basis for defining property distributions and tracking how they change during processing. Chapters 4–6 cover processes which generate single particles, while Chapters 7 and 8 cover processes that build particulate delivery forms. Chapters 9 and 10 give important product performance models that predict important behavior of the product in use. For each chapter:

1. the key rate processes are defined;
2. the relevant physics of the processes is presented leading to identification of the formulation properties and process parameters that control them; and



**Table 1.2** Structure of the book

Essential tools	2. Particle Characterization
	3. The Population Balance
Particle formation processes	4. Crystallization
	5. Particle Size Reduction
	6. Aerosol Processes
Particulate delivery forms	7. Spray drying and spray cooling
	8. Wet Granulation
Product Models	9. Strength and attrition of agglomerates
	10. Dispersion, disintegration and dissolution

3. the population balance is used as a framework to quantify these processes for synthesis and analysis.

Each chapter begins with a messy case study based on a real industrial example. The case study helps you to empathize with the engineer or technologists who face such challenges on a regular basis, and puts the chapter in context.

This book is primarily for use as a textbook for students studying courses in particulate processing and particle technology more broadly. Hopefully, it is also a resource for practitioners wanting to bring a more rigorous approach to product or process development. Chapters 2 and 3 give the students the tools necessary for the analysis in the following chapters. Students, lecturers or practitioners can cherry-pick from the unit operations covered in Chapters 4–8. We recommend that at least one of the product modeling chapters is included. I hope your course of study convinces you that quantitative engineering with a sound scientific basis can and should be applied to these complex products and processes. Enjoy!

## 1.4 Discussion Questions and Problems

- 1.1. Visit your supermarket and make a list of the particulate products you see on the shelf. Remember to visit the cleaning and laundry aisles as well as the food aisles. Group the products by their physical type: crystal, powder, granule, table, paste, and so on. For each product, list the product attributes important to its performance – e.g., fast dissolving, good shelf life. Look at the ingredient list. Is the product a single component (sugar) or a complex formulation (laundry detergent)? Based on your observations of the product, how do you think it is manufactured? Is the same product available in several different physical forms?
- 1.2. Repeat problem 1.1 at the pharmacy (drug store). Don't forget to look in the cosmetics and personal care aisles as well as the pharmaceuticals.
- 1.3. Repeat problem 1.1 at the hardware store.

- 1.4. Using an encyclopedia of chemical technology or web-based resources, look up typical manufacturing flowsheets for the following products (or any other you can think of):
- a. carbon black
  - b. table sugar
  - c. paracetamol (acetaminophen) tablets
  - d. laundry detergent
  - e. ammonium nitrate for (a) fertilizer; or (b) explosive production
  - f. pyrotechnic fireworks
  - g. toothpaste
  - h. catalyst for using in catalytic cracking of petroleum fractions
  - i. cement

In each case, identify the unit processes that form new particles, change the particle properties, or form them into structured particulate products.

## 2 Particle Characterization and Particle Property Distributions

---

### 2.1 Consider a Case Study ...

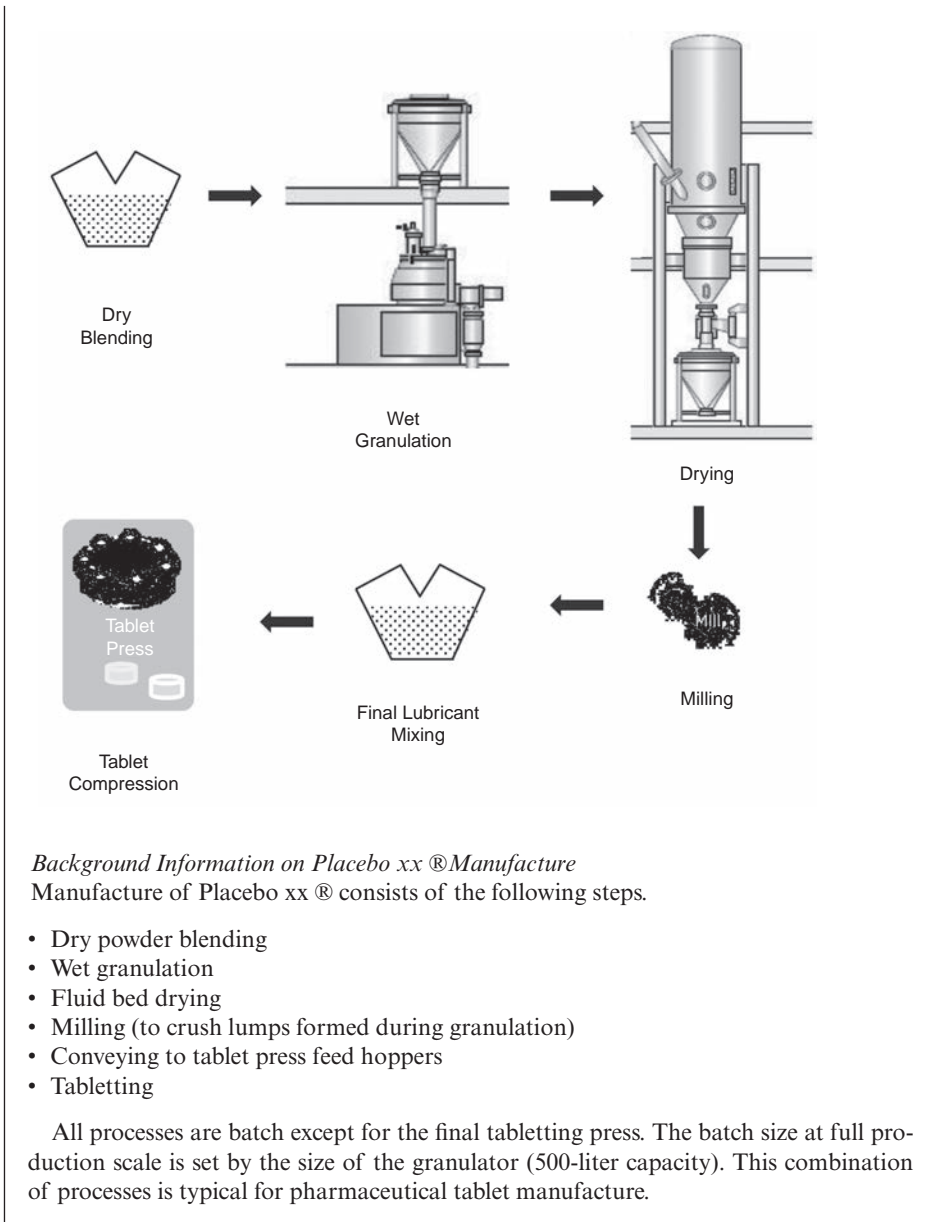
*Acme Modern Drugs*

Memo to: Physical Characterization Lab.

From: Jim Litster, Placebo xx Development Team

Date: January 6, 2011

We have had serious problems in transferring our new antidepressant Placebo xx® from production in our Puerto Rican plant to the Rocklea facility in Brisbane, Australia. In the development batch, granulation was very poor. Tablets formed had low crush strength and high friability. This formulation has previously given no problems in Puerto Rico and none were anticipated in Australia, so production schedules have been pushed back. This is a serious issue as demand for Placebo xx® in Australia is booming. We suspect that the change in behavior of the formulation is due to sourcing of lactose powder which comprises 94.2% w/w of Placebo xx®. The lactose used at Rocklea is from the Delicious Dairy Co. in Hamilton, New Zealand, while Puerto Rico uses lactose from the US supplier. We have already established there is no difference in chemical properties between the two sources of lactose. Can you please: (1) identify any differences in physical properties of the two types of lactose that could explain their different granulation and tableting behavior; (2) recommend a standard set of characterization tests to be performed on all newly sourced formulation ingredients in the future. We are receiving a visit from the Australian Food and Drug Agency next month so it is imperative we receive your memo by February 11 at the latest.



You may be surprised to know that problems like the one described above are very common and create continuous headaches for engineers and technologists.

- A new batch of material for processing behaves differently in processing to previous batches even though it meets the same specifications.

- Different process plants within the same company with apparently the same equipment produce different quality product.
- Powders behave differently in the summer to in the winter, or on a rainy day when compared to a dry day.

Particulate materials cannot be characterized by their thermodynamic state alone. Their behavior during processing and their final product attributes also depend on their *particulate state*, which is a function of their past history.

As an individual reflective exercise, or as a group brainstorm discussion, make as long a list as you can of possible causes for the problems observed by the Placebo xx® team. What is a list of particle and/or bulk powder properties you would wish to measure in order to test your differential diagnosis? What learning goals related to particle characterization does this case study inspire for you, and how do they compare with the chapter learning goals given below? How much do you know about the various unit operations in the process flowsheet? Some of them are the topic of chapters in this book.

## 2.2 Learning Goals

At the completion of this chapter, the student should be able to:

1. Explain to a peer the importance and the difficulty of characterizing particle properties.
2. Write the definitions of a range of particle properties related to size, shape, density, and porosity and describe how to measure them.
3. State the definitions of the frequency and cumulative distributions.
4. Correctly calculate and plot cumulative and frequency distributions from a set of raw data and make conversions between distributions with different measures of quantity and property.
5. Calculate parameters of the frequency and cumulative size distributions.
6. Critically analyze the quality of particle property data.
7. Manipulate size distribution data for engineering problem-solving.

## 2.3 Defining Properties of a Single Particle

There are many particle properties that may influence their behavior in handling, processing, and performance in use (see Figure 2.1). Broadly speaking, we can classify these under several headings, including:

- size and size distribution;
- morphological properties such as shape, density, porosity, and structure;
- surface properties such as surface energy, roughness, and electrical charge; and
- mechanical properties.

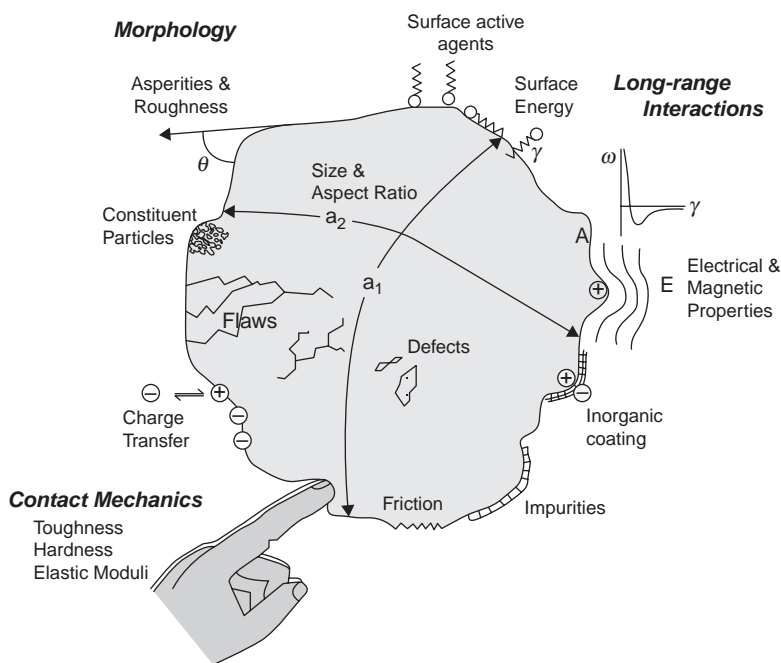


**Figure 2.1** Illustration of some of the many particle properties of interest in particle design and processing (Litster and Ennis, 2004).

In practice, we can never measure all the properties (and their distributions) that we need. In this chapter we define some important properties related to particle size, shape, and morphology. Other particle properties are introduced and defined as necessary in the applications chapters.

### 2.3.1 Particle Size

The most fundamental property of particulate materials is the size of the particles. Particle size affects many important attributes of individual particles and particle assemblies (see Table 2.1). One of the main reasons for this effect is that the behavior of particulate systems is often a balance between surface forces (such as adhesion) and body forces (such as gravity). Let us consider a particle of size  $x$ . The surface force is proportional to the particle surface area  $\sim x^2$ , whereas the body force is proportional to the particle mass  $\sim x^3$  so that the ratio of surface forces to body force is proportional to  $x^{-1}$ .

Despite its universal importance, and our intuitive understanding of its meaning, particle size only has a unique definition if the particle is a sphere. Ask yourself what is the size of the particles shown in Figure 2.2. We must clearly define the particle size we are measuring, or using in a calculation.

**Table 2.1** Properties of particles, granules, and particle assemblies that depend on particle size (Litster and Ennis, 2004)

Property	Trend with decreasing size	Other relevant particle properties
Properties of single particles		
1. Homogeneity	Increasing	
2. Elastic-plastic behavior (ductility)	Increasing	Elastic moduli
Probability of breakage	Decreasing	Toughness
Particle strength	Increasing	Hardness
Wear behavior	Decreasing	Flaw distribution
3. Properties resulting from competition between volume and surface forces, e.g.: adhesion agglomeration suspendability	Increasing	Surface energy Charge distribution Surface groups Impurities Hardness Surface asperities Density Shape Interparticle forces
Properties of particle assemblies and granules		
1. Bulk density	Decreasing	Density, shape, friction, interparticle forces
2. Rheological behavior: elasticity, yield point	Mostly increasing	Size distribution, density, shape, interparticle forces, friction
3. Wetting	Decreasing	Surface energy, contact angle
4. Strength of agglomerates and briquettes	Increasing	Fracture toughness, hardness, elasticity voidage, flaws
5. Powder mechanics: shear stress, unconfined yield stress, cohesive stress, wall friction	Increasing	Surface energy, friction, asperities, hardness, elasticity
6. Fluid mechanics: permeability, fluidizability	Usually decreasing	Density, interparticle forces
7. Ignitability, explosive behavior	Increasing	Chemical and surface properties
8. Reactivity, dissolution rate	Increasing	Surface energy Flaw distribution

As the diameter of a sphere is clearly defined, a common class of particle size definitions is the *equivalent diameter*. The equivalent diameter of a particle is the diameter of the sphere that has the same relevant property as the particle. Thus, the volume equivalent diameter of a particle  $d_v$  is defined as:

$$V_p = \frac{\pi}{6} d_v^3 \quad 2.1$$

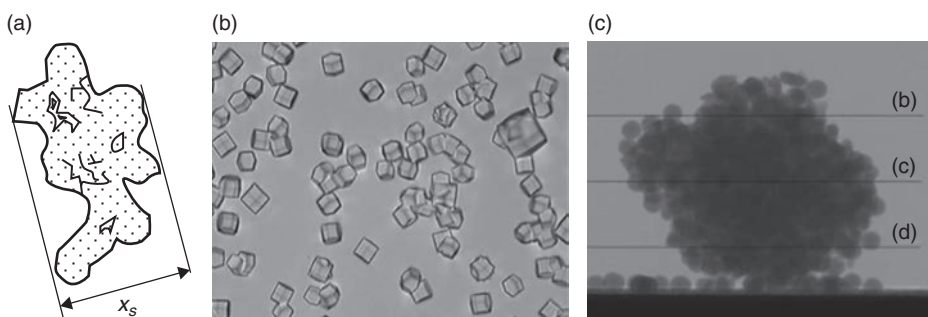


**Figure 2.2** Some different particle morphologies. How would you define their size and shape?

where  $V_p$  is the volume of the particle. In a similar way, we can define other equivalent diameters for other properties such as the particle surface area. Table 2.2 lists some common definitions of particle size based on equivalent diameters.

It is very important to realize that an equivalent diameter size can only match one particle property. Calculating the particle surface area using the volume equivalent diameter will yield the incorrect answer:

$$S_p = \pi d_s^2 \neq \pi d_v^2 \quad 2.2$$

Ideally, our choice of particle size definition should relate to the application of interest. If we wish design a hydrocyclone to separate particles from a fluid by settling in a centrifugal field, then the Stokes diameter  $d_{St}$ , the diameter of a sphere with the same settling velocity as the particle, is a good choice. In many cases, however, the particle size definition depends on how we measure particle size. Thus, the sieve size  $d_{sieve}$  is the maximum diameter of a sphere that will pass through a sieve with a certain square aperture. There are a number of measures of particle size derived directly from microscopy and image analysis including the projected area diameter  $d_a$ , and the Feret diameter  $d_F$  (see Table 2.2 for definitions).

### 2.3.2 Particle Shape

Particle shape is also an important property which impacts on flowability, particle packing, and particle–particle and particle–fluid interactions. It is perhaps more difficult to define than particle size. Ask yourself how you would define particle shape for the particles in Figure 2.2. For crystals and other regular shapes we have clear definitions of the particle shape (see Chapter 4 for more details). Most particles are irregular, however. For these particles, we define shape factors that relate to specific particle properties. Thus, we define the volume, surface area, and specific surface area shape factors as follows:

$$V_p = \alpha_v x^3 \quad 2.3$$



$$S_p = \alpha_s x^2 \quad 2.4$$

$$\left(\frac{S}{V}\right)_p = \frac{\alpha_{sv}}{x} \quad 2.5$$

Here,  $x$  is some arbitrary measure of particle size. Thus, the numerical value of these shape factors depends on the definition of particle size chosen! One important shape factor has a definition which does not include an arbitrary particle size, the particle sphericity:

$$\psi = \frac{\text{surface area of sphere of same volume}}{\text{surface area of particle}} \quad 2.6$$

By definition,  $\psi$  will always lie in a range between 0 and 1. Typical equidimensional granular particles have sphericities of order 0.85–0.9.  $\psi < 0.6$  indicates a large deviation from a sphere – e.g., plates or needles. The sphericity can be used to convert between some of the common equivalent diameters. From the definition in Equation 2.6, it follows that:

$$d_v = \psi^{0.5} d_s \quad 2.7$$

Other useful approximations relate the Stokes diameter and the sieve size to the volume equivalent diameter:

$$d_{sieve} \approx \psi d_v \quad 2.8a$$

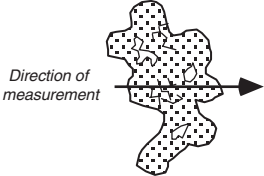
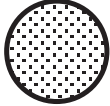
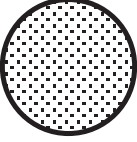




$$d_{St} \approx \psi^{0.25} d_v \quad 2.8b$$

For very rough two-dimensional or three-dimensional shapes, it is very difficult to distinguish surface roughness from the particle “shape.” Consider, for example, flocculated particles in the settling tank for a waste treatment plant, or agglomerated particles formed during the manufacture of pigments via aerosol processes. For such systems, fractal analysis provides a useful way to characterize the “shape” of the particle. The size of the agglomerate is related to the number primary particles  $p$  by:

$$d_{agg} \propto p^{1/D_f} \quad 2.9$$

where  $D_f$  is the fractal dimension. The fractal dimension is in the range 1 to 3. An agglomerate with a fractal dimension of 1 is a line of primary particles, while a fractal dimension of 3 represents a tightly packed, spherical agglomerate. A truly fractal agglomerate will have the same fractal dimension, independent of the scale of observation. In reality, the analysis will break down as we approach the scale of the primary particle in the agglomerate. In this book, we will use fractal dimensions when analyzing aerosol processes (Chapter 6).

**Table 2.2** Eight typical measures of size or length scale for irregularly shaped particles (Litster and Ennis, 2004)

Particle under study		
		
Volume diameter	Diameter of a sphere having the same volume as the particle $V_p = \frac{\pi}{6} d_v^3$	
Surface diameter	Diameter of a sphere having the same surface area as the particle $S_p = \pi d_s^2$	
Stokes' diameter	Diameter of a sphere having the same terminal velocity as the particle $u_t = \frac{g(\rho_p - \rho)d_{St}^2}{18\mu}$	
Specific surface diameter	Diameter of a sphere having the same specific surface area as the particle $(S/V)_p = 6/d_{sv}$	
Particle sieve diameter	Width of the minimum square aperture through which the particle will pass	
Projected area diameter	Diameter of a sphere having the same projected area as the particle $A_p = \pi d_a^2$	
Feret's diameter	Projection of the particle's outline onto a line perpendicular to the direction of measurement	
Scattering diameter	Diameter of a sphere scattering light at the same intensity	

**Example 2.1 Shape Factors and Equivalent Diameters** Common table salt (NaCl) forms cubic crystals. Write down an expression for the volume-equivalent diameter  $d_v$  in terms of the side length of the cubic crystal  $L$ . What is the volume shape factor for the crystal when the size of the crystal is expressed in terms of (a)  $L$  and (b)  $d_v$ ? What is the sphericity of this particle?

*Solution*

The volume of a cubic particle is:

$$V_p = L^3$$

By comparison with Equation 2.1, we have:

$$\begin{aligned} V_p &= \frac{\pi}{6} d_v^3 = L^3 \\ \Rightarrow d_v &= \left(\frac{6}{\pi}\right)^{1/3} L = 1.24L \end{aligned}$$

Given the definition of  $\alpha_v$  from Equation 2.3, it follows that  $\alpha_v = 1$  when  $x = L$ ; and  $\alpha_v = \pi/6$  when  $x = d_v$ . From Equation 2.6:

$$\psi = \frac{\pi d_v^2}{6L^2} = \frac{\pi (6/\pi)^{2/3} L^2}{6L^2} = (\pi/6)^{1/3} = 0.806$$

This almost trivial example emphasizes the importance of clear and thoughtful definition of particle size and shape factor. The volume shape factor is almost halved when the definition of particle size is changed from  $L$  to  $d_v$ . In fact, the nature of their definitions means that  $\alpha_v = \pi/6$  for *any particle shape* when volume-equivalent diameter is chosen as particle size!

### 2.3.3 Particle Density and Porosity

The way a mass of solid occupies space is an important property for many applications, from the packaging of foods (why is the cornflake box never full when I open it?) to mineral separation processes based on particle density. As for particle size and shape, we need to be very careful with our definition of particle density. There are three basic definitions of solids density important in powder processing, which vary according to the length scale of interest (see Figure 2.3):

- the bulk density  $\rho_b$ , which measures the volume occupied by a known mass of powder including the void space between the particles;
- the particle or envelope density  $\rho_p$ , which measures the volume occupied by a single particle including the pores within the particle; and
- the true or skeletal density  $\rho_s$ , which measures the true solids density of the material.

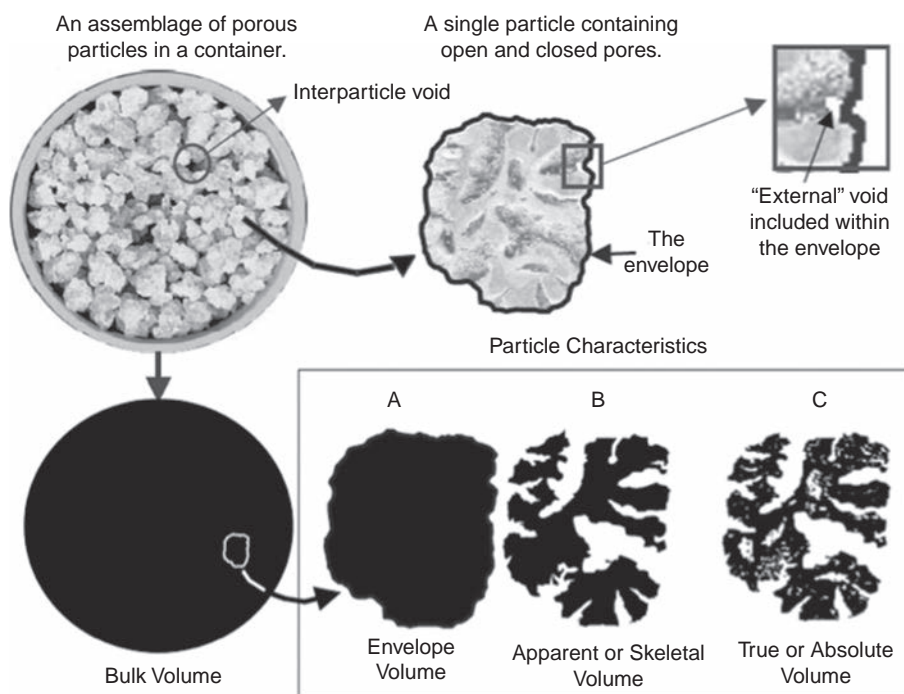


**Figure 2.3** The basis for defining density at different length scales (Webb, 2001).

Of these three density definitions, only the skeletal density is a thermodynamic property of the material. The particle and bulk densities strongly depend on the particle morphology (size, shape, porosity), which depends on the history of the sample. Particle density is difficult to measure directly because the “envelope” around the particle is virtual, rather than real. The particle density is important in determining properties related to particle–fluid interactions – e.g., the terminal settling velocity and minimum fluidization velocity. The bulk density is important for bulk solids handling and packaging applications. In general,  $\rho_b$  is a strong function of sample history – loose-filled, tapped, compressed, and so on.

The voidage of a bulk powder  $\varepsilon$  and the porosity of a particle  $\varepsilon_p$  are closely related to our definitions of density. The bulk powder voidage  $\varepsilon$  is the volume fraction of a powder bed that is voids *between* the particles. The particle porosity  $\varepsilon_p$  is the volume fraction of a particle (within its virtual envelope) that is pores within the particle. Thus, we can relate the densities, voidage, and porosity as follows:

$$\rho_b = \rho_p (1 - \varepsilon) \quad 2.10$$

$$\rho_p = \rho_s (1 - \varepsilon_p) \quad 2.11$$

## 2.4 The Mathematics of Property Distributions for Particle Populations

### 2.4.1 Basic Definitions

So far, we have defined some key particle properties related to their size, shape and porosity. However, we never deal with only one particle, but with a heterogeneous population of particles. Therefore, particle properties do not have single values. Instead, there is a *distribution* of values of the property. We will use the particle size as the example property to develop the mathematics of particle property distributions, but the approach is general to any property.

There are two basic ways to represent the particle size distribution.

- The cumulative distribution,  $N(x)$ , is the number of particles per unit control volume less than size  $x$  (dimensions of  $L^{-3}$ ).
- The frequency distribution,  $n(x)$ , is defined such that  $n(x)dx$  is the number of particles per unit control volume between sizes  $x$  and  $x + dx$ . Thus,  $n(x)$  has dimensions of  $L^{-4}$ .

Clearly,  $N(x)$  and  $n(x)$  are related. From their definitions:

$$N(x) = \int_0^x n(x')dx' \quad 2.12$$

$$n(x) = \frac{d}{dx} N(x) \quad 2.13$$

From Equation 2.12, it follows that the total area under the  $n(x)$  curve must be  $N_T$ , the total number of particles per unit control volume:

$$\int_0^\infty n(x)dx = N_T \quad 2.14$$

We often express the cumulative and frequency distributions as *normalized* distributions:

$$f(x) = \frac{n(x)}{N_T}; \quad F(x) = \frac{N(x)}{N_T} \quad 2.15$$

Figure 2.4 and Table 2.3 show the definitions of the normalized size distributions.

Note that the frequency distribution  $f(x)$  is not the same as the number fraction in the size interval. The number of particles of exactly size  $x$  is impossible to define. Instead, we define the number in a size interval  $x$  to  $x + dx$  so that the fraction of particles in that interval is *the area under the curve*. Thus,  $f(x)$  has the dimensions  $L^{-1}$ . *Always plot the true frequency distribution, not the fraction in a size interval, against size.*

Equations 2.12 to 2.15 are written for a continuous distribution. Most real data are divided into sections (intervals). By convention, the top size of the interval is  $x_i$  and  $\Delta x_i = x_i - x_{i-1}$  is the size interval breadth. Particle properties such as  $f(x)$  are considered constant across the interval. Table 2.3 and Figure 2.4 summarize the different definitions associated with the cumulative and frequency size distributions

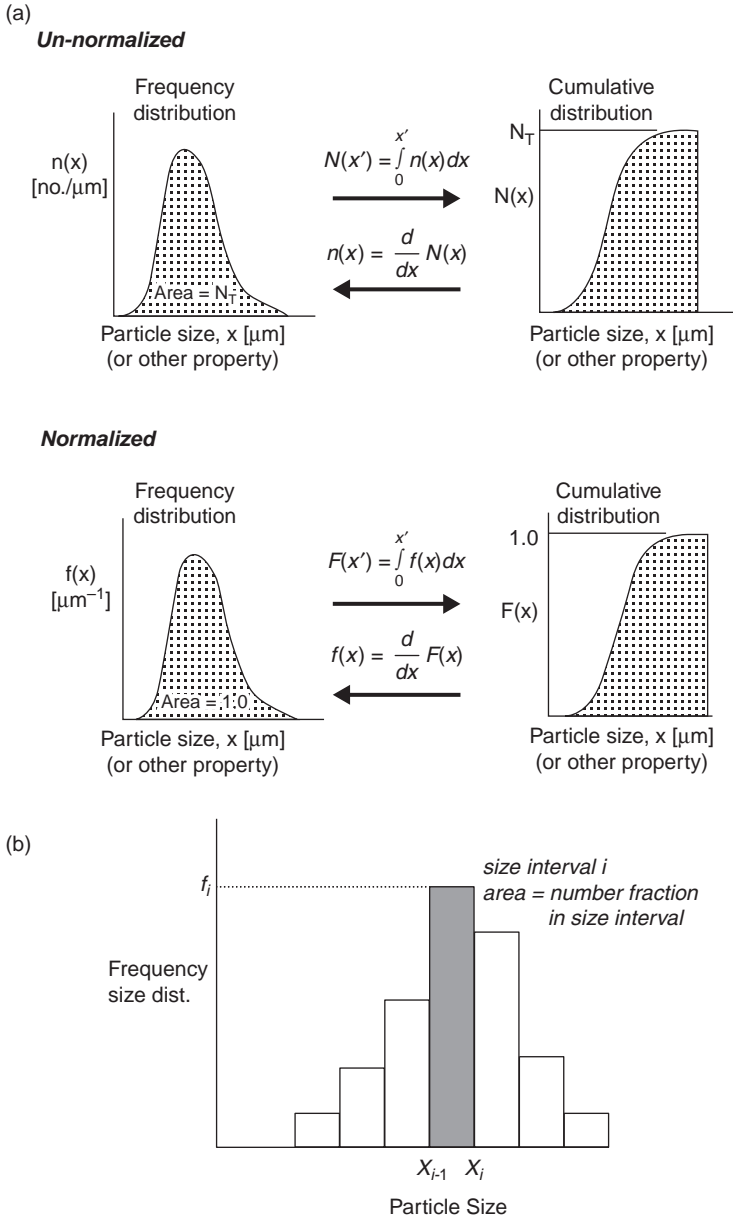


**Figure 2.4** Representing the frequency and cumulative particle size distributions (a) for continuous distributions and (b) for discrete distributions (Litster and Ennis, 2004).

represented as both continuous functions and discrete (sectional) distributions. A quick look at Table 2.3 shows an impressive list of different symbols. In fact, much of the difficulty in handling size distributions comes from confusion in nomenclature, rather than in concepts! Use Table 2.3 as a reference guide as you work through this book.

**Table 2.3** Summary of particle size distribution definitions

Type of distribution	Definition	Relationships
Un-normalized/continuous $N(x)$ $n(x)dx$	No. of particles per unit volume less than size $x$ No. of particles per unit volume between size $x$ and $x + dx$	$N(x) = \int_0^x n(x')dx'$ $n(x) = \frac{d}{dx} N(x)$ $\int_0^\infty n(x)dx = N_T$
Normalized/continuous $F(x)$ $f(x)dx$	No. fraction of particles less than size $x$ No. fraction of particles between size $x$ and $x + dx$	$F(x) = \int_0^x f(x')dx'$ $f(x) = \frac{d}{dx} F(x)$ $\int_0^\infty f(x)dx = 1$ $f(x) = \frac{n(x)}{N_T}$ $F(x) = \frac{N(x)}{N_T}$
Un-normalized/sectional $x_i$ $\Delta x_i = x_i - x_{i-1}$ $N_i$ $n_i^* = n_i \Delta x_i$	Maximum size of particles in size interval $i$ Width of size interval $i$ No. of particles in all intervals up to and including $i$ No. of particles in size interval $i$	$N_i = \sum_{j=1}^i n_i^* = \sum_{j=1}^i n_j \Delta x_j$ $n_i \Delta x_i = n_i^* = N_i - N_{i-1}$ $\sum_{i=1}^\infty n_i \Delta x_i = N_T$ $n_i = \frac{\int_{x_{i-1}}^{x_i} n(x)dx}{\Delta x_i}; N_i = N(x_i)$
Normalized/sectional $F_i$ $y_i = f_i \Delta x_i$	No. fraction of particles in all intervals up to and including $i$ No. fraction of particles in size interval $i$	$F_i = \sum_{j=1}^i y_j = \sum_{j=1}^i f_j \Delta x_j$ $f_i \Delta x_i = y_i = F_i - F_{i-1}$ $\sum_{i=1}^\infty f_i \Delta x_i = 1$ $f_i = \frac{\int_{x_{i-1}}^{x_i} f(x)dx}{\Delta x_i}; F_i = F(x_i)$

**Example 2.2 Calculating Size Distributions from Size Distribution Data** A feed powder to a granulator has the following size distribution, as measured by a Coulter counter. Plot the data as a normalized frequency histogram and normalized cumulative distribution.

Size interval	Range (μm)	Number of particles ( $n_i^*$ )
6	-64 + 32	2
5	-32 + 16	66
4	-16 + 8	117
3	-8 + 4	57
2	-4 + 2	26
1	-2	12
		$N_T = 280$

*Solution*

Take the example of the third (-8 + 4 μm) size interval. Using relationships from Table 2.3 we can calculate the frequency and cumulative normalized distributions:

$$y_3 = \frac{n_3^*}{N_T} = \frac{57}{280} = 0.204$$

$$f_3 = \frac{y_3}{\Delta x_3} = \frac{0.204}{4\mu\text{m}} = 0.0509\mu\text{m}^{-1}$$

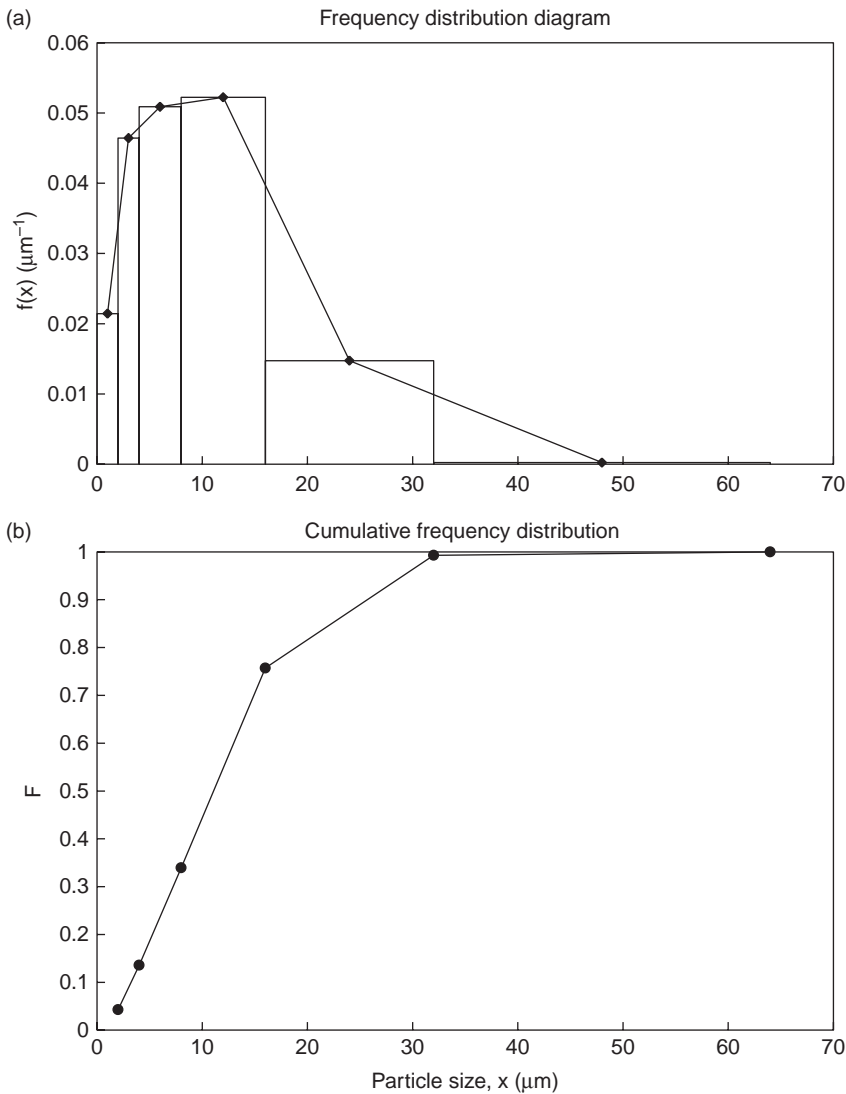
$$F_3 = \frac{\sum_1^3 n_i^*}{N_T} = \frac{12 + 26 + 57}{280} = 0.339$$

These calculations are done for all size intervals and summarized below.

Size interval	Range (μm)	Number of particles ( $n_i^*$ )	$f_i$ (μm <sup>-1</sup> )	$F_i$
6	-64 + 32	2	0.0002	1.000
5	-32 + 16	66	0.0147	0.993
4	-16 + 8	117	0.0522	0.757
3	-8 + 4	57	0.0509	0.339
2	-4 + 2	26	0.0464	0.136
1	-2	12	0.0214	0.043
		$N_T = 280$		

The frequency histogram and cumulative distribution are plotted below:





Note that the cumulative distribution is always plotted against the maximum size of the size interval  $F_i$  vs.  $x_i$ , whereas the frequency distribution is plotted against the midpoint of the size interval,  $f_i$  vs  $\bar{x}_i$ .

## 2.4.2 Changing the Way that We Represent the Distributions

$f(x)$  uses *number* as the measure of *quantity* of particles and *size* as the *property* of interest. More generally, we should be able to express the distribution of any measure of quantity ( $y$  axis of a frequency plot) and property ( $x$  axis of a frequency plot). We write a generalized distribution as  $f_\alpha(\xi)$ , where  $\xi$  is the particle property of interest and the subscript  $\alpha$  denotes the measure of quantity of particles. Thus,

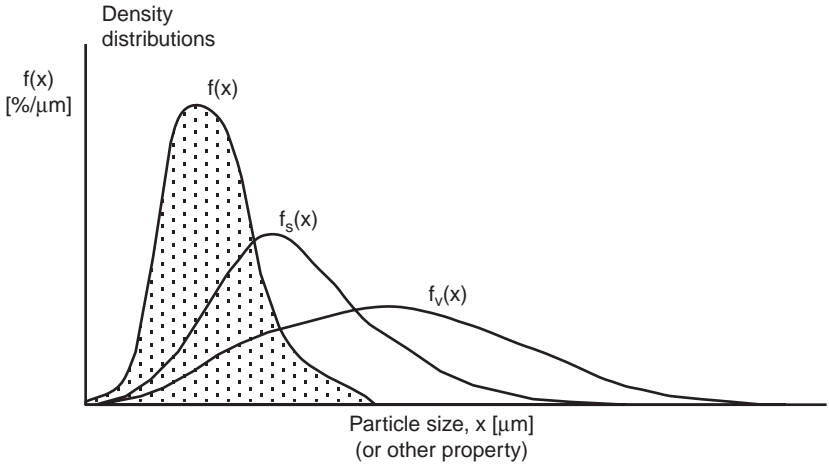


Figure 2.5 Examples of different frequency size distributions.

the general definition of the frequency distribution  $f_{\alpha}(\xi)$  is that the fraction of  $\alpha$  between  $\xi$  and  $\xi + d\xi$  is  $f_{\alpha}(\xi)d\xi$ . Figure 2.5 illustrates three different frequency distributions where the quantity is expressed in terms of number, surface area, and volume. The subscript is omitted when  $\alpha$  is the number of particles.

We regularly convert from a number to a volume (mass) basis as most particle sizers either count or weigh particles. Typical particle properties  $\xi$  are size  $x$ , volume  $v$  and  $\ln(x)$ .

One distribution can be converted to another if the relationship between the two measures of quantity or property is known. Below, we derive the volume size distribution  $f_v(x)$  from the number distribution  $f(x)$  – i.e., changing the measure of quantity:

- The number of particles of size  $x$  to  $x + dx = N_T \cdot f(x) dx$
- The volume of an individual particle of size  $x = \alpha_v \cdot x^3$
- Therefore, the volume of particles of size  $x$  to  $x + dx = \alpha_v \cdot x^3 \cdot N_T \cdot f(x) dx$ .

The total volume of particles is  $V_T = \int_0^{\infty} \alpha_v \cdot x^3 \cdot N_T \cdot f(x) dx$

Assuming the volume shape factor is size-independent, the volume frequency distribution is given by

$$f_v(x) dx = \frac{\alpha_v \cdot x^3 \cdot N_T \cdot f(x) dx}{V_T}$$

$$\Rightarrow f_v(x) = \frac{x^3 f(x)}{\int_0^{\infty} x^3 f(x) dx} \tag{2.16}$$

Note from Figure 2.5 that the volume (mass) size distribution is very different to the number size distribution, with much greater weighting to the larger particles.

**Table 2.4** Converting between different frequency distributions

Property ( $\xi$ )	Quantity ( $\alpha$ )	Continuous	Discrete
Size	Number	$f(x)$	$f_i$
Size	Surface area	$f_s(x) = \frac{x^2 f(x)}{\int_0^\infty x^2 f(x) dx}$	$f_{si} = \frac{\bar{x}_i^2 f_i}{\sum_j \bar{x}_j^2 f_j \Delta x_j}$
		$f(x) = \frac{x^{-2} f_s(x)}{\int_0^\infty x^{-2} f_s(x) dx}$	$f_i = \frac{\bar{x}_i^{-2} f_{si}}{\sum_j \bar{x}_j^{-2} f_{sj} \Delta x_j}$
Size	Volume or mass	$f_v(x) = \frac{x^3 f(x)}{\int_0^\infty x^3 f(x) dx}$	$f_{vi} = \frac{\bar{x}_i^3 f_i}{\sum_j \bar{x}_j^3 f_j \Delta x_j}$
		$f(x) = \frac{x^{-3} f_v(x)}{\int_0^\infty x^{-3} f_v(x) dx}$	$f_i = \frac{\bar{x}_i^{-3} f_{vi}}{\sum_j \bar{x}_j^{-3} f_{vj} \Delta x_j}$
Volume	Number	$f(v) = \frac{f(x)}{3\alpha_v x^2}$	$f_i^v = \frac{f_i}{3\alpha_v \bar{x}_i^2}$
ln(size)	Number	$f(\ln x) = xf(x)$	$f_i^{\ln x} = \bar{x}_i f_i$

Let us now convert from a linear to a logarithmic frequency distribution (changing the property from  $x$  to  $\ln(x)$ ). By definition, the number of particles between size  $x$  and  $x + dx$  must be the same as between  $\ln(x)$  and  $\ln(x) + d\ln(x)$ . That is:

$$\begin{aligned}
 f(x).dx &= f(\ln x).d \ln x \\
 \Rightarrow f(\ln x) &= \frac{dx}{d \ln(x)}.f(x) \\
 \text{but } \frac{d \ln(x)}{dx} &= \frac{1}{x} \\
 \therefore f(\ln x) &= xf(x)
 \end{aligned}
 \tag{2.17}$$

It is very common for particle size to be measured with geometric size intervals where  $x_i = k x_{i-1}$ . Typical values for the geometric constant  $k$  are  $2^{1/q}$ , where  $q = 1, 2, 3, \text{ or } 4$ . In this case, the width of the histogram on the  $x$  axis is constant on a plot of  $f(\ln(x))$  vs.  $\ln(x)$ , making this a very useful way to plot data, especially for skewed distributions. Table 2.4 gives the relationships between a number of common size distribution representations.

**Example 2.3 Converting Size Distribution Data** Calculate the volume (mass) size distribution for the size distribution data in Example 2.2.

*Solution*

$$\text{From Table 2.4: } f_{vi} = \frac{f_i \bar{x}_i^3}{\sum f_i \bar{x}_i^3 \Delta x_i}$$

Results are tabulated below:

Size interval	$\bar{x}_i (\mu\text{m})$	$\Delta x_i (\mu\text{m})$	$f_i (\mu\text{m}^{-1})$	$f_i \bar{x}_i^3 (\mu\text{m}^2)$	$f_i \bar{x}_i^3 \Delta x_i (\mu\text{m})$	$f_{vi} (\mu\text{m}^{-1})$
6	48	32	0.0002	22.1	708	0.0047
5	24	16	0.0147	203.2	3251	0.0430
4	12	8	0.0522	90.2	721	0.0191
3	6	4	0.0509	11.0	44	0.0023
2	3	2	0.0464	1.2	2.5	0.0003
1	1	2	0.0214	0.02	0.04	0
					$\sum = 4726$	

### 2.4.3 Properties of the Frequency and Cumulative Distributions

Ideally, we prefer not to have to work with all the information contained in the full distribution if we can avoid it. Are there a limited set of parameters that capture most of the information in the distribution more efficiently than the amount of particles in each of 50 size intervals?

The first property that springs to mind is the mean of the distribution:

$$\bar{x} = \int_0^\infty x f(x) dx = \sum_{i=1}^\infty \bar{x}_i f_i \Delta x_i \tag{2.18}$$

In fact,  $\bar{x}$  as defined in Equation 2.18 is the first *moment* of the frequency size distribution. A more general definition of the *k*th moment is:

$$\mu_k = \int_0^\infty x^k f(x) dx = \sum_{i=1}^\infty \bar{x}_i^k f_i \Delta x_i ; \quad k \geq 1 \tag{2.19}$$

Equation 2.19 gives the definition of the *normalized* moments of the frequency distribution. Sometimes un-normalized moments are defined:

$$\mu'_k = \int_0^\infty x^k n(x) dx = \sum_{i=1}^\infty \bar{x}_i^k n_i \Delta x_i \tag{2.20}$$

Note that:

$$\mu_k = \left( \frac{\mu'_k}{\mu'_0} \right) \quad 2.21$$

A limited number of moments tell us a lot about the frequency distribution:

- $\mu'_0$  is the total number of particles ( $N_T$ ).
- $\mu_1$  is the mean of the distribution.
- $\mu_2$  is a measure of the spread of the distribution. It is related to the variance of the distribution ( $\sigma^2 = \mu_2 - \mu_1^2$ ).
- The volume fraction of particles in the control volume ( $V_T$ ) is  $\alpha_v \mu'_3$ .

Given we have many moments to choose from, the mean size definition can be tailored to our application. A more general definition than Equation 2.18 is:

$$\bar{x}_{m,n} = \left( \frac{\mu'_m}{\mu'_n} \right)^{\frac{1}{m-n}} = \left( \frac{\mu_m}{\mu_n} \right)^{\frac{1}{m-n}} \quad 2.22$$

Important examples of mean sizes based on this definition are:

- $\bar{x}_{1,0} = \mu_1$
- $\bar{x}_{3,2} = \mu_3 / \mu_2$  (the specific surface mean)
- $\bar{x}_{4,3} = \mu_4 / \mu_3$  (the mass-moment mean)

Use the mean size relevant to your application. As an example, to calculate the minimum fluidization velocity using the Ergun equation, we need the surface area per unit volume of the powder. Therefore, we should use  $\bar{x}_{3,2}$  as the mean size in this calculation. Other mean size definitions give the wrong answer.

Moments and mean sizes are properties of the *frequency* distribution. We can define parameters based on the cumulative distribution as well. We define  $x_a$  as follows:

$$F(x_a) = \frac{a}{100} \quad 2.23$$

i.e.,  $x_a$  is the  $a\%$  passing size at which  $a\%$  of the particles are smaller than this size. Thus, the median size  $x_{50}$  is the 50% passing size – i.e.,  $F(x_{50}) = 0.5$ . Similarly, we can define the range of the distribution as the difference between the 95% passing size and the 5% passing size ( $x_{95} - x_{05}$ ). Often, the “maximum” size of the distribution is taken as  $x_{95}$ .

Properties of the cumulative distribution are often faster to calculate than the moment-based properties of the frequency base distribution. However, the properties of the cumulative distribution do not have the same direct relationship to important properties of the particulate system (surface area, volume, and so on).

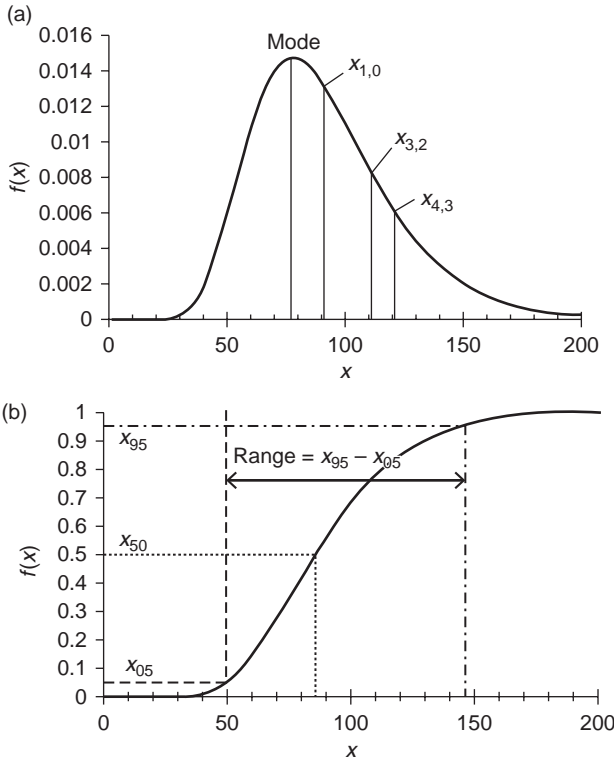


**Figure 2.6** Some properties of the frequency and cumulative distributions.

**Example 2.4** Take the size distribution data in Example 2.2 and calculate the following parameters:  $\bar{x}_{1,0}$ ,  $\bar{x}_{3,2}$ ,  $x_{50}$

*Solution*

From the definitions we have:

$$\bar{x}_{10} = \sum \bar{x}_i f_i \Delta x_i = 12.7 \mu\text{m}$$

$$\bar{x}_{32} = \frac{\sum \bar{x}_i^3 f_i \Delta x_i}{\sum \bar{x}_i^2 f_i \Delta x_i} = \frac{4726 \mu\text{m}^3}{218.6 \mu\text{m}^2} = 21.6 \mu\text{m}$$

The median size can be interpolated from the data table or cumulative plot from Example 2.2 to give  $x_{50} = 11 \mu\text{m}$ .

### 2.4.4 Some Special Distributions

The analysis of the frequency and cumulative size distributions given above makes no a priori assumptions about the shape of the distribution and so is applicable to any

arbitrary size distribution data. The downside is that we have to carry around a lot of information to describe the distribution – i.e., the frequency in each size interval.

For particular applications, researchers have found that unimodal frequency distributions often follow a similar shape and can be described by a mathematical formula with only two or three parameters. This has advantages in terms of the amount of information we need to keep to describe the distribution and simplifies our mathematical modeling efforts of unit processes. Borrowing from statistics, one might think that the first distribution to consider would be the Gaussian (normal) distribution:

$$f(x) = \frac{1}{\sigma\sqrt{2\pi}} \exp\left[-\frac{(x - \mu_1)^2}{2\sigma^2}\right] \quad 2.24$$

In fact, the normal distribution is rarely a good representation of particle size distributions unless they are very narrow. Most real particle size distributions are skewed towards the fine particle sizes. Therefore, a log-normal distribution is a better representation of many data sets:

$$f(z) = \frac{1}{\sigma_z\sqrt{2\pi}} \exp\left[-\frac{(z - \bar{z})^2}{2\sigma_z^2}\right] \quad 2.25$$

where

$$z = \ln(x) \quad 2.25a$$

$$\bar{z} = \ln(x_g) \quad 2.25b$$

$$\sigma_z = \ln(\sigma_g) \quad 2.25c$$

$x_g$  is the geometric mean size and  $\sigma_g$  is the geometric standard deviation of the distribution. The log-normal distribution has some special properties. In particular, if the number-based distribution  $f(x)$  is log-normal, then the surface area and volume-based distributions  $f_s(x)$  and  $f_v(x)$  are also log-normal with the same geometric standard deviation.

Another common two-parameter distribution is the Rosin–Rammler distribution, often used to describe the fragment size distribution during milling. It is usually represented in cumulative form:

$$F(x) = 1 - \exp(-bx^n) \quad 2.26$$

where  $b$  and  $n$  are the two fitting parameters in the distribution.

More than 15 different mathematical formulae have been proposed for representing different types of particle size distributions (Allen, 2003). We will refer to these special distributions occasionally in this book. However, caution should be used in trying to force real data to fit the formulae. This is often done by plotting the cumulative

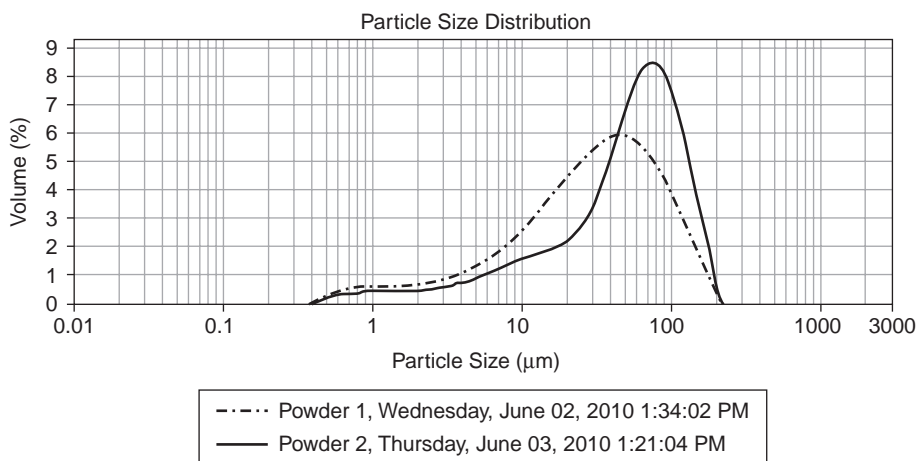


**Figure 2.7** Size distributions for two lactose powders measured by laser light scattering (Malvern Mastersizer E). Distributions were measured with the powder suspended in a saturated ethanol solution after 5 min in an ultrasonic bath to break up agglomerates.

distribution on graphs with transformed axes designed to give a straight line for a particular formula – e.g., a plot of the log-normal distribution on log-probability axes will yield a straight line. Similarly, for the Rosin–Rammler distribution, a plot of  $\ln(-\ln(1 - F(x)))$  against  $\ln(x)$  should yield a straight line. Transforming the axes in this fashion dramatically and artificially reduces scatter in the data, especially in the tails of the distribution, and is not a good way to test the validity of the model.

## 2.5 Measuring Properties of Populations of Particles

### 2.5.1 Particle Size

There are many different approaches to measuring particle size and size distributions. Some of the most important ones are listed in Table 2.5. For particles greater than 100 μm in size, sieving remains the most common approach to size measurement. For smaller particles, laser light diffraction techniques are the most common sizing technique if the majority of the volume of particles is greater than 1 μm. For particles in the range 0.05–1 μm, dynamic light scattering is commonly used. Microscopy (either optical or electron-based) combined with image analysis software can cover the full range of particle sizes and is a powerful tool when particle shape or morphology is also an important parameter. Figure 2.7 gives an example of particle size distribution data from two lactose powders using a light-scattering approach (in fact, the two lactose powders from the introductory case study for this chapter). Many of the size distribution statistics we discussed in Section 2.4.3 are calculated automatically by the software associated with the sizer analysis equipment.



Detailed descriptions of the methods for particle size analysis is beyond the scope of this text. *Powder Sampling and Particle Size Measurement* (Allen, 2003) gives an excellent description of particle size measurement techniques. However, there are several important lessons to learn in order to get high-quality, relevant data from your particle size analysis and avoid many tears.

1. Getting a representative sample is *vital*. Poor sampling is the major error source in any particle characterization problem.
2. Different techniques measure different definitions of size. Use the technique that measures the “size” of interest. For example, the opacity of a paint pigment is related to the projected area of the platelet particles. Microscopy with image analysis directly measures the projected area equivalent diameter of the particles and is therefore a good choice for this application.
3. Choose a number (counting)-based or a volume (mass)-based technique depending on the application. Beware of error propagation in converting from number or volume distributions and vice versa unless the distribution is quite narrow.
4. For fine powders, the level of dispersion of the powder – i.e., the extent to which particle aggregates are broken down – will have a dramatic effect on the measured particle size distribution. In particular, be very careful comparing data from wet-dispersed and dry-dispersed powders.
5. Don't compare apples with oranges. Comparison between size distributions measured in different ways is dangerous!

Note that points 1, 4, and 5 above apply to the measurement of any particle or bulk powder property. *Always view data from particle characterization with a critical eye.*

## 2.5.2 Particle and Powder Density Measurement

Particle and powder density are obtained by measuring the volume occupied by the powder, or the volume of fluid displaced by the particles. As for all particle characterization, the density we measure is very dependent on sample preparation. Comments on measurement of the three types of density we defined in Section 2.3.3 are:

### 1. *Bulk density*

- The volume occupied by a known mass of bulk solid measured by pouring into a container. The loose-filled bulk density is not a very reliable measurement.
- The maximum settled density (tapped density) is measured by vibrating or tapping the container until no further settling is observed.
- For fine solids, bulk density may increase significantly under pressure.

**Table 2.5** Commonly employed methods of particle size analysis (Litster and Ennis, 2004)

Method	Size range ( $\mu\text{m}$ )	Condition	Particle size measured	Type of distribution
<b>Microscopy</b>				
Optical	1–500	Dry or wet	A range of geometric diameters	Number
Electron (e.g., TEM, SEM)	0.01–100	Dry		
Image analysis		Dry or wet		
<b>Sieving</b>				
Wire-woven	37–4000	Dry or wet	Sieve diameter	Mass
Electro-formed	5–120	Dry or wet		
<b>Sedimentation</b>				
Micromerograph	5–75	Dry/gravity	Stoke's diameter	Mass
Pipette extraction	2–75	Wet/gravity or		
Photosedimentation	2–75 (0.05–5 centrifugal)	centrifugal		
X-ray sedimentation	0.1–75 (0.05–5 centrifugal)			Mass Mass
Sediment balance	2–75			
Elutriation/cyclone tech.	2–100	Dry or wet		
<b>Sensing zones</b>				
Electrical (e.g., Coulter)	0.5–1000	Wet	Volume diameter	Number
<b>Optical laser based</b>				
Diffraction/scattering (e.g., Sympatec Helos or Malvern)	0.1–100 1–3500	Wet or dry	Scattering diam. Scattering diam.	Volume Volume
Dynamic light scattering	0.003–3	Wet	Scattering diam.	Number
Scanning IR laser (e.g., Lasentec FBRM)	3–100	Wet	Chord length	Number
<b>Surface methods</b>				
Surface permeametry	0.1–75	Dry	Surface-volume mean diameter	Surface
Gas adsorption		Dry		
Thermal conductivity		Dry		
Adsorption from solution		Wet		
Heats of solution/wetting		Wet		
<b>Miscellaneous</b>				
Ultrasonic attenuation	1–500	Wet	Volume diameter	Volume

## 2. *Skeletal (true) density*

- Measured by the volume of a liquid or gas displaced by the solid using a pycnometer.
- Gas pycnometers are now common, using an ideal gas such as helium as the displacement fluid. The sample is first evacuated and the volume of gas taken up by the sample at several different pressures is measured.

## 3. *Particle (envelope) density*

- This is the most problematic measurement. A “smart” fluid is needed that can distinguish between external voids and internal pores (Figure 2.3).

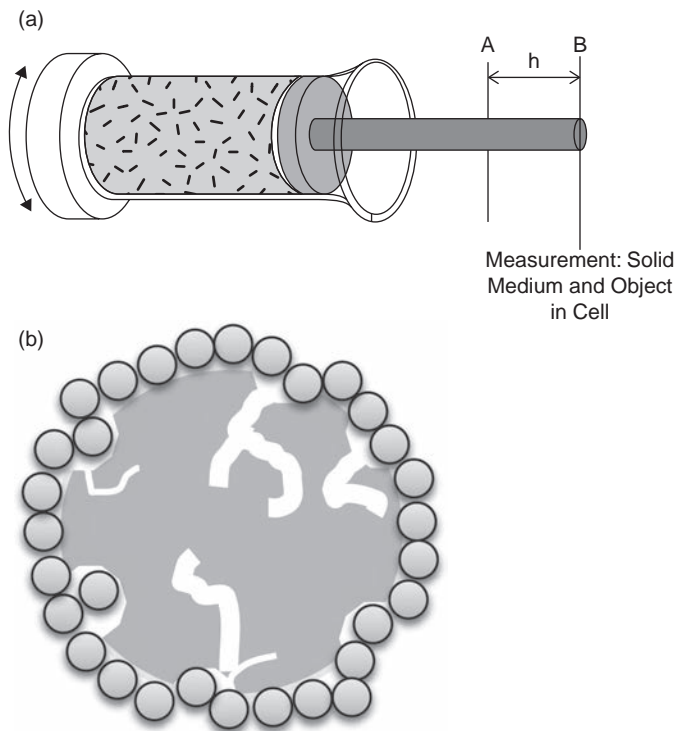


**Figure 2.8** The principle for measuring envelope density of a porous particle using a dry powder technique (Micromeritics GeoPyc) (Webb, 2001).

One method for measuring envelope density using liquid displacement consists of three steps: (1) soak the particles in boiling water; (2) drain the particles; and (3) measure water displaced by the drained but saturated particles. It is easy to see that such a method will be inaccurate for small particles because the surface liquid film on the particles will bias the results. An alternative approach is to use a free-flowing dry powder as the “fluid” to surround the particles but not enter the particle pores. This is the basis for the Micromeritics GeoPyc® envelope density pycnometer (Figure 2.8). Results from both wet and dry powder methods are strongly influenced by particle size for particles less than 1 mm. For particles less than 1 mm, the envelope density can be inferred from other measurements – e.g., combining measurements of particle porosity and skeletal density in Equation 2.11.

### 2.5.3 Porosity and Pore Size Distribution Measurement

Equation 2.11 can be used to calculate porosity where independent measurements of  $\rho_s$  and  $\rho_p$  are available. Alternatively, mercury porosimetry can be used to measure both porosity and pore size distribution. Mercury does not wet most solids – i.e., the contact angle between mercury and the solid is greater than  $90^\circ$ . Therefore,

pressure must be applied to force the mercury into the particle pores. The required pressure is given by the Laplace–Young equation:

$$\Delta P = \frac{4\gamma^{lv} \cos \theta}{d_{pore}} \quad 2.24$$

where  $\gamma^{lv}$  is the surface tension of mercury,  $\theta$  is the contact angle between mercury and the solid, and  $d_{pore}$  is the size of the pore in the particle. Note that the pressure is inversely proportional to the pore size, assuming cylindrical pores, and this is the basis for the method. First the powder sample is evacuated. Then the amount of mercury taken up by a given mass of the powder is measured as the pressure is slowly increased. The measured cumulative volume basis pore size distribution  $V(\Delta P)$  is converted to  $V(d_{pore})$  using Equation 2.24.  $d_{min}$  is the pore size corresponding to the maximum applied pressure and  $V(d_{min})$  is the total pore volume. From  $V(d_{min})$  we can calculate the porosity:

$$\varepsilon_p = V(d_{min})\rho_p; \text{ or } \varepsilon_p = \frac{V(d_{min})\rho_s}{1 + V(d_{min})\rho_s} \quad 2.25$$

Note that  $V(d_{min})$  has the units  $\text{m}^3 \text{kg}^{-1}$  and  $dV/d(d_{pore})$  is the frequency distribution of pore volume. An example of pores size distributions measured for five different formulated products is shown in Figure 2.9.

Like any particle characterization technique, data from mercury porosimetry should be treated with caution. Pore size down to several nanometers can be measured depending on the maximum applied pressure. So this technique is not applicable for measuring micropores. In reality, there is a network of interconnected, complex-shaped pores, not cylinders. This may lead to hysteresis in the pore size distribution results. For very fine powders, or agglomerates with very large pores, the mercury cannot distinguish between a void between particles and a pore inside a particle easily. Finally, the heterogeneous nature of real powder surfaces means there is a distribution of contact angles that cannot be deconvoluted from the pore size distribution.

A range of modern and highly sophisticated tomographic techniques can now be used to give great detail of the morphology and structure of complex and porous particles. For example, X-ray microtomography (XRCT) is a technique adapted from medical X-ray CAT scanning technology. A beam of X-rays is sent through the sample and the absorbance level is recorded. By rotating either the X-ray source or the sample and repeating many times, a three-dimensional absorbance shadow of the particle is produced. Such tomographic images can be analyzed to give information about non-uniform density and pore structures and possibly the position of particular phases or components in the particle (see Figure 2.10). Recent technology has a voxel size of less than  $1 \mu\text{m}^3$  and can therefore detect characteristics only a few microns in size.

XRCT techniques are very powerful but also very expensive and time-consuming, and therefore typically used only for research and development purposes, rather than routine measurements during production.

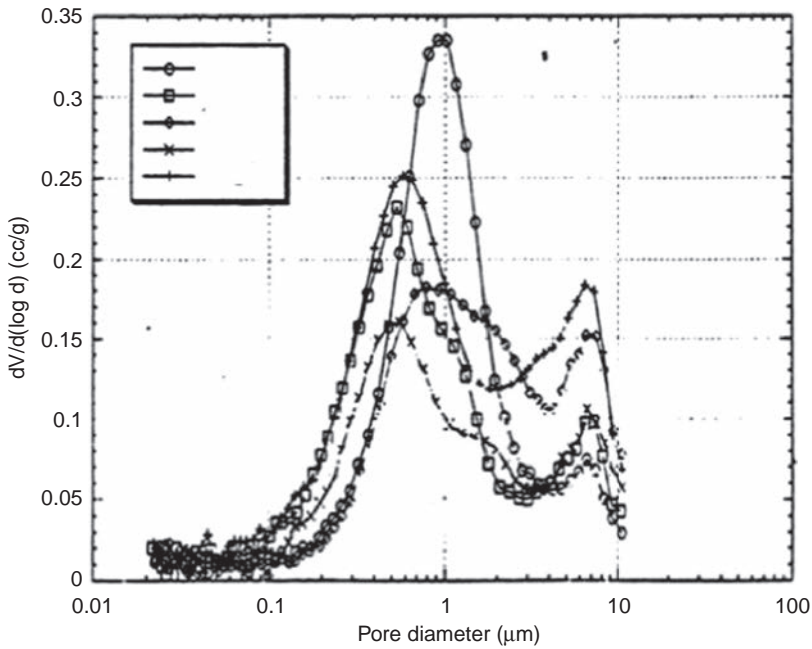


**Figure 2.9** An example of mercury porosimetry data shown as a frequency distribution on pore volume. The total pore volume is the area under the curve.

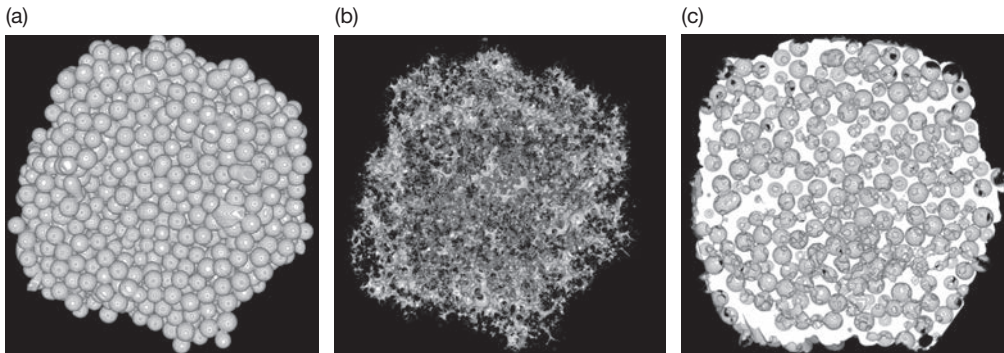


**Figure 2.10** XRCT images of a model granule showing (a) the position of the primary particles (glass ballotini), (b) the polymeric binder, and (c) the pore structure.

---

**Example 2.5 Consistency of Density and Porosity Data** Density measurements made on porous granules yield the following results:

bulk density = 1,900 kg/m<sup>3</sup>

envelope density = 3,100 kg/m<sup>3</sup>

skeletal density = 4,600 kg/m<sup>3</sup>

In addition, interparticle voidage and total pore volume were measured by permeability and mercury porosimetry, respectively:

$$\begin{aligned}\text{voidage} &= 0.385 \\ \text{pore volume } (-100 \mu\text{m}) &= 7.2 \times 10^{-5} \text{ m}^3/\text{kg}\end{aligned}$$

Are these measurements consistent? If not, what are the possible reasons for the discrepancy?

*Solution:*

First, look at the relationship between bulk density, envelope density, and voidage.

$$\varepsilon = 1 - \frac{\rho_b}{\rho_p} = 1 - \frac{1900}{3100} = 0.387$$

By comparison,  $\varepsilon_{meas} = 0.385$ . Therefore, the measurements of  $\varepsilon$ ,  $\rho_b$ , and  $\rho_p$  are consistent.

Now, look at the relationship between envelope density, skeletal density, and porosity.

$$\varepsilon_p = 1 - \frac{\rho_p}{\rho_s} = 1 - \frac{3100}{4600} = 0.326$$

The porosity data are given as  $\text{m}^3$  (of pores)/ $\text{kg}$  (of solid). Therefore, we can calculate the porosity as:

$$\begin{aligned}\varepsilon_p &= \frac{V_{pore}}{V_{pore} + V_s} = \frac{V_{pore}}{M_s / \rho_p} = \rho_p \left( \frac{V_{pore}}{M_s} \right) \\ &= 3,100 \text{ kg m}^3 \times 7.2 \times 10^{-5} \text{ m}^3 \text{ kg}^{-1} = 0.223\end{aligned}$$

The two measures of porosity are not consistent. There are many possible reasons for the discrepancy.

- The envelope density measurement may be underestimated, especially if the particles are smaller than 1 mm in size or very rough.
- The mercury porosimetry measurement may not be capturing very big pores  $> 100 \mu\text{m}$  or very small pores  $< 20 \text{ nm}$ .
- The particle may contain enclosed pores that the mercury cannot penetrate, or the particle may be compressed during porosimetry, closing off pore space.

How would you go about further troubleshooting to pin down the real problem here?

## 2.6 Another Case Study

Pectin in a food polymer used in cooking and food processing because of its gelling properties. It is a common ingredient in jams and jellies. Pectin exists naturally in



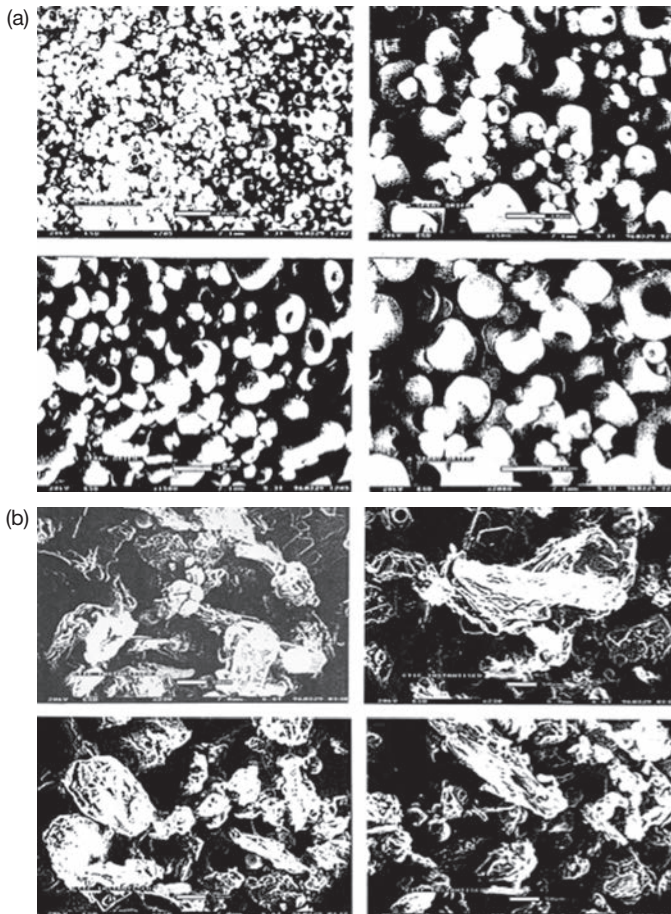


**Figure 2.11** SEM micrographs of (a) spray-dried pectin and (b) precipitated pectin.

many fruits. Commercially, pectin is extracted from citrus fruit peel. Traditionally, pectin powder is produced by precipitation by adding alcohol, and then milling. An alternative process is to spray dry the extract to produce a pectin powder. Scanning electron micrography (SEM) micrographs of the two types of pectin, and particle size distributions from a laser light diffraction size analyzer, are shown in Figures 2.11 and 2.12. As a small group, discuss your observations about the pectin size distribution from the two different preparation methods. Why are the properties of the two powders so different? Which one will flow more easily? Which one will dissolve more easily? Why?

Without answering all of the above questions, we can make some immediate observations. First, it is remarkable how much the particle size distribution and morphology of the particles vary with the method of manufacture. The milled granules are coarse, with a mean size around  $120\ \mu\text{m}$ . They have a broad, unimodal size distribution and rough, irregular-shaped particles. This morphology and size

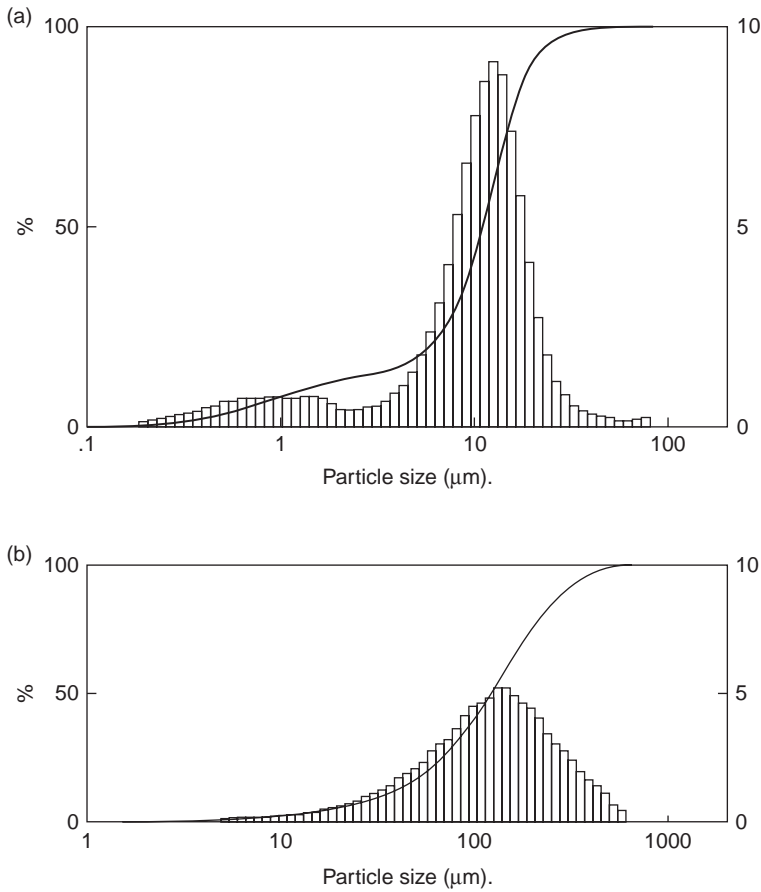


**Figure 2.12** Particle size distributions of (a) spray-dried pectin and (b) precipitated pectin measured using laser light diffraction.

distribution is quite typical of milled materials. On the other hand, the spray-dried particles are “doughnut”-shaped. In fact, they are collapsed hollow spheres. The particles are much smaller than the milled granules. The size distribution is bimodal, with one mode around 10  $\mu\text{m}$  and one around 1  $\mu\text{m}$ . These characteristics are common for spray-dried materials.

This case study is a nice introduction to this book. We wish to predict and control the particle property distributions we produce by controlling the formulation and the process conditions. We will see how particle property distributions are controlled in crystallization, milling, and spray drying in Chapters 4, 5, and 7, respectively. The relationship between particle properties and disintegration and dissolution is covered in Chapter 10.



## 2.7 Summary

Good particle characterization is essential for any particle design and processing problem, and the key to many. The particulate nature of the systems we study means that the behavior of systems cannot be fully characterized by the thermodynamic state of the system alone. We must also know its *particulate state* (size, morphology, density, structure).

Particle properties must be carefully defined. There is no single unique definition for particle size or shape (see Table 2.2). Equivalent diameters are a common way to define particle size. The particle size definition used should be fit for purpose – i.e., it should lead to knowledge of the property or attribute of the system that is of interest. You should know the most common particle size and shape factor definitions.

Particulate systems are heterogeneous. Particle properties have *distributions* and for many problems knowledge of the property distribution, rather than just a single value, is required. Particle size and other properties can be represented as frequency or cumulative distributions. For particle size, the basic representation is the distribution of size by number,  $f(x)$ . However, we can change the measure of *quantity* we use (e.g., number to volume) or the measure of the *property* we use (e.g.,  $x$  to  $\ln(x)$ ). You should know the definitions of the frequency and cumulative distributions, be able to correctly calculate and plot these distributions from a set of raw data, and make conversions between distributions with different measures of quantity and property.

There a wide range of techniques available to measure particle size, density, and porosity. In all cases, correct sampling and careful sample preparation and presentation are essential. Different measurement techniques measure different properties of the distribution of particles. Beware of comparing apples and oranges. Always view particle characterization data sets with a critical eye.

For more detail on particle size and other property measurement techniques and correct sampling procedures see Allen *Particle Sampling and Particle Size Determination*, Elsevier (2003).

## 2.8 Bibliography

- Allen, T., 2003. *Powder Sampling and Particle Size Measurement*, 1st Edition, Elsevier, Amsterdam.
- Gy, P., 1979. *Sampling of Particulate Materials – Theory and Practice*, Elsevier Press, Amsterdam.
- Litster, J.D., and Ennis, B.J. (2004). *The Science and Engineering of Granulation Processes*, chapters 2 and 6, Kluwer Press, Dordrecht.

- Perry, R.H., Green, D.W., and Maloney, J.O., 2008. *Perry's Chemical Engineers Handbook*, 8th edition, McGraw-Hill, New York. (Chapters 8.5 to 8.9 on particle size analysis, and 21.10 to 21.13 on sampling techniques.)
- Webb, P.A., 2001. Volume and density determinations for particle technologists. Micromeritics Instrument Corp 2.16 (2001): 01.

## 2.9 Problems

- 2.1. Evaluate the sphericity of crystals which are in the shape of hexagonal prisms with prism height equal to four times the distance ( $x$ ) across opposite flats of the hexagonal base.  
Also evaluate, in terms of  $x$
- the volume-equivalent size
  - the projected area-equivalent size (in expected orientation)
  - the surface area-equivalent size
  - $\alpha_V, \alpha_S$ .

- 2.2. Calculate the volume-equivalent size ( $d_V$ ) of a rectangular parallelepiped of length 3 mm, width 2 mm and depth 1 mm.
- 2.3. Show that the specific surface diameter,  $d_{SV}$ , may be written in terms of the equivalent volume diameter,  $d_V$ , and equivalent surface area diameter,  $d_S$ , as

$$d_{SV} = \frac{d_V^3}{d_S^2}$$

- 2.4. Show that the equivalent volume diameter,  $d_V$ , of a particle can be related to the particle's equivalent surface area diameter,  $d_S$ , by

$$d_V = \sqrt{\psi} d_S,$$

where  $\psi$  is the particle's sphericity, defined as the ratio of the surface area of a sphere with the same volume as the particle to the surface area of the particle.

- 2.5. For an irregular-shaped particle, the specific surface area can be given by the expression:

$$\frac{S}{V} = \frac{6}{\psi d_V}$$

Derive this expression starting from the definition of the sphericity  $\psi$  and the volume-equivalent size  $d_V$ .

- 2.6. Show that for a geometric sieve series, the logarithmic frequency size distribution (mass basis) is proportional to the mass fraction of particles in the size range. What is the proportionality constant if it is a  $2^{1/4}$  series of sieves?

- 2.7. Derive an expression to give the specific surface mean size  $\bar{x}_{32}$  for a continuous distribution from the volume frequency distribution  $f_v(x)$ .
- 2.8. Derive an expression for the weighted average volume diameter  $\bar{x}_{43}$  given:
- a size distribution by volume  $f_v(x)$ , or
  - a size distribution by surface area  $f_s(x)$ .

You may assume that particle shape and density do not change appreciably over the range of sizes.

- 2.9. Write down an expression to calculate the specific surface area mean size ( $\bar{x}_{32}$ ) of a powder sample if you are given a discrete size distribution where the number fraction in each size interval is  $y_i$ , the top size of the  $i$ th interval is  $x_i$ , and the mean size within each interval is  $\bar{x}_i$ . Write a similar expression for  $\bar{x}_{32}$  if the data are given in terms of mass fraction in each size interval  $y_{m,i}$ .
- 2.10. Consider three spherical particles with diameters of 1 mm, 2 mm, and 3 mm. Determine:
- the arithmetic average length diameter ( $\bar{x}_{1,0}$ ),
  - the arithmetic average surface area diameter ( $\bar{x}_{2,0}$ ),
  - the arithmetic average volume diameter ( $\bar{x}_{3,0}$ ),
  - the Sauter mean diameter (the weighted average surface area diameter,  $\bar{x}_{32}$ ), and
  - the de Brouckere mean diameter (the weighted average volume diameter,  $\bar{x}_{43}$ ).

- 2.11. Consider the following raw data from a sieve size distribution:

Size range (mm)	Mass retained in that range (g)
>1.0	5
0.855–1.0	15
0.71–0.855	25
0.5–0.71	30
0.25–0.5	20
<0.25	5

- Calculate the mass frequency of particle size for each size fraction ( $f_{mi}$ )
  - Calculate the mass frequency of log of particle size ( $f_{mi}^{\ln x}$ )
  - Calculate the number frequency of particle size ( $f_i$ )
  - Plot each of these frequency distributions as a histogram
- 2.12. The results given below were obtained from a sieve analysis. Present the results as:
- a cumulative mass distribution
  - a cumulative number distribution

Also calculate the  $\bar{x}_{32}$  and  $\bar{x}_{43}$  mean sizes, the median, and mode of the distribution.

Sieve size ( $\mu\text{m}$ )	Weight retained on sieve (g)
500	2.46
420	5.11
355	11.52
300	11.88
250	11.43
210	5.51
pan	1.94

State clearly any assumption made in development these answers.

- 2.13. A sieve size analysis of a 24 oz box of Great Value™ Crunchy Nuggets™ cereal gives the following data.

Sieve No.	Mass retained (g)
¼ in.	0.0
3.5	2.0
4	17.1
5	207.5
6	91.0
7	109.9
8	80.9
10	51.9
14	88.4
16	22.6
pan	17.4

- What type of size is being measured?
- Plot the frequency, cumulative fraction finer, and cumulative fraction coarser distributions.
- What type of distributions are being measured, e.g., by number, by area, etc.?
- Determine the arithmetic mean particle size of the distribution.
- Determine the  $x_{10}$ ,  $x_{50}$ ,  $x_{90}$ , and span.
- How much mass is contained between the sizes of 0.1 and 0.2 in.?

- 2.14. My lab group for senior lab was allocated the lactose crystallization experiment. To get the size distribution of lactose crystals we took a 1 ml sample of suspension from the crystallizer at set time intervals. We used a microscope combined with image analysis software to get a number distribution of the crystals in the sample. I am really struggling with analyzing the data and I need your help. An example of one of our data sets is given below.

Size interval ( $\mu\text{m}$ )	Crystals in that interval (no./ml of suspension)
0–10	0
10–20	$5 \times 10^5$
20–25	$20 \times 10^5$
25–30	$15 \times 10^5$
30–40	$15 \times 10^5$
40–60	$5 \times 10^5$

- (a) Please calculate the normalized number frequency distribution of these crystals ( $f(x)$ ) and plot the distribution as a histogram.
- (b) Please calculate the specific surface area mean size of these crystals ( $\bar{x}_{32}$ ).
- (c) My lab partner has lost all our mass balance data. Our crystallizer had a volume of one liter and we looked up the density of lactose crystals ( $1540 \text{ kg m}^{-3}$ ). Is there any way we can back-calculate the mass of crystals in our crystallizer from our size distribution data? Please show me how using the data from the table above. (To make it easier for you, I am willing to assume the crystals are spheres for this calculation.)
- 2.15. I am characterizing some porous spherical activated carbon beads to use in the packed bed filter in my fish tank. I have measured the size distribution using sieves (see table below).

Size interval (mm)	Mass in that interval (g)
0.125–0.25	5
0.25–0.5	10
0.5–1.0	20
1.0–2.0	5

I have also measured the bulk density of the (dry) packed bed of beads in my filter, the internal porosity of the beads using mercury porosimetry, and the skeletal density of beads using helium pycnometry:

$$\begin{aligned} \rho_b &= 975 \text{ kg m}^{-3} \\ \rho_s &= 1,900 \text{ kg m}^{-3} \\ \text{pore volume} &= 1.4 \times 10^{-4} \text{ m}^3 \text{ kg}^{-1} \end{aligned}$$

- (a) Plot the carbon bead size distribution of as a frequency histogram  $f_m(x)$  vs.  $x$ .
- (b) To calculate the pressure drop across my packed bed filter, I need to estimate the average capillary size in my packed bed using the Carman–Kozeny expression:

$$R_{cap} = \frac{\bar{x}_{32}\epsilon}{3(1-\epsilon)}$$

- Given the data above, calculate  $\epsilon$ ,  $\bar{x}_{32}$ , and  $R_{cap}$  for my activated carbon filter.
- 2.16. The raw data for the size distribution of particles measured using an electronic zone sensing size analyzer is given below. From these data, calculate (1) the normalized number frequency  $f(x)$  and (2) normalized volume frequency  $f_v(x)$  for each size interval. Show the frequency histogram for  $f(x)$  vs.  $x$ .

Size range ( $\mu\text{m}$ )	Number in size range
125–180	10
180–250	20
250–355	15
355–500	5

- This sizing technique measures volume-equivalent size. The particle sphericity  $\psi$  is 0.8. Calculate the specific surface area of these particles.
- 2.17. The Carman–Kozeny equation is a commonly used expression relating the pressure drop,  $\Delta p$ , across a bed of particles with bed length,  $L$ ,

$$\frac{-\Delta p}{L} = K \frac{(1-\epsilon)^2}{\epsilon^3} S_v^2 \mu_f U,$$

where  $K$  is a dimensionless constant,  $\epsilon$  is the bed porosity (the ratio of void volume to the total volume in the bed),  $S_v$  is the specific surface area of the bed (the ratio of the total particle surface area to the particle volume),  $\mu_f$  is the fluid’s dynamic viscosity, and  $U$  is the superficial speed of the fluid

through the bed (equal to the volumetric flow rate through the bed divided by the bed's cross-sectional area).

If the particles in the bed consist of a distribution of sizes, given in terms of a number distribution, but all particles have identical shape, what mean particle size should be reported in place of the specific surface area? If the particles are spheres, relate this mean size to the specific surface area.

- 2.18. The following size data are measured using sieving.

Nominal sieve size ( $\mu\text{m}$ )	Mass retained (g)
500	0.0
425	0.2
355	5.7
300	50.0
250	175.3
212	206.3
180	224.8
150	100.4
pan	53.4

Determine the constants  $n$  and  $b$  in the Rosin–Rammler size distribution for the given data.

# 3 The Population Balance

## 3.1 Consider a Case Study ...

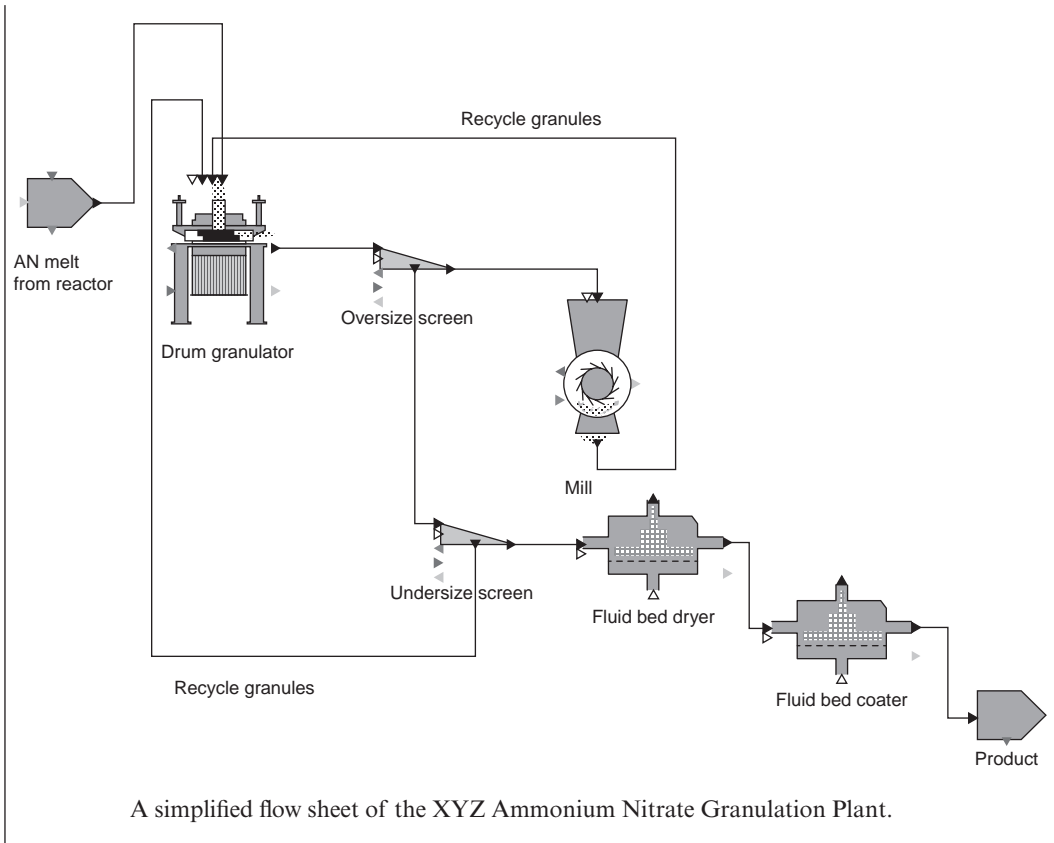
XYZ Ltd. manufacture fertilizer-grade ammonium nitrate in a drum granulator. A simplified flow sheet of the process is given below. Ammonium nitrate melt is sprayed onto recycled seed granules in a rotating drum granulator. Granules then pass an “oversize” and an “undersize” screen. Product granules are cooled and given a thin wax coating. Undersize granules are returned as seed to the drum. Oversize granules are crushed and also return to the drum as seed.

You are the newly appointed “Process Engineer – Granulation” and you discover in your first few days that the granulation plant has some serious problems. The plant was commissioned two years ago using a drum previously used for ammonium sulfate granulation. Since then, the plant has never reached more than 75% of design capacity and currently contracts are not being filled on time. The ideal granule size distribution is 1.7–3 mm for use in farm machinery, and to avoid segregation when blended with other granular fertilizers. Contracts specify 95% of granules should be in this range. This is apparently very difficult to achieve. Chatting with operators and engineers, you get a range of contradictory advice. Distilling this down, you note:

- The granulation drum seems to produce a lot of raspberry-shaped agglomerates, rather than smooth spheres.
- The impact crusher (a hammer mill) seems to produce a lot of dust as well as some uncrushed lumps.
- The granule recycle ratio is very large at about 4:1 – i.e., for every 1 tonne of product granules, 4 tonnes of oversize and undersize granules are recycled.
- The plant never appears to be in stable steady-state operation, with cyclic behavior in the recycle and product flow rates.
- There does not seem to have been a proper sampling audit of the plant performed.

Reviewing the literature, you find there is a different type of granulator (a fluidized drum granulator) (Litster and Sarwono, 1996) that claims to grow the granules by a different mechanism with much reduced recycle ratios. You propose replacing the granulation drum to your manager. She replies that such a major capital expense would require a rigorous technical and economic feasibility study, and reminds you she is looking for a quick fix. “How do you know a new granulator will really work? Can’t we optimize the granulator we’ve got? What about fixing the crusher – will that help us out?”





As an individual reflective exercise, or as a group brainstorming discussion, make a list of possible causes of the problems in this plant (and don't just limit yourself to hearsay from the operators and engineers). How can you identify which of these possible causes has the most impact? How can you evaluate the effectiveness of the proposed solutions, so you can present a proper engineering and economic case to the manager? Do you have the necessary technical tools at your disposal for this evaluation?

Process engineers have a wealth of technical knowledge and tools to bring to a process troubleshooting and optimization problems, including mass and energy balances. However, that toolbox is not sufficient to address the problem described above. We need a mathematical tool to track the distribution of the important particle property (size in this case), including through processes where the property is changed (such as the granulator and the crusher in this plant). That tool is called the population balance and this chapter introduces this new and powerful tool to you. (Oh, by the way, don't worry if you know nothing about granulation. We cover that in detail in Chapter 8.)

## 3.2 Learning Goals

At the completion of this chapter, the student should be able to:

1. Explain what the population balance is to a peer using the analogy of a chemical reactor, and describe the usefulness of the population balance to analyze particulate processes.
2. Write down the one-dimensional population balance and its moments for a well-mixed system.
3. Explain the terms in the population balance and relate them to specific rate processes – e.g., crystal growth, particle breakage.
4. Do a total numbers balance on any particulate process using the moments of the population balance.
5. Use the population balance to solve closed problems similar to those presented in the chapter, including making appropriate assumptions and analytical or numerical solutions.
6. Use the population balance to critically analyze and interpret real data sets from laboratory data or plant trials.
7. Use the population balance as a tool to attack open-ended problems, and to solve classes of problems not previously encountered.

## 3.3 Modeling a Well-mixed Particle Generator

There is a strong analogy between any operation that changes the properties of a particulate material and a chemical reactor. A chemical reactor transforms chemical species in the feed to give the desired product. To design a reactor, we must predict the chemical composition of the product given the feed composition, equipment parameters, and operating conditions. The process engineering tools used in the design are mass and energy balances, reaction kinetics, thermodynamics, and mixing analysis (residence time distributions).

Many processes we are interested in transform a particulate or liquid feed to a particulate product. For engineering design and operation we must predict the product particle property of interest (e.g., size or porosity) as a function of feed properties, equipment parameters, and operating variables. As for the chemical reactor, to do this we must apply process engineering analysis. The performance of any such process – e.g., crystallizer, granulator, or grinding mill – is described by a series of important equations:

- the mass balance;
- the energy balance;
- the population balance(s) for property(ies) of interest;
- rate expressions to describe the kinetics for the change in the property; and
- an expression for mixing (residence time distribution).

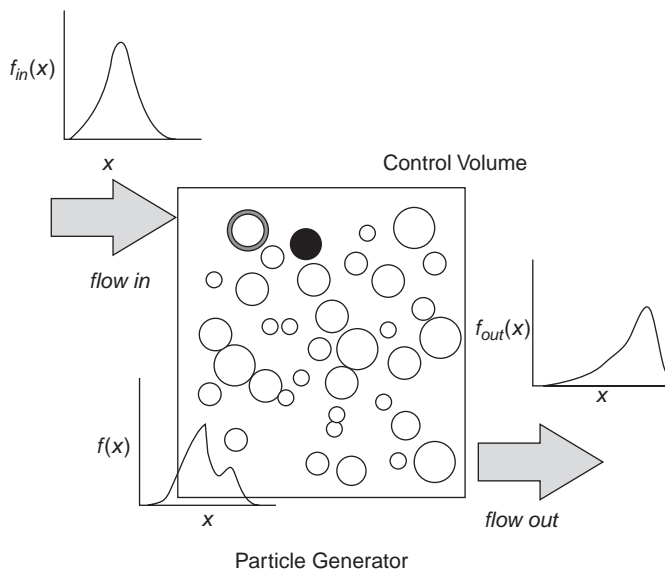


**Figure 3.1** The conceptual framework for modeling a well-mixed particle generator.

You are probably already familiar with mass and energy balances. For a system containing a discrete (particulate) phase we also need the population balance for the particle properties of interest. The population balance is a rate equation which follows the change in number of particles of a given property. It includes a kinetic expression for each mechanism which changes the particle property analogous to chemical reaction kinetics in reactor design.

The population balance was introduced as a general equation for particulate systems independently by Hulbert and Katz (1964) and Randolph and Larsen (1968). It is a powerful tool with uses including:

- critical evaluation of data to determine controlling mechanisms;
- in design, to predict the mean size and size distribution of product particles;
- sensitivity analysis to analyze quantitatively the effect of changes in operating conditions or feed variables on product quality; and
- optimization and process control.

There are many particulate properties of interest. However, particle size and properties directly related to size are nearly always important, so we will begin with size as our example property. This chapter develops the population balance as a general tool and looks at examples of its use where different mechanisms dominate the change in particle properties. The application of the population balance to particulate unit processes is demonstrated in the following chapters.

### 3.4 Derivation of the Macroscopic Population Balance

We start by deriving the macroscopic population balance for following the distribution of a single property, size. Consider a well-mixed particle generator as shown in Figure 3.1. It could be a granulator, grinding mill, crystallizer, chemical reactor, or any number of processes that give a particulate product. We want to keep track of how the number of particles between sizes  $x$  and  $x + dx$  in the process changes with time. The number of particles of this size  $n(x)dx$  within the process control volume  $V$  can change for a number of reasons. Let us divide these into three categories:

(a) Flows into and out of the control volume:

The flow of particles of size  $x$  into and out of the process at a rate of  $\dot{Q}_{in}n_{in}(x)dx$  and  $\dot{Q}_{ex}n_{ex}(x)dx$ , respectively, where  $\dot{Q}_{in}$  and  $\dot{Q}_{ex}$  are the volumetric flows entering and leaving the control volume ( $m^3 s^{-1}$ ) and  $n_{in}(x)$  and  $n_{ex}(x)$  are the inlet and exit size distributions ( $m^{-4}$ ).

(b) Sudden processes that generate or destroy particles of size  $x$ :

The sudden “birth” of new particles of size  $x$  in the control volume is defined as occurring at a rate of  $V\dot{b}(x)dx$ . Here,  $\dot{b}(x)$  is the frequency distribution of the new-born particles.  $\dot{b}(x)$  has similar properties to the particle size distribution  $n(x)$ . However, as  $\dot{b}(x)$  represents a birth rate, it has the units  $m^{-4} s^{-1}$ . Nucleation of a new crystal from solution is an example of a birth process. Similarly, the sudden “death” of particles of size  $x$  in the control volume occurs at a rate of  $V\dot{d}(x)dx$  where  $\dot{d}(x)$  is the death rate frequency distribution ( $m^{-4} s^{-1}$ ). Disappearance of a particle of size  $x$  due to a sudden breakage event is an example of a death process.

(c) Growth processes:

Here, a particle slightly smaller than size  $x$  grows to that size, or a particle of size  $x$  grows to give a particle that is slightly larger in size. The growth term needs some explanation. It is a gradual (differential) process, not a sudden process like the birth and death terms. We define the growth rate of an individual particle as:

$$\left(\frac{\partial x}{\partial t}\right)_x = G(x, t) \quad 3.1$$

We can think of growth as a convective process analogous to flow of a fluid down a pipe. Just as fluid will flow down the pipe at some velocity  $v$ , growing particles move along the size axis with a “velocity”  $G$ . The flux of particles into a size range between  $x$  and  $x + dx$  from smaller sizes is  $VnG|_x$  and the flux leaving the size range to larger sizes is  $VnG|_{x+dx}$  (see Figure 3.2).

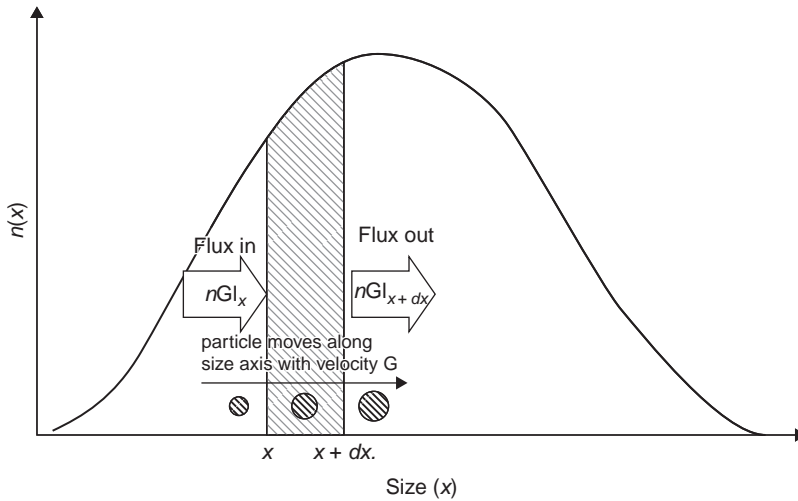


**Figure 3.2** Change in the particle size distribution due to differential growth. The growth rate  $G$  is the velocity along the size axis.

The rate of accumulation of particles in the size range between  $x$  and  $x + dx$  by all these processes (flow, sudden birth and death, differential growth) is then:

$$\frac{\partial Vn(x,t)dx}{\partial t} = \dot{Q}_{in}n_{in}(x)dx - \dot{Q}_{ex}n_{ex}(x)dx + VnG|_x - VnG|_{x+dx} + V\dot{b}(x)dx - V\dot{d}(x)dx \quad 3.2$$

Dividing by  $dx$  and taking the limit as  $dx \rightarrow 0$  gives:

$$\frac{\partial Vn(x,t)}{\partial t} = \dot{Q}_{in}n_{in}(x) - \dot{Q}_{ex}n_{ex}(x) - \frac{\partial VGn(x,t)}{\partial x} + V\dot{b}(x) - V\dot{d}(x) \quad 3.3$$

This is the *one-dimensional macroscopic population balance* for a well-mixed control volume with the particular example of particle size as the property of interest. Note that it is written in terms of volumetric flows and un-normalized size distributions – e.g., the inlet volumetric flow rate is  $\dot{Q}_{in}$  ( $\text{m}^3 \text{s}^{-1}$ ) and the inlet size distribution is  $n_{in}$  ( $\text{m}^{-4}$ ).

*The population balance (Equation 3.3) is an essential part of the tool kit for analyzing all particulate systems. It is as important as the mass balance and the energy balance. In combination with appropriate kinetic expressions, these balances define the system for process engineering analysis.*

### 3.4.1 Variations on a Theme

The energy balance for the system (1st Law of Thermodynamics) can be written in several forms depending on the likely application. It is the same with the population balance. Other equations equivalent to Equation 3.3 are possible:

1. We can rewrite Equation 3.3 in terms of number flows and normalized size distributions – e.g., the inlet number flow rate is  $\dot{v}_{in}$  ( $s^{-1}$ ) and the normalized inlet size distribution is  $f_{in}(x)$ . Thus  $\dot{Q}_{in}n_{in}(x) = \dot{v}_{in}f_{in}(x)$  and the full population balance is:

$$\frac{\partial VN_T f(x,t)}{\partial t} = \dot{v}_{in}f_{in}(x) - \dot{v}_{ex}f_{ex}(x) - \frac{\partial VGN_T f(x,t)}{\partial x} + V\dot{B}f_B(x) - V\dot{D}f_D(x) \quad 3.4$$

Here,  $\dot{B}$  and  $\dot{D}$  are the total birth and death rates per unit volume, and  $f_B(x)$  and  $f_D(x)$  are the normalized birth and death frequency distributions, respectively.

2. Equation 3.3 is written in terms of the linear size as the particle property. The balance is easily rewritten in terms of any property of the particle – e.g., the distribution of particle volume  $n(v)$ .
3. Equation 3.3 is suitable for analyzing well-mixed vessels as it implicitly assumes particle properties are uniform within the control volume. It is also possible to derive a much more general *multidimensional microscopic population balance*. The microscopic balance is needed to examine processes where the particle property distribution varies with position in the vessel – i.e., distributed parameter systems. The adjective “multidimensional” applies because the equation can, in principle, be used to follow any combination of particle properties that have distributions (size, concentration, porosity, strength, etc.). This is the more general form of the population balance and is written:

$$\frac{\partial n}{\partial t} + \nabla \cdot \bar{v}_e n + \nabla \cdot \bar{v}_i n + \dot{d} - \dot{b} = 0 \quad 3.5$$

The particle distribution  $n$  is a function of the particle position with respect to its *external* coordinates ( $l, y, z$ ) and its *internal* coordinates or properties which define the state of the particle (size, concentration, porosity, strength, etc.).  $\bar{v}_e$  is a vector of the components of the particle external velocity in the  $l, y$ , and  $z$  directions.  $\bar{v}_i$  is the vector of velocity components with respect to the internal coordinates – e.g.,  $G$  is the velocity component with respect to particle size as discussed above. The internal and external coordinates define the *phase-space* for the particle distribution  $n$ . For the full derivation of this equation, see Ramkrishna (2000) or Randolph and Larsen (1988).

Equation 3.5 is the most general form of the population balance. Many very useful simplifications can be derived from this general equation, including the macroscopic population balance (Equation 3.3). Another important simplification is the microscopic population balance in one internal coordinate for a plug flow system:

$$\frac{\partial n}{\partial t} + \frac{\partial v_l n}{\partial l} + \frac{\partial Gn}{\partial x} + \dot{d} - \dot{b} = 0 \quad 3.6$$

where  $v_l$  is the velocity through the vessel,  $l$  is the distance from the start of the vessel, and  $n = n(x, l, t)$ .

### 3.4.2 Moments Form of the Population Balance

The population balance (Equation 3.3) is a complex partial differential equation which is sometimes difficult to solve. In Section 2.4.3 we defined the *moments* of the particle frequency size distribution as important properties of the distribution (Equations 2.19 and 2.20). It is often useful to solve the population balance equation for the moments of the distribution:

$$\int_0^\infty x^k (eqn.3-3) dx \Rightarrow \frac{dV\mu'_k}{dt} = \dot{Q}_{in}\mu'_{k,in} - \dot{Q}_{ex}\mu'_{k,ex} - \int_0^\infty x^k \frac{\partial VGn(x)}{\partial x} dx + V\mu'_{k,B} - V\mu'_{k,D} \tag{3.7}$$

The growth term can be simplified further if  $G$  is not a function of size. This is called *size-independent growth*. In this case, the growth term simplifies to:

$$\int_0^\infty x^k \frac{\partial VGn(x)}{\partial x} dx = -VGk\mu'_{k-1} \tag{3.8}$$

Substituting from Equation 3.8 into Equation 3.7 gives:

$$\boxed{\frac{dV\mu'_k}{dt} = \dot{Q}_{in}\mu'_{k,in} - \dot{Q}_{ex}\mu'_{k,ex} + VGk\mu'_{k-1} + V\mu'_{k,B} - V\mu'_{k,D} \quad \text{for } k \geq 1} \tag{3.9}$$

Note that Equation 3.9 is an ordinary differential equation and therefore much easier to solve than Equation 3.3. For many practical examples, analytical expressions are available for the solution to Equation 3.9 when solution of the full particle size distribution from Equation 3.3 is only available numerically.

Let us look at some specific examples. For  $k = 0$ , Equation 3.9 reduces to:

$$\frac{dV\mu'_0}{dt} = \dot{Q}_{in}\mu'_{0,in} - \dot{Q}_{ex}\mu'_{0,ex} + V\mu'_{0,B} - V\mu'_{0,D} \tag{3.10}$$

Here,  $\mu'_0 = N_T$ ,  $\mu'_{0,in} = N_{T,in}$ ,  $\mu'_{0,ex} = N_{T,ex}$ ,  $\mu'_{0,B} = \dot{B}$ , and  $\mu'_{0,D} = \dot{D}$ . Thus, Equation 3.10 is rewritten as:

$$\boxed{\frac{dVN_T}{dt} = \dot{Q}_{in}N_{T,in} - \dot{Q}_{ex}N_{T,ex} + V\dot{B} - V\dot{D}} \tag{3.11}$$

This is the total numbers balance for the particle generator. As you would expect, the total number of particles in the control volume is affected by the numbers flowing in and out, dying, and being born. Note that the differential growth term has disappeared. This makes sense because differential growth does not change the number of particles in the system, only their properties.

$k = 3$ , the third moment, is important because the mass concentration of particles in the control volume  $m$  is:

$$m = \rho_p \alpha_v \mu'_3 \quad 3.12$$

Substituting  $k = 3$  into Equation 3.9 gives:

$$\frac{dV\mu'_3}{dt} = \dot{Q}_{in}\mu'_{3,in} - \dot{Q}_{ex}\mu'_{3,ex} + 3VG\mu'_2 + V\mu'_{3,B} - V\mu'_{3,D} \quad 3.13$$

Multiply Equation 3.13 by  $\rho_p \alpha_v$  and combine with Equation 3.12 to give:

$$\boxed{\frac{dVm}{dt} = \dot{Q}_{in}m_{in} - \dot{Q}_{ex}m_{ex} + 3VG\rho_p\alpha_v\mu'_2 + V\dot{m}_B - V\dot{m}_D} \quad 3.14$$

Equation 3.14 provides the link between the population balance and the mass balance for the particulate system.

Equations 3.3, 3.9, 3.11, and 3.14 represent the population balance for any well-mixed particle generator and its key moments and are powerful tools for analyzing many particulate processes. Of course, we can generate the moments of other forms of the population balance, such as Equations 3.5 and 3.6, in a similar way.

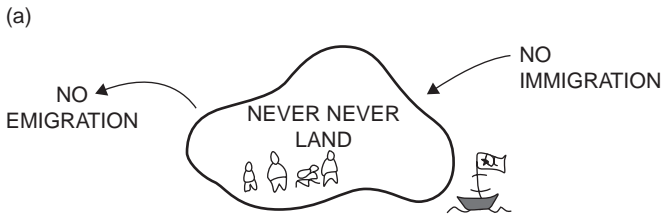
### 3.4.3 An Example

To make the abstract concept of the population balance more concrete, let us look at an introductory example.

**Example 3.1 The Population of Never Never Land** Never Never Land is an isolated Island. To avoid overpopulation, the birth rate is carefully controlled at 5,000 per year. The isolation has meant that many modern medical facilities are not available; 5% of people of every age die each year. Under these conditions, the population is constant.

- (a) What is the total population of Never Never Land?
- (b) How many people draw the pension (available to everyone over 65)?





### Solution

First, let us look at the total number of people on Never Never Land. We apply the total numbers balance (Equation 3.11):

$$\frac{dVN_T}{dt} = \dot{Q}_{in}N_{T,in} - \dot{Q}_{ex}N_{T,ex} + V\dot{B} - V\dot{D}$$

Total numbers are constant (no accumulation) and there is no immigration or emigration ( $\dot{Q}_{in}N_{T,in} = \dot{Q}_{ex}N_{T,ex} = 0$ ). Therefore, the total numbers balance becomes:

$$V\dot{B} = V\dot{D} = 5,000 / \text{year}$$

We also know that 5% of people of all ages die each year; i.e.,

$$V\dot{D} = \frac{0.05}{\text{year}} VN_T$$

$$\Rightarrow VN_T = \frac{5,000}{\text{year}} \cdot \frac{\text{year}}{0.05} = 10^5$$

i.e., the total population of Never Never Land is  $10^5$ . This is the answer to part (a). Note only the total numbers balance was needed to solve this part of the problem.

Now, let's look at the full population balance. We will use Equation 3.3:

$$\frac{\partial Vn(x,t)}{\partial t} = \dot{Q}_{in}n_{in}(x) - \dot{Q}_{ex}n_{ex}(x) - \frac{\partial VGn(x,t)}{\partial x} + V\dot{b}(x) - V\dot{d}(x)$$

As for the total number balance, the accumulation, inflow and outflow terms are all zero. Therefore, the population balance reduces to:

$$0 = -\frac{\partial VGn(x,t)}{\partial x} + V\dot{b}(x) - V\dot{d}(x)$$

We can simplify further. The "growth" rate for people (rate of aging) is 1 year/year, independent of their age:

$$G = 1 \text{ year/year}$$

All people are born at age zero, meaning that the birth distribution is given mathematically as:

$$V\dot{b}(x) = V\dot{B}\delta(x)$$

where  $\delta(x)$  is the Dirac delta function. People of all ages die in equal proportion. Thus:

$$\dot{d}(x) = \dot{D} \frac{n(x)}{N_T} = \dot{B} \frac{n(x)}{N_T}$$

Taking account of all these simplifications, the population balance becomes:

$$VG \frac{dn(x)}{dx} = V\dot{B}\delta(x) - \frac{V\dot{B}}{N_T} n(x)$$

So we now have reduced the population balance to a simple ordinary differential equation (ODE) which we can solve directly. It is convenient to solve for  $x > 0$  because the birth distribution will always be zero in this range. Thus we have:

$$VG \frac{dn(x)}{dx} = -\frac{V\dot{B}}{N_T} n(x) \quad \text{for } x > 0$$

$$\Rightarrow \frac{dn(x)}{n(x)} = -\frac{\dot{B}}{GN_T} dx$$

$$\Rightarrow \ln \left[ \frac{n(x)}{n(0)} \right] = -\frac{\dot{B}}{GN_T} (x-0)$$

$$\Rightarrow n(x) = n(0) \exp \left[ -\frac{\dot{B}}{GN_T} x \right]$$

We still have an unknown parameter  $n(0)$ . However we know, by definition:

$$\int_0^{\infty} n(x) dx = \int_0^{\infty} n(0) \exp \left[ -\frac{\dot{B}}{GN_T} x \right] dx = N_T$$

$$\Rightarrow n(0) = \frac{\dot{B}}{G} \text{ and } n(x) = \frac{\dot{B}}{G} \exp \left[ -\frac{\dot{B}}{GN_T} x \right]$$

Substituting the known values of the total number, birth and growth rates gives:

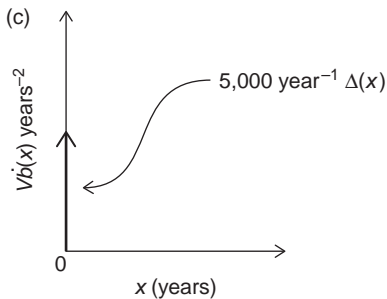
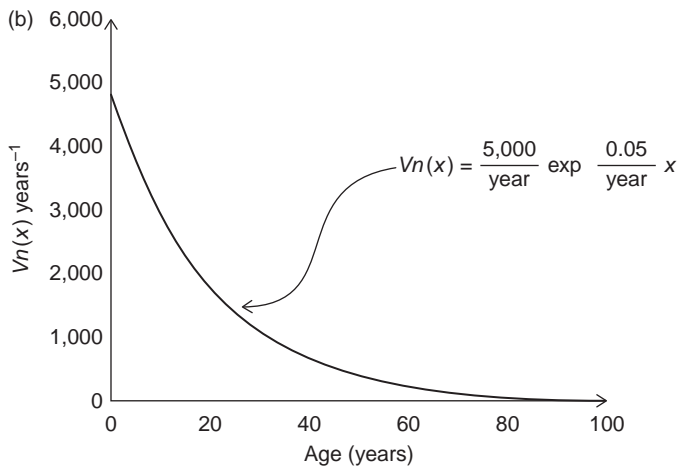
$$\frac{\dot{B}}{GN_T} = \frac{5,000 / \text{year}}{\left(\frac{1 \text{ year}}{\text{year}}\right) 10^5} = \frac{0.05}{\text{year}}$$

$$Vn(x) = \frac{5,000}{\text{year}} \exp\left[-\frac{0.05}{\text{year}} x\right]$$

Now we have the age distribution on the island, the number of people collecting the old age pension can be calculated:

$$OP = \int_{65}^{\infty} Vn(x) dx = 10^5 \exp\left[-\frac{0.05}{\text{year}} 65 \text{ year}\right] - 0 = 3877$$

Thus, just under 4% of the population is receiving the pension. This is the answer to part (b) of the problem.



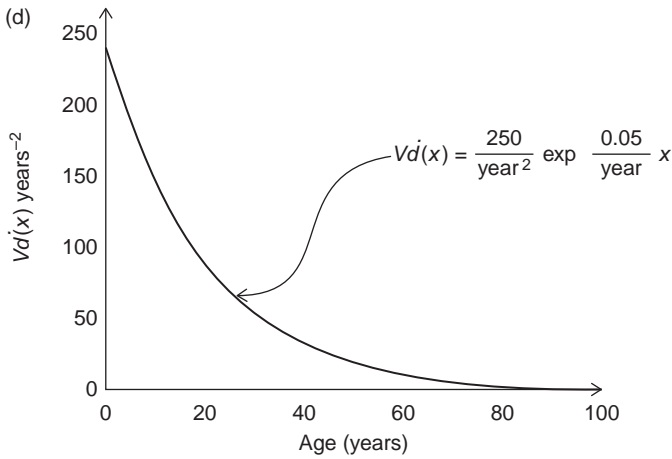


**Figure E3-1b,c,d** The age frequency distributions for (a) the population, (b) the birth rate, and (c) the death rate of people on Never Never Land.

Example 3.1 illustrates the approach to using the population balance to analyze processes involving birth, death, and growth. The general procedure is similar to those used for performing momentum, mass or energy balances on process systems.

1. Define the control volume clearly.
2. Write down the relevant balance equations – i.e., the population balance, the total numbers balance, and often the mass balance.
3. State clearly any assumptions. Especially consider assumptions that simplify the population balance by allowing some of the terms to be neglected (taken as zero).
4. State clearly the initial and boundary conditions for the problem.
5. Provide rate expressions for the key growth, birth, and death processes.
6. Simplify the equation set based on decisions made in steps 3, 4, and 5.
7. Solve the equation numerically or analytically.

Example 3.1 also gives a feeling for the meaning of the growth, birth and death terms in the population balance in a way that will be understood by most readers. For particulate systems, having good rate equations and reliable parameters in those equations for the rate processes of interest is the key to the power of the population balance as an analysis and design tool. Particles can also undergo processes not generally allowable for people. While a person being born is a good analogy to nucleation in particulate processes, people generally do not break into several smaller people, or agglomerate together.

The remainder of this chapter looks in some more detail at the mathematical expressions for important rate processes in particulate systems, highlighting that the same mathematics is applicable in both smog formation in the atmosphere and detergent granulation; growth of a crystal in an industrial crystallizer and coating a tablet. The differences lie in the physics that control the processes. The process physics are covered in detail in later chapters.

### 3.5 Differential Growth Processes

There is a range of particulate rate processes where the size of the particles gradually changes with no change to the number of particles, including:

- crystal growth;
- condensation onto existing drops during aerosol processes;
- condensation onto particles from the vapor phase in a reactor – e.g., fluidized bed polymerization;
- particle coating;
- crystal dissolution;
- attrition and erosion;
- shrinking core reaction of a particle.

Notice that this list includes processes that both increase and decrease the particle size.

In the population balance, all of these processes are modeled by the differential growth term  $\frac{\partial VGn}{\partial x}$  in Equation 3.3. The single model parameter is  $G$ , the growth rate.  $G$  is defined as the growth rate of a single particle within the local environment (Equation 3.1).  $G$  is positive if the particle is increasing in size (e.g., crystal growth, particle coating) and negative if the particle is decreasing in size (e.g., dissolution, attrition). It is very useful to think of the growth rate as a *velocity* corresponding to the flux of particles along the size axis as shown in Figure 3.2. This makes the transition from a one-dimensional population balance to a multidimensional microscopic balance given by Equation 3.5 easier to understand.

The rate expression for  $G$  will depend on the type of process being modeled and the governing physics. For example, particle dissolution into solution controlled by external film mass transfer can be represented as:

$$G(x, t) = \frac{k_l}{\rho_p} (c - c_s) \quad 3.15$$

where  $k_l$  is the mass-transfer coefficient in solution,  $c$  is the concentration of the solute, and  $c_s$  is the equilibrium solubility of the solid in solution. Note that as  $c < c_s$  during dissolution,  $G$  will be negative and the particle size will decrease with time.

A special case for differential growth processes is *size-independent growth*, mathematically defined as:

$$G(t) = \left( \frac{\partial x}{\partial t} \right)_x = \frac{dx}{dt} \neq G(x) \quad 3.16$$

Size-independent growth dramatically simplifies the mathematical analysis of growth processes. It is also a reasonable starting assumption for many physical processes – e.g., crystallization, particle coating.

The change in number and volume of particles due to growth is related to the moments of growth term in the population balance (Equations 3.10, 3.13):

$$\left[ \frac{dVN_T}{dt} \right]_{growth} = \left[ \frac{dV\mu'_0}{dt} \right]_{growth} = 0 \quad 3.17$$

$$\left[ \frac{dV.V_T}{dt} \right]_{growth} = \alpha_v \left[ \frac{dV\mu'_3}{dt} \right]_{growth} = 3\alpha_v VG\mu'_2 \quad 3.18$$

Note that growth does not change the total number of particles, but does change the total volume of particles.

**Example 3.2 Fattening Ammonium Nitrate Prills** The ACME explosives company produces ammonium nitrate (AN) particles by a prilling (spray cooling) process for use in explosive manufacture. The AN prills are very circular and have a very tight size distribution (effectively 1.4 mm diameter monosized). The company wishes to diversify its product range by producing fertilizer granules in competition with XYZ Ltd. (see the case study at the start of this chapter). Engineers propose to do this using a single-stage continuous fluidized bed to “fatten” the AN prills by spraying AN melt onto the granules so that they grow by layering (agglomeration is undesirable and will be avoided).

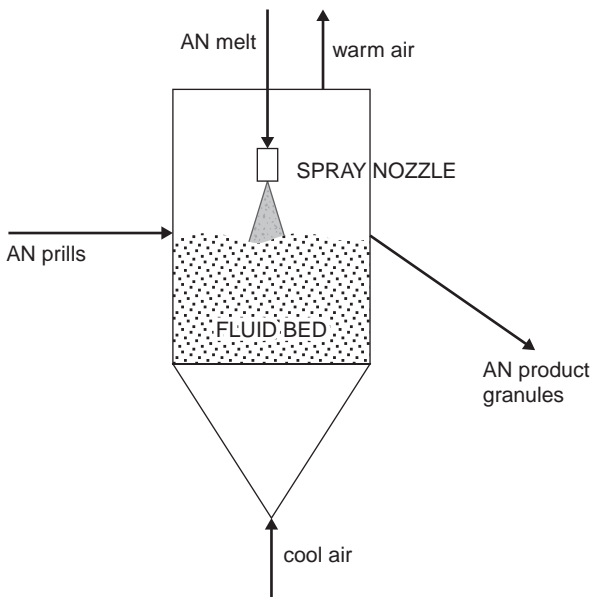


**Figure E3.2** Schematic of the AN prill-fattening process.

- (a) If the product granule size distribution has a mean size  $\bar{x}_{3,0} = 1.85\text{mm}$  and the feed rate of seed AN prill particles is 1 tonne per hour, what is the feed rate of AN melt to the granulator?
- (b) Derive an expression to give the growth rate  $G$  in terms of the flow rate of AN melt and the moments of the product granule size distribution. If the residence time in the fluid bed is 30 minutes, what is  $G$ ?
- (c) Derive an expression for the particle size distribution of product prills.

*Solution:*

From the problem statement we can make the following assumptions:

1. Steady-state operation:  $\partial Vn / \partial t = 0$ .
2. No coalescence, nucleation or breakage:  $\dot{b} = \dot{d} = 0$ .
3. The granulator is well mixed, and the overflow granules have the same size distribution as the granules in the fluid bed:  $n_{ex} = n$ .
4. The granule growth rate by layering is size independent:  $G \neq G(x)$ .

To solve part (a), we will use the total number and the mass balance. The total numbers balance (Equation 3.11) reduces to a simple statement of constant numbers:

$$\dot{Q}_{in} N_{in} = \dot{Q}_{ex} N_{ex} = \dot{Q}_{ex} N_T$$

In addition, the inlet granule size distribution is given by:

$$n_{in}(x) = N_{in} d(x - x_{in})$$

where  $x_{in} = 1.4\text{ mm}$ . The mass flow rate of seed granules can be linked to the third moment of the seed size distribution:

$$\begin{aligned} \dot{M}_{seed} &= \dot{Q}_{in} m_{in} = \dot{Q}_{in} \rho_p \alpha_v \mu'_{3,in} = 1\text{tonne / hr} \\ \Rightarrow \dot{M}_{seed} &= \dot{Q}_{in} \rho_p \alpha_v N_{T,in} x_{in}^3 \\ \Rightarrow \dot{M}_{seed} &= \rho_p \alpha_v \dot{Q}_{ex} N_T x_{in}^3 \end{aligned}$$

Similarly, we can write an expression for the product mass flow rate:

$$\dot{M}_{product} = \rho_p \alpha_v \dot{Q}_{ex} \mu'_3$$

Noting that:

$$\frac{\mu'_3}{\mu'_0} = \frac{\mu'_3}{N_T} = \bar{x}_{3,0}^3$$

we derive:

$$\dot{M}_{product} = \rho_p \alpha_v \dot{Q}_{ex} N_T \bar{x}_{3,0}^3$$

$$\Rightarrow \dot{M}_{product} = \left( \frac{\bar{x}_{3,0}^3}{x_{in}^3} \right) \dot{M}_{seed}$$

where  $\bar{x}_{3,0}^3 = 1.85 \text{ mm}$ . The overall mass balance gives:

$$\begin{aligned} \dot{M}_{melt} &= \dot{M}_{product} - \dot{M}_{seed} \\ &= \left[ \left( \frac{\bar{x}_{3,0}^3}{x_{in}^3} \right) - 1 \right] \dot{M}_{seed} \\ &= \left[ \left( \frac{1.85^3}{1.4^3} \right) - 1 \right] \cdot 1 \text{ tonne / h} \\ &= 1.31 \text{ tonne / h} \end{aligned}$$

To solve part (b), let us look at the general moments balance. With the assumptions for this example included, Equation 3.9 becomes:

$$\begin{aligned} 0 &= \dot{Q}_{in} \mu'_{k,in} - \dot{Q}_{ex} \mu'_k + kVG \mu'_{k-1} \\ &= \dot{Q}_{in} N_{in} x_{in}^k - \dot{Q}_{ex} m'_k + kVG \mu'_{k-1} \\ &= \dot{Q}_{ex} N_T x_{in}^k - \dot{Q}_{ex} \mu'_k + kVG \mu'_{k-1} \end{aligned}$$

If we divide by  $\dot{Q}_{ex}$ , this equation can be rearranged to give:

$$\mu'_k = N_T x_{in}^k + kG \tau \mu'_{k-1}$$

where the mean particle residence time in the granulator is  $\tau = V / \dot{Q}_{ex}$ . If this equation is used in sequence for  $k = 1, 2, 3$ , we derive the following expressions:

$$\begin{aligned} \mu'_1 &= N_T (x_{in} + G\tau) \\ \mu'_2 &= N_T (x_{in}^2 + 2G\tau x_{in} + 2(G\tau)^2) \\ \mu'_3 &= N_T (x_{in}^3 + 3G\tau x_{in}^2 + 6(G\tau)^2 x_{in} + 6(G\tau)^3) = N_T \bar{x}_{3,0}^3 \end{aligned}$$

Rearranging this equation gives:

$$\left( \frac{\bar{x}_{3,0}^3}{x_{in}^3} \right)^3 = 1 + 3 \left( \frac{G\tau}{x_{in}} \right) + 6 \left( \frac{G\tau}{x_{in}} \right)^2 + 6 \left( \frac{G\tau}{x_{in}} \right)^3$$



In this cubic equation, the only unknown is  $G$ . We solve to give:

$$G = 2.04 * 10^{-7} \text{ ms}^{-1}$$

Finally, we can solve the full population balance to give the product size distribution. For this exercise, the population balance (Equation 3.3) reduces to:

$$\begin{aligned} 0 &= \dot{Q}_{in} N_{in} \delta(x - x_{in}) - \dot{Q}_{ex} n(x) - \frac{VGdn(x,t)}{dx} \\ &= \dot{Q}_{ex} N_T \delta(x - x_{in}) - \dot{Q}_{ex} n(x) - \frac{VGdn(x,t)}{dx} \end{aligned}$$

Divide by  $\dot{Q}_{ex}$  and rearrange to give:

$$\frac{dn(x)}{dx} = \frac{N_T \delta(x - x_{in}) - n(x)}{G\tau}$$

Solving this equation, we follow a similar procedure to that in used in Example 3.1. For  $x > x_{min}$ :

$$\frac{dn}{dx} = -\frac{n}{G\tau}$$

Integrating the equation gives:

$$n(x) = n(x_{in}) \exp\left[-\frac{x - x_{in}}{G\tau}\right]$$

Noting that  $N_T = \int_{x_{in}}^{\infty} n(x) dx$ , it follows that  $n(x_{in}) = N_T / G\tau$ . Therefore, the granule product size distribution is:

$$n(x) = \frac{N_T}{G\tau} \exp\left[-\frac{x - x_{in}}{G\tau}\right]$$

There are a few take home points from Example 3.2. First, note that for this layered growth example, the growth rate of the prills is simply set by the mass balance and the surface area of prills available on which the melt is sprayed. Thus, this is a coupled mass balance and population balance problem. Such coupling is very common. Second, note that we could establish the melt flow rate and the particle growth rate using the moments form of the population balance without needing to solve the whole population balance. Equations 3.9 and 3.11

often provide a lot of information fairly simply for even quite complex problems. Third, note that this continuous, well-mixed granulator gives a very broad product size distribution, even though the seed particles were monosized. Can you explain why this is so?

### 3.6 The Birth and Death Terms: Nucleation, Agglomeration, and Breakage

Equation 3.9 gives the general form of the population balance for a well-mixed system. A whole host of important rate processes for unit operations that make or transform particles are described simply by two terms, birth  $\dot{b}$  and death  $\dot{d}$ . We will now explore in more detail the mathematical expressions for the birth and death terms related to (1) nucleation, (2) agglomeration, and (3) breakage.

#### 3.6.1 Nucleation

Nucleation can be described as any process in the control volume which produces new particles from a continuous phase. Thus, nucleation involves a birth term only. A good example is particle formation by crystallization or precipitation from solutions, melts, and gases. Each nucleus is formed from a relatively small number of ions or molecules and we often assume the nuclei have negligible size. The mathematical expression for nucleation at zero size is:

$$\dot{b}_{nuc} = \dot{B}_{nuc} \delta(x) \tag{3.19}$$

where  $\delta(x)$  is the Dirac delta function which has the following properties:

$$\delta(x) = \begin{cases} 0, & x \neq 0 \\ \infty, & x = 0 \end{cases} \tag{3.20}$$

$$\int_{-\infty}^{+\infty} \delta(x) dx = 1 \tag{3.21}$$

$$\int_{-\infty}^{+\infty} x^k \delta(x) dx = 0 \text{ for } k \geq 1 \tag{3.22}$$

It follows from Equations 3.20 to 3.22 that the moments of the nucleation terms are:

$$\mu'_{0,nuc} = \dot{B}_{nuc} \tag{3.23}$$

$$\mu'_{k,nuc} = 0 \text{ for } k \geq 1 \tag{3.24}$$

In other words, we can count the nuclei, but they do not add length, surface area, or volume to the particulate phase.

In a variation on this theme, we can model the nucleation process as producing particles of a small but finite size  $x_{min}$ :

$$\dot{b}_{nuc} = \dot{B}_{nuc} \delta(x - x_{min}) \quad 3.25$$

Equation 3.23 still defines the rate of generation of number of particles, but the higher moments are given by:

$$\mu'_{k,nuc} = \dot{B}_{nuc} x_{min}^k \text{ for } k \geq 1 \quad 3.26$$

Not all nucleation processes produce very small nuclei. Consider a spray-drying or spray-cooling process. A continuous liquid phase is atomized to produce a “particulate phase” of drops of finite size and often broad size distribution. This is still a nucleation process as new particles are being formed from a continuous phase. Models for this type of process are described in Chapter 7.

Example 3.1 shows how to include nuclei at zero size (or zero age in this case) in the population balance.

### 3.6.2 Agglomeration

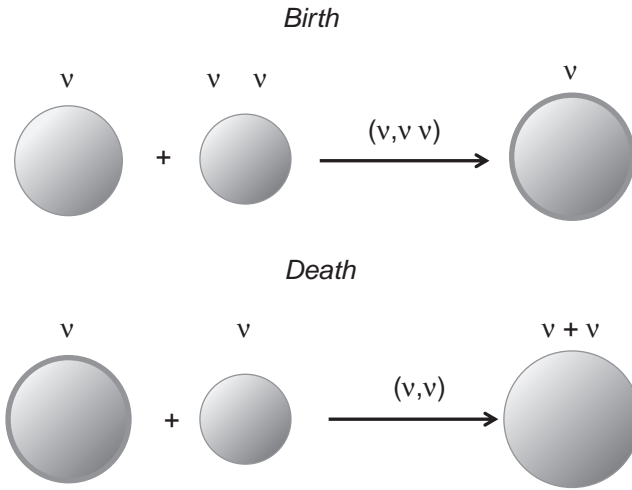
Agglomeration, aggregation, coalescence, and flocculation are a family of related rate processes in which several particles come together to form a single larger particle. In its simplest form, we model such processes as binary coalescence (think of two raindrops colliding and combining). Binary coalescence involves both a birth term and a death term in the population balance because two small particles disappear (die) and one larger particle appears (is born). Let us derive the birth and death terms for binary coalescence.

Figure 3.3 shows schematically the “birth” and “death” of a particle of volume  $v$  by coalescence. Coalescence preserves the particle volume. Therefore, a particle of volume  $v$  will be formed from a particle of arbitrary smaller volume  $v'$  coalescing with a particle of volume  $v - v'$ . The number of particles of volume  $v'$  is  $n(v')dv'$ . Let us assume that the rate of coalescence is proportional to the number of particles available for coalescence as this should set the frequency of collisions between particles. Thus, the rate of birth of particles of volume  $v$  from collisions involving particles of volume  $v'$  is:

$$\left. \frac{dn(v)dv}{dt} \right|_{v'} = \dot{b}(v)_{coal} \left. dv \right|_{v'} = \beta n(v') n(v - v') dv' d(v - v') \quad 3.27$$

$$\Rightarrow \dot{b}(v)_{coal} \left. dv \right|_{v'} = \beta n(v') n(v - v') dv' \quad 3.27a$$

Equation 3.27a is analogous to a second-order chemical reaction with the number densities  $n(v')$  and  $n(v - v')$  equivalent to the concentrations of two reactants  $c_A$  and  $c_B$ .  $\beta$  is the coalescence rate constant, often called the *coalescence kernel*.  $v'$  is any



**Figure 3.3** Schematic representation of appearance (birth) and disappearance (death) of particle of volume  $v$  due to coalescence. Note the analogy to a second-order chemical reaction.

arbitrary size less than  $v$ , so to calculate the total rate of birth of particles of volume  $v$  we must integrate across the range of  $v'$  from  $0$  to  $v$ :

$$\dot{b}(v)_{coal} = \frac{1}{2} \int_0^v \beta n(v') n(v - v') dv' \tag{3.28}$$

Here the  $\frac{1}{2}$  factor is to avoid double counting interactions.

The death term for coalescence is the result of coalescence of a particle of volume  $v$  with any particle of arbitrary volume  $v'$  across the whole range of particle volumes. Following a similar approach to our derivation of the birth term, we find:

$$\dot{d}(v)_{coal} = \int_0^\infty \beta n(v) n(v') dv' = n(v) \int_0^\infty \beta n(v') dv' \tag{3.29}$$

Equations 3.28 and 3.29 are the birth and death terms for coalescence that can be used in any form of the population balance, such as Equations 3.3 or 3.5. Note, however, that we have written the coalescence expressions in terms of  $n(v)$  rather than  $n(x)$ . Can you explain the reason for this given the derivation described above?

Remember, there is a simple relationship between  $n(v)$  and  $n(x)$ . From Table 2.4:

$$n(v) = \frac{n(x)}{3\alpha_v x^2} \tag{3.30}$$

so that the number distribution in terms of particle volume can always be derived if the distribution in terms of particle size is known.

The key parameter in the coalescence rate expression is the coalescence kernel  $\beta$ . In general:

$$\beta = \beta(v, v'; p_i; e_i) \quad 3.31$$

where  $p_i$  is a list of other relevant particle properties, and  $e_i$  is a list of relevant process (environmental) parameters. The exact form of this function depends on the physics of the process under study. For aerosols of low-viscosity liquid drops, the coalescence kernel is primarily determined by the frequency of collision between drops (see Chapter 6). In granulation, the coalescence kernel is primarily determined by the probability that a collision leads to particles sticking together, which is a strong function of the particle liquid content (see Chapter 8). The magnitude of the coalescence kernel determines the rate of change of mean particle size due to coalescence, while the functional dependence of the kernel on  $v$  and  $v'$  determines the change of shape of the particle size distribution.

Inserting the coalescence birth and death terms from Equations 3.28 and 3.29 into the population balance Equation 3.3 creates a messy integro-differential equation which is difficult to solve analytically. Some analytical solutions exist for particular kernel functions. The simplest of these is the size independent kernel:

$$\beta = \beta(v, v') \quad 3.32$$

With this simplification, Equations 3.28 and 3.29 become:

$$\dot{b}(v)_{coal} = \frac{\beta}{2} \int_0^v n(v') n(v-v') dv' \quad 3.33$$

$$\dot{d}(v)_{coal} = \beta n(v) \int_0^\infty n(v') dv' = \beta n(v) N_T \quad 3.34$$

Table 3.1 lists some analytical solutions for the PB with coalescence only with some simple kernel forms. However, most practical applications require numerical solution of the population balance equation. We can, however, get some joy from the moments analysis for the coalescence terms. It is possible to show that for any form of  $\beta$ , the first moment in terms of  $v$  (third moment in terms of  $x$ ) of the coalescence terms is 0:

$$\mu'_{1,v coal} = \int_0^\infty [\dot{b}(v)_{coal} - \dot{d}(v)_{coal}] v dv = 0 \quad 3.35$$

i.e., coalescence events do not change the total volume of particles. This is logical as we derived the coalescence terms on the assumption that total volume was conserved. However, the total number of particles in the system is decreased by coalescence. For the size-independent kernel, we can derive an analytical expression for first moment:

**Table 3.1** Examples of analytical solutions to the population balance with agglomeration

Mixing state	Coalescence kernel	Initial size distribution	Final size distribution
Batch	$\beta(v, v') = \beta_0$	$n_0(x) = N_0 \delta(v - v_0)$	$n(v) = \frac{N_0}{\bar{v}} \exp\left[-\frac{v}{\bar{v}}\right]$  where $\bar{v} = v_0 \exp\left[\frac{\beta_0 t}{6}\right]$
Batch	$\beta(v, v') = \beta_0$	$n_0(x) = \frac{N_0}{v_0} \exp\left[-\frac{v}{v_0}\right]$	$n(v/v_0) = \frac{4N_0}{v_0(2 + N_0\beta_0 t)^2} \exp\left[-\frac{v/v_0}{2 + N_0\beta_0 t}\right]$
Batch	$\beta(v, v') = \beta_0(v + v')$	$n_0(x) = \frac{N_0}{v_0} \exp\left[-\frac{v}{v_0}\right]$	$n(v/v_0) = \frac{N_0(1-T)}{vT^{1/2}} \exp\left[-v/v_0(1+T)\right] I_1(2T^{1/2}v/v_0)$ where $T = 1 - \exp(-(2 + N_0\beta_0 t))$

\* For other analytical solutions see Gelbard and Seinfeld (1980) and Hounslow (1990).

$$\mu'_{0, coal} = \int_0^\infty [\dot{b}(v)_{coal} - \dot{d}(v)_{coal}] dv \tag{3.36}$$

Substituting from Equations 3.28 and 3.29 gives:

$$\begin{aligned} \mu'_{0, coal} &= \frac{\beta}{2} \int_0^\infty \int_0^v n(v')n(v-v')dv'dv - \int_0^\infty \beta n(v)N_T dv \\ \Rightarrow \mu'_{0, coal} &= \frac{\beta N_T^2}{2} - \beta N_T^2 = -\frac{\beta N_T^2}{2} \end{aligned} \tag{3.37}$$

**Example 3.3 Exploring the Effect of the Functional Form of the Coalescence Kernel** How will the shape of the product particle size distribution change with the functional form of the coalescence kernel for a batch coalescence process with an initial mono-sized seed particle distribution?

*Solution*

Let us consider three forms of the coalescence kernel:

1. the constant kernel  $\beta(v, v') = \beta_0$  ;

2. the Smoluchowski shear kernel  $\beta(v, v') = \beta_1 (v^{1/3} + v'^{1/3})^3$  originally developed for aerosols; and
3. the equikinetic energy (EKE) kernel  $\beta(v, v') = \beta_3 (v^{1/3} + v'^{1/3})^2 (v^{-1} + v'^{-1})^{1/2}$ , sometimes used in fluid bed granulation.

For a batch coalescence process with no other rate processes occurring, Equation 3.3 combined with Equations 3.28 and 3.29 gives:

$$\frac{dVn(v)}{dt} = \frac{V}{2} \int_0^v \beta n(v') n(v-v') dv' - V \int_0^\infty \beta n(v) n(v') dv'$$

As volume is conserved during coalescence, we expect  $V$  to be constant. Therefore:

$$\frac{dn(v)}{dt} = \frac{1}{2} \int_0^v \beta n(v') n(v-v') dv' - \int_0^\infty \beta n(v) n(v') dv'$$

The initial condition is given by:

$$n_0(v) = N_0 \delta(v - v_0)$$

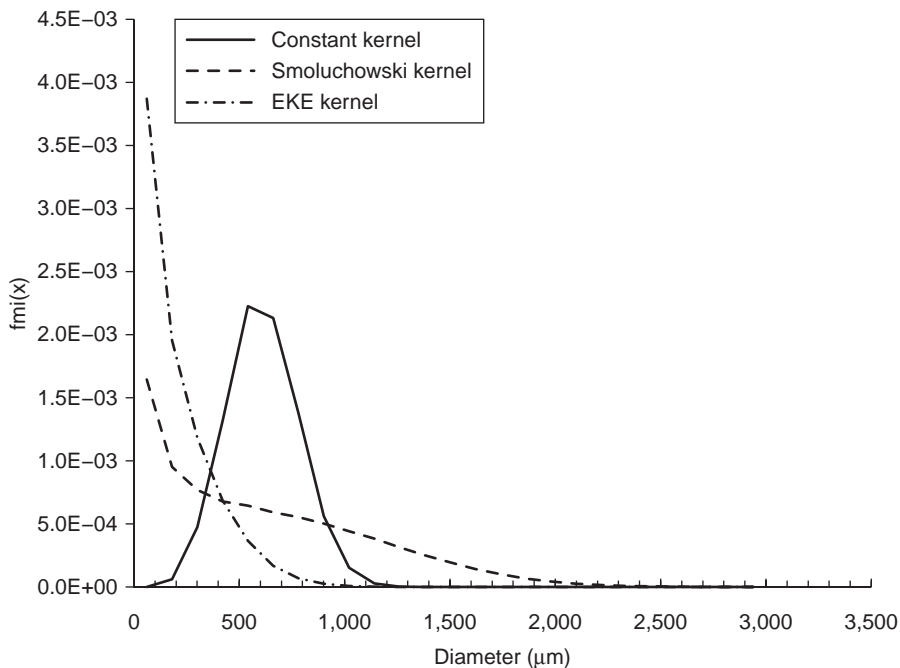


**Figure E3.3** Particle size distributions for three different agglomeration kernels.

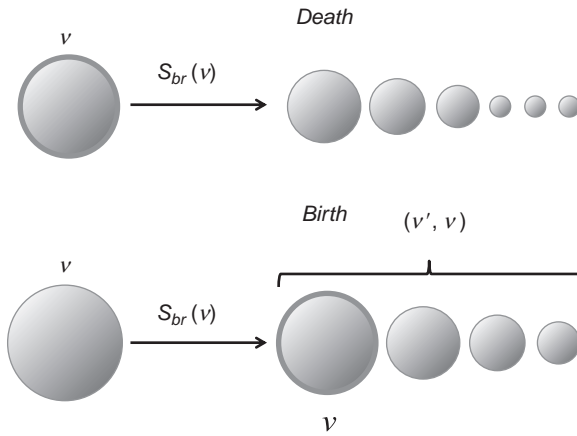


**Figure 3.4** Illustration of the breakage process: (a) breakage of a particle of volume  $v$ ; (b) breakage of a particle of volume  $v' > v$ , where some of the fragments are of size  $v$ .

From Table 3.1, we see there is an analytical solution for this equation and initial condition for coalescence kernel 1, but not for kernels 2 and 3. Therefore, we will solve the population balance equation numerically. Numerical solutions for the three different kernels for batch coalescence are shown in Figure E3.3, all with  $\bar{v} = \mu'_{1,v} / \mu'_0 = 10v_0$ . We can note several features. First, all the coalescence kernels substantially broaden the particle size distribution. Second, the final shape of the particle size distribution is a strong function of the form of the coalescence kernel. The larger the net dependence on particle volume (the “order” of the kernel) the broader the particle size distribution produced.

### 3.6.3 Breakage

We normally associate particle breakage with crushing and grinding (Chapter 6). However, breakage can also occur in many other particulate processes, including crystallization, granulation, flocculation, and emulsion formation. We use the same mathematical approach to model breakage in each case. Figure 3.4 illustrates the birth and death terms for breakage.

We generally treat breakage as a first-order process in which particle volume is conserved. It is simplest to look at the death term first. The rate at which particles of size  $v$  disappear due to breakage is proportional to number of particles of that size (Figure 3.4a):

$$-\left[ \frac{\partial Vn(v,t) dv}{\partial t} \right]_{death, br} = VS_{br}(v)n(v,t) dv$$

$$\Rightarrow \dot{d}_{br} = S_{br}(v)n(v,t) \tag{3.38}$$



where  $S_{br}(v)$  is the *breakage selection function* or *breakage rate constant*.

New particles of size  $v$  can be formed from the breakage of a larger particle of arbitrary size  $v'$  (Figure 3.4b):

$$\left[ \frac{\partial Vn(v,t)dv}{\partial t} \right]_{birth,v'} = V \varphi(v',v) dv S_{br}(v') n(v',t) dv' \quad 3.39$$

where  $\varphi(v',v)dv$  is the number of particles from a breakage event of a particle of size  $v'$  that are in the size range  $v$  to  $v + dv$ . As  $v'$  is an arbitrary size, we need to integrate over the full range  $v' > v$  to give the total birth term:

$$\begin{aligned} \left[ \frac{\partial Vn(v,t)dv}{\partial t} \right]_{birth} &= \int_v^{\infty} V \varphi(v',v) dv S_{br}(v') n(v',t) dv' \\ \Rightarrow \dot{b}_{br}(v) &= \int_v^{\infty} \varphi(v',v) S_{br}(v') n(v',t) dv' \end{aligned} \quad 3.40$$

We call  $\varphi(v',v)$  the *breakage function*. It defines the fragment size distribution for any single breakage event. We can only make fragments smaller than the original size. Therefore:

$$\varphi(v',v) \Big|_{v>v'} = 0 \quad 3.41$$

and

$$\int_0^{\infty} \varphi(v',v) dv = \int_0^{v'} \varphi(v',v) dv = N_{fragment} \quad 3.42$$

where  $N_{fragment}$  is the number of fragments from a single breakage event. Also, as any breakage event conserves particle volume:

$$\int_0^{\infty} v \varphi(v',v) dv = \int_0^{v'} v \varphi(v',v) dv = v' \quad 3.43$$

Equations 3.38 and 3.40 give the birth and death terms for breakage. Although breakage is, in general terms, the “opposite” of coalescence, Equations 3.38 and 3.40 are not the inverse of Equations 3.28 and 3.29. This is because (1) we treat breakage as a first-order process, and (2) we only consider binary coalescence but we allow the breakage event to produce many fragments, not just two. To use the population balance for breakage we need to specify two functions: the breakage selection function (breakage rate constant)  $S_{br}(v)$  and the breakage function (breakage fragment distribution)  $\varphi(v',v)$ . Of course, the form and magnitude of these functions are defined by the physics of the breakage process. Often, single particle breakage experiments are used to give these functions. We will discuss measurement of  $S_{br}(v)$  and  $\varphi(v',v)$  in Chapter 5.

As for coalescence, volume is conserved in the breakage event:

$$\mu'_{1,v br} = \int_0^\infty [\dot{b}(v)_{br} - \dot{d}(v)_{br}] v dv = 0 \tag{3.44}$$

The zeroth moment for breakage terms in the population balance is:

$$\begin{aligned} \mu'_{0 br} &= \int_0^\infty [\dot{b}(v)_{br} - \dot{d}(v)_{br}] dv \\ &= \iint_{0 v}^{\infty \infty} \varphi(v', v) S_{br}(v') n(v', t) dv' dv - \int_0^\infty S_{br} n(v) dv > 0 \end{aligned} \tag{3.45}$$

The number of particles in the control volume always increases due to breakage. The rate of increase will depend on how  $S_{br}$  and  $\varphi(v', v)$  vary with particle volume  $v$ .

---

**Example 3.4 Forming an Emulsion by Drop Breakage** Consider the process of forming an emulsion of viscous oil drops in water in a stirred tank. Let us neglect drop coalescence. Assume the drop breakage rate is independent of drop size with a breakage rate constant  $S_{br}$  and each breakage event gives two daughter drops of equal size.

- (a) How will the mean size  $\bar{x}_{3,0}$  will change with time?
- (b) Derive an expression for the breakage function  $\varphi(v', v)$  suitable to describe this problem.
- (c) Derive the population balance equation for this process.

*Solution:*

We can solve part (a) using only the total numbers balance and knowing that volume is conserved during the breakage process. Noting this is a batch process and the only birth and death terms are due to breakage, Equation 3.11 gives:

$$\frac{dN_T}{dt} = V\dot{B}_{br} - V\dot{D}_{br} \Rightarrow \frac{dN_T}{dt} = \dot{B}_{br} - \dot{D}_{br}$$

because the total system volume is conserved. Let us derive an expression for the total death term:

$$\dot{D}_{br} = \int_0^\infty \dot{d}_{br}(v) dv = \int_0^\infty S_{br} n(v) dv$$

In this case  $S_{br} \neq S_{br}(v)$  so we can write:

$$\dot{D}_{br} = \int_0^\infty S_{br} n(v) dv = S_{br} \int_0^\infty n(v) dv = S_{br} N_T$$

Each breakage event yields two fragments. Therefore we can write:

$$\dot{B}_{br} = 2\dot{D}_{br} = 2S_{br}N_T$$

Substituting the birth and death terms into the numbers balance gives:

$$\frac{dN_T}{dt} = \dot{B}_{br} - \dot{D}_{br} = 2S_{br}N_T - S_{br}N_T = S_{br}N_T$$

Integrating the equation gives:

$$N_T(t) = N_T(0) \exp[S_{br}t]$$

From Equation 3.44, we know:

$$\frac{d\mu'_{1,v}}{dt} = 0 \Rightarrow V_T(t) = V_T(0)$$

Combining these two equations:

$$\bar{v}_{1,0}(t) = \frac{V_T(t)}{N_T(t)} = \frac{V_T(0)}{N_T(0) \exp[S_{br}t]} = \bar{v}_{1,0}(0) \exp[-S_{br}t]$$

The drops will be spherical. Therefore:

$$\bar{x}_{3,0} = \left( \frac{6\bar{v}_{1,0}}{\pi} \right)^{1/3}$$

Thus, we have an expression for how the drop mean size decreases with time. For example, if  $S_{br} = 0.3 \text{ s}^{-1}$ , it will take 23 s to achieve a 10-fold decrease in  $\bar{x}_{3,0}$ .

To answer part (b), consider that only the breakage of a drop of *exactly* volume  $2v$  can produce a fragment of volume  $v$ . Thus, the breakage function must be of the form:

$$\varphi(v', v) = C\delta(2v - v')$$

To evaluate the value of the constant  $C$ , we note that each breakage event gives two fragments and substitute into Equation 3.42:

$$\int_0^{\infty} \varphi(v', v) dv = \int_0^{\infty} C\delta(2v - v') dv = N_{\text{fragment}} = 2$$

With a little mathematical manipulation:

$$\begin{aligned} \int_0^{\infty} C\delta(2v - v') dv &= 2 \\ \Rightarrow \int_0^{\infty} \frac{1}{2} C\delta(2v - v') d(2v) &= 2 \end{aligned}$$

$$\Rightarrow C / 2 = 2$$

$$\Rightarrow C = 4$$

Thus we can write:

$$\begin{aligned} \dot{b}_{br} &= \int_v^{\infty} \varphi(v', v) S_{br} n(v') dv' \\ &= \int_v^{\infty} 4\delta(2v - v') S_{br} n(v') dv' \\ &= 4S_{br} \int_v^{\infty} \delta(2v - v') n(v') dv' \\ &= 4S_{br} n(2v) \end{aligned}$$

Now we have expressions for both the birth and death terms, the full population balance can be written:

$$\frac{dn}{dt} = 4S_{br} n(2v) - S_{br} n(v)$$

If we know the initial drop size distribution  $n(v, 0)$  we can solve the population balance equation either analytically or numerically to give the evolution of drop distribution with time  $n(v, t)$ .

### 3.7 Summary

The population balance is a rate equation that follows the change in the distribution of a particle (property) with time in phase space. It is an important tool to add to your process engineering tool kit which already includes mass and energy balances for analyzing particulate processes.

The balance includes terms for birth, death, flows, accumulation, and growth. There are many equivalent forms of the population balance. The *macroscopic* population balance is most useful for well-mixed systems. The *microscopic* population balance is more general and covers systems where particle properties vary with position. The *moments* form of the population balance leads to useful simplifications including balances for total number and total mass in particulate process.

Important rate processes such as growth, dissolution, nucleation, coalescence, and breakage are represented as rate expressions within the population balance. Table 3.2 summarizes the most important of these expressions and the impact of these processes on the total number and volume (mass) of particles. The rate constants

**Table 3.2** Modeling rate processes in the population balance

Rate process	Term in the population balance	Parameter	$\mu'_0$ number	$\mu'_3$ volume
Growth Dissolution Coating Attrition	$-\frac{\partial VGn}{\partial x}$	$G$	0	$2VG\mu'_2$ $G \neq G(x)$
Nucleation	$\dot{b}(x) = \dot{B}_{nuc} f_{nuc}(x)$	$\dot{B}_{nuc}, f_{nuc}(x)$	$V\dot{B}_{nuc}$	$V\mu'_{3,nuc}$
– at zero size	$\dot{b}(x) = \dot{B}_{nuc} \delta(x)$			0
– at $x_{min}$	$\dot{b}(x) = \dot{B}_{nuc} \delta(x - x_{min})$	$x_{min}$		$Vx_{min}^k$
Coalescence	$\dot{b} = \frac{1}{2} \int_0^v \beta n(v') n(v - v') dv'$	$\beta = \beta(v, v'; p_i; e_i)$	Decreases	0
Agglomeration Flocculation Aggregation	$\dot{d} = \int_0^\infty \beta n(v) n(v') dv'$			
Breakage	$\dot{b} = \int_v^\infty \varphi(v', v) S_{br}(v') n(v', t) dv'$ $\dot{d} = S_{br}(v) n(v, t)$	$S_{br}, \varphi(v', v)$	Increases	0

(model parameters) in these expressions are key to the application of the population balance. If we can (1) predict the parameters from first principles, or (2) measure them easily in small-scale tests, *and* understand how they change with scale, then the population balance becomes a powerful tool for the engineer and technologist.

At this point, the population balance may seem quite abstract. Those of you that are intuitive learners<sup>1</sup> will be excited to have this very general and powerful tool at your disposal. Those of you who are sensing learners, don't panic! In the following chapters, we will provide many concrete examples of how to use the population balance for applications in crystallization, grinding, aerosol processes, granulation, and many other processes.

### 3.8 Bibliography

- Freidlander, S.K., 1977. *Smoke, Dust and Haze*, Wiley, NY.  
 Gelbard, F. and Seinfeld, J.H., 1980. Simulation of multicomponent aerosol dynamics. *Journal of Colloid and Interface Science*, 78, 485.

<sup>1</sup> See Felder and Brent on learning styles, [www.ncsu.edu/effective\\_teaching](http://www.ncsu.edu/effective_teaching)

- Hounslow, M.J., 1990. A discretized population balance for continuous systems at steady state. *AIChE Journal*, 36, 106.
- Hulbert, H.M. and Katz, S. 1964. Some problems in particle technology: A statistical mechanical formulation. *Chemical Engineering Science*, 19, 555.
- Litster, J. and Sarwono, R., 1996. Fluidized drum granulation: Studies of agglomerate formation. *Powder Technology*, 88, 165–172.
- Ramkrishna, D., 2000. *Population Balances: Theory and Practice to Particulate Systems in Engineering*, Academic Press, New York.
- Randolph, A.D. and Larsen, M.A., 1988. *Theory of Particulate Processes 2nd edition*, Academic Press, New York.

### 3.9 Problems

- 3.1. The table below lists several rate processes that will change the particle size distribution in some way. Indicate in the table how each process will change the listed properties of the size distribution by indicating in every table cell either “increase,” “decrease,” or “no change.” For example, crystal growth by layering will increase the particle mean size.
- 3.2. Consider the “Never Never Land” example (Example 3.1).
- What is the median age of the population of Never Never Land? What is the mean age  $\bar{x}_{10}$ ?
  - The Governor of Never Never Land needs to cut budget spending so he can buy a new luxury yacht. To reduce spending on old age pensions, he introduces “voluntary” euthanasia for all citizens on their 70th birthday. What will be the age distribution of citizens once the new steady-state population is achieved? What is the percentage savings on old age pensions?
  - Perhaps not surprisingly, the Governor is overthrown in a geriatric coup. The new Governor rescinds the voluntary euthanasia legislation and plans to pay for looking after the senior citizens by using immigration to stimulate

**Table for Problem 3.1** Effect of rate processes on particle size distribution properties

Rate process	0th moment (total number) $\mu'_0$	3rd moment (total volume) $\mu'_3$	Particle mean size $\bar{x}_{1,0}$
Crystal growth by layering			
Crystal nucleation during crystallization			
Agglomeration during powder granulation			
Drop-controlled nucleation during powder granulation			
Rock breakage during grinding			

- economic growth and bring in more young people. There will be a steady influx of 1,000 people per year aged exactly 25. Birth rates on the island will also rise by 20% as a result. Does the proportion of potential workers (aged 20–65) increase by these policies?
- 3.3. The figure below gives information on the population distribution of people in Australia in 1996 and 2006. It is extracted from an Australian newspaper article on the consequences of Australia's aging population. Given the data in the figures, answer the following questions:
- Comment on the statement "Australia's population is aging" by comparing  $F(\theta \text{ years})$  for the population in 1996 and 2006.
  - The mode of the distribution for both men and women is 40–44 years. Give an estimate of the frequency  $f(x)$  ( $\text{years}^{-1}$ ) of men in this age range.
  - Give an estimate of the birth rate for women in 2006, assuming it is unchanged for the previous five years.
  - It is often stated that women live longer than men. Is there any evidence for this statement in the population distributions? Be as quantitative as possible in your answer.
  - For both men and women, the population distribution of people greater than 50 years is approximately an exponential decay, similar to the "Never Never Land" example. If we assume that the peak in the population distribution between ages 40 and 50 is entirely due to high birth rates during the "baby boomer" generation from 1955 to 1965, then the "steady-state" population distribution would be almost flat between 0 and 50 years. For the steady-state distribution, propose a reasonable functional form for the death rate distribution  $d(x)$  for (a)  $x > 50$ , and (b)  $0 < x < 50$ . Justify your answer as quantitatively as possible and state clearly any assumption you make.
- 3.4. For a granulation process with a size-independent kernel, the total birth and death rates associated with agglomeration are given by Equation 3.37. Consider a well-mixed granulator operating at steady state with representative overflow. Seed granules are fed to the granulator where they grow by agglomeration only (no layering, no nucleation). Derive an expression which gives the total number density  $N_T$  as a function of the inlet number density  $N_{T,in}$  and the residence time in the granulator  $\tau$ . State clearly all assumptions you make.
- 3.5. In Example 3.2, how will the growth rate change if (a) the spray rate is doubled; or (b) the seed size is doubled?
- 3.6. Consider a modification of Example 3.2 in which the prill fattening is done in a batch-fluidized bed granulator. One tonne of 1.4 mm-diameter ammonium nitrate prills is used as initial seed granule charge.
- What is the spray rate of melt added to the granulator if the product mean size is 1.85 mm and the melt is added at a constant rate over 30 minutes?
  - What is the initial growth rate  $G(0)$ ? What is the final growth rate  $G(30 \text{ min})$ ? Explain why the initial and final growth rates are different.

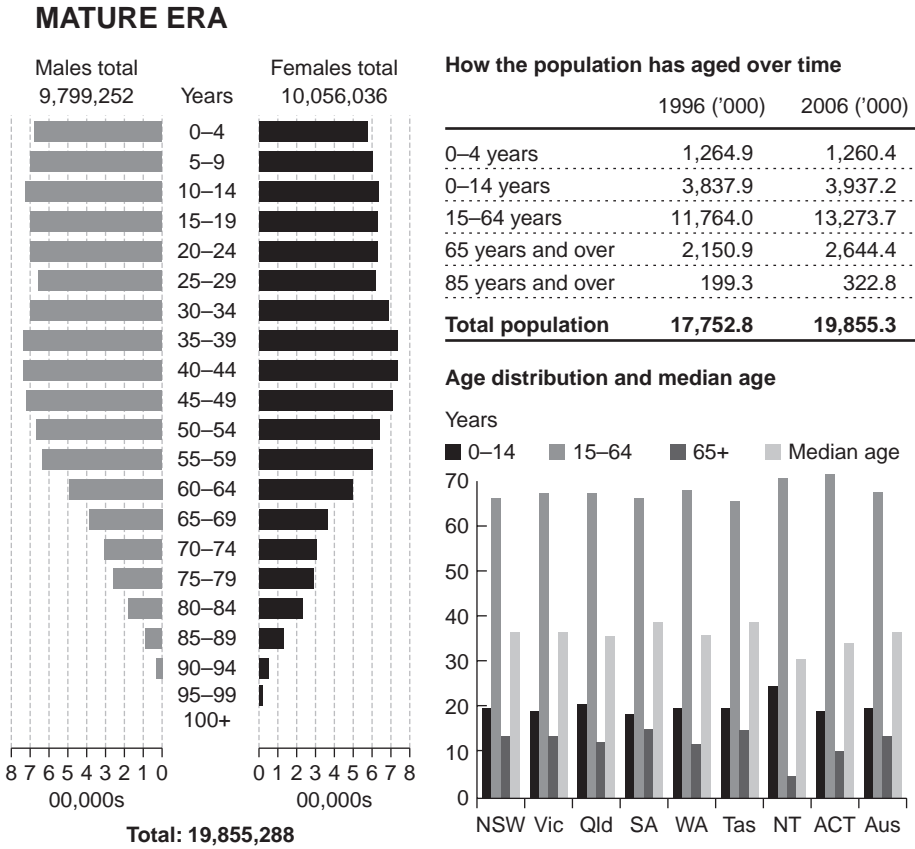


Figure for problem 3.3 Australian population statistics for 1996 and 2006.

- c. Derive an expression for the final granule size distribution. This batch process gives a much narrower product size distribution than the continuous granulator in Example 3.2. Why is this so?
- 3.7. The assumption made in Example 3.4 that the breakage rate is independent of drop size is not very realistic. Usually, things are more difficult to break the smaller they get. We could capture this effect if we allow the breakage rate to vary with size:  $S_{br} = Av$ . Redo Example 3.4 with this breakage rate expression.
- 3.8. A continuous stirred tank fermenter is used to grow genetically modified *Escherichi coli* bacteria. The feed to the tank is water containing the carbon substrate at a concentration  $c_{s,in}$ . In the fermenter the bacteria grow until they reach a volume  $v_{max}$ . At this point they divide to form two new bacteria of equal volume. The growth rate of the bacteria is limited by the concentration of carbon substrate as given by the following equation:

$$\frac{dv}{dt} = \frac{Ac_s}{B + c_s}$$



where  $v$  is the volume of a bacteria,  $A$  and  $B$  are constants, and  $c_s$  is the concentration of the carbon substrate in the fermenter. The yield on the carbon substrate is  $Y$  – i.e., 1 gram of carbon substrate consumed yields  $Y$  grams of cells. The cell density is  $\rho_c$ . Bacteria carried out of the fermenter contain a valuable protein product which is later extracted.

- a. Draw a sketch of the system under study.
  - b. Derive a population balance model for the fermenter operating at steady state. In doing this, clearly define any variables used and state clearly all assumptions made.
  - c. Write a steady-state mass balance for the bacteria in the fermenter.
  - d. Solve the population balance to give, quantitatively, the bacteria volume distribution in terms of the parameters defined above.
  - e. Sketch the shape of the bacteria volume distribution leaving the fermenter.
- 3.9. The continuous crystallizer at our pilot plant is prone to suffer from nucleation bursts that give a large number of undesirable small crystals. To overcome the problem, we are planning to install a “fines dissolver” (FD) after the crystallizer. The FD is a heated, well-mixed tank. In the dissolver, the liquor will be undersaturated so crystals will dissolve. Our aim is to remove small crystals by dissolution without losing too much size or mass from the larger crystals. From mass-transfer considerations, the dissolution rate of a single crystal is given by Equation 3.15. As a starting point for building a design model, we can assume the FD operates at steady state, and there is a representative overflow; i.e., the crystal content and size distribution in the exit stream from the FD are the same as those in the FD ( $n_{ex}(x) = n(x)$ ).
- a. Starting from the general form of the population balance, derive a simplified expression of the form:

$$\frac{dn}{dx} = g(n_{in}, \tau, G_d, \dot{D})$$

where  $\tau$  is the mean residence time in the dissolver,  $n_{in}(x)$  is the distribution of crystals entering the fines dissolver, and  $\dot{D}$  is the rate of disappearance of crystals due to dissolution.

- b. Can you write an expression that relates  $\dot{D}$  to dissolution rate  $G_d$  and the parameter(s) of crystal size distribution? Briefly justify your answer. Derive an expression for the number concentration of crystals  $N_T$  in the exit stream from the FD.
- c. Having reviewed my heat and mass transfer notes, I realize that  $k_l$  is actually likely to be a function of crystal size  $x$ . Will this affect my model assumptions and derivations above?

# 4 Industrial Crystallization

## 4.1 Consider a Case Study ...

*Particulate Products Inc.*

Memo to: New Process Development Team  
Memo from: Manager Product Development  
February 12, 2015

**re: Design of an industrial-scale protein crystallizer**

The year is 2016. A new company Plant Power Products (PPP) has been formed to exploit new technology based on genetically modified plants. In this technology the process plant is the plant. A raft of chemical products are now planned to be produced by this (almost) natural process using largely renewable energy at room temperature and pressure. The new “plant process plant” is being touted as the basis for the sustainable chemical industry for the twenty-first century.

Genetically modified soy plants can now produce a range of potentially important proteins for use as pharmaceuticals and food supplements (nutraceuticals). PPP is looking to exploit this technology and wishes to purify the proteins by crystallization. Crystallization gives a very pure product and the protein in crystal form guarantees it remains in its active form. A new protein product *superpro*<sup>TM</sup> has just received FDA approval. The protein is extracted from the soy plants. After removal of other materials via a series of separation techniques, very pure *superpro*<sup>TM</sup> can be produced by crystallization at neutral pH with the addition of ammonium sulfate as a precipitant.

PPP has limited engineering expertise and no crystallization expert. They have commissioned our team to design a full-scale continuous crystallizer to produce a crystalline *superpro*<sup>TM</sup> for their new 1-tonne-per-day facility. Your job is to provide the process design for a continuous crystallizer to produce 1 tonne per day of *superpro*<sup>TM</sup> in crystalline form in a concentrated clean suspension. The feed to the crystallizer is a solution of 50 g/l *superpro*<sup>TM</sup> at pH 7 and 25°C. A crystal yield needs to be at least 85% for economic viability. For ease of handling and separation downstream at least 95% of the crystals (by mass) need to be larger than 20 μm and a relatively narrow crystal size distribution is preferred. PPP is also looking to us to recommend how to instrument and control the crystallizer effectively so that product quality can be maintained.

Unfortunately, there are limited thermodynamic and kinetic data immediately available to help with the design. (We do know that the protein denatures above 50°C and at pH values below 5 and above 9 it reverts to an inactive form.) In fact, bulk crystallization of proteins is a relatively new technology at industrial scale. Luckily, Purdue University has an excellent protein crystallization laboratory that can make these measurements for us (for a price, of course). I have attached an example of some experimental data on the thermodynamics and kinetics of protein crystallization from this laboratory.

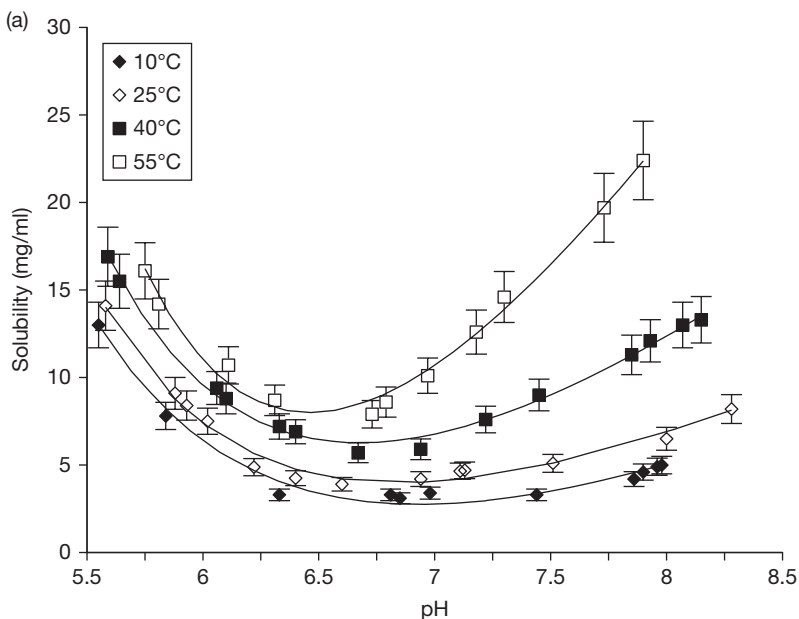
The task, therefore, needs to be completed in a number of stages:

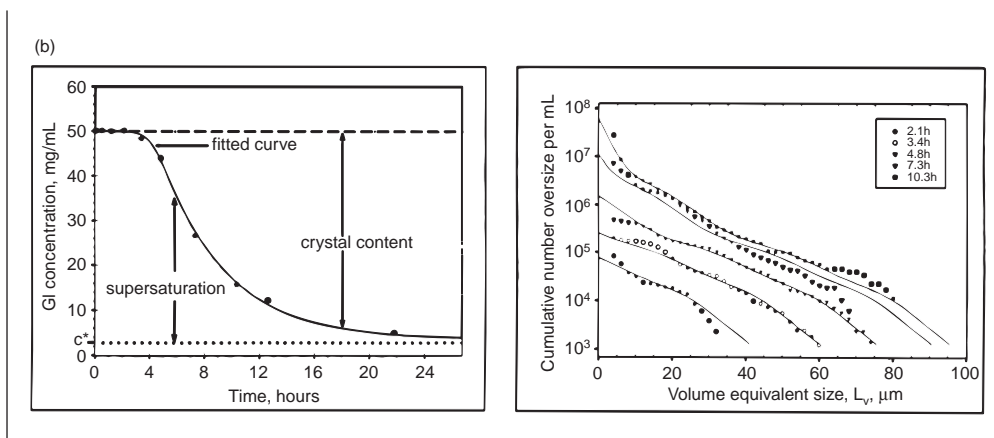
1. Establish the data that need to be obtained from laboratory studies on the crystallization thermodynamics and kinetics and suggest an experimental plan to achieve this.
2. Develop a continuous crystallizer design to meet the specifications described above. In doing this, you should develop a model, using gCrystal or other simulation software, that will give as an output the yield and crystal size distribution from the crystallizer as a function of design parameters for the system.
3. Propose how to instrument and control the crystallizer, and provide advice on operational issues.

Could you please provide me with a one-page memo request to Purdue outlining the proposed kinetic and thermodynamic experiments that need to be conducted. I would like to meet with the team in a week's time to discuss your request and your preliminary thoughts on the crystallizer design. Your final report should be submitted in two months, to coincide with your oral presentation of the design to representatives of the DPP *superpro*<sup>TM</sup> product development team.

### Example Data from Purdue Laboratory

- (a) Solubility of a protein system as a function of temperature and pH
- (b) Crystallization kinetic data for a protein system





Crystallization is an excellent *separation* process. The crystalline product usually has very high purity because the crystal lattice is very selective of the ion or molecule it will allow. However, it is also a *particle design* process. New particles are formed in the process and their properties dramatically impact on downstream processing and end use performance. This is our main interest.

As an individual reflective exercise, or as a group brain-storming discussion, list the design specifications required to complete the process design of the crystallizer and associated equipment – it is quite a long list! Classify your list into *process design* specifications – e.g., impeller motor power – and *product design* specification – e.g., parameters of the crystal size distribution. What types of calculation are required to get these specifications? What data are needed for these calculations? Are such data likely to be available – e.g., from a thermodynamic database, or must it be measured in the lab at Purdue University?

What learning goals related to crystallization does this case study inspire for you and how do they compare with the chapter learning goals given below?

## 4.2 Learning Goals

At the completion of this chapter, the student should be able to:

1. Describe concepts of saturation and supersaturation, the different methods by which supersaturation can be achieved in industrial crystallization, and the use of solubility data to set conditions and calculate yields in industrial crystallizers.
2. State the definitions of key terms in industrial crystallization (saturation, supersaturation, size-independent growth, crystal shape descriptors, etc.).
3. Describe the key mechanisms that control the crystal size distribution (especially nucleation and growth), and what controls the rates of these mechanisms and mathematical descriptions.
4. State the major crystallizer designs/configurations, their advantages and disadvantages and typical applications.

5. Define the shape of a crystal using Miller indices and how shape can be controlled or predicted.
6. Use crystallizer mass, energy, and population balances to address simple problems related to crystallizer design and operation problems similar to those at the end of this chapter.
7. Critically analyze and interpret real crystallization data sets from laboratory or plant trials using appropriate analysis tools.
8. Attack open-ended particle design or troubleshooting problems in crystallization of similar nature to the introductory case study for this chapter.

### 4.3 The Driving Force for Crystallization – Solubility and Supersaturation

Crystallization from solution occurs when there is a thermodynamic driving force for the solute to form a solid phase – i.e., when the crystalline solid has a lower Gibbs free energy than the material as solute in solution. Under these conditions, the solution is said to be *supersaturated*. The driving force for crystallization is the difference between the solute concentration,  $c$  and the concentration at equilibrium at the given thermodynamic state,  $c^*$ . We call this concentration difference the supersaturation,  $s$ :

$$s = c - c^* \quad 4$$

Other measures of crystallization driving force are the relative supersaturation,  $\sigma$  and the supersaturation ratio:

$$\sigma = \frac{c - c^*}{c^*} \quad 2$$

$$\sigma + 1 = \frac{c}{c^*} \quad 3$$

Figure 4.1a gives an example of a simple constant pressure phase diagram where the  $c^*$  increases with temperature in a simple two-component system. In such a system, supersaturation can be achieved by cooling a saturated solution. However, providing a thermodynamic driving force for crystallization does not guarantee crystals will form. The supersaturated portion of the phase diagram is divided into (at least) three regions.

- The *metastable* region. In this region no new crystals will nucleate. If seed crystals are present, they will grow until the supersaturation is depleted. If no seed crystals are present, the solution will remain in a metastable state.
- The *primary nucleation* region. In this region of very high supersaturation, the clear solution will spontaneously form new nuclei crystals. The primary nucleation threshold (PNT) defines the minimum concentration of solute required for primary nucleation and is the lower bound for the primary nucleation regime.

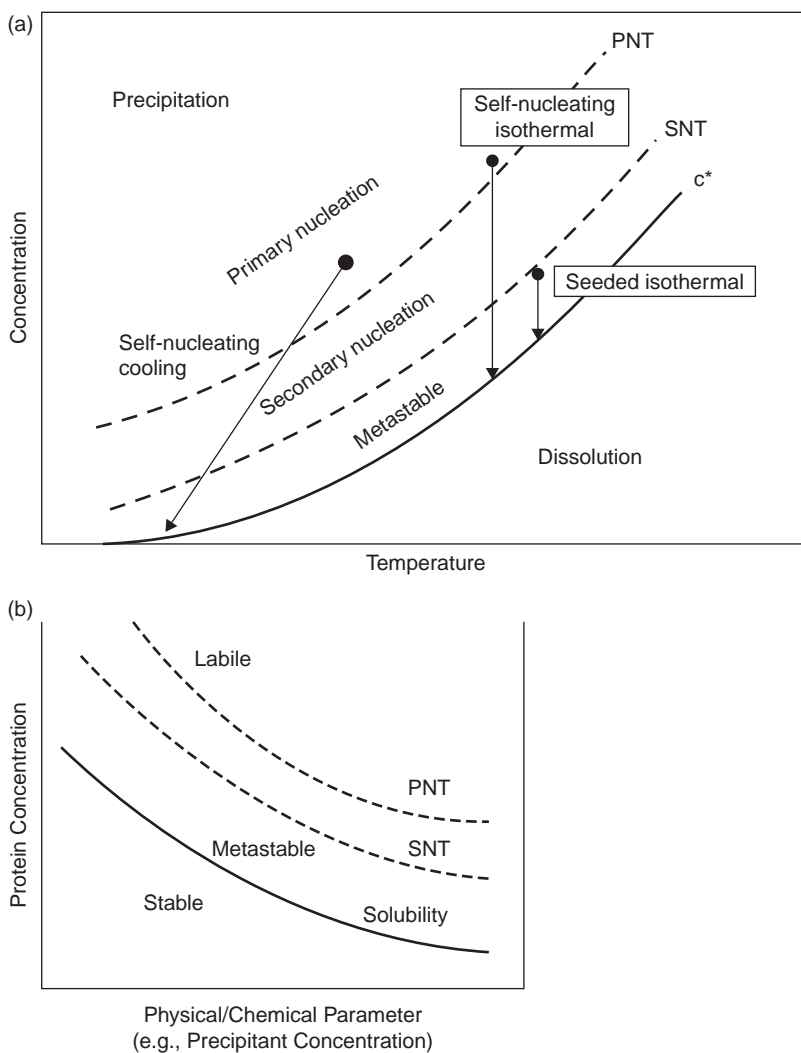


**Figure 4.1** The solubility–supersolubility diagram for a simple two-component system at constant pressure (a) for cooling crystallization, (b) for precipitant or antisolvent crystallization. PNT, primary nucleation threshold; SNT, secondary nucleation threshold;  $c^*$ , solubility.

- The *secondary nucleation* region. In this region, new nuclei crystals will occur only in the presence of existing seed crystals. The lower bound for this region is called the secondary nucleation threshold (SNT) and the upper bound is the PNT.

At very high supersaturation, the precipitation of amorphous solid or the separation of a concentrated liquid phase (“oiling out”) may occur.

Note that the SNT and PNT are not true thermodynamic limits, but also depend on nucleation kinetics. Thus, their position on the phase diagram depends on how they are measured.

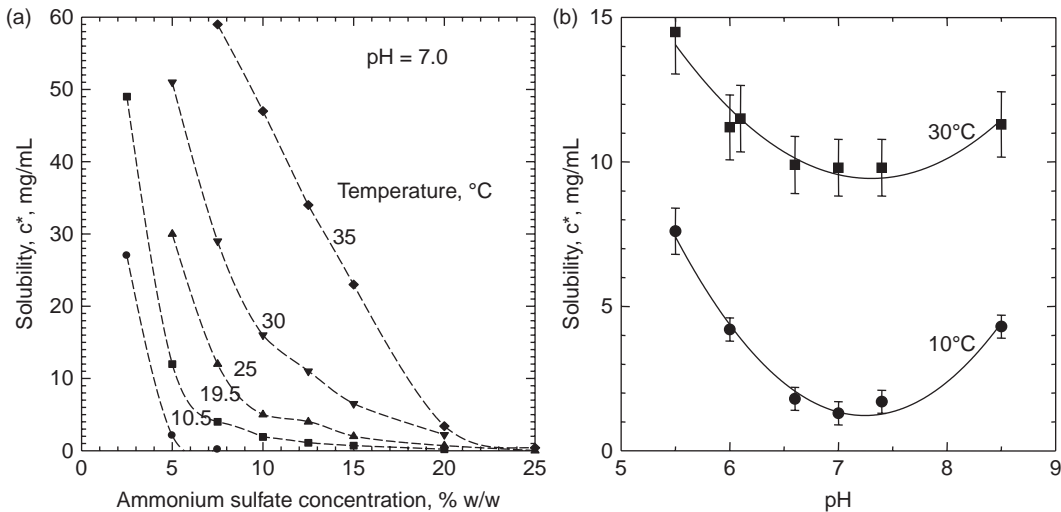


**Figure 4.2** The phase diagram for the enzyme, glucose isomerase. (a) Effect of ammonium sulfate concentration and temperature; (b) effect of pH (Dalziel, 1999).

**Table 4.1** Methods for inducing supersaturation during solution crystallization

Method of inducing supersaturation	Examples
Cooling	Aluminum trihydroxide (alumina refining)
Evaporation	Sucrose
Salting out	Proteins
Antisolvent	Lactose, fructose, ibuprofen

Figure 4.1b shows the solubility–supersolubility for a system where supersaturation is induced by the addition of a precipitant. The phase diagram can be more complex if (1) there are different crystalline phases that can form because there are several polymorphs, or different hydrates may crystallize; or (2) the system has more than two components. Multicomponent systems occur if a second liquid is added to induce crystallization (an antisolvent) or a salt is added for the same reason (salting out). Figure 4.2 shows an example of a phase diagram for a system in which solubility is controlled by the addition of a salt as a precipitant, but is also sensitive to pH and temperature. There are many ways to induce supersaturation for industrial crystallization which depend primarily on the details of the phase diagram. Table 4.1 lists the most common of these approaches with some industrial examples. Establishing the phase diagram is always the first step in developing an industrial crystallization system. Sometimes the solubility curve can be predicted from thermodynamic models, although experimental measurement is still common. The PNT and SNT usually need to be measured.

## 4.4 Crystallizer Design Choices and Configurations

The simplest conceptual design of an industrial crystallizer is a single, well-mixed tank. Many crystallizer designs incorporate a draft tube and propeller-style impeller to promote gentle mixing to avoid crystal breakage while still keeping the crystals fully suspended. Heat transfer, either through internal tubing or via circulation of the contents through an external heat exchanger, is usually necessary.

More complex designs may include fines dissolution or product classification to reduce the fines content in the product. The crystallizer design also depends on the method of generation of supersaturation. Antisolvent crystallizers need to take great care in placement of the antisolvent addition point to maximize good micro-mixing. Evaporative crystallizers often operate under vacuum to prevent degradation of thermally labile materials.

In designing the crystallizer, ancillary operations also need to be considered:

- slurry pumping from the crystallizer. Care is necessary to avoid crystal breakage particularly if a centrifugal pump is used;
- washing of the crystals to remove liquor from the crystal surface to improve purity;
- solid–liquid separation by filtration, centrifugal separation or sedimentation; and
- drying.

Readers are referred to the Bibliography (Section 4.9) for details of the wide variety of equipment designs for crystallizers.

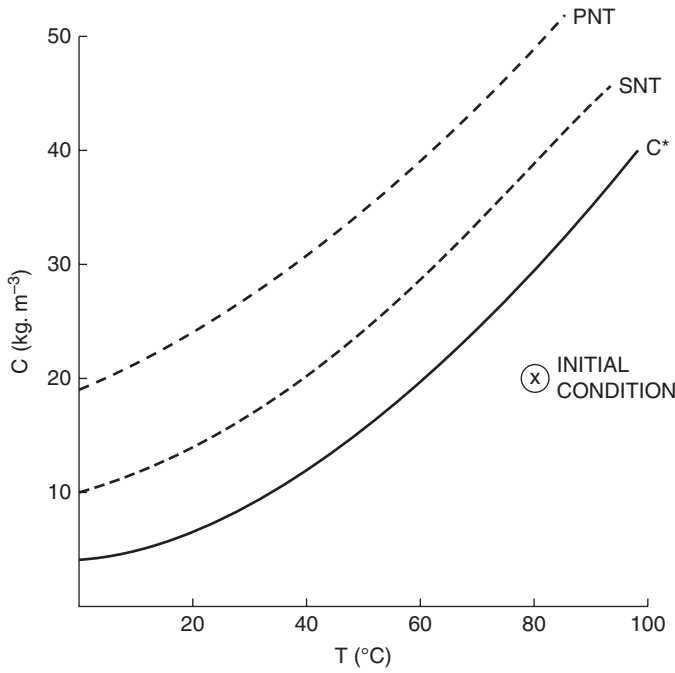
One key design choice in a crystallizer is whether to operate using seed crystals, or using nucleation to generate new crystals. Seeded crystallizers will generally give narrower crystal size distributions provided that the crystallizer is operated in the metastable region to avoid secondary nucleation. Thus, the width of the metastable zone is key to this design choice.

---

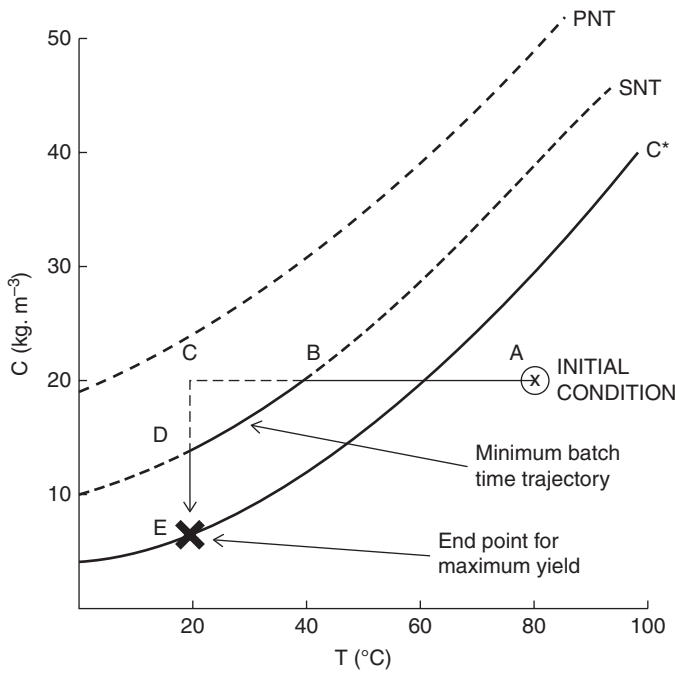
**Example 4.1 Solubility and Crystallization Calculations** The figure below shows the solubility–supersolubility diagram for a particular material A including the primary and secondary nucleation thresholds (PNT and SNT). We have a stream of solution of A at 80°C with a concentration of A of 20 kg m<sup>-3</sup> from which I wish to produce crystalline A.

- (a) In a batch cooling crystallizer, my final temperature is 20°C. What is the maximum crystal yield I can achieve?
- (b) Is it possible to operate the batch cooling crystallizer in part (a) without seed crystals?
- (c) Your crystallizer has excellent online measurement of both temperature and concentration. You have the ability to control the cooling rate based on this information. Sketch a desirable temperature–concentration trajectory for a *seeded* batch cooling crystallizer starting from the given initial conditions and finishing at 20°C subject to the following constraints: (1) no nucleation is allowed, (2) yield should be maximized, (3) batch time should be minimized.





Solubility-supersolubility diagram



Endpoint and optimum trajectory

*Solution:*

(a) Point E is the end point for maximum yield:

$$c = c^*(20^\circ\text{C}) = 6 \text{ kg m}^{-3}$$

Thus the yield is:

$$Y = \frac{(20 - 6)\text{kg.m}^{-3}}{20\text{kg.m}^{-3}} = 0.7$$

- (b) No. The maximum supersaturation that can be achieved is at point C which is still below the PNT. Nucleation will not occur from clear solution, so no crystallization will occur without seed crystals.
- (c) The optimum trajectory is ABDE. The crystallizer is quickly cooled to  $40^\circ\text{C}$  (AB). Following the path BD gives the maximum supersaturation (and therefore maximum growth rate) without entering the secondary nucleation zone. Once the crystallizer is cooled to  $20^\circ\text{C}$ , hold at this temperature until the supersaturation is fully depleted (DE).

## 4.5 Crystallization Rate Processes

A number of the most important product attributes for any crystalline product relate to its crystal size distribution (CSD). Often, relatively large crystals ( $50\text{--}500 \mu\text{m}$ ) are required for efficient solid–liquid separation or to ensure a free-flowing product. For some poorly soluble pharmaceutical drugs, very small crystals ( $< 1 \mu\text{m}$ ) are preferred to maximize the surface area for dissolution. The desired crystal size may be set by downstream processing operations such as blending, granulation, or compaction. For sophisticated applications, the shape of the CSD may also be controlled.

The population balance gives us the ideal mathematical framework for following the generation of the CSD in a crystallizer (Chapter 3). Before we can apply the population balance we need to have suitable rate expression for the key mechanisms that change the number and size of crystals. These mechanisms are nucleation, growth, agglomeration, and breakage. The rate processes of agglomeration and breakage are considered in later chapters. Here, we will address crystal nucleation and growth.

### 4.5.1 Crystal Growth Kinetics

Crystals grow by ions or molecules adding to the crystal lattice on the surface or edge of a crystal. Macroscopically, we can represent the growth rate of a single crystal in terms of the linear growth rate:

$$G = \frac{dx}{dt} \quad 4$$

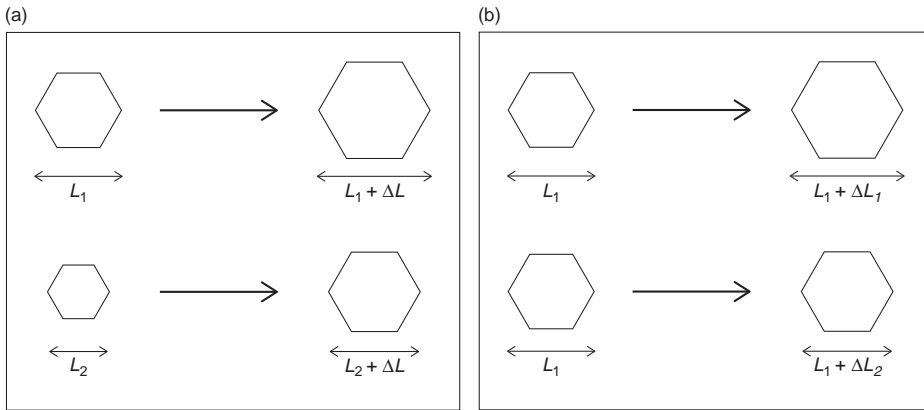


**Figure 4.3** Different growth behaviors of crystals. (a) A system obeying the McCabe  $\Delta L$  law; (b) a system displaying growth rate dispersion.

Here, we will generally use the volumetric equivalent diameter  $d_v$  to represent the crystal size  $x$ . The length of a defined crystal face  $L$  is also commonly used. We commonly assume that  $G$  is independent of size: i.e., small crystals and large crystals have the same linear growth rate (Figure 4.3):

$$G = \frac{dx}{dt} \neq G(x) \quad \text{4}$$

Equation 4.4 is called the *McCabe  $\Delta L$  Law* and holds for a wide variety of systems. This is serendipitous, as it allows us to more easily calculate moments of the CSD and find analytical solutions for the population balance (see Equations 3.7 to 3.9). Industrially relevant growth rates are typically in the range 1–10  $\mu\text{m}/\text{min}$ . Growth rates less than 1  $\mu\text{m}/\text{h}$  are considered too slow to be economically viable, even for high-value products.

Crystal growth rate is a strong function of supersaturation. We represent the growth rate by one of the two following expressions:

$$G = k_g s^a \quad \text{5}$$

$$G = k_g \sigma^a \quad \text{6}$$

The growth rate is controlled by some combination of mass transfer to the crystal surface by diffusion through a stagnant liquid layer and integration of molecule or ion into the crystal lattice (surface integration) (Figure 4.4). For mass transfer-controlled growth,  $a = 1$  and the growth expression is given by:

$$G = \left( \frac{\alpha_{sv} k_l}{3\rho_c} \right) s \quad \text{7}$$

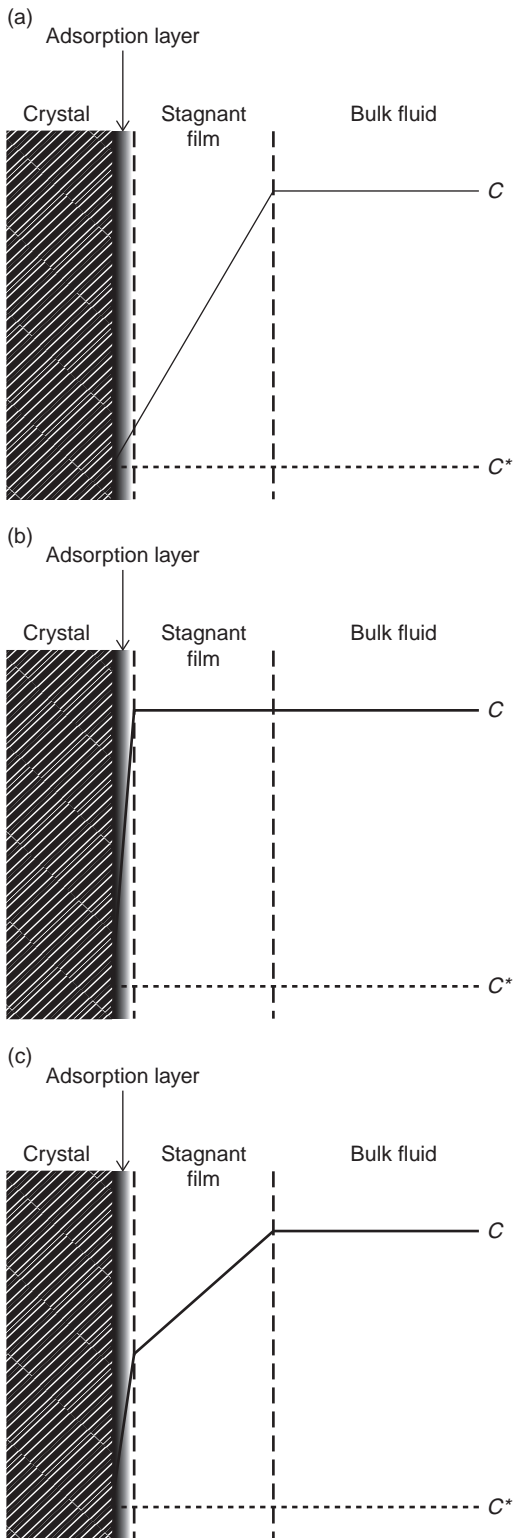


**Figure 4.4** Concentration profiles near the crystal surface for different mechanisms of crystal growth. (a) Mass transfer-controlled; (b) surface integration-controlled; (c) mixed mechanism.

where  $k_l$  is the liquid-phase mass-transfer coefficient for the solute and  $\rho_c$  is the crystal density.

In highly agitated industrial crystallizers, the mass transfer rate is usually fast. Therefore, the crystal growth rate is often controlled by surface integration. There are various theories for the kinetics of crystal growth by surface integration. For example, the Burton, Cabrera, and Frank expression for growth controlled by a screw dislocation is:

$$G \propto \sigma^2 \tanh(B / \sigma) \quad \text{8}$$

where  $B$  is a constant. Equation 4.8 reduces to Equation 4.6b with  $a = 2$  for low relative supersaturation and  $a = 1$  for high relative supersaturation.

In practice, it is difficult to predict the crystal growth rate of a system *a priori* from theoretical calculations. However, for most industrial systems, crystal growth can be represented by either Equation 4.6a or 4.6b where  $a$  lies somewhere in the range 1–2. The growth rate constant  $k_g$  is a function of temperature given by the Arrhenius expression:

$$k_g = k_g^* \exp \left[ -\frac{E_{a,g}}{RT} \right] \quad \text{9}$$

Crystal growth rates are relatively easy to measure in seeded batch crystallization at laboratory scale (Section 4.6). These growth rates scale fairly reliably to large crystallizers. Sometimes problems occur if laboratory measurements are made with pure solutions, but impurities in the industrial liquor reduce the growth rate by adsorbing to active sites on the crystal surface. This is sometimes referred to as *poisoning*.

Figure 4.5 gives an example of laboratory growth rate data for the enzyme glucose isomerase. Note that in this case, the growth order is 2, indicating surface integration-controlled growth. The growth rate increases with temperature as described in Equation 4.9. Figure 4.6 gives an indication of the range of growth rates as a function of relative supersaturation for different types of materials. In general, growth rate decreases with the size and complexity of the ion or molecule to be crystallized.

Some systems display *growth rate dispersion* (GRD) (Figure 4.3b) where not all crystals of the same size display the same growth rate and we have a distribution of growth rates around some mean value. Growth rate dispersion is identified by a broadening of the crystal size distribution during seeded growth experiments. Interestingly, the crystals have a memory. “Slow” growers maintain their slow growth rate no matter how large they grow and the same is true for “fast” growers. For a system displaying GRD, we can usually represent the growth rates with a log-normal distribution (Equation 2.25) with mean growth rate  $G_M$  and geometric

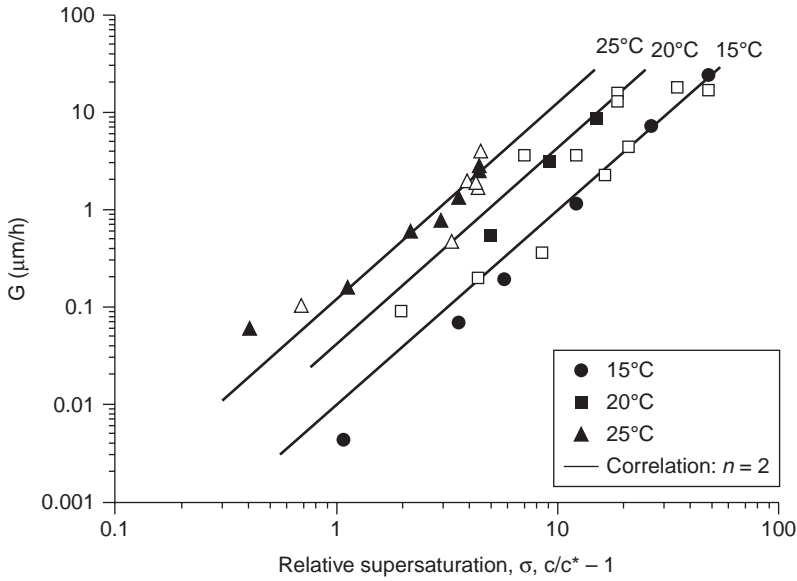


**Figure 4.5** Laboratory growth rate data for glucose isomerase (Dalziel, 1999). The data fit the growth

rate expression  $G = k_g \exp\left[-\frac{165 \text{ kJ mol}^{-1}}{RT}\right] \sigma^2$ .

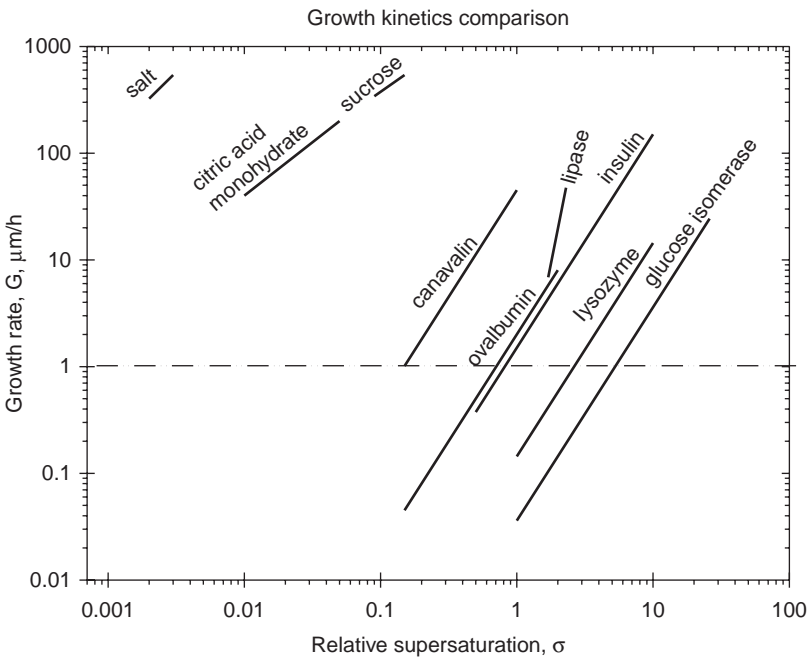


**Figure 4.6** Growth rates as a function of relative supersaturation for different materials (Dalziel, 1999).

standard deviation  $\sigma_g(G)$ . Equations 4.6 to 4.10 are still applicable for correlating  $G_M$ . Typical values of  $\sigma_g(G)$ , which is closely related to the CV of the distribution, are in the range 0.2–0.5. Greater care is required in producing seed crystals for growth rate experiments for systems displaying GRD and a more sophisticated analysis of the data is needed. For further discussion on GRD see White *et al.* (1998).

#### 4.5.2 Crystal Nucleation Kinetics

Crystal nucleation is a complex and stochastic process that is less well understood than crystal growth. We can divide nucleation into two main categories: *primary* and *secondary* nucleation (Figure 4.7). Primary nucleation is the spontaneous creation of new crystals from crystal-free solutions. Secondary nucleation is the creation of new crystals in the presence of seed crystals of the same material. Primary nucleation can be further divided into *homogeneous* and *heterogeneous* primary nucleation. Homogeneous primary nucleation occurs spontaneously from clear solution without the aid of foreign surfaces or particles. Heterogeneous primary nucleation occurs near such surfaces that often reduce the energy barriers for nucleation to occur. In industrial practice, foreign surfaces and particles are always present, so heterogeneous rather than homogeneous primary nucleation will occur. However, only the theory of homogeneous primary nucleation has been fully developed and it is instructive to understanding nucleation processes more broadly so we will briefly describe it here.

Primary nuclei form in solution if a stable cluster of ions or molecules of solute can form spontaneously and reorganize into a crystal lattice. The free energy change,  $\Delta G$  required for a spherical cluster of radius  $r$  to form is given by the expression:

$$\Delta G = 4\pi r^2 \gamma_{ls} - \frac{4}{3}\pi r^3 \frac{kT \ln(\sigma + 1)}{V_m} \quad 40$$

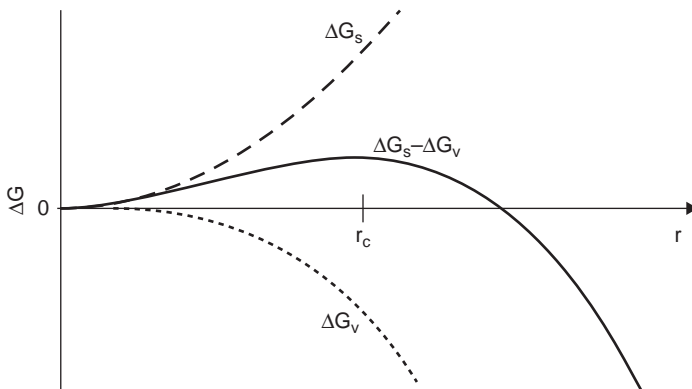


**Figure 4.7** The net free energy to form a spherical cluster is a balance between an increase in surface energy and a decrease in bulk energy.

where  $\gamma_{ls}$  is the liquid–solid interfacial tension at the cluster surface,  $k$  is Boltzmann’s constant, and  $V_m$  is the molar volume of the solute. Note there is a positive contribution due to interfacial energy. It takes energy to create the new surface between the phases. However, there is a negative contribution from the bulk Gibbs energy of the nuclei. The solution is supersaturated, so the solute prefers to be in the solid phase. As  $r$  increases,  $\Delta G$  goes through a maximum (Figure 4.8).

The nucleus will be stable if adding an additional molecule to the cluster reduces  $\Delta G$ . Thus the critical cluster size  $r_{crit}$  and corresponding critical Gibbs energy change  $\Delta G_{crit}$  are calculated at the maximum of Gibbs energy curve:

$$\frac{d(\Delta G)}{dr} = 0 \tag{4.1}$$

Combining Equations 4.10 and 4.11 and performing some calculus gives:

$$r_{crit} = \frac{2\gamma_{ls}}{\Delta G_{crit}} \tag{4.2}$$

$$\Delta G_{crit} = \frac{16\pi\gamma_{ls}^3V_m^2}{3(kT)^2(\ln(\sigma + 1))^2} \tag{4.3}$$

The rate of nucleation can then be given as follows:

$$\dot{B}_{muc} = A \exp\left[\frac{-\Delta G_{crit}}{kT}\right] = A \exp\left[\frac{-16\pi\gamma_{ls}^3V_m^2}{3(kT)^3(\ln(\sigma + 1))^2}\right] \tag{4.4}$$

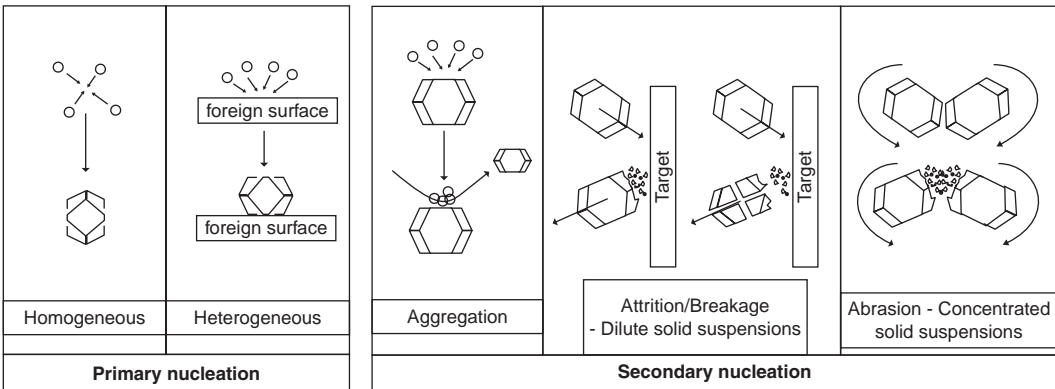


**Figure 4.8** Different mechanisms for primary and secondary nucleation of crystals (Tait, 2005).



In practice, the real value of  $\gamma_{ls}$  is unknown, so  $\gamma_{ls}$  and the pre-exponential factor  $A$  become fitting parameters for nucleation rate expressions for both homogeneous and heterogeneous primary nucleation. Nevertheless, the nucleation theory highlights some important points of practical relevance:

1. Equation 4.14 shows that  $\Delta G_{crit}$  is infinite when  $\sigma = 0$  ( $c = c^*$ ). Until the supersaturation reaches a larger value, the probability of a cluster of size  $r_{crit}$  randomly forming is vanishingly small. This explains the presence of a metastable zone in which crystal growth can occur but there is no nucleation (Figure 4.1).
2. Hot spots due to poor mixing will lead to local areas where the supersaturation exceeds the PNT and nucleation can occur, especially when supersaturation is achieved by the addition of small amounts of a precipitant or antisolvent.
3. Typical values for  $r_{crit}$  are 1–100 nm, so nuclei have often grown substantially before they are observed in the crystallizer, contributing to the nucleation induction time in batch crystallization.

Purely empirical expressions are also used to fit primary nucleation data similar to Equations 4.6 for crystal growth:

$$\dot{B}_{nuc} = k_B s^b \quad 45$$

$$k_B = k_B^* \exp\left[-\frac{E_{a,B}}{RT}\right] \quad 46$$

The nucleation exponent  $b$  can be in the range 5–10, emphasizing how sensitive nucleation rate is to supersaturation level.

Secondary nucleation has lower effective energy barriers than primary nucleation and therefore usually dominates when crystals are present. Two main mechanisms are postulated (Figure 4.8). One is aggregation, in which new nuclei form at or near an existing crystal surface and then separate to form a nucleus crystal. The second is where small fragments of existing crystal are shed by impact with a wall or impeller (attrition) or with other crystals (abrasion). Thus, secondary nucleation rates will be a function of equipment geometry, impeller speed and power, the volume concentration and CSD of existing crystals as well as supersaturation. Empirical correlations of the following form are sometimes used to correlate nucleation rate data in terms of the mass concentration of the crystals and the energy input from the impeller:

$$\dot{B}_{nuc} = k_B (\rho_c \alpha_v \mu'_3)^j s^b \quad 47$$

$$\dot{B}_{nuc} = k_B \left(\frac{N_Q}{N_P}\right) \left(\frac{P}{V}\right) (\rho_c \alpha_v \mu'_3)^j s^b \quad 48$$

where  $N_Q$ ,  $N_p$ , and  $P/V$  are the flow number, power number, and power per unit volume for the mixing tank, respectively, and  $\mu'_3$  is the third moment of the CSD.

Given the discussion above, it is easy to understand why nucleation kinetics are difficult to measure accurately and hard to scale effectively:

- nucleation is a highly non-linear function of supersaturation;
- nucleation thresholds and rates are sensitive to the presence of foreign surfaces, scratches, accretion, etc;
- nucleation rate is a strong function of fluid flow patterns and mixing. Micromixing as well as macromixing is very important. “Hot spots” of supersaturation near feed, precipitant or antisolvent addition points cause nucleation bursts; and
- secondary nucleation is very sensitive to crystal content and CSD.

It is no wonder there are few reliable data available for crystal nucleation compared with crystal growth. This is also one reason why seeded batch crystallization operating in the metastable zone is a preferred mode to operate batch crystallizers.

#### Example 4.2 Estimating Nucleation and Growth Rates

- (a) Data from experimental studies of lactose nucleation at 25°C (Dombrowski *et al.*, 2007) suggest the following values for the pre-exponential factor and interfacial tension in the homogeneous nucleation expression:  $A = 2.9 \times 10^8 \text{ m}^{-3} \text{ s}^{-1}$ ;  $\gamma^v = 5.9 \text{ m Nm}^{-1}$ . How does nucleation rate vary with supersaturation for this system?
- (b) If I assume that the lactose growth rate in my crystallizer is mass-transfer-controlled, estimate the growth rate of 5  $\mu\text{m}$  crystals as a function of supersaturation if we can assume a stagnant liquid layer around the crystal is providing the resistance to mass transfer.

*Solution:*

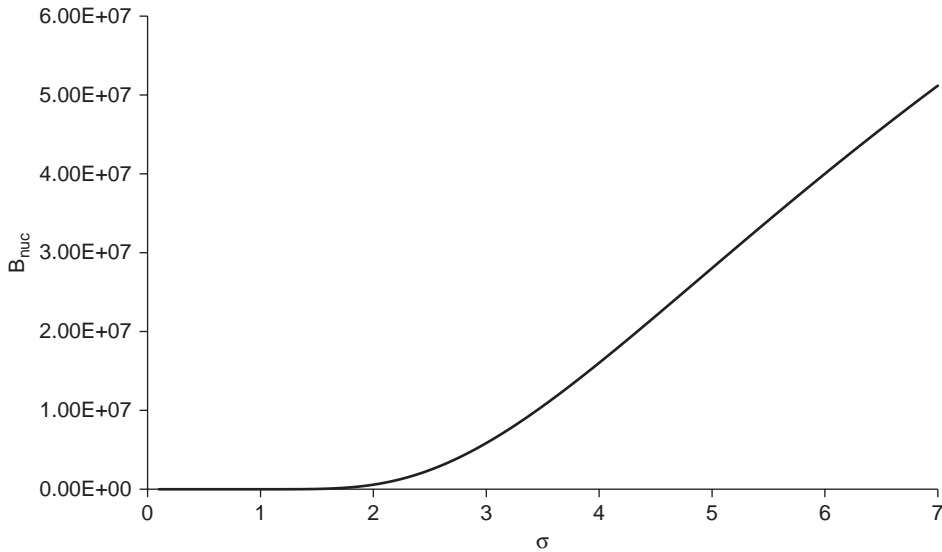
- (a)  $V_m$  is the molecular volume of lactose equal to  $3.9 \times 10^{-28} \text{ m}^3$ .  $T = 298 \text{ K}$ ;  
 $k = 1.38 \times 10^{-23} \text{ J K}^{-1}$ .

Substituting into Equation 4.14:

$$\dot{B}_{nuc} = A \exp \left[ \frac{-16\pi\gamma_{ls}^3 V_m^2}{3(kT)^3 (\ln(\sigma+1))^2} \right] = 2.9 \times 10^8 \text{ m}^{-3} \text{ s}^{-1} \exp \left[ \frac{-7.5}{(\ln(\sigma+1))^2} \right]$$

We can plot the nucleation rate as a function of supersaturation below. Note how the nucleation rate is negligible at low supersaturation and increases very sharply

between  $\sigma = 1$  and 2 for this system. This helps explain the concept of the primary nucleation threshold.



- (b) For mass transfer-controlled growth, the growth expression is given by Equation 4.7.  $\rho_c$  is the density of lactose monohydrate crystal, which is reported to be  $1540 \text{ kg m}^{-3}$ .  $\alpha_{sv}$  is the volume shape factor, estimated as  $1/12$  when the crystal size is defined as the height of the tomahawk shaped crystal (Dombrowski *et al.*, 2007). By assuming that a stagnant liquid layer around the crystal is providing the resistance to mass transfer, the mass-transfer coefficient is given by the Ranz–Marshall equation at zero velocity (refer to Chapter 10 for more details):

$$\text{Sh} = \frac{k_l d_p}{D} = 2$$

where Sh is the Sherwood number,  $d_p = 2r = 5 \text{ }\mu\text{m}$  is the particle diameter, and  $D$  is the mass diffusivity of the solute in the solvent. The mass diffusivity  $D$  for  $0.1 \text{ M}$  lactose aqueous solution at  $25^\circ\text{C}$  is reported as  $5.41 \times 10^{-10} \text{ m}^2 \text{ s}^{-1}$  (Ribeiro *et al.*, 2006). The liquid-phase mass-transfer coefficient for lactose can then be calculated with the above equation:

$$k_l = \frac{\text{Sh}D}{d_p} = \frac{2 \times 5.41 \times 10^{-10} \text{ m}^2 / \text{s}}{5 \times 10^{-6} \text{ m}} = 2.16 \times 10^{-4} \text{ m / s}$$

Therefore, the growth rate of lactose can be expressed as a function of supersaturation by substituting into Equation 4.7:

$$G = \frac{\left(\frac{1}{12}\right) \times 2.16 \times 10^{-4} \text{ m/s}}{3 \times 1540 \text{ kg/m}^3} \times s = 3.9 \times 10^{-9} \left[ \frac{\text{m}^3}{\text{kg}} \right] \left[ \frac{\text{s}}{\text{m}} \right] s$$

For example, if  $s = 100 \text{ kg m}^{-3}$  then  $G = 0.39 \text{ } \mu\text{m s}^{-1} = 23 \text{ } \mu\text{m min}^{-1}$ . This is a relatively high growth rate, suggesting that for small lactose crystals, growth rate may be controlled by surface integration.

## 4.6 Crystallizer Analysis and Design

### 4.6.1 Batch Crystallizers

The population balance developed in Chapter 3 provides a powerful tool for analysis of both batch and continuous crystallizers. First, let us consider the growth of crystals in a seeded batch crystallizer operating within the metastable zone so there is no nucleation occurring. If we assume no breakage or agglomeration of crystals, then the population balance (Equation 3.3) reduces to:

$$\frac{\partial n(x,t)}{\partial t} = -\frac{\partial Gn(x,t)}{\partial x} \quad 49$$

If we further assume size-independent growth:

$$\begin{aligned} \frac{\partial n(x,t)}{\partial t} &= -G \frac{\partial n(x,t)}{\partial x} \\ \Rightarrow G &= -\frac{\partial n / \partial t \Big|_x}{\partial n / \partial x \Big|_t} = \frac{\partial x}{\partial t} \Big|_n \end{aligned} \quad 20$$

i.e., the size distribution will be shifted to increasing size but will maintain the same shape (Figure 4.9):

$$n(x, t + \Delta t) = n(x - \Delta x, t) \quad \text{where} \quad \Delta x = \int_t^{t+\Delta t} G dt \quad 21$$

The corresponding moments form of the population balance, derived from Equation 3.8, is:

$$\frac{d\mu'_k}{dt} = kG\mu'_{k-1} \quad k \geq 1 \quad 22a$$

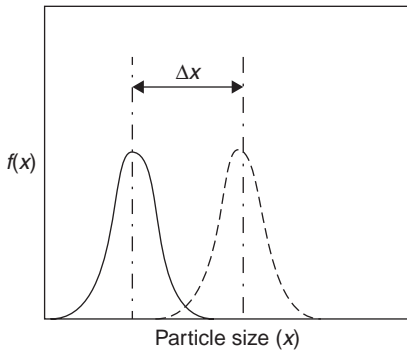


**Figure 4.9** Movement of the CSD along the size axis for size-independent growth in a seeded batch crystallizer.

$$\frac{d\mu'_0}{dt} = 0 \Rightarrow \mu'_{0,t} = \mu'_{0,i} \quad 42b$$

As we intuitively expect, the total number of crystals in the system does not change with time, but all the higher moments do. We can use Equation 4.22 directly to write the rate of change of many properties of the CSD. For example:

$$\frac{d\bar{x}_{1,0}}{dt} = G \Rightarrow \bar{x}_{1,0}(t) - \bar{x}_{1,0}(0) = \int_0^t G dt = \Delta x \quad 43$$

**Example 4.3 Measuring Growth Kinetics from a Seeded Batch Crystallizer** Figure E4.3 shows data for a seeded batch crystallization of ovalbumin. The crystal size distribution (shown as  $100(1 - F(x))\%$ ) is plotted for samples taken from the crystallizer at various times in Figure 4.E3a. Figure E4.3b shows the corresponding supersaturation data for ovalbumin in solution. What useful conclusions can you draw from the form of the size distribution data? Calculate the growth rate as a function of supersaturation and compare the data with Equation 4.6a.

*Solution:*

Note that the cumulative distribution curves are approximately parallel, indicating that the size-independent growth assumption is reasonable. From Equation 4.21, it follows that:

$$F(x, t + \Delta t) = F(x - \Delta x, t)$$

$$\Delta x = \int_t^{t+\Delta t} G dt \approx G \Delta t$$

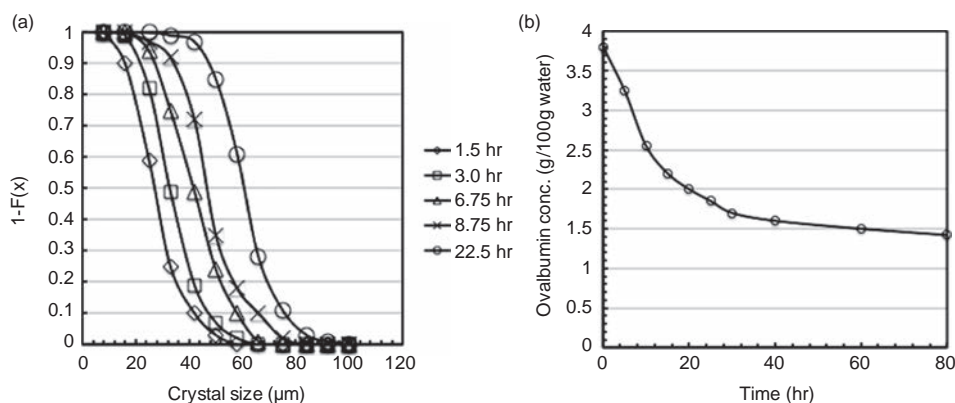


**Figure E4.3** Data from the seeded, batch crystallization of ovalbumin. (a)  $100\%(1 - F(x))$  vs.  $x$ , (b)  $c$  vs.  $t$  (Judge, 1995).

We can use these equations for any value of  $F$ . For example, for  $F = 0.5$ , comparing the size distributions after 1.5 h and 3.0 h gives:

$$G = \frac{x_{50,3\text{hr}} - x_{50,1.5\text{hr}}}{(3 - 1.5)\text{hr}} = \frac{(33 - 27)\mu\text{m}}{1.5\text{hr}} = 4\mu\text{m}\cdot\text{hr}^{-1}$$

This is the average growth rate over the period 1.5–3 h, which we take as the estimate of the growth rate at the mid point of the interval  $\bar{t} = 2.25\text{hr}$ . From Figure 4. E3b, the associated ovalbumin concentration at this time is 3.3 g/100 g water, and the supersaturation is:

$$s = c - c^* = 33 - 12\text{g} / 100\text{g} = 21\text{g} / 100\text{g}$$

Repeating this process, we can produce a table of growth rate vs. supersaturation:

$t_i$ (h)	$x_{50}$ ( $\mu\text{m}$ )	$\bar{t}$ (h)	$G = \Delta x / \Delta t$ ( $\mu\text{m h}^{-1}$ )	$c$ (g/100 g)	$s$ (g/100 g)
1.5	27	2.25	4	3.3	2.1
3.0	33	4.88	2.4	3.0	1.8
6.75	42	7.75	2.5	2.75	1.55
8.75	47	15.6	1.02	2.1	0.9
22.5	61				

Growth rate increases with increasing supersaturation, as expected, although there is clearly some scatter in this set of real data.

Batch crystallizer analysis can also be useful to answer design questions. Given known crystallization kinetics, we can do calculations to answer questions such as:

- What are the properties of the final CSD?
- What is the required batch time if the required recovery is 95%?

To answer such questions, we need to realize that the crystallizer mass balance and population balance are coupled. For a seeded, batch crystallizer with no nucleation, from Equation 4.21 we can write:

$$\Delta x_f = x|_{n,f} - x|_{n,i} = \int_0^{t_f} G dt \quad 24$$

where the subscripts  $f$  and  $i$  denote the final and initial batch conditions, respectively. However,  $G$  is a function of supersaturation that is changing with time as the growing crystals remove solute mass from the solution. We can write the solute mass balance as:

$$V(c_f - c_i) = V(s_f - s_i) = V\rho_c\alpha_v(\mu'_{3,f} - \mu'_{3,i}) \quad 25$$

We can write an expression for  $\mu'_3$  by repeated application of Equation 4.22:

$$\mu'_{3,f}(t) = \mu'_{3,i} + 3\mu'_{2,i}\Delta x_f + \mu'_{1,i}\Delta x_f^2 + 6\mu'_{0,i}\Delta x_f^3 \quad 26$$

If the growth kinetics are known, we can solve Equations 4.6, 4.24, 4.25, and 4.26 simultaneously to give the CSD and the solution concentration as a function of time.

## 4.6.2 The MSMPR Continuous Crystallizer

The simplest design of a continuous crystallizer is a single, mixed tank fed by a stream containing the feed solution. There may be a separate inlet stream containing seed crystals, antisolvent, or precipitant. The crystal-containing slurry overflows from the crystallizer as the exit stream.

Our starting point for analyzing such a system is to consider it as a *mixed suspension, mixed product removal crystallizer (MSMPR)*. We consider the fluid in the crystallizer to be perfectly mixed (no concentration or temperature gradients) and the product overflow fluid has the same properties as the fluid in the crystallizer. This is exactly analogous to the CSTR in classical reactor engineering analysis. Furthermore, we make the same assumptions about the particulate phase; i.e., the CSD is the same everywhere in the crystallizer and also in the product overflow. In practice, this is much more difficult to achieve as gravity is always acting to encourage the crystals to settle. A propeller-type impeller, a central draft tube, wall baffles, and perhaps a round bottom are often used to prevent settling and keep the crystallizer “well-mixed.”

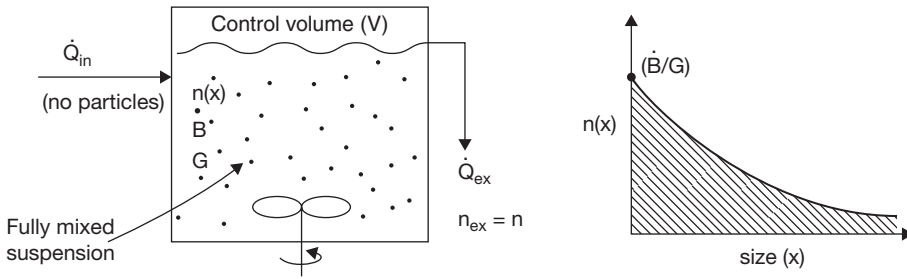


Figure 4.10 A nucleating MSMPR crystallizer.

Let us start by analyzing the MSMPR as shown in Figure 4.10. Growth (size-independent) and nucleation (at zero size) occur in our well-mixed vessel, but no particles enter with the feed. First we write the population balance. From Equation 3.3 we have:

$$\frac{\partial Vn(x,t)}{\partial t} = \dot{Q}_{in}n_{in}(x) - \dot{Q}_{ex}n_{ex}(x) - V \frac{\partial Gn(x,t)}{\partial x} + V\dot{b}(x) - V\dot{d}(x) \tag{33}$$

Based on our assumptions, we can make the following simplifications:

- no particles in the feed  $n_{in}(x) = 0$ ;
- no breakage or agglomeration  $\dot{d}(x) = 0$ ;
- consider steady-state only  $\frac{\partial Vn(x,t)}{\partial t} = 0$ ;
- representative overflow  $n_{ex}(x) = n(x)$ ;
- nucleate at zero size  $\dot{b}_{nuc}(x) = \dot{B}\delta(x)$ ; and
- size-independent growth  $\frac{\partial Gn}{\partial x} = G \frac{\partial n}{\partial x}$

Making all these substitutions into Equation 3.3 gives:

$$\begin{aligned} 0 &= -\dot{Q}_{ex}n(x) - VG \frac{\partial n(x,t)}{\partial x} + V\dot{B}\delta(x) \\ \Rightarrow G \frac{\partial n(x,t)}{\partial x} &= \dot{B}\delta(x) - \frac{n(x)}{\tau} \quad \text{where} \quad \tau = \frac{V}{\dot{Q}_{ex}} \end{aligned} \tag{47}$$

where  $\tau$  is the mean residence time of a crystal in the vessel. Equation 4.25 is a first-order linear differential equation that we can solve analytically. First, note that the zeroth moment this population balance, derived from Equation 3.11, is:

$$\dot{B} = \frac{\dot{Q}_{ex}N_T}{V} = \frac{N_T}{\tau} \tag{48}$$



Then solve Equation 4.25 for the domain  $x > 0$  because the nucleation term is zero in all this domain. Integrating Equation 4.25 gives:

$$\begin{aligned}\frac{dn}{n} &= -\frac{dx}{G\tau} \\ \Rightarrow \ln n \Big|_{n(0)}^{n(x)} &= -\frac{x}{G\tau} \Big|_0^x \\ \Rightarrow n(x) &= n(0)\exp\left(-\frac{x}{G\tau}\right)\end{aligned}\quad 29$$

Finally, by definition:

$$N_T = \int_0^\infty n(x)dx = \int_0^\infty n(0)\exp\left(-\frac{x}{G\tau}\right)dx = n(0)G\tau \quad 30$$

Substituting from Equations 4.26 and 4.28 into Equation 4.27 gives the final solution:

$$n(x) = \frac{\dot{B}}{G} \exp\left(-\frac{x}{G\tau}\right) \quad 31$$

This size distribution in the crystallizer (and in the representative overflow) is exponential and is therefore very broad. This is really because the residence time distribution of particles in the crystallizer is exponential. The longer particles remain in the control volume, the larger they grow.

The seeded MSMPR (Figure 4.11) is very similar to the nucleating MSMPR except that new crystals are supplied by the inlet stream as seed, not by nucleation; i.e., we have the same assumptions and simplifications except that  $n_{in}(x) \neq 0$  but  $\dot{b}(x) = 0$ . With these new assumptions, the population balance reduces to:

$$G \frac{dn(x)}{dx} = \frac{(n_{in}(x) - n(x))}{\tau} \quad 32$$

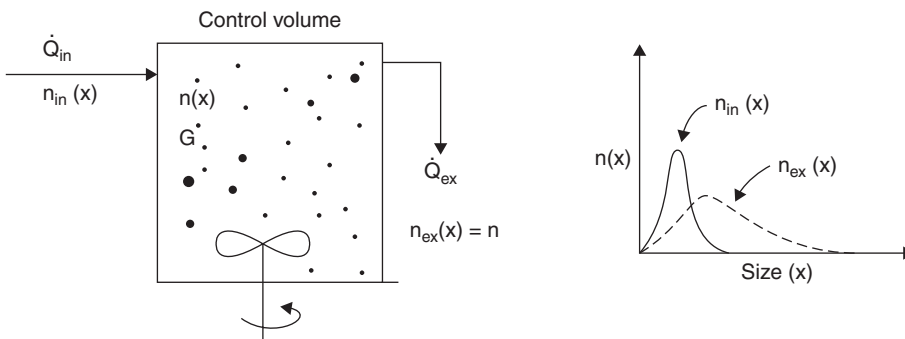


Figure 4.11 A seeded MSMPR crystallizer.

and the zeroth moment balance is:

$$\dot{Q}_{in} N_{in} = \dot{Q}_{ex} N_T \quad 33$$

Equation 4.32 is a linear ODE, which is true for any inlet size distribution. Once  $n_{in}(x)$  is specified, it can be solved numerically, or analytically by using the integration factor approach to give:

$$n(x) \exp\left(-\frac{x}{G\tau}\right) - n(0) = \frac{I}{G\tau} \int_0^x n_{in}(x) \exp\left(-\frac{x}{G\tau}\right) dx \quad 34$$

For example, if the control volume is fed with particles which all have the same size,  $x_{in}$ , then  $n_{in}(x) = N_{in} \delta(x - x_{in})$ . Equation 4.32 or 4.34 is solved to give:

$$n(x) = \frac{N_{in}}{G\tau} \exp\left[-\frac{x - x_{in}}{G\tau}\right] \text{ for } x > x_{in} \quad 4.35$$

Note the similarity to Equation 4.31. Of course, in practice,  $n_{in}(x)$  will be a more complex distribution for which we may have little information. Nevertheless, we can always get an analytical solution for the moments of the distribution:

$$\frac{I}{\tau} (\mu'_k - \mu'_{k,in}) = kG\mu'_{k-1} \Rightarrow \mu'_k = \mu'_{k,in} + kG\tau\mu'_{k-1} \quad 36$$

For example:

$$\bar{x}_{10} = \mu'_1 / \mu'_0 = \bar{x}_{10,in} + G\tau \quad 37$$

No matter what shape the inlet size distribution, the mean size will always be shifted by a distance  $G\tau$ .

Note that in this analysis of an MSMPR we assume size-independent growth. The analysis of an MSMPR for a system exhibiting GRD is also available but not included here (see White, 2002).

---

**Example 4.4 MSMPR Analysis** An MSMPR crystallizer operates with the growth rate of crystals is  $50 \mu\text{m h}^{-1}$  and the nucleation rate is  $10^{10} \text{m}^{-3} \text{h}^{-1}$ . The slurry flow rate out of the crystallizer is  $10 \text{m}^3 \text{h}^{-1}$  and the crystallizer volume is  $5 \text{m}^3$ .

- What fraction of the crystal product is less than  $10 \mu\text{m}$ ?
- Explain qualitatively what changes could be made to the crystallizer configuration or operating conditions to give a narrower crystal size distribution.

We propose to remove the fines problem by controlling the crystallizer to give no nucleation. Instead, we will input monosized seed crystals that are  $10 \mu\text{m}$  in size at a number rate equivalent to the previous nucleation rate.

- (c) What is the mean size of the product crystals?  
 (d) What will be the standard deviation of the product CSD?

*Solution:*

First, the total numbers balance for the MSMPR gives (Equation 4.28):

$$N_T = \dot{B}\tau$$

Here, the mean residence time  $\tau$  is:

$$\tau = \frac{V}{\dot{Q}} = \frac{5\text{m}^3}{10\text{m}^3\text{hr}^{-1}} = 0.5\text{hr}$$

The frequency size distribution for a nucleating MSMPR is given by Equation 4.31:

$$n(x) = \frac{\dot{B}}{G} \exp\left(-\frac{x}{G\tau}\right)$$

The normalized cumulative distribution can be written as:

$$F(x) = \frac{\int_0^x n(x) dx}{N_T} = \frac{\int_0^x \dot{B}/G \exp\left(-\frac{x}{G\tau}\right) dx}{\dot{B}\tau} = 1 - \exp\left(-\frac{x}{G\tau}\right)$$

Thus, the fraction of crystals less than 20  $\mu\text{m}$  is:

$$F(20\mu\text{m}) = 1 - \exp\left(-\frac{20\mu\text{m}}{50\mu\text{m}\cdot\text{hr}^{-1}\cdot 0.5\text{hr}}\right) = 0.551$$

This is the answer to part (a). For part (b), first note that a simple MSMPR always gives an exponential crystal size distribution because the residence time distribution in the well-mixed tank is exponential (Equation 4.31). Consider the moments of the distribution. From Equation 4.36, with nucleation only (no seed), we can write:

$$\mu'_k = kG\tau\mu'_{k-1} \text{ for } k \geq 1$$

Thus, the mean size  $\bar{x}_{10}$  is given by:

$$\bar{x}_{10} = \frac{\mu'_1}{\mu'_0} = \frac{G\tau\dot{B}\tau}{\dot{B}\tau} = G\tau$$

A good indicator of the spread of the distribution is the relative standard deviation:

$$\frac{\sigma}{\mu_1} = \frac{(\mu_2 - \mu_1^2)^{1/2}}{\mu_1} = \frac{(2(G\tau)^2 - (G\tau)^2)^{1/2}}{G\tau} = 1$$

Note that the relative standard deviation is constant. Simply changing the process conditions to change  $G$  or  $\tau$  is not helpful. Three other approaches might be tried.

1. Modifying the residence time distribution to make it narrower. This could be achieved by placing several smaller MSMPR crystallizers in series, or by using a plug flow crystallizer such as a tubular crystallizer or oscillatory baffle crystallizer.
2. Fines dissolution. In this approach, nucleation is controlled by circulating the slurry through a heat exchanger so that the solution becomes undersaturated. Small crystals will disappear due to dissolution.
3. Classified product stream. An external or internal classifier only lets large crystals leave the crystallizer. This effectively makes the crystal residence time closer to plug flow while not effecting the fluid residence time distribution.

To answer parts (c) and (d), we can use the moments form of the population balance for a seeded MSMPR (Equation 4.36):

$$\mu'_0 = N_{in}$$

$$\mu'_1 = \mu'_{1,in} + G\tau\mu'_0 = N_{in} (x_{in} + G\tau)$$

$$\mu'_2 = \mu'_{2,in} + 2G\tau\mu'_1 = N_{in} (x_{in}^2 + 2G\tau x_{in} + 2(G\tau)^2)$$

Knowing these moments, we can calculate the mean size:

$$\bar{x}_{1,0} = \mu_1 = \frac{\mu'_1}{\mu'_0} = x_{in} + G\tau = 10\mu\text{m} + 50\mu\text{m}\cdot\text{hr}^{-1} \cdot 0.5\text{hr} = 35\mu\text{m}$$

Similarly, after some algebraic manipulation, we can show:

$$\sigma = (\mu_2 - \mu_1^2)^{1/2} = G\tau = 25\mu\text{m}$$

Interestingly, the CSD standard deviation from the seeded crystallizer is the same as for the nucleating crystallizer, but the mean size can be independently controlled by varying the size of the seed crystals.

To this point, we have ignored the mass balance in our analysis of the MSMPR. In practice, the mass balance usually constrains the growth rate that can be achieved. The mass flowrate of crystals leaving the crystallizer can be written in terms of the third moment of the product CSD:

$$\dot{m}_{c,p} = \alpha_v \rho_c \dot{Q} \mu'_3$$

Our mass balance relates the crystal production to the decrease in concentration of the solute in solution:

$$\dot{m}_{c,p} - \dot{m}_{c,in} = \dot{Q}(s_{in} - s) \quad 39$$

Substituting for  $\mu'_3$  from Equation 4.36 into Equation 4.38 gives the following expression for the mass flow rate of product crystals:

$$\dot{m}_{c,p} = \rho_c \alpha_v \dot{Q} (\mu'_{3,in} + 3G\tau\mu'_2) \quad 40$$

If there is no seed (nucleation at zero size provides all new particles), by repeated use of Equation 4.34, we can derive:

$$\dot{m}_{c,p} = 6\rho_c \alpha_v \dot{B}_{nuc} G^3 \tau^4 \dot{Q} \quad 41$$

Then Equations 4.39, 4.41 and expressions for  $G$  and  $\dot{B}_{nuc}$  such as Equations 4.6 and 4.15 can be solved simultaneously to give  $s$ ,  $\dot{m}_{c,p}$ ,  $G$ , and  $\dot{B}_{nuc}$ . Then, Equation 4.31 is applied to give the full CSD. Figure 4.12 shows graphically how the operating point for the crystallizer is set by the balance between the mass balance (Equation 4.39) and the population balance (Equation 3.41).

On the other hand, if we have a seeded MSMPR with no nucleation, we can derive the following equation for the mass flow rate of product crystals:

$$\dot{m}_{c,p} = \rho_c \alpha_v \dot{Q} (\mu'_{3,in} + 3G\tau\mu'_{2,in} + 6(G\tau)^2 \mu'_{1,in} + 6(G\tau)^3 \mu'_{0,in}) \quad 42$$

Equations 4.6, 4.39, and 4.42 can then be solved to give  $s$ ,  $\dot{m}_{c,p}$ , and  $G$  provided the moments of the seed crystal size distribution are known.

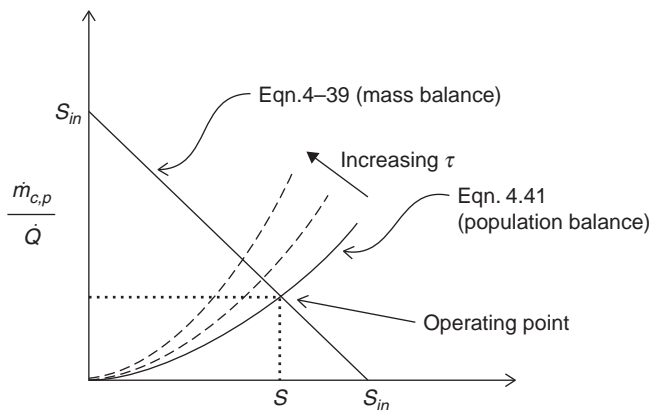


**Figure 4.12** The operating point of an MSMPR is set by the mass balance and the population balance.

## 4.7 Crystal Engineering

To this point, we have focused on design of the *crystallizer*, specifically the requirements to achieve a certain crystal mean size and size distribution while maximizing the yield of crystals. However, other crystal properties are also important, including the shape and morphology. Control of shape and morphology requires us to examine crystallization at the scale of the single crystal – i.e., crystal design.

All crystal shapes are based on seven basic crystal systems (see Table 4.2). The systems are defined in terms of three axes  $x$ ,  $y$ , and  $z$ , where  $z$  is the vertical axis and the angles between the axes  $\alpha$ ,  $\beta$ , and  $\gamma$ . The different crystal systems lead to different classes of crystal shape. However, within one crystal system, a wide variety of shapes can still be seen due to differences in the relative growth rates of the different crystal faces.

To quantify such effects, we need a nomenclature to identify the crystal faces. For this we use *Miller Indices*. Figure 4.13a illustrates the Miller Indices for two types of crystal faces seen in the regular crystal system: cubic and octahedral faces. The cubic face A intersects the  $x$  axis at unity [1], and intersects the  $y$  and  $z$  axes at infinity. The indices of this face are  $\left(\frac{1}{1} \frac{1}{\infty} \frac{1}{\infty}\right)$  or (100). Face B is a similar type of face that intersects only the  $y$  axis and is designated as (010). The face opposite face A will intersect the  $x$  axis at  $-1$  and is designated as  $(\bar{1}00)$ , and so on. The octahedral faces intersect the  $x$ ,  $y$ , and  $z$  faces at equal distances from the origin. Thus face A is (111), face B is  $(1\bar{1}\bar{1})$ , and so on. Figure 4.13b shows that an array of crystal shapes (habits) can be generated for the regular crystal system from just (100)- and (111)-type faces with the cube and the octahedron being the extremes.

**Table 4.2** The seven crystal systems (modified from Mullin, 2001).

System	Angle between axes	Length of axis	Examples
Regular	$\alpha = \beta = \gamma = 90^\circ$	$x = y = z$	Sodium chloride Diamond
Tetragonal	$\alpha = \beta = \gamma = 90^\circ$	$x = y \neq z$	Rutile Zircon
Orthorhombic	$\alpha = \beta = \gamma = 90^\circ$	$x \neq y \neq z$	Iodine Silver nitrate
Monoclinic	$\alpha = \beta = 90^\circ \neq \gamma$	$x \neq y \neq z$	Sucrose Oxalic acid
Triclinic	$\alpha \neq \beta \neq \gamma \neq 90^\circ$	$x \neq y \neq z$	Copper sulfate
Trigonal	$\alpha = \beta = 90^\circ \neq \gamma$	$x = y = z$	Sodium nitrate
Hexagonal	$z$ axis perpendicular to $x$ , $y$ , and $u$ axes which are inclined at $60^\circ$	$x = y = u \neq z$	Graphite Water (ice)

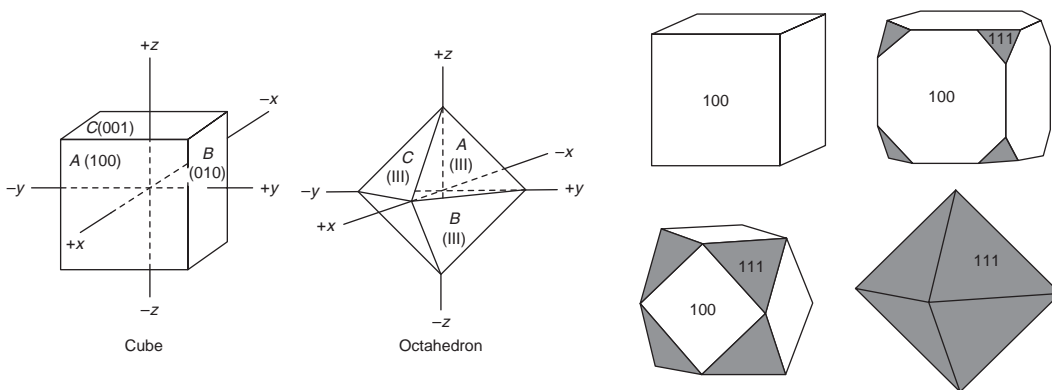


**Figure 4.13** (a) Illustration of the Miller Indices for cubic and octahedral faces of regular system crystals; (b) variety of different crystal shapes from the regular crystal system.

The crystal shape (habit) changes as the relative growth rate of the crystal faces changes. Counterintuitively, the largest faces on the crystal are the *slowest*-growing faces. The fast-growing faces grow out to a point. So for a cubic crystal, the (100)-type faces are slow-growing and the (111)-type faces show only as the eight corners of the cube. Figure 4.14 illustrates this phenomenon for a real system, the protein lysozyme. The (110) and (101) face growth rates have different dependencies of lysozyme concentration (supersaturation). At low concentration, the (110) faces grow slowly and dominate the crystals, which are needle-shaped. At high concentration the (101) faces grow slowly and plate-like crystals are formed.

Crystal face growth rates are a function of the same parameters of the overall crystal growth rate: supersaturation, temperature, type of solvent, and the presence of additives that may preferentially poison growth on particular faces. Traditionally, controlling the crystal habit was very much a black art and handbooks contain long lists of additives that influence the habit of different types of crystals. More recently, sophisticated modeling and simulation techniques are used to predict the relative growth rates of crystal faces and hence the crystal habit, although these are beyond the scope of this text.

While predicting crystal shape and habit may already seem tricky enough, a number of other factors can influence the shape of a crystal.

- (a) *Polymorphism*. Polymorphism occurs when a particular molecular species can pack into different unit cell arrangements, leading to the possibility of one substance crystallizing in different crystal systems, called polymorphs. This can occur when crystallizing under different conditions, or from different solvents, or by using seed crystals of a particular polymorph. Sometimes, polymers of the same materials can have different properties; e.g., chemical stability of an active pharmaceutical ingredient.

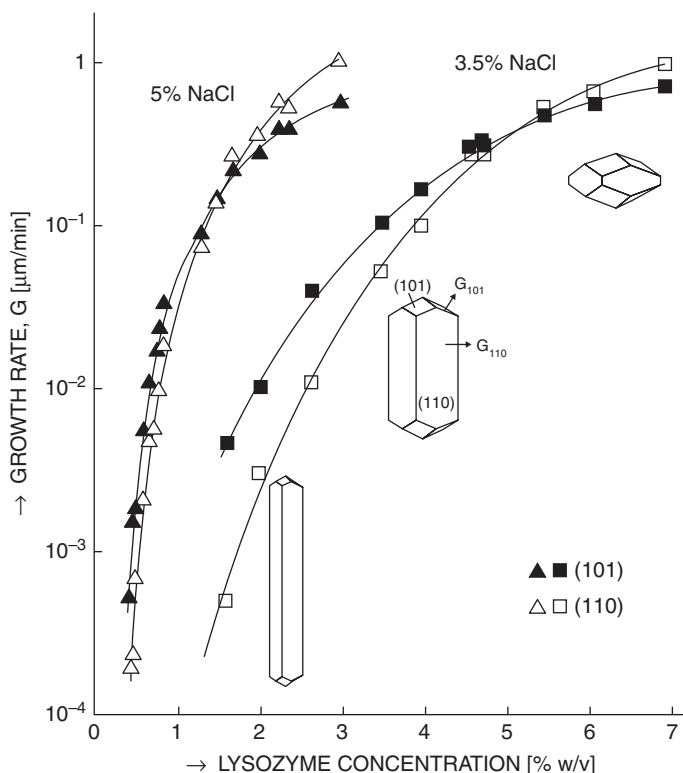


**Figure 4.14** Growth rates of lysozyme crystal faces as a function of lysozyme concentration at 24°C, pH 4.6, and 3.5% NaCl and dependence of crystal shape on concentration (Durbin and Feber, 1986).

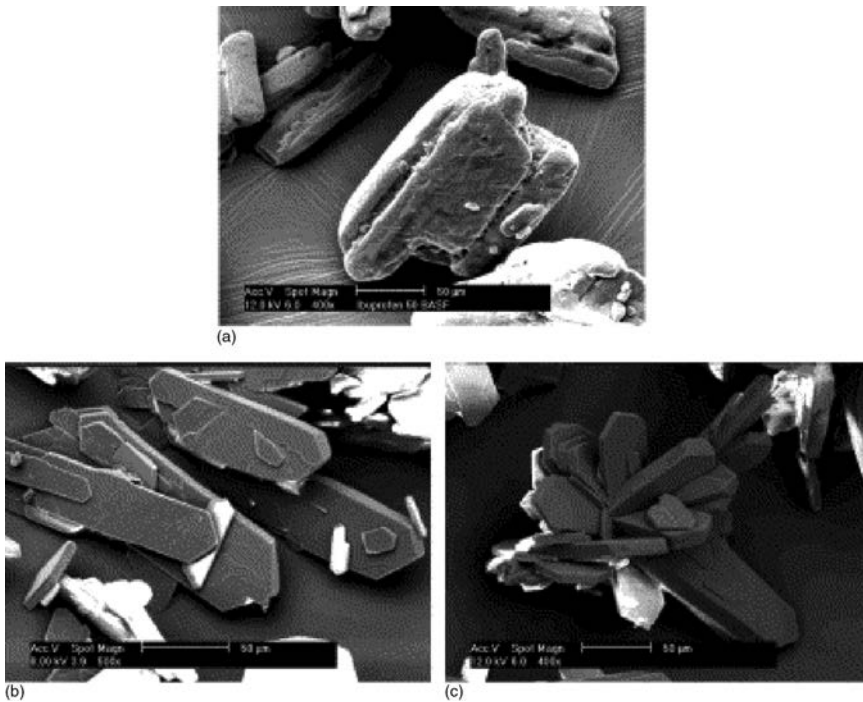
- (b) *Twinning and composite crystals.* Two or more crystals grow together and interpenetrate.
- (c) *Dendritic growth.* Rapid crystallization at high supersaturation can lead to dendritic growth of crystals leading to tree-like fractal shapes.
- (d) *Agglomeration.* Small crystals can agglomerate to form irregular shapes.

Figure 4.15 illustrates the wide variety of crystal shapes and morphologies that can be produced from the same material.

## 4.8 Summary

The first step in designing an industrial crystallizer is to establish the phase diagram for the system in the solvent system of choice including the solubility, the primary nucleation threshold (PNT), and the secondary nucleation threshold (SNT). These thermodynamic parameters allow important design decisions to be made, including choice of solvent, method of inducing supersaturation, seeded or nucleating crystallization, batch or continuous crystallization. It is important to understand the





**Figure 4.15** Some examples of different crystal shapes and morphology for ibuprofen crystals due to changes in solvent type and supersaturation conditions. (a) Habit 1; (b) habit 2 (platelets); (c) crystal agglomerate formed from platelets (Raesenack and Muller, 2002).

key regions on the phase diagram – metastable, secondary nucleation, and primary nucleation – in order to make these decisions. Crystal yield is primarily related to the crystallization thermodynamics.

To specify a crystallizer and predict the product size distribution, the kinetics of the key rate processes, growth, and nucleation must be known. Crystal growth rate can be controlled by external mass transfer (rate proportional to  $s^1$ ) or by surface integration (rate proportional to  $s^2$ ). Nucleation rate is a strong function of supersaturation and many other factors. In general, the systems kinetics are difficult to predict *a priori* and must be measured in the laboratory. Growth kinetics are easy to measure and scale. Nucleation is a stochastic process and nucleation kinetics are more difficult to measure accurately and notoriously difficult to scale.

The population balance provides an excellent framework for design of both batch and continuous crystallizers. In batch crystallizers, relatively narrow crystal size distributions are produced, especially if crystal seed is used and nucleation is avoided. The simplest continuous crystallizer is the MSMPR. This well-mixed crystallizer gives broad crystal size distributions because of the broad residence time distribution of crystals in the crystallizer. In this chapter, we presented solutions to the population balance for batch and continuous crystallizers, for both nucleating and

seeded crystallizers. However, for most real crystallization problems, the population balance and mass balance are coupled and analytical solutions are difficult. The problems can be solved numerically in general mathematical software like Matlab, or using specialized software such as gCrystal. Note that sometimes, simpler or even analytical solutions are available for the moments of the crystal size distribution. Readers should all be familiar with solutions to standard configurations, and also ready to take up the challenge to model more complex configurations such as crystallizers in series, and fines dissolution or recycling.

Finally, readers should be familiar with the different crystal lattices and the Miller Index notation for identifying crystal faces. Crystal shape is a function not only of the crystal lattice type (polymorph) but also the relative growth rate of faces, and the presence of composite crystals, dendritic growth, and agglomeration. Predicting crystal morphology requires sophisticated molecular simulation tools beyond the scope of this text.

## 4.9 Bibliography

- Dalziel, S., 1990. *Crystallisation Studies on Glucose Isomerase*. PhD thesis, University of Queensland.
- Dombrowski, R.D., Litster, J.D., Wagner, N.J., and He, Y., 2007. Crystallization of alpha-lactose monohydrate in a drop-based microfluidic crystallizer. *Chemical Engineering Science*, 62, 4802–4810.
- Durbin, S.D. and Feher, G., 1986. Crystal growth studies of lysozyme as a model for protein crystallization. *Journal of Crystal Growth*, 76, 583–592.
- Jones, A.G., 2002. *Crystallisation Process Systems*, Butterworth Heinmann, Oxford.
- Judge, R., Forsythe, E.L., and Pusey, M.L., 1998. Effect of protein impurities on lysosyme crystal growth. *Biotechnology and Bioengineering*, 59, 776–785.
- Mullin, J.W., 2001. *Crystallisation*, 4th Edition, Butterworth Heinmann, Oxford.
- Myerson, A.S. (ed.), 1999. *Molecular Modelling Applications in Crystallisation*, Cambridge University Press, Cambridge.
- Nyvt, J., 1992. *Design of Crystallisers*, CRC Press, Boca Raton, FL.
- Perry, R.H., Green, D.W., and Maloney, J.O., 2009. *Perry's Chemical Engineers Handbook*, 8th edition, McGraw-Hill, New York. Chapter 19.
- Raesack, N. and Muller, B.W., 2002. Crystal habit and tableting behaviour. *International Journal of Pharmaceutics*, 244, 45–57.
- Ribeiro, A.C., Ortona, O., Simoes, S.M., *et al.*, 2006. Binary mutual diffusion coefficients of aqueous solutions of sucrose, lactose, glucose, and fructose in the temperature range from (298.15 to 328.15) K. *Journal of Chemical & Engineering Data*, 51(5), 1836–1840.
- Tait, S., 2007. *Secondary Nucleation Characteristics of Protein Crystals*. PhD Thesis, The University of Queensland, 177 pp.
- White, E.T., 2002. A simple procedure to analyse size distributions from an MSMR with growth rate dispersion. *Proc. 4th World Congress on Particle Technology*, paper 710.
- White, E.T., Mackintosh, D.L., Butler, B.K., Zhang, H., and Johns, M.R., 1998. Modelling growth rate dispersion in sugar crystallization. *Proc. Aust. Sugar Cane Technol.*, 20, 524–531.

## 4.10 Problems

- 4.1. The rate of mass transfer through a liquid boundary layer to a solid surface can be written as:

$$\dot{m} = k_l A (c_b - c_s)$$

where  $A$  is the surface area available for mass transfer and  $c_s$  is the solute concentration at the surface. Starting from this equation, derive Equation 4.7 for the mass transfer-controlled crystal growth rate.

- 4.2. The following size distributions were measured at the start and finish of a batch crystallization experiment using a wet screening technique. Confirm that nucleation, breakage, and agglomeration can all be safely ignored in analyzing this system.

Size interval ( $\mu\text{m}$ )	Mass fraction (initial)	Mass fraction (final)
38–45	0.014	0
45–63	0.287	0.017
63–74	0.586	0.313
74–90	0.112	0.536
90–125	0	0.134

Initial mass of crystals = 50.0 g/l

Final mass of crystals = 93.8 g/l

Hint: Sieves measure mass size distributions. Agglomeration, breakage, and nucleation all change the total number of particles.

- 4.3. Refer to the solubility–supersolubility diagram in Example 4.1. I want to design a continuous nucleating MSMPR crystallizer operating at 20°C using my 80°C, 20 kg m<sup>-3</sup> A stream as my inlet to the crystallizer. Is this possible? What is the maximum yield I can achieve? Explain with reference to the phase diagram. Will your continuous crystallizer give a narrower CSD than the batch-seeded crystallizer in Example 4.1? Explain your answer in two or three sentences with the aid of sketches of the expected crystal size distributions.
- 4.4. Figure 4.P4 below is experimental data on the solubility, primary nucleation threshold (PNT) and secondary nucleation threshold (SNT) for a protein, alpha amylase. I wish to perform a seeded-batch crystallization of alpha amylase at 25°C, pH 7, 7.5 wt% sodium sulfate with no nucleation. What is the maximum starting concentration of alpha amylase and corresponding maximum crystal yield I can achieve from this crystallization?
- 4.5. Ovalbumin crystals are not spherical. In fact, they look more like surfboards. We can assume they are rectangular parallelipeds with length to width ratio of 4:1 and width to depth ratio 5:3. The data for Example 4.3 are given in terms of crystal length. Convert the growth rates to be in terms of volume-equivalent size.

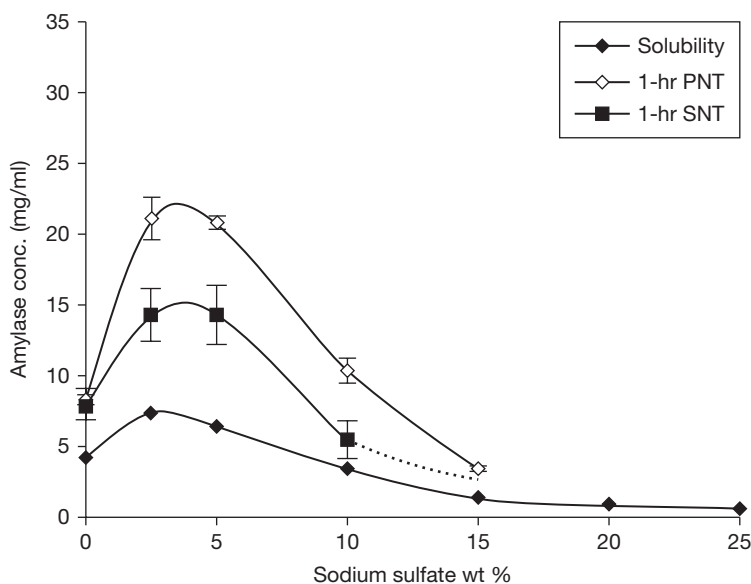


**Figure 4.P4** Solubility–supersolubility diagram for  $\alpha$ -amylase in 20 mM sodium phosphate buffers at pH 7 and 25°C.

4.6. A pilot plant MSMPR crystallizer operates at steady state with a clear liquor feed (no seed crystals). Crystal growth and nucleation occur in the crystallizer but no agglomeration or crystal breakage occurs. Data from this crystallizer are collected to assist with the design of a full-scale crystallizer. Figure 4.P6 shows the size distribution data from the crystallizer as cumulative number oversize  $N_T - N(x)$  (log scale) against crystal size for one set of conditions where:

$$\begin{aligned} V &= 1 \text{ m}^3 \\ \dot{Q}_{ex} &= 2 \text{ m}^3 \text{ hr}^{-1} \\ \rho_c &= 1,200 \text{ kg m}^{-3} \\ \alpha_v &= 0.5 \end{aligned}$$

In Figure 4.P6, the units of  $N_T$  and  $N_T - N(x)$  are crystal number per  $\text{m}^3$  of slurry in the crystallizer. All symbols are as defined in the course notes.

- (a) Derive the following expression for the cumulative number oversize distribution for the crystallizer:

$$N_T - N(x) = \dot{B}\tau \exp\left[-\frac{x}{G\tau}\right]$$

- (b) From the data in Figure 4.P6, estimate the crystal growth rate  $G$  and nucleation rate  $\dot{B}$  for this set of conditions.  
 (c) What is the median crystal size  $x_{50}$ ?  
 (d) What is the mass flowrate of crystals leaving the crystallizer (kg crystals/h)?

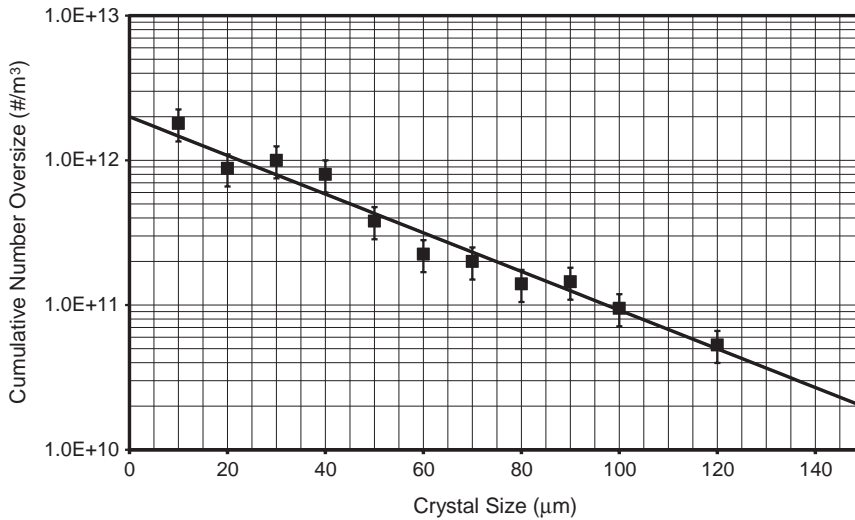


**Figure 4.P6** Measured CSD for problem 4.6.

4.7. An MSMPR crystallizer with a mean residence time of 60 minutes gives a mass mean product size of 200 μm crystallizing a salt that shows size-independent growth behavior. The growth rate and nucleation rate are proportional to supersaturation and supersaturation squared, respectively; 98% recovery of the salt is achieved.

- If the flow rate to the crystallizer is doubled, what will the new steady-state product mean size be?
- What will be the new recovery?
- Specify the performance of a fines dissolver to lift the product mean size back to 200 μm.

4.8. A nucleating MSMPR crystallizer operates under the following conditions:

$$\begin{aligned}
 V &= 10 \text{ m}^3 \\
 G &= 20 \text{ } \mu\text{m min}^{-1} \\
 \dot{Q}_{ex} &= 20 \text{ m}^3 \text{ hr}^{-1} \\
 \dot{B} &= 10^9 \text{ m}^{-3} \text{ min}^{-1}
 \end{aligned}$$

Feed to the crystallizer is clear liquor (no seed crystals). Answer the following questions about this system.

- What is the residence time in the crystallizer?
- What is the mean size of the crystals  $\bar{x}_{10}$  leaving the crystallizer?
- What is the total number concentration of crystals leaving the crystallizer (#/m³)?
- What fraction of crystals leaving the crystallizer is greater than 100 μm in size?

4.9. An MSMR crystallizer is used as a cooling crystallizer to produce potassium sulfate crystals. The crystallizer is fed with monosized seed crystals (50  $\mu\text{m}$ ) at a rate of 2.5 tonne per hour. The required residence time and measured growth rate are available from pilot plant trials and given below.

- Calculate the product CSD and median crystal size.
- What must the inlet liquor concentration be?
- What is the required crystallizer volume?

$$\rho_{crystal} = 2,660 \text{ kg m}^{-3}$$

$$\alpha_v = 0.7$$

$$\rho_{magma} = 250 \text{ kg m}^{-3}$$

$$G = 1.27 \times 10^{-8} \text{ m s}^{-1}$$

$$\tau = 4 \text{ hr}$$

$$\dot{B} = 0$$

4.10. Sketch the product size distribution for problem 4.9. On the same plot, sketch the product size distribution if the following changes were made (all else being equal).

- The rate of seed addition is doubled.
- The size of the seed particles is doubled.
- No seed is added. Instead nucleation occurs at the same (number) rate.
- The inlet liquor flow rate is halved.

Justify your answers qualitatively (and quantitatively if possible).

4.11. Consider a seeded-batch crystallizer (no nucleation, breakage, or growth; size-independent growth) using the same size distribution seed crystals as specified in Problem 4.2. The crystals are cubic and have a density of 2,000  $\text{kg m}^{-3}$ . Seed crystals, 10  $\text{g l}^{-1}$ , are placed in a crystallizer where the initial supersaturation is 70  $\text{g l}^{-1}$  and the crystals are grown until supersaturation drops to 5  $\text{g l}^{-1}$ .

- (a) Derive the following expression for the 3rd moment of the crystal size distribution at the end of the crystallization starting with the moment form of the general population balance:

$$\mu'_3(t) = \mu'_3(0) + 3\mu'_2(0)\Delta x + 6\mu'_1(0)\Delta x^2 + 6\mu'_0(0)\Delta x^3$$

where  $\mu'_k(0)$  is the  $k$ th moment of the seed size distribution, and  $\Delta x$  is the shift in the size distribution during crystallization; i.e.,  $\Delta x = \int_0^t G dt$ .

- (b) Calculate the 0th, 1st, 2nd, and 3rd moments of the seed size distribution given the data above.
- (c) For the final crystal size distribution, calculate the following:  $\Delta x$ , the volume and number concentration of crystals in the crystallizer, the specific surface mean size, and the fraction of crystals smaller than 90  $\mu\text{m}$ .

# 5 Particle Size Reduction

## 5.1 Consider a Case Study ...

### Ground down with problems

*Wassgren Agricultural Chemicals Inc.*

Memo to: Solids Processing Team  
Memo from: Manager Product Development  
February 12, 2015

### Analysis of grinding options for agricultural chemicals

The market for our new crop protection formulation is growing dramatically in the USA. *Pestaway*<sup>TM</sup> is a herbicide used on corn. It contains an active ingredient that kills harmful pest larvae without affecting bees and other good insects. However, we have some issues with manufacturing the formulations specifically related to our grinding step.

Our manufacturing plant in Crossroads, Indiana is struggling to meet demand. We have identified the bottleneck in the grinding plant, where the precipitated active ingredient must be ground from 500  $\mu\text{m}$  to 80% passing 65  $\mu\text{m}$  to ensure fast dissolution when the granular formulation is reconstituted on the farm. Currently, we use a continuous ball mill to grind the active at a rate of 10 tonnes/h. At higher throughput, we cannot achieve the quality specification on particle size. Engineering division has suggested installing a second, identical ball mill in parallel. However, this is a very expensive option. Are there any cheaper options to modify the existing grinding circuit, or the operation of the existing mill that can achieve the debottlenecking and still meet product specification?

At the same time, our new products team at the Purdue Research Park in West Lafayette is developing a new form of the active ingredient that is much less soluble in water. A new synthesis and spray-drying process gives submicron primary crystals ( $d_p = 0.5 \mu\text{m}$ ) that form large agglomerates approximately 50  $\mu\text{m}$  in size. Our aim is to use the grinding circuit for deagglomeration down to the primary particle size so a colloidal suspension, rather than a solution, is sprayed onto the crops. This colloidal suspension is less likely to be washed into the soil in the next spring thunderstorm than our current formulation. However, I don't think our ball mill can grind down to this size. Is this right? The economics of the new process are also heavily dependent on energy costs during grinding, which I fear will be very high to produce such small particles.

I request your team undertake the following tasks and report within a month.

1. Brainstorm a number of possible process flow sheet modification options for debottlenecking our grinding circuit with purchase of an additional ball mill.

2. For the two most promising of these, do an initial process design and specification suitable for our engineering division to undertake preliminary costing and economic analysis.
3. Assess the grindability of our new agglomerate formulation and recommend an appropriate grinding mill for the deagglomeration process with an estimate of the energy requirements.

Our R&D facility at Purdue Research Park has a range of bench-scale grinding mills that you can use, as well as several ways to measure particle strength and grindability. As a first step, please prepare a list of the desired characterization and bench-scale test you wish to use. You will also have access to the gSOLIDS simulation software for developing your new process flowsheets.

Crushing and grinding processes (comminution) are very important in many process plants producing structured particulate products where the primary particle or product size is a key quality attribute. Comminution is also practiced at very large scale for commodity materials such as minerals, cement, and pulverized coal for power generation. It is estimated that between 2% and 10% of the world's energy production is used for particle size reduction.

As an individual reflective exercise, or as a group brainstorming discussion, brainstorm a list of modifications that might be made to the grinding circuit. What sort of design models are needed to simulate these different scenarios? What data are needed for these models and how might they be measured? Discuss the similarities and differences between grinding hard precipitated particles compared to deagglomeration of submicron particles.

Reflect on learning goals related to crushing and grinding inspired by this case study. How do they compare with the chapter learning goals given below?

## 5.2 Learning Goals

At the completion of this chapter, the student should be able to:

1. Recognize different types of particle size reduction equipment, and state their advantages and disadvantages.
2. Understand modes of stress transmission during particle size reduction and the definitions of particle properties relevant to breakage.
3. Write down the mass–size balance for a particle size reduction process and show how it is derived from the general population balance.
4. Explain to a peer the definition the key parameters in the mass–size balance, (a) the breakage rate constant, and (b) the breakage function, and how these parameters can be measured.
5. Use empirical grindability and energy correlations for scaling particle size reduction processes.
6. Solve simple problems related to particle design in particle size reduction for batch milling, continuous mills in open circuit, and in closed circuit with a



- classifier – e.g., given mill conditions and kinetic parameters, predict exit size distribution from the mill.
7. Critically analyze and interpret real particle size reduction data sets from laboratory or plant trials using appropriate analysis tools.
  8. Attack open-ended particle design or troubleshooting problems in particle size reduction of similar nature to the introductory case study for the chapter.

### 5.3 Breakage Mechanisms and Fracture Mechanics

To reduce the size of a particle in comminution equipment, stress must be applied to the particle until it yields or breaks. There are many ways to impose stress on the particle. The three most common in industrial mills are (see Figure 5.1) as follows.

1. Single particle crushing: a single particle is compressed between two surfaces at relatively low velocity.
2. Particle bed crushing: a bed of particles is compressed between two surfaces. Stress is transmitted through the bed. Stress chains form so that some particles receive much more stress than others.
3. Impact: a particle is accelerated to high velocity where it hits a hard surface and breaks.

For crushing or impact, it may appear that particles fail in compression. However, failure is usually caused by induced tensile stress because the tensile strength of most materials is much lower than the compressive strength. When a sphere of diameter  $d$  undergoes unconfined compression, tensile stress is induced along a plane parallel to the compression points (Figure 5.2a) where the tensile stress is given by:

$$\sigma_T = \frac{4F_c}{\pi d^2} \quad \text{51}$$

where  $F_c$  is the applied compression force and  $\pi d^2/4$  is the cross-sectional area under tension. For an irregular-shaped particle, similar failure in tension occurs, although the exact relationship is dependent on the geometry. By analogy, we define the crush strength of a single particle as:

$$\sigma_p = \frac{kF_c}{x^2} \quad \text{52}$$

where  $x$  is some representative particle size – e.g.,  $d_{\text{sieve}}$  or  $d_v$  – and  $k$  is a constant which depends on the choice of definition of size and the shape of the particle. While a perfectly brittle material will fail by a single crack, real semi-brittle materials will often plastically deform at the contact point before failure, generating fines in the contact zone.

Similarly, when a particle undergoes an impact with a surface, initially the particle is compressed at the point of contact. Pressure waves then rebound through the particle causing tensile stress by which the particle fails (Figure 5.2b). At low

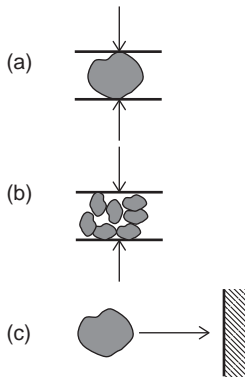


**Figure 5.1** Common modes of stress application in crushers and mills: (a) single particle crushing; (b) crushing a bed of particles; (c) impact against a surface.

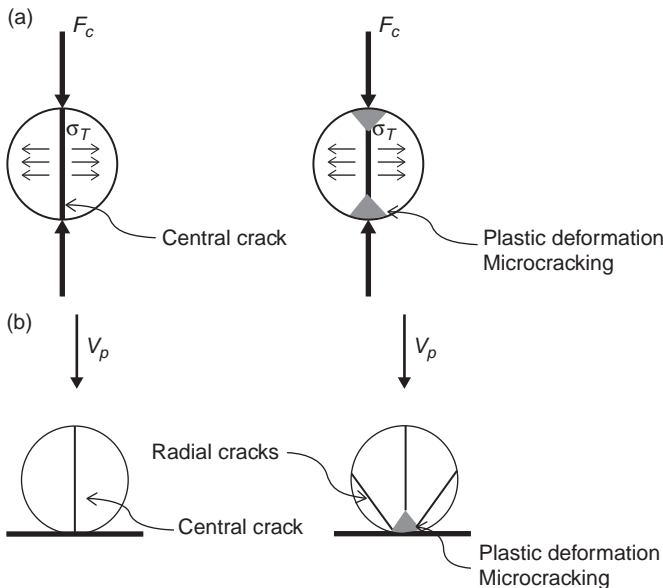


**Figure 5.2** Failure of single particles via (a) uniaxial compression: pure brittle and semi-brittle failure; (b) impact: failure mode and fragment distribution varies with impact velocity.

impact velocity, failure may be via a central crack. At higher impact velocity, a conical zone of fines is found due to deformation at the contact point, with a pattern of radial cracks growing from this point being observed.

The response to the applied tensile stress depends on the type of material. A brittle material will deform elastically (reversibly) until it reaches its yield stress when sudden catastrophic failure occurs (Figure 5.3a). The slope of the stress–strain curve is the elastic modulus. A ductile (elastic–plastic) material will deform elastically until it reaches its yield stress, at which point it will deform plastically and absorb much more energy until it finally fails at significant strain (Figure 5.3b). The energy

absorbed before failure is called the toughness of the material. Many materials of industrial interest exhibit semi-brittle failure with some plastic deformation at the contact point prior to crack propagation from either single particle compression or impact (see Figure 5.2).

The measured strength of a brittle material is usually much lower than the theoretical strength based on the work required to create new surfaces of a given surface energy. This is because brittle materials fail in tension by *crack propagation*. All real particles have faults or cracks. When a tensile stress is applied to the material, the stress concentrates around the crack tip. The ratio of the stress at the crack tip to the applied average stress is called the stress intensity factor,  $K$  and is related to the crack shape by:

$$K = \left[ 1 + 2\sqrt{\frac{L}{R}} \right] \quad \text{5}$$

where  $L$  is the crack length and  $R$  is the radius of curvature of the crack.

A crack will propagate if the strain energy exceeded the surface energy created as the crack propagated. This leads to the Griffith criterion for the critical stress required to propagate a crack  $\sigma_T$ :

$$\sigma_T \propto \left( \frac{2\gamma^{sv}E}{L} \right)^{1/2} \quad \text{54}$$

where  $\gamma^{sv}$  is the surface energy of the material and the proportionality constant depends on the geometry of the crack. This is precisely the reason that glaziers score (make a crack in) a pane of glass in order to cut it. As glass is very brittle, it will fail easily by crack propagation from the end of the scored crack.

Tough materials require more work to propagate cracks, and we can define an important property of the material, the fracture toughness  $K_c$  by considering the form of Equations 5.3 and 5.4:

$$K_c = Y\sigma_T (\pi L)^{1/2} \quad \text{5}$$

where  $Y$  is a geometric factor that varies with specimen geometry but is of order 1. For particles,  $K_c$  can be measured from indentation tests when cracks appear at the edge of the indent.

As the stored strain energy (crack distribution) within a population of particles will vary, so the crush strength of particles will vary and measuring the crush strength of a material usually involves testing 100–200 particles. For brittle materials, this distribution is typically skewed towards smaller values, and is often correlated by a log normal distribution (Equation 2.25), or the Weibull distribution:

$$P = 1 - \exp\left(-\frac{W}{W_m}\right)^n \quad \text{56}$$

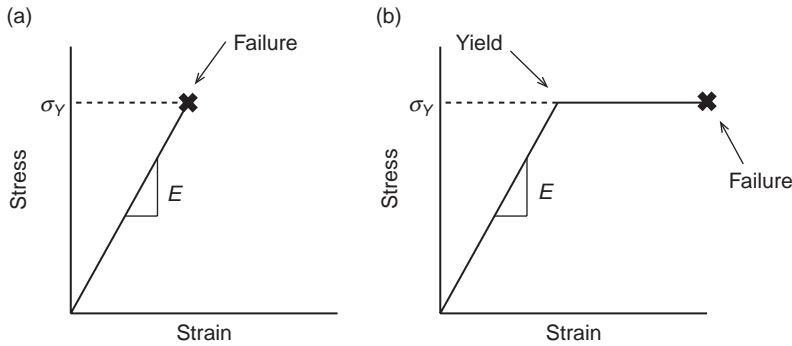


**Figure 5.3** Stress–strain relationships for (a) brittle, and (b) elastic–plastic materials.

where  $P$  is the probability that a particle will fail,  $W$  is the applied work, and  $W_m$  and  $n$  are material parameters related to the median strength and the spread of the strength distribution.

The strength and attrition resistance of particles and agglomerates are important product attributes for the performance of many particulate products during handling and transport, and in use. Measuring and modeling particle strength will be discussed further in Chapter 9. However, for application to crushing and grinding, we can draw a number of important conclusions from our understanding of how particles break.

1. The strain energy and related crack distribution will be different for each particle so a particle distribution also has a distribution of strengths. Thus, the breakage rate is a macroscopic average of many stressing events, not all of which lead to a particle breaking.
2. Generally, large particles break faster than small particles because the size of the largest crack can be bigger, increasing the value of  $K$  and increasing the probability of crack propagation.
3. The fragment size distribution from a breakage event will depend on the mode of breakage. When a single particle is compressed, it will break into a small number of fragments via brittle fracture (*cleavage*). For breakage due to *impact*, a larger number of fragments are formed. Where breakage only occurs at the contact point due to plastic deformation or microcracking, we see *attrition*, which is characterized by a bimodal size distribution (see Figure 5.4).
4. Ductile materials are more difficult to break than brittle materials because the strain energy is dissipated via plastic deformation. Even for brittle materials, very small particles (a few microns or smaller) do not have cracks and may behave in a more ductile manner. Different breakage modes and more energy are required for breakage.

These observations are important as we choose types of mill and develop mathematical models of the milling processes.

**Example 5.1**

- (a) What force is required to crush a single particle of size 2 mm if  $K_C = 0.7$  MPa and the maximum crack size in the fracture plane is 200  $\mu\text{m}$ ?
- (b) How do you expect particle strength and breakage force to change with particle size if particles fail by brittle fracture?

*Solution:*

From Equation 5.5, if we assume the geometric factor  $Y$  is equal to one:

$$\sigma_T = \frac{K_C}{Y(\pi L)^{1/2}} = \frac{0.7 \text{ MPa} \cdot \text{m}^{1/2}}{(\pi \cdot 2 \cdot 10^{-4} \text{ m})^{1/2}} = 27.9 \text{ MPa}$$

If the particle is spherical, from Equation 5.1, the force required to break the particle is:

$$F_c = \frac{\pi d^2 \sigma_T}{4} = \frac{\pi (2 \cdot 10^{-4} \text{ m})^2 27.9 \text{ MPa}}{4} = 0.88 \text{ N}$$

The answer will vary a little with changes in the particle and crack geometry.

As particles increase in size, the increase in size of the largest crack (flaw) in the particle can also increase. If we assume that  $L_{max} \propto d$ , then it follows that:

$$\sigma_T \propto d^{-1/2}$$

$$F_c \propto \sigma_T d^2 \propto d^{3/2}$$

## 5.4 Population Balance Models

The population balance framework developed in Chapter 3 is an ideal tool for tracking the development of the product size distribution from a size reduction process, and for designing or optimizing crushing and grinding circuits. In fact, modeling milling processes is the earliest example of application of population balances in industry with the approach being extensively used in the mineral processing industry since the 1970s. However, at first glance, you may not always recognize the population balance, as it is often presented as a discretized mass–size balance.

### 5.4.1 Derivation of the Mass–Size Balance for Particle Size Reduction

Particle breakage appears as birth and death terms in the population balance. In Section 3.6.3, these birth and death terms were derived and their properties examined:

$$\dot{d}_{br} = S_{br}(v)n(v,t) \quad \text{B}$$

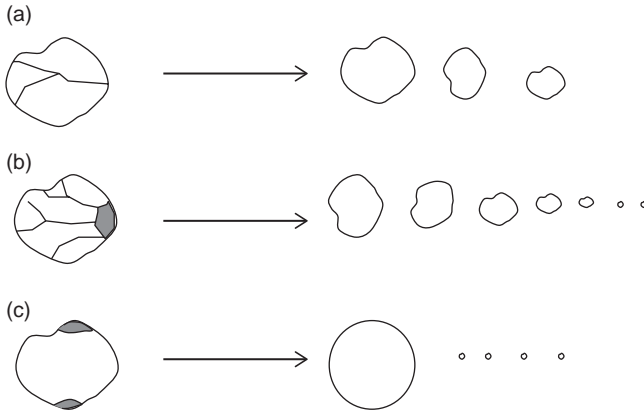


**Figure 5.4** Different fragment distributions formed by (a) cleavage, (b) impact, and (c) attrition.

$$\dot{b}_{br}(v) = \int_v^\infty \varphi(v', v) S_{br}(v') n(v', t) dv' \tag{30}$$

$$\int_0^{v'} v \varphi(v', v) dv = v' \tag{33}$$

$$\mu'_{1,vbr} = \int_0^\infty [\dot{b}(v)_{br} - \dot{d}(v)_{br}] v dv = 0 \tag{34}$$

$$\mu'_{0,vbr} = \int_0^\infty [\dot{b}(v)_{br} - \dot{d}(v)_{br}] dv > 0 \tag{35}$$

Review Section 3.6.3 before reading on. Remember that  $S_{br}(v)$  is the breakage selection function (rate constant) assuming that breakage is a first-order process.  $\varphi(v', v)$  is the breakage function that defines the fragment size distribution from the breakage of a single particle of size  $v'$ .

Consider a simple, well-mixed grinding mill in which only breakage needs to be considered (Figure 5.5). Combining Equations 3.4, 3.38, and 3.40 yields the following population balance equation for grinding:

$$\frac{\partial Vn(v, t)}{\partial t} = \dot{Q}_{in} n_{in}(v) - \dot{Q}_{ex} n_{ex}(v) + V \int_v^\infty \varphi(v', v) S_{br}(v') n(v', t) dv' - VS_{br}(v) n(v, t) \tag{57}$$

Remember, we write the population balance in terms of the distribution of particle volume  $n(v)$  because particle volume is conserved during a breakage event. For mill

models, it is more common to write the equation in terms of the mass frequency distribution:

$$m(v, t)dv = \rho_p vn(v)dv \tag{5.8}$$

Multiplying Equation 5.7 by  $\rho_p v$  and substituting from Equation 5.8 gives:

$$\begin{aligned} \frac{\partial Vm(v, t)}{\partial t} &= \dot{Q}_{in}m_{in}(v) - \dot{Q}_{ex}m_{ex}(v) \\ &+ V \int_v^\infty (v/v')\varphi(v', v)S_{br}(v')m(v', t)dv' - VS_{br}(v)m(v, t) \end{aligned} \tag{5.9}$$

Let us define the mass-based breakage function as:

$$\varphi^*(v', v) = (v/v')\varphi(v', v) \tag{5.10}$$

Substituting into Equation 5.9 gives the population balance written in terms of the mass-frequency distribution:

$$\frac{\partial Vm(v, t)}{\partial t} = \dot{Q}_{in}m_{in}(v) - \dot{Q}_{ex}m_{ex}(v) + V \int_v^\infty \varphi^*(v', v)S_{br}(v')m(v', t)dv' - VS_{br}(v)m(v, t) \tag{5.11}$$

Equations 5.7 and 5.11 look very similar, but note that while the same rate constants  $S_{br}(v)$  are used in each equation, the mass-based fragment size distribution is different from the number-based fragment size distribution; i.e.,  $\varphi^*(v', v) \neq \varphi(v', v)$ . Furthermore, it is common to use Equation 5.11 discretized in the size domain:

$$\frac{dm_i}{dt} = \dot{m}_{i,in} - \dot{m}_{i,ex} + \sum_{j=1}^{i-1} \Phi_{i,j} S_j m_j - S_i m_i \tag{5.12}$$

where  $m_i$  is the mass of material in the mill in size fraction  $i$ ,  $S_i$  is the average breakage rate for particles in size fraction  $i$ ,  $\Phi_{i,j}$  is the mass fraction of fragments in size interval  $i$  produced from the breakage of particles in size fraction  $j$ , and  $\dot{m}_{i,in}$  and  $\dot{m}_{i,ex}$  are the mass flow rates of particles in size fraction  $i$  into and out of the mill, respectively.

For a total of  $N$  size intervals, Equation 5.12 must be solved  $N$  times to give the full size distribution. For grinding, it is the convention to number the size intervals from largest to smallest; i.e.,  $i = 1$  is the largest size fraction. While Equation 5.12

holds for any arbitrary discretization of the size intervals, it is almost always used with a geometric discretization where (Section 2.3.2):

$$v_{i-1} = kv_i \tag{5.13}$$

By discretizing the size distribution, the continuous function for the breakage rate constant becomes a vector of values of  $S_i$  and the breakage function becomes a breakage matrix of values of  $\Phi_{i,j}$  where  $\Phi_{i,j} = 0$  for  $i \leq j$  and  $\sum_{i=j+1}^N \Phi_{i,j} = 1$ .

From Equation 3.14, we can also write the total mass balance for the mill:

$$\frac{dM_T}{dt} = \dot{M}_{in} - \dot{M}_{ex} \tag{5.14}$$

where  $M_T = \sum_{i=1}^N m_i$ ,  $\dot{M}_{in} = \sum_{i=1}^N \dot{m}_{i,in}$  and  $\dot{M}_{ex} = \sum_{i=1}^N \dot{m}_{i,ex}$ . Equation 5.12 can be solved for  $i = 1$  to  $N-1$  along with Equation 5.14 to give the full size distribution of particles in the mill.

Now we consider three useful special cases of the general mill model.

**Batch Grinding**

For a batch grinding mill, there are no flow terms and Equations 5.12 and 5.14 reduce to:

$$\frac{dm_i}{dt} = \sum_{j=1}^{i-1} \Phi_{i,j} S_j m_j - S_i m_i \tag{5.15}$$

$$\frac{dM_T}{dt} = \dot{M}_{in} - \dot{M}_{ex} \Rightarrow M_T = \text{constant} \tag{5.16}$$

We can rewrite Equation 5.15 in terms of the mass fraction in the size interval  $i$ :

$$\frac{dy_{mi}}{dt} = \sum_{j=1}^{i-1} \Phi_{i,j} S_j y_{mj} - S_i y_{mi} \tag{5.15}$$

where  $y_{mi} = m_i / M_T$ .

**Plug Flow Grinding at Steady State**

The plug flow grinding equation is formally derived starting from Equation 3.6 with the birth and death terms for breakage inserted:

$$\frac{dv_l n(v,l)}{dl} = \int_v^\infty \phi(v',v) S_{br}(v') n(v',t) dv' - S_{br}(v) n(v,t) \tag{5.17}$$



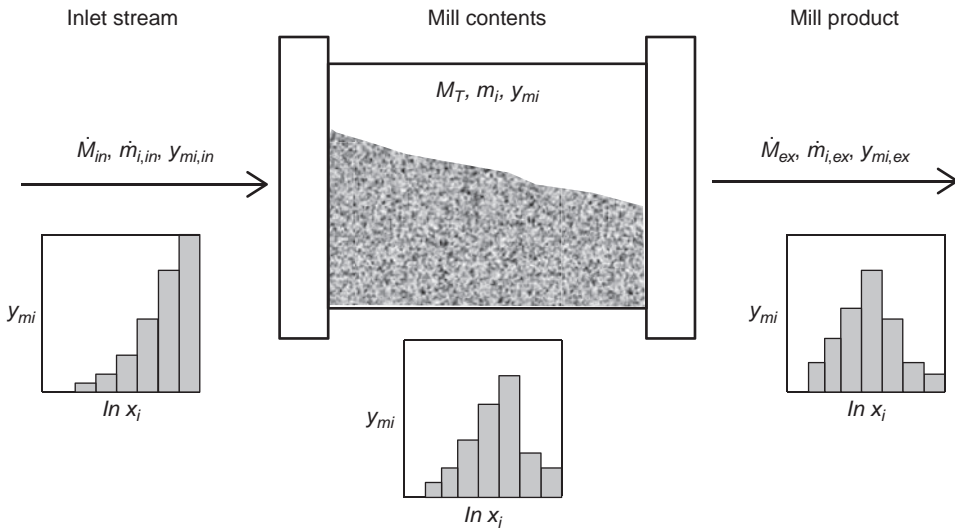


**Figure 5.5** Schematic of a well-mixed grinding mill showing nomenclature for the mass–size balance form of the population balance.

Converting to a mass basis and discretizing as we did for the well-mixed mill gives:

$$v_l \frac{dm_i}{dl} = \sum_{j=1}^{i-1} \Phi_{i,j} S_j m_j - S_i m_i \quad 518$$

$$v_l \frac{dy_{mi}}{dl} = \sum_{j=1}^{i-1} \Phi_{i,j} S_j y_{mj} - S_i y_{mi} \quad 518$$

$$M_T(l) = M_T(0) \quad 519$$

where  $v_l$  is the particle superficial velocity in the mill. Equation 5.18a or b can be solved to give the profile of the particle size distribution as a function of position in the mill.

#### Continuous, well-mixed mill at steady state

At steady state, Equations 5.12 and 5.14 become:

$$0 = \dot{m}_{i,in} - \dot{m}_{i,ex} + \sum_{j=1}^{i-1} \Phi_{i,j} S_j m_j - S_i m_i \quad 520$$

$$\dot{M}_{in} = \dot{M}_{ex} = \dot{M} \quad 521$$

If we assume the exit stream from the mill is representative of the mill contents (similar to the MSMPR assumption for crystallization), then:

$$y_{mi,ex} = \frac{\dot{m}_{i,ex}}{\dot{M}} = y_{mi} = \frac{m_i}{M_T} \tag{5.22}$$

where  $y_{mi}$  is the mass fraction of particles of size interval  $i$  in the mill. Substituting from Equation 5.22 into Equation 5.20 gives:

$$0 = y_{mi,in}\dot{M} - y_{mi}\dot{M} + \sum_{j=1}^{i-1} \Phi_{i,j} S_j y_{mj} M_T - S_i y_{mi} M_T \tag{5.23}$$

We define the average residence time of particles in the mill as:

$$\tau = \frac{M_T}{\dot{M}} \tag{5.24}$$

Combining Equations 5.23 and 5.24 gives:

$$0 = y_{mi,in} + \tau \sum_{j=1}^{i-1} \Phi_{i,j} S_j y_{mj} - (1 + \tau S_i) y_{mi} \tag{5.25}$$

**Example 5.2 Analysis of a Well-mixed Mill** Consider a well-mixed ball mill in continuous operation with a residence time of 5 min. The mill parameters are:

$$\bar{X} = \begin{bmatrix} 300 \mu\text{m} \\ 212 \mu\text{m} \\ 150 \mu\text{m} \\ 106 \mu\text{m} \\ 75 \mu\text{m} \\ 53 \mu\text{m} \\ 37 \mu\text{m} \end{bmatrix} \quad \bar{Y}_{in} = \begin{bmatrix} 0.25 \\ 0.45 \\ 0.2 \\ 0.1 \\ 0 \\ 0 \\ 0 \end{bmatrix} \quad \bar{S} = \begin{bmatrix} 0.5 \text{ min}^{-1} \\ 0.45 \text{ min}^{-1} \\ 0.42 \text{ min}^{-1} \\ 0.4 \text{ min}^{-1} \\ 0.38 \text{ min}^{-1} \\ 0.25 \text{ min}^{-1} \\ 0.2 \text{ min}^{-1} \end{bmatrix} \quad \bar{\Phi} = \begin{bmatrix} 0 & 0 & 0 & 0 & 0 & 0 & 0 \\ 0.25 & 0 & 0 & 0 & 0 & 0 & 0 \\ 0.24 & 0.29 & 0 & 0 & 0 & 0 & 0 \\ 0.19 & 0.27 & 0.33 & 0 & 0 & 0 & 0 \\ 0.12 & 0.2 & 0.3 & 0.45 & 0 & 0 & 0 \\ 0.1 & 0.16 & 0.25 & 0.3 & 0.6 & 0 & 0 \\ 0.1 & 0.1 & 0.12 & 0.25 & 0.4 & 1 & 0 \end{bmatrix}$$

- (a) What is the product size distribution leaving the mill?
- (b) How does this compare with the product size distribution if the mill is run in batch mode for 5 minutes?

*Solution:*

First, check the properties of the data associated with the mill. The particle size distribution is represented by seven size intervals in a  $\sqrt{2}$  geometric series. The vector  $\bar{X}$  contains the top size of each interval with  $x_1 = 300 \mu\text{m}$ , and so on. The vectors  $\bar{Y}_{in}$  and  $\bar{S}$  are the inlet size distribution and breakage rate constants by size interval.  $\bar{\Phi}$  is the matrix of values of  $\Phi_{ij}$  where each column of the matrix gives the fragment size distribution when a particle in size interval  $j$  is broken. Therefore, each column should sum to 1  $\left( \sum_{i=j+1}^N \Phi_{i,j} = 1 \right)$  and all the values are zero for  $i \leq j$ .

We can solve part (a) by solving the set of Equations 5.25 for  $i = 1$  to 7. We represent the equations in matrix notation and solve using an appropriate mathematical solver:

$$0 = \bar{Y}_{in} + \tau \bar{\Phi} \bar{S} \bar{Y} - (I + \tau \bar{S}) \bar{Y}$$

Note that  $\bar{\Phi}$  is a lower triangular matrix and we can solve the equations easily, if a little tediously, by hand, starting with  $i = 1$ . Below, we show the solution for the first two size intervals. For  $i = 1$ :

$$0 = y_{m1,in} + 0 - (1 + \tau \cdot S_1) y_{m1}$$

Note that no particles can break into the largest size fraction. Substituting in the numerical values:

$$0 = 0.25 + 0 - (1 + 5 \text{min} \cdot 0.5 \text{min}^{-1}) y_{m1}$$

$$\Rightarrow y_{m1} = 0.071$$

For  $i = 2$ :

$$0 = y_{m2,in} + \tau \phi_{2,1} S_1 y_{m1} - (1 + \tau \cdot S_2) y_{m2}$$

Substituting the numerical values:

$$0 = 0.45 + 5 \text{min} \cdot 0.25 \cdot 0.5 \text{min}^{-1} \cdot 0.071 - (1 + 5 \text{min} \cdot 0.45 \text{min}^{-1}) y_{m2}$$

$$\Rightarrow y_{m2} = 0.152$$

The other size intervals can be solved in a similar fashion.

For part (b), we need to solve the set of ODEs Equation 5.15 for  $i = 1$  to 7 using  $\bar{Y}_{in}$  as the initial particle size distribution at  $t = 0$ . Again, the linear ODEs are easily

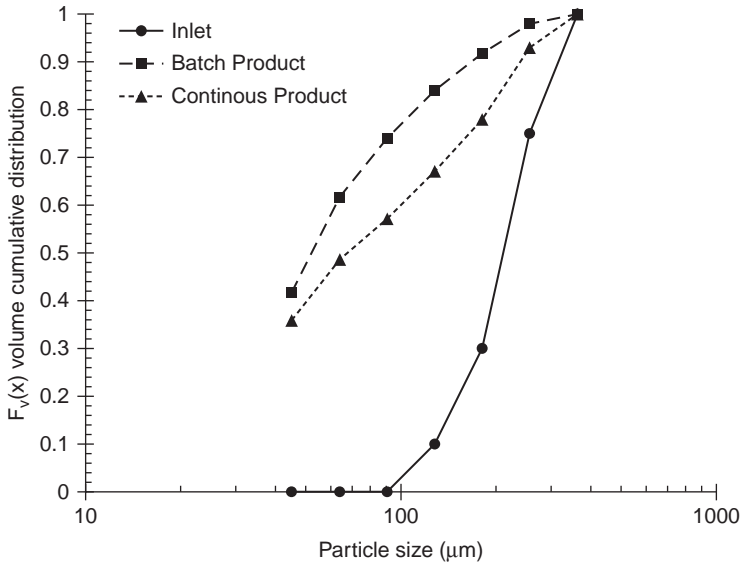


Figure E5.2 Product size distributions for Example 5.2.

solved using appropriate mathematical software. Here, we will solve just the first size interval as an example. For  $i = 1$ :

$$\frac{dm_1}{dt} = -S_1 m_1$$

$$\Rightarrow \frac{dy_{m1}}{dt} = -S_1 y_{m1}$$

We solve this simple ODE to give:

$$y_{m1}(t) = y_{m1}(0) \exp(-S_1 t)$$

$$\Rightarrow y_{m1}(5\text{min}) = 0.25 \exp(-0.5\text{min}^{-1} 5\text{min}) = 0.021$$

Observe that the batch grinding mill is more effective at grinding the particles in the largest size fraction than the continuous well-mixed mill with the same average residence time. Figure E5.2 shows the full cumulative size distributions for each case. Why is the batch mill “better” than the continuous mill?

### 5.4.2 The Breakage Rate Constant and the Breakage Kernel

The key parameters in the population balance for breakage are (1) the breakage rate constant  $S_{br}$  or  $S_i$ ; and (2) the breakage function  $\phi(v', v)$  or  $\Phi_{i,j}$ . These are functions of particle size, material properties, mill type, and process conditions.

The breakage rate constant generally decreases with particle size. For brittle particles, this is because the number and size of cracks is likely to be larger in the larger particles. For many systems, breakage rate follows a power law function with respect to particle size:

$$S_i = a \left( \frac{x_i}{x_1} \right)^\alpha \quad \text{5.26}$$

where  $a$  and  $\alpha$  are parameters. For some systems, breakage rate decreases past a certain optimum size. For example, in ball milling large particles cannot be effectively pinched between the grinding media, so that the optimum particle size for breakage is related to the size of the grinding media balls. For such systems, Equation 5.26 can be replaced by a four-parameter model:

$$S_i = a \left( \frac{x_i}{x_1} \right)^\alpha \left[ 1 + (x_i / \mu)^\eta \right]^{-1} \quad \text{5.27}$$

$\alpha$  and  $\eta$  are taken as global constants, while  $a$  and  $\mu$  are functions of the media size.

This is an example of the effect of process parameters on breakage rate constant. For example, in a ball mill,  $S_i$  is a function of the load of grinding media, the size, shape, and density of the grinding media, and the rotational speed of the drum.  $S_i$  will also be a function of material properties. It will be inversely proportional to particle strength or toughness, and increase with increasing flaw size and density in the material.

The breakage function will be dependent of the mode of breakage. Typical breakage functions for cleavage and attrition are shown in Figure 5.6. Cleavage yields a small number of fragments mainly in the next two or three size intervals smaller than the particle being broken. In contrast, attrition gives a bimodal distribution of fragments – eroded cores in the next smaller size interval, and fines.

While the breakage function depends on the breakage mode, unlike the breakage rate it is relatively insensitive to changes in operating conditions in the mill, e.g., mill size. It is mainly related to the properties of the material to be broken, and the energy involved in the breakage event – e.g., the kinetic energy of impact in an impact mill.

The breakage function is often presented in the cumulative form:

$$\Phi'_{i,j} = \sum_{k=i+1}^N \Phi_{k,j} \quad \text{5.28}$$

A number of functional forms for  $\Phi'_{i,j}$  are available. For example, a simple power law form of the breakage function can be used:

$$\Phi'_{i,j} = \left( \frac{x_i}{x_j} \right)^\gamma \quad \text{5.29}$$

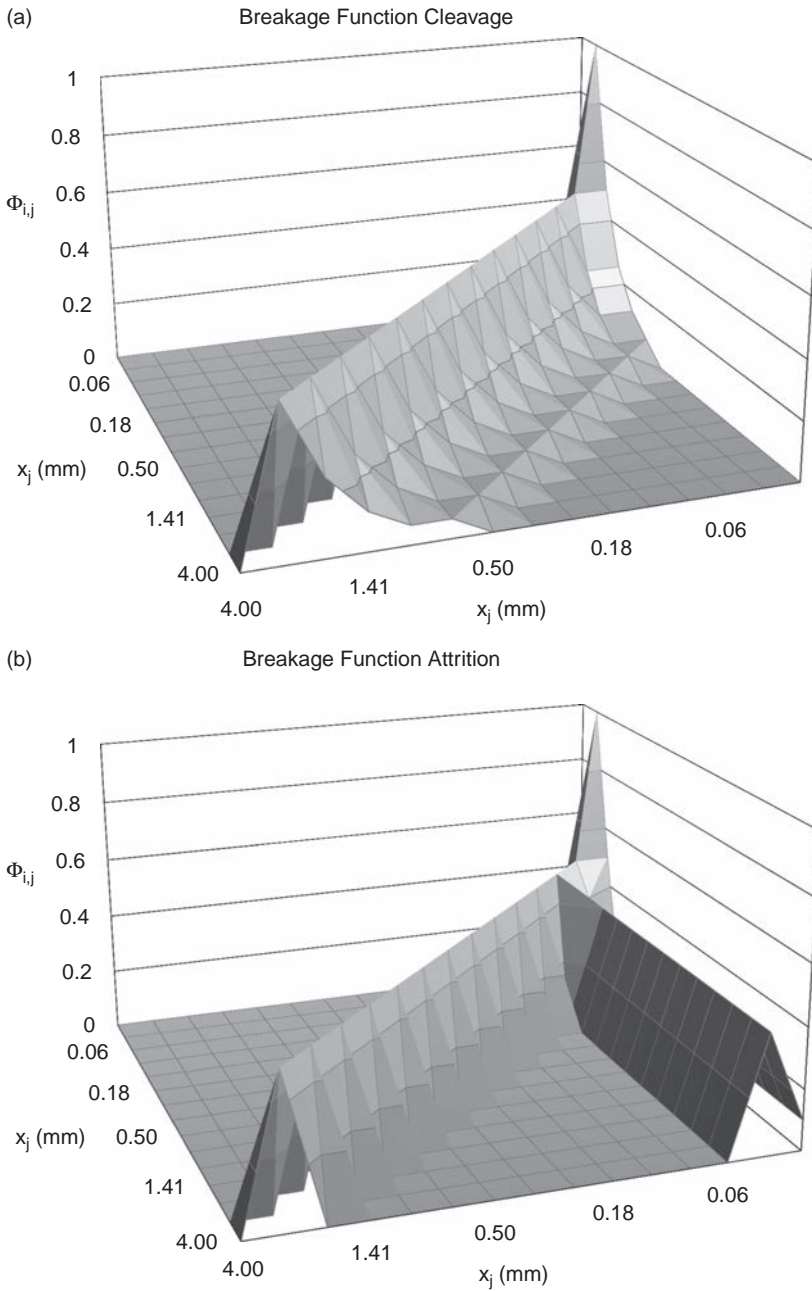


Figure 5.6 Typical breakage functions for breakage by (a) cleavage, and (b) attrition.

A more flexible three-parameter function is:

$$\Phi'_{i,j} = \alpha \left( \frac{x_i}{x_j} \right)^\gamma + (1 - \alpha) \left( \frac{x_i}{x_j} \right)^\beta \quad \text{59}$$

Other more general forms of the breakage function are given in Diemer and Olsen (2002).

Note that Equation 5.29 and 5.30 have the property of being *top size independent*; i.e.,  $\Phi'_{i,j} = \Phi'_{i+1,j+1} = \Phi'_{i+2,j+2} = \Phi'_{i-j}$ . This is a very useful property as it reduces an  $N \times N$  matrix of values to a vector of  $N$  values for storing the breakage function information. Referring to Figures 5.4 and 5.6, which breakage mode is unlikely to meet the top size independent criteria?

To use the population balance model effectively, we need to measure or estimate the values of  $S_i$  and  $\Phi_{i,j}$ . In Example 5.2, there are 21 different parameters for seven size intervals. By using correlating equations of the form shown in Equations 5.26 and 5.30, we reduce the number of required parameters to of order 3 to 7 for any given material and mill process conditions, independent of the number of size intervals. Values of the parameters are not available in handbooks because they depend on the particle morphology and history (size, shape, flaw distribution) as well as on thermodynamic properties of the material. Therefore, they must be measured or estimated by one or more of the following techniques:

1. single particle testing;
2. laboratory batch grinding tests;
3. back-calculated from particle size distribution from the operating mill; or
4. combinations of the above methods.

Single particle test methods break a single particle under known energy conditions – e.g., by swinging a pendulum of known weight at a known velocity into a stationary particle. This process is repeated for several hundred particles and the combined fragment size distribution measured. As each impact is a single breakage event, the breakage function is measured directly, for a given impact energy. Figure 5.7 shows the range of different single particle breakage tests that are used. Tavares (chapter 1 of Salman *et al.*, 2007) gives a detailed description of these tests. This method is particularly suitable for design and scaling of crushers.

Laboratory batch grinding tests measure the breakage rate  $S$  directly. A single size fraction of particles is loaded into the laboratory mill, and the fraction of particles remaining in that size fraction is measured as a function of time. From Equation 5.15 it follows that:

$$\frac{dm_1}{dt} = -S_1 m_1 \quad \text{58}$$

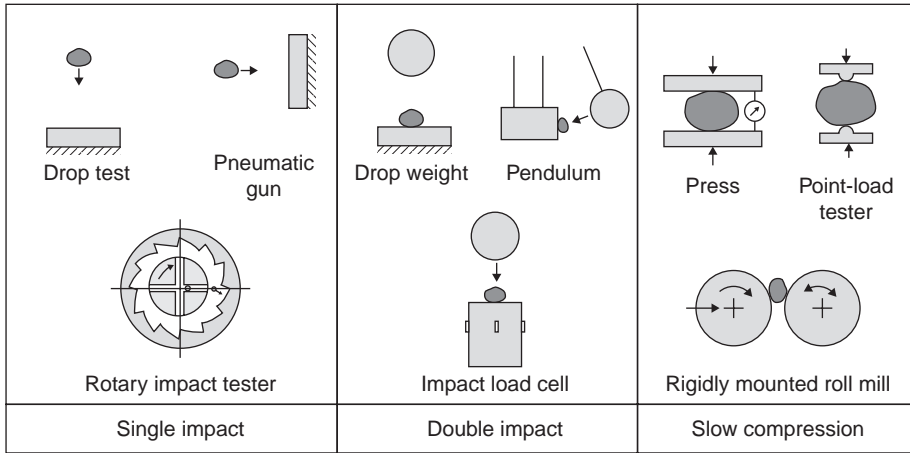


Figure 5.7 Single particle breakage tests (Salman *et al.*, 2007, chapter 1).

which can be integrated to give:

$$\ln\left(\frac{m_1(t)}{m_1(0)}\right) = \ln(y_{m1}(t)) = -S_1 t \tag{5.8}$$

A plot of  $\ln(y_{m1}(t))$  vs.  $t$  will yield a straight line of slope  $-S_1$  (see Figure 5.8). By repeating the test with different size fraction particles, the full breakage rate vector can be established. Notice in Figure 5.8 that the breakage rate increases with increasing particle size.

It is not possible to measure the breakage function  $\Phi_{i,1}$  directly from the size distribution of such a test because particles may have undergone more than one breakage event. Several approximations can be used for estimating  $\Phi_{i,1}$ . For example:

$$\Phi_{i,1} \approx \frac{\ln[(1 - F_i(0)) / (1 - F_i(t))]}{\ln[(1 - F_2(0)) / (1 - F_2(t))]} \tag{5.9}$$

Another approach is to back fit  $\Phi_{i,j}$  to the data using Equation 5.15 with standard parameter estimation techniques. Usually, this is done by assuming a functional form of the breakage function and estimating the best values breakage function parameters to match the generated particle size distributions.

Back-fitting data from an operating mill is useful for characterizing an existing piece of equipment.  $\bar{S}$  and  $\bar{\Phi}$  must be extracted simultaneously. However, these parameters are highly correlated so it is difficult to deconvolute the effect of the breakage rate and breakage function in the parameter estimation step. Clearly, this approach is of little use in designing a new grinding mill or circuit from scratch.



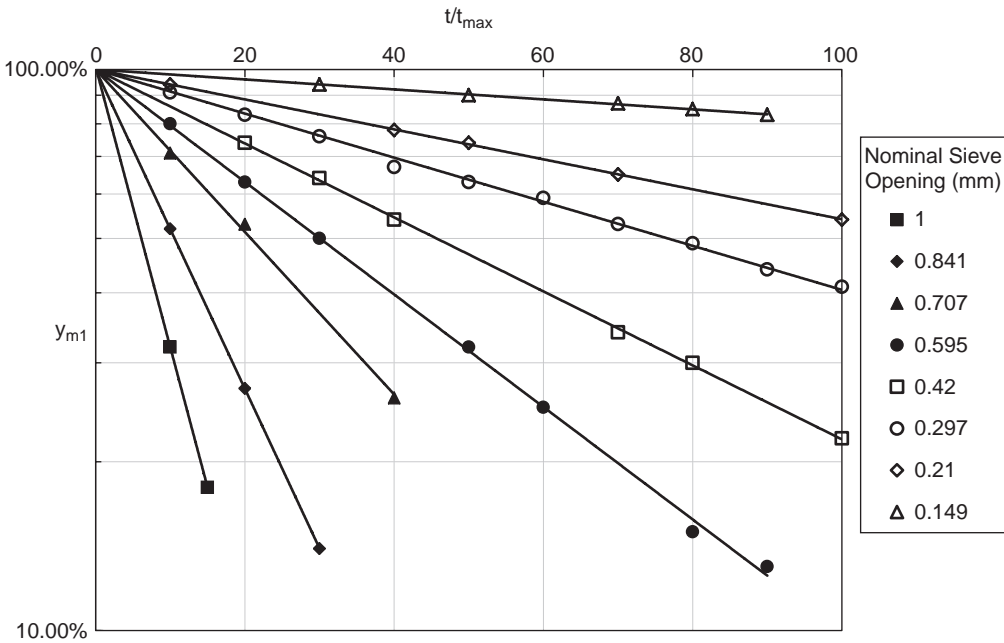


**Figure 5.8** Analysis of batch grinding data to measure breakage rate constants.

**Example 5.3 Parameter Estimation Example for Grinding Model Parameters** Use the data from Figure 5.8 to get an expression for breakage rate as a function of particle size for this system if  $t_{max} = 10$  min.

*Solution:*

Note that all the data sets follow the relationship set by Equation 5.32:

$$\ln\left(\frac{m_1(t)}{m_1(0)}\right) = \ln(y_{m1}(t)) = -S_1 t$$

For example, for sieve size 0.42 mm, the breakage rate is calculated from the slope of the line:

$$S_5 = -\frac{\ln(y_a / y_b)}{t_a - t_b} = -\frac{\ln(80 / 30)}{(1.43 - 8.0) \text{ min}} = 0.15 \text{ min}^{-1}$$

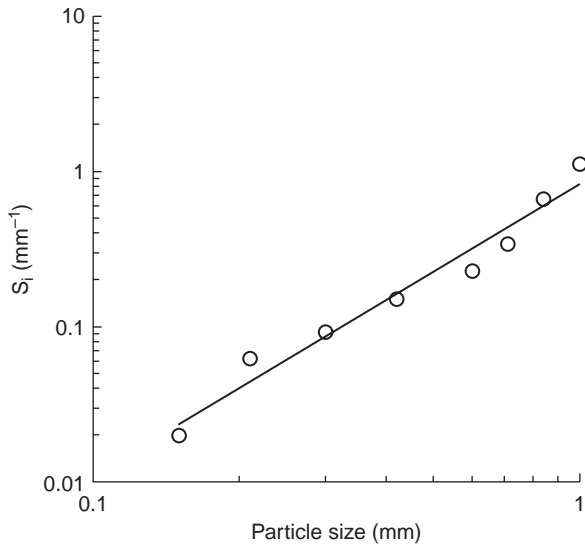
This process can be repeated for all the size fractions. Results are summarized in the table below:

$i$	$x_i$ (mm)	$S_i$ ( $\text{min}^{-1}$ )
1	1.0	1.13
2	0.84	0.66
3	0.71	0.34

$i$	$x_i$ (mm)	$S_i$ (min <sup>-1</sup> )
4	0.60	0.23
5	0.42	0.15
6	0.30	0.093
7	0.21	0.062
8	0.15	0.020

We can plot this data on a log-log plot to test whether the breakage rate data fits a power law function as given by Equation 5.26 (see below). There is a reasonable fit to the equation with:

$$S_i = 0.87 \left( \frac{x_i}{x_1} \right)^{1.9} \text{ min}^{-1}$$



### 5.4.3 Size Reduction with Classification

Many mills and crushers operate with the aid of a classifier that separates particles on the basis of their size. In some cases, the classification is built into the size reduction equipment. For example:

1. A hammer mill may have a screen at the exit to prevent uncrushed material escaping the mill.
2. A jet mill may have an inbuilt centrifugal classifier for the airborne particles leaving the mill that recycles oversize into the mill chamber.

We will call this *internal* classification. In other cases, an *external* classifier is used. Common external classifiers are screening stations, hydro cyclones and air cyclones. The choice of classifier depends on the desired product size, as well as whether wet milling or dry milling is used.

Classifiers divide an inlet stream into two exit streams, one containing large particles (the coarse fraction) and one containing fine particles (the fine fraction) (see Figure 5.9a). Both internal and external classifiers are modeled in a similar way. We define the total efficiency as the mass fraction of all material entering the classifier that is captured in coarse fraction:

$$E_T = \frac{\dot{M}_c}{\dot{M}} \quad \text{5.35a}$$

where  $\dot{M}_c$  is the mass flowrate of the coarse fraction stream. The *grade efficiency*  $Q(x)$  or  $Q_i$  is defined as the mass fraction of particles of a given size that are captured in the coarse stream:

$$Q(x) = \frac{\dot{M}_c f_{m,c}(x)}{\dot{M} f_m(x)} \quad \text{5.35b}$$

$$Q_i = \frac{\dot{m}_{i,c}}{\dot{m}_i} = \frac{\dot{M}_c y_{mi,c}}{\dot{M} y_{mi}} \quad \text{5.35c}$$

The grade efficiency and the total efficiency are related by the total mass balance for the system. Summing Equation 5.35b over all size fractions:

$$\dot{M}_c \sum y_{mi} = \dot{M}_c = \dot{M} \sum Q_i y_{mi} \quad \text{5.35d}$$

Combining with Equation 5.34 gives:

$$E_T = \sum Q_i y_{mi} \quad \text{5.35e}$$

While the total classifier efficiency is a strong function of the size distribution of the inlet stream, the grade efficiency is generally not, and is considered a performance parameter of the classifier. The grade efficiency as a function of particle size is called the *grade efficiency curve* (Figure 5.9b). A key parameter of the grade efficiency curve is the cut size  $x_{50}$  where:

$$Q(x_{50}) = 0.5 \quad \text{5.35f}$$

When operated in closed loop, the classifier returns oversize or unmilled material to the mill for further size reduction (Figure 5.11). Operating with a classifier in closed circuit gives a narrower product size distribution. The population balance model is needed to correctly size the mill due to the contribution of the recycle stream to increasing the actual throughput to the mill.

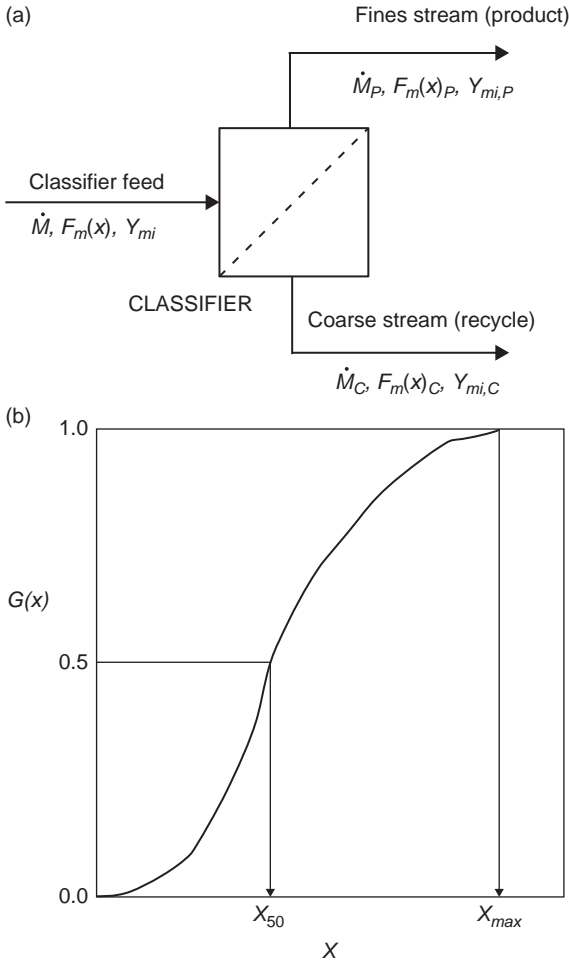


Figure 5.9 Particle classifier models. (a) Schematic of a generic classifier; (b) the grade-efficiency curve.

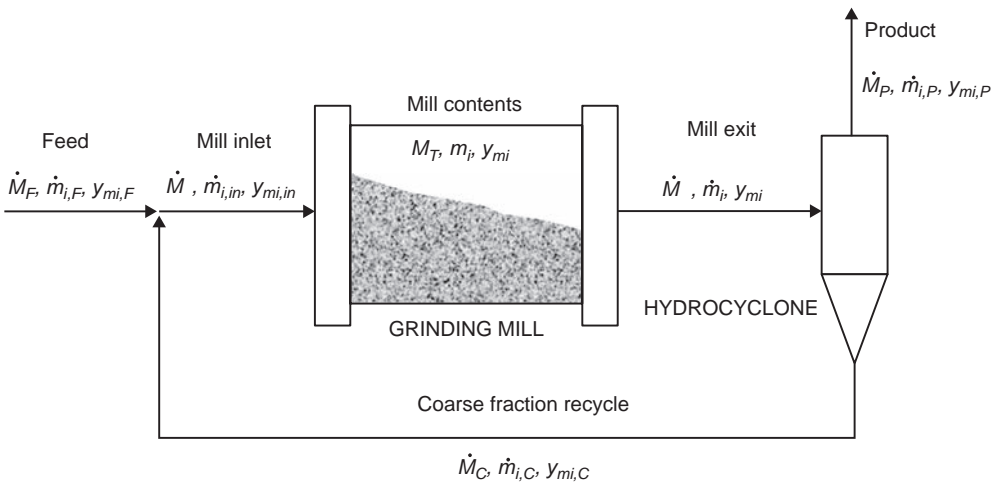


Figure 5.10 Closed loop operation of a mill with classifier.

**Example 5.4** Consider the well-mixed mill described in Example 5.2. This mill now operates with a hydrocyclone classifier on the mill exit operating in closed circuit. The classifier grade efficiency curve is given in vector form below.

- Derive an expression for the product size distribution  $y_{mi,p}$  in terms of the feed size distribution and the parameters of the mill and classifier.
- Calculate the product size distribution, assuming the hold up in the mill is the same as when the mill is run without the classifier as in Example 5.2.

$$\bar{Q} = \begin{bmatrix} 0.95 \\ 0.85 \\ 0.6 \\ 0.4 \\ 0.15 \\ 0.05 \\ 0 \end{bmatrix}$$

*Solution:*

- Referring to the nomenclature as shown in Figure 5.10, we can write the total mass balance for the the overall circuit, the recycle-feed mixer, and the classifier when operated at steady state:

$$\dot{M}_P = \dot{M}_F \quad \text{E 1}$$

$$\dot{M} = \dot{M}_C + \dot{M}_F = E_T \dot{M} + \dot{M}_F \quad \text{E 2}$$

Rearranging gives:

$$\dot{M}_F = (1 - E_T) \dot{M} \quad \text{E 3}$$

where  $E_T$  is given by Equation 5.37.

The mass balance on the  $i$ th size fraction for recycle feed mixer is:

$$\dot{M}_{y_{mi,in}} = \dot{M}_F y_{mi,F} + \dot{M}_C y_{mi,C} \quad \text{E 4}$$

while the performance equation of the classifier (Equation 5.35b) gives:

$$\dot{M}_C y_{mi,C} = Q_i \dot{M} y_{mi} \quad \text{E 5}$$

Combining Equations 5.E3, 5.E4, and 5.E5 gives:

$$y_{mi,in} = (1 - E_T) y_{mi,F} + Q_i y_{mi} \quad \text{E 6}$$

Substituting into the well-mixed mill size-mass balance (Equation 5.25) and rearranging:

$$0 = (1 - E_T)y_{mi,F} + \tau \sum_{j=1}^{i-1} \Phi_{i,j} S_j y_{mj} - (1 - Q_i + \tau S_i)y_{mi} \tag{5.7}$$

In matrix form, we have:

$$0 = (1 - E_T)\bar{Y}_F + \tau \bar{\Phi} \bar{S} \bar{Y} - (I - \bar{Q} + \tau \bar{S})\bar{Y} \tag{5.8}$$

where

$$E_T = \bar{Q} \cdot \bar{Y} \tag{5.9}$$

We can solve Equations 5.E8 and 5.E9 to get  $\bar{Y}$  and then calculate the product size distribution from the classifier equation:

$$\bar{Y}_P = \frac{(I - \bar{Q})}{(1 - E_T)} \bar{Y} \tag{5.10}$$

(b) If the mill hold up in closed loop is the same as in open loop, the residence time for each pass through the mill will be smaller, as we have a higher throughput to the mill:

$$\begin{aligned} M_{T,cl} &= M_{T,op} \\ \Rightarrow \dot{M} \tau_{cl} &= \dot{M}_F \tau_{op} \\ \Rightarrow \tau_{cl} &= (1 - E_T) \tau_{op} \end{aligned} \tag{5.11}$$

Combining Equation 5.E11 with 5.E7 or 5.E8 we have:

$$0 = (1 - E_T)y_{mi,F} + (1 - E_T) \tau_{op} \sum_{j=1}^{i-1} \Phi_{i,j} S_j y_{mj} - (1 - Q_i + (1 - E_T) \tau_{op} S_i)y_{mi} \tag{5.12a}$$

$$0 = (1 - E_T)\bar{Y}_F + (1 - E_T) \tau_{op} \bar{\Phi} \bar{S} \bar{Y} - (I - \bar{Q} + (1 - E_T) \tau_{op} \bar{S})\bar{Y} \tag{5.12b}$$

where  $\tau_{op}$  is given as 5 min.

Solving Equations 5.E12, 5.E9, and 5.E10 gives the product size distribution. Similarly to Example 5.2, we can solve the equations by hand, starting with  $i = 1$ , or more conveniently using appropriate mathematical software, we solve the equations to give the full size distributions. These are shown in the figure below and compared to the results from Example 5.2.

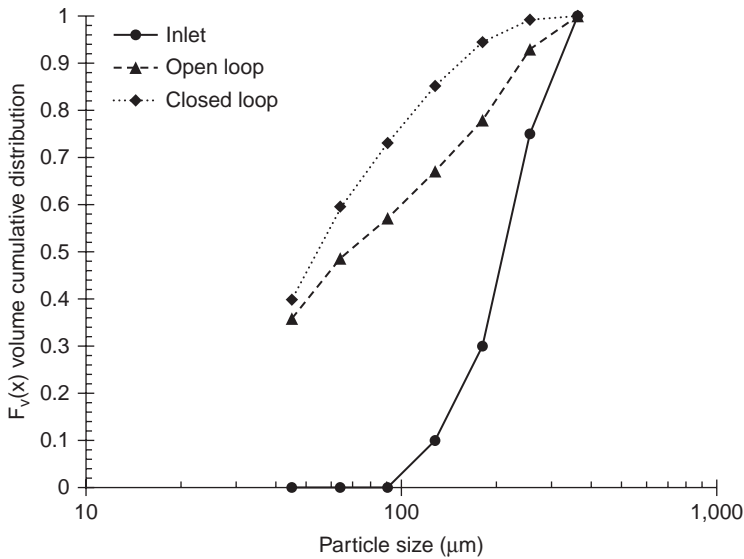


**Figure E5.4** Product size distributions from the mill with and without closed loop classification.

## 5.5 Particle Size Reduction Equipment

Particle size reduction equipment is used for a huge variety of applications, from crushing large rocks to grinding material to less than 100 nm. Not surprisingly, there is a very wide variety of equipment available which we will describe only briefly here. See the references in the Bibliography for more detailed descriptions of equipment. A useful way to categorize crushing and grinding equipment is by the mechanism by which stress is applied to the particles.

### 5.5.1 Crushers

Crushers apply stress to individual particles, or thin beds of particles, by squeezing them between two surfaces at relatively low velocity (0.1–10 m s<sup>-1</sup>). Crushers are generally used for reducing the size of large lumps of material. The jaw crusher (Figure 5.11) handles large rocks up to over 1 m in diameter. One jaw is static while the other is hinged to squeeze the material, similar to the operation of a nutcracker. The gyratory or cone crusher uses an eccentric-driven central cone to crush material against an outside conical casing. The roll crusher pinches individual particles between two counter-rotating rolls. Roll crushers are usually choke-fed by gravity and the feed size to gap width is limited to 4:1.

As the force is applied directly to the particle, crushers are relatively energy-efficient for comminution equipment. Many designs have inherent classification. Particles greater than the maximum gap between the jaws or rolls cannot leave without being crushed. Some designs have a screen to prevent oversize from leaving. Most particles undergo only a small number of breakage events in the crusher.

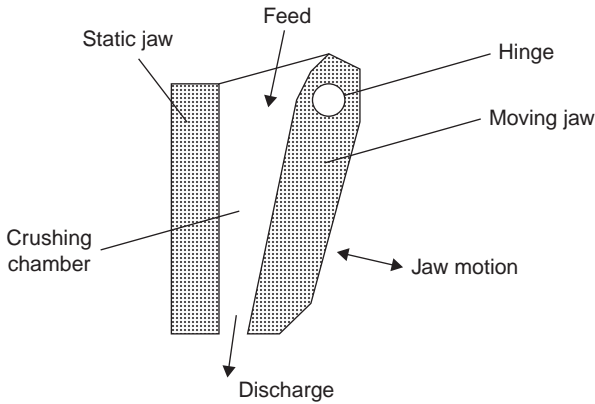


**Figure 5.11** A jaw crusher (from Rhodes, 2008).

### 5.5.2 Impact Mills

Impact mills break particles by high-speed impact at velocities from 20 to 150  $\text{m s}^{-1}$  between particles and stationary or rotating surfaces within the mill. The hammer mill (Figure 5.12) is the most common impact mill. Particles are fed by gravity to the top of the mill. Hammers rotate around a central shaft. Particles may break both by impact with the hammer and when they hit the impact plates around the shell of the mill. An outlet screen can be used to increase residence time in the mill.

A pin mill consists of two parallel plates with protruding pins. One plate rotates at high speed. Particles are flung by centripetal force towards the outside of the disc and are broken by high-speed impact with the pins. Air entrainment aids the flow of particles through the mill.

Impact mills are robust to handle a wide variety of materials and yield a broader size distribution of product than crushers because the impact energy is often well in excess of that required to break the particle. Large particles may also escape through the mill unbroken.

### 5.5.3 Tumbling Mills

Tumbling mills impart stress to the particles indirectly. The machine, typically a tumbling drum, rotates. Grinding media are placed within the drum: rods, balls, or large rocks of the same material for rod mills, ball mills, and autogenous mills, respectively (Figure 5.13). As the grinding media cascade and cataract within the mill, the particles are broken by a combination of impact from grinding media and crushing when particles are pinched between the media. Tumbling mills are used extensively in the mineral processing industry for fine grinding to give product in the range 10–100  $\mu\text{m}$ . However, they have high power consumption. The mills can be operated with wet or dry.



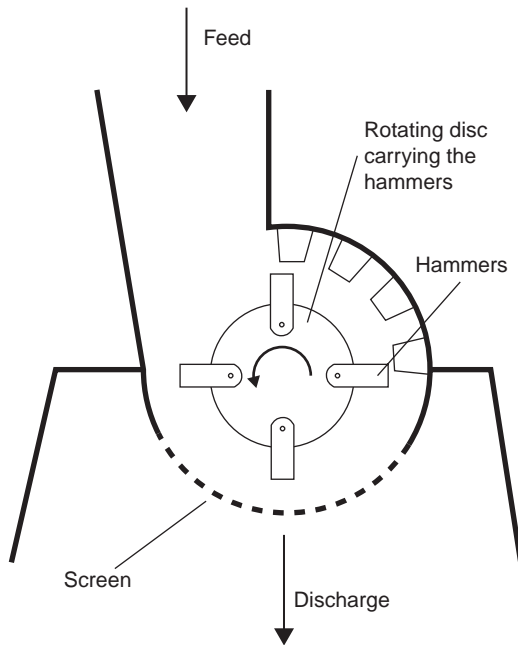


**Figure 5.12** A hammer mill (from Rhodes, *Introduction to Particle Technology* 2nd ed., 2008).

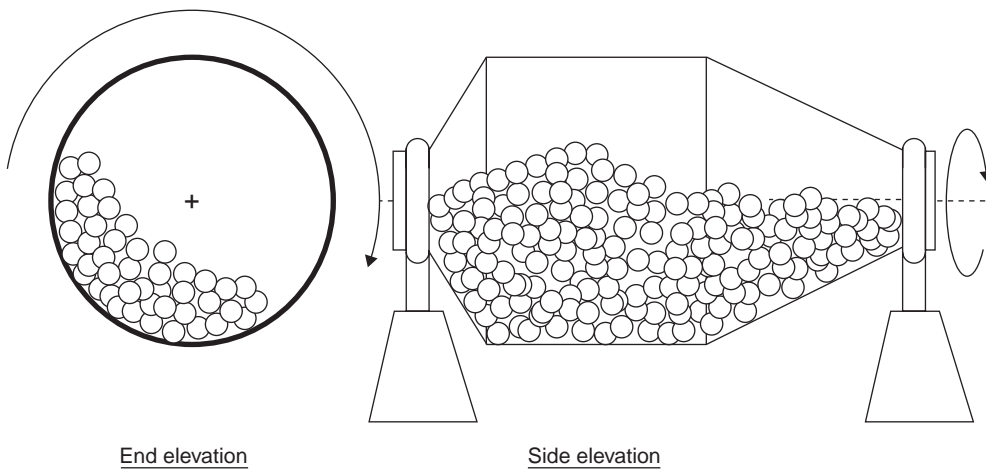


**Figure 5.13** Schematic of a ball mill (from Rhodes, *Introduction to Particle Technology*, 2nd ed., 2008).

Tumbling mills operate in the cataracting regime. The grinding media are lifted and partly thrown across the mill. To achieve this, the mill is operated at Froude numbers in the range 0.65–0.80 where the Froude number is defined as:

$$Fr_m = \frac{\omega R^2}{g} \quad \text{59}$$

where  $\omega$  is the rotational velocity (rad/s),  $R$  is the drum radius, and  $g$  is gravitational acceleration.  $Fr_m = 1$  corresponds to the speed required to suspend a single grinding ball or rod on the rim of the drum due to centripetal forces alone.

#### 5.5.4 Stirred Media Mills

Similar to tumbling mills, stress is imparted to particles indirectly via grinding media. However, the media are set in motion by high-speed rotating impellers, typically operating with tip speeds in the range 5–15 m s<sup>-1</sup> (Figure 5.14). The media consist of sand, glass, ceramic, or steel beads. Hence, stirred media mills are sometimes called bead mills. The media completely fill the mill with a slurry of the particles to be ground filling the interstitial spaces. The energy intensity in stirred media mills is very high and they are used for very fine grinding to produce sizes from 10 μm to less than 100 nm. They are often used for soft materials such as dyes, paints, and foods where the feed particles may actually be soft aggregates of much finer primary particles. Media mills can only handle low throughputs less than 10 tonnes h<sup>-1</sup> and are only suitable for wet milling operations. Some of the design principles for media mills are covered in Section 5.6.3.

#### 5.5.5 Jet Mills

Jet mills, also known as fluid energy mills, use turbulent eddies in a high-velocity fluid stream to entrain particles and cause high-velocity collisions between particles, or between a particle and the wall of the mill. Hence, the breakage mechanism is impact. Air is usually used as the fluid. The air velocity, and hence the particle velocity, is very high, up to several hundred m s<sup>-1</sup>. Several geometries are available including the spiral jet mill, the loop jet mill, and the opposed jet mill (see Figure 5.16). Jet mills give a dry grinding alternative to stirred media mills for producing ultrafine powders. They usually include an internal classifier such as a cyclone or other centrifugal separator. The product size increases as the powder feed rate increases.

#### 5.5.6 Selection of Particle Size Reduction Equipment

There are a number of factors to be considered when selecting the type of particle size reduction equipment. These include the following.

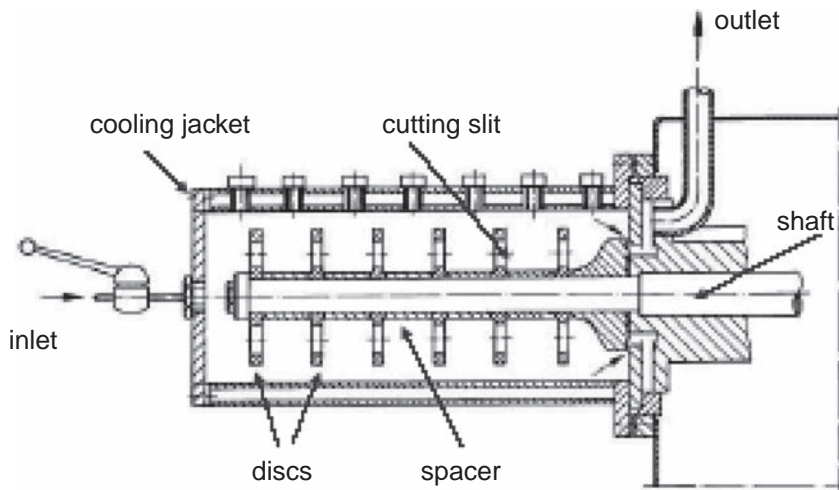


**Figure 5.14** Schematic of a stirred media mill (Kwade and Schwedes, 1997).

1. Size of the feed material and desired size of the product material.
2. Type of material: brittle, ductile, soft aggregates.
3. Capacity or production rate.
4. Wet or dry grinding.
5. Wear of equipment and grinding media, related maintenance costs, and risk of product contamination.
6. Cost.
7. Past experience with equipment and suppliers.

Points 6 and 7 may dominate decision-making. However, a classification of some of the more common equipment based on points 1–4 is given in Table 5.1 as a guide for first-pass screening of equipment options.

## 5.6 Energy Relationships and Scaling

Particle size reduction is a very intensive user of energy so a very reasonable question is:

*How much energy do I need to grind a material from size A to size B?*

As the energy input to a mill is usually related to its size, answering this question also gives us information on the size of mill we need to use – i.e., the development of scaling relationships.

Answering the energy question has challenged engineers for 150 years. As grinding produces new surfaces with higher energy than the bulk material, one might

**Table 5.1** Useful information to aid particle size reduction equipment selection

Equipment	Feed size (mm)	Product size (mm)	Maximum capacity* (tonne h <sup>-1</sup> )	Wet or dry	Breakage mode
Jaw crusher	100–2,000	25–100	4,000	Dry	Crushing
Cone crusher	100–500	5–50	2,400	Dry	Crushing
Hammer mill	5–350	1–25	850	Dry	Impact
Roll crusher	1–5	0.1–1	850	Dry	Crushing
Rod mill	0.15–1.5	0.05–0.5	300	Wet or dry	Media
Ball mill	0.15–1.5	<0.05	300	Wet or dry	Media
Media mill	0.05–0.5	<0.05	10	Wet	Media
Jet mill	0.05–1.5	<0.05	6	Dry	Impact

\* Capacity is very dependent on desired product size.

assume that the energy requirement per unit mass (the specific energy requirement) is proportional to the increase in specific surface energy of the particles:

$$E_m = C_R \left[ \frac{1}{x_2} - \frac{1}{x_1} \right] \quad 50$$

where  $E_m$  is the specific energy requirement (kJ kg<sup>-1</sup>),  $x_1$  and  $x_2$  are the feed size and product size, respectively, and  $C_R$  is a constant. This relationship was proposed by Rittinger in 1867. However, in grinding equipment as little as 0.3% of the energy is actually used to create new surface, and Equation 5.40 overpredicts the energy requirements for milling. Some more modern approaches for energy requirements for milling are summarized in this section.

### 5.6.1 The Bond Work Index

Bond developed an empirical modification to Equation 5.40 which gives a better estimate of the specific energy  $E_m$  required for grinding:

$$E_m = W_I \left[ \frac{10}{\sqrt{x_2}} - \frac{10}{\sqrt{x_1}} \right] \mu\text{m}^{1/2} \quad 51$$

where  $W_I$  is the Bond Work Index and the particle size is measured in microns.  $W_I$  represents the specific energy required to reduce a particle from infinite size to 100  $\mu\text{m}$ , usually measured in units of kW-h t<sup>-1</sup> or kJ kg<sup>-1</sup>. Of course, both the feed and product streams will be size distributions, not monosized. Bond used  $x_{80}$  as the representative particle size in his equations, although there is no fundamental reason for this choice.

**Table 5.2** Example values of Bond Work Index for different materials\*

Material	Bond Work Index (kJ kg <sup>-1</sup> )
Bauxite	37.4
Basalt	80.8
Copper ore	52.0
Limestone	46.0
Phosphate fertilizer	51.6
Quartz	50.6
Calcined clay	5.7

\* For a more complete list of materials, see Green and Perry (2008), chapter 20.

Although purely empirical, this approach is robust and has been used extensively, especially in the mineral industry.  $W_I$  is measured by standard laboratory equipment with different equipment for use in crusher design and grinding mill design. Some typical values of  $W_I$  are given in Table 5.2.

### 5.6.2 Energy–Size Relationships from Single Particle Impacts

Single particle crushing tests, such as those described in Section 5.4.2, can be used to relate the particle size distribution generated to the energy input to the breakage event. This is done using a set of characteristic  $t$  values for the size distribution.  $t_n$  is defined as the fraction of the fragment size distribution that is less than  $(1/n)$ th the size of the particle being broken.  $t_{10}$  is often taken as a representative value of the distribution and will vary with the energy input (see Figure 5.15).  $t_{10}$  can be correlated with the energy input to the crush test:

$$t_{10} = A[1 - \exp(-bE_c)] \quad \text{5.42}$$

where  $A$  and  $b$  are material-specific parameters. Notice that the curves for this example have similar shapes and we can extract the full fragment size distribution by relating  $t_n$  to the value of  $t_{10}$  calculated from Equation 5.42 (Figure 5.15b).

The  $t$  value approach can be used directly to estimate the energy requirement for crushing, where each particle undergoes only one or two breakage events. An appropriate crusher can then be chosen based on its energy rating. This method gives more detailed information on the product size distribution than the Bond Work Index.

There are a couple of things to note with this approach. First, Equation 5.42 and Figure 5.15b assume the  $t$  curves are top size-independent, something that is often true for single particle crushing but not for all breakage modes – e.g., attrition.

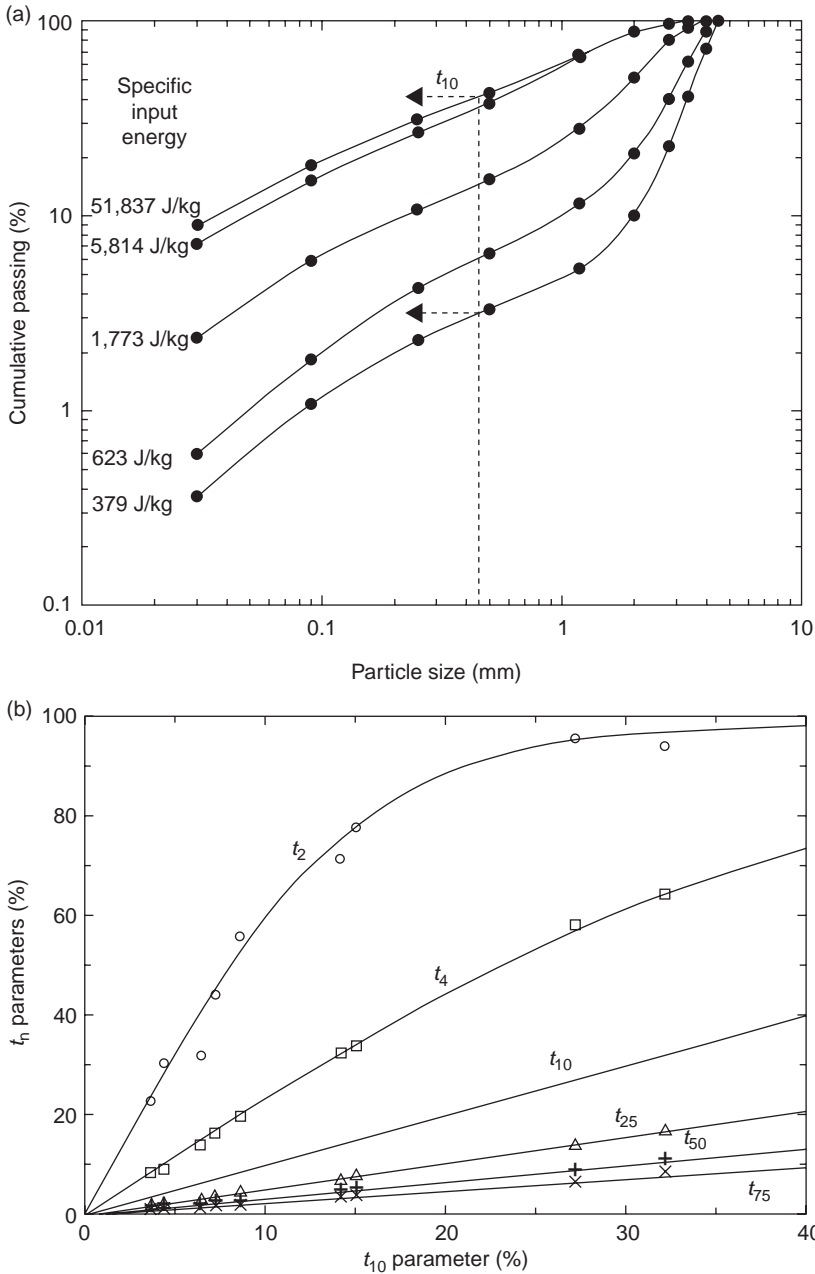


**Figure 5.15** The  $t$  curve approach for energy–size relationships. (a) Calculation of  $t_{10}$  for a copper ore with different specific energy input; (b) characteristic  $t$  curves for the same ore (Salman *et al.*, 2007, chapter 1).

Second, the  $t$  curves are very closely related to breakage function:

$$\Phi'_{j,i} = t_{x_i/x_j}$$

3

For example, if a  $\sqrt{2}$  geometric series is used for the size intervals, then:

$$\Phi'_{5,1} = t_{(\sqrt{2})^{5-1}} = t_4 \quad \text{54}$$

### 5.6.3 Semi-mechanistic Approaches for Stirred Media Mills

The Bond Work Index and  $t$  characteristic approaches do not allow one to easily predict the effect of process parameters on energy requirements and product size distribution. Kwade and Schwedes (2007) introduced a more mechanistic approach to characterizing the energy–size relationships for stirred media mills. The size distribution of product from the grinding mill will be related to two key parameters:

1. the stress energy seen by a single particle when it is crushed between two grinding media  $SE$ ; and
2. the number of such stress events seen by the particle,  $SN$ .

The stress energy seen by a particle is related to the stress energy between two grinding media which collide while rotating in grinding mill  $SE_{GM}$  and which can be written in terms of the kinetic energy of the grinding media:

$$SE \propto SE_{GM} = \rho_{GM} d_{GM}^3 V_t^2 \quad \text{55}$$

where  $\rho_{GM}$ ,  $d_{GM}$ , and  $V_t$  are the density, diameter, and tangential velocity of the grinding media, respectively.

The number of stress events that each particle sees in the mill depends on the number of collisions between grinding media  $N_c$ , the probability that a particle is stressed in such a collision  $P_s$  and the number of particles in the mill  $N_p$ :

$$SN = \frac{N_c P_s}{N_p} \quad \text{56}$$

By considering the factors that control  $N_c$ ,  $P_s$ , and  $N_p$ , we can write an expression for  $SN$  in terms of process variables:

$$SN = \frac{N_c P_s}{N_p} \propto \frac{\phi_{GM} (1 - \varepsilon)}{(1 - \phi_{GM} (1 - \varepsilon)) c_v} \cdot \frac{nt}{d_{GM}^2} \quad \text{57}$$

where  $\phi_{GM}$  is filling ratio of the grinding media,  $\varepsilon$  is the porosity of the bed of grinding media,  $n$  is the impeller rotational speed,  $t$  is the grinding time, and  $c_v$  is the volume fraction of particles in the feed slurry.

It is useful to relate  $SN$  and  $SE$  to the specific energy input to the mill  $E_m$ :

$$E_m \propto SE \cdot SN \quad \text{58}$$

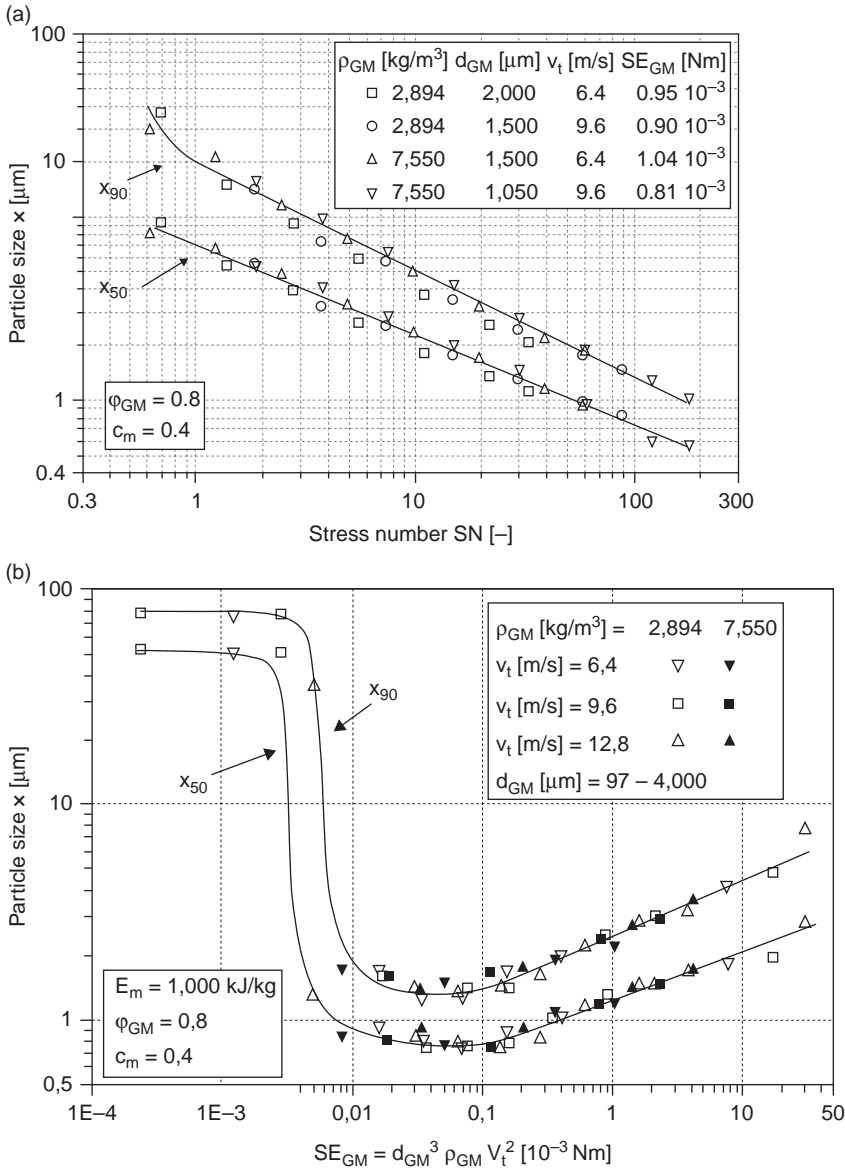


**Figure 5.16** Variation in product particle size with (a)  $SE$  ( $SN$  constant) and  $SN$  ( $E_m$  constant) for grinding limestone (Kwade and Schwedes, 2007)

Thus, we can write the expected product size in terms of any two of  $SE$ ,  $SN$ , and  $E_m$ :

$$x_{50} = f_1(SE, SN) \tag{5.1}$$

$$x_{50} = f_2(SE, E_m) \tag{5.2}$$

$$x_{50} = f_3(SN, E_m) \tag{5.3}$$



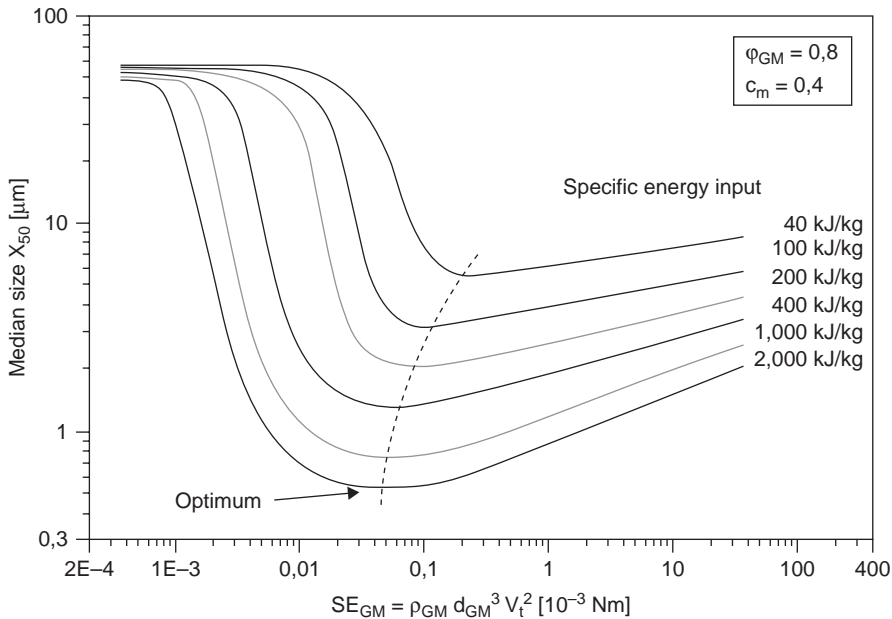


**Figure 5.17** Effect of specific energy and stress energy for media milling of limestone (Kwade and Schwedes, 2007).

The relationship expressed in Equations 5.49 can be measured in laboratory grinding tests for any material of interest. Figure 5.16 shows an example of the effect of  $SN$  and  $SE$  on product size.

As one would expect, the product size decreases monotonically with the number of successful stress events. However, there is an optimum stress energy to minimize the product particle size for a given specific energy input to the mill. If the  $SE$  is too low, the particles may not break. If  $SE$  is above the optimum, more energy is dissipated rather than producing new surface area of particles. Figure 5.17 gives an example of a series of characteristic curves for media milling that can be used for design calculations.

The advantage of such semi-mechanistic approaches is that the effect of important process variables is explicit in the equations, allowing for sensible optimization and design. Equations 5.45–5.49 hold for most crystalline materials. For very hard materials, and for deagglomeration processes, slightly different forms of the equations are used.

#### 5.6.4 Energy Relationships and the Population Balance

The energy–size relationships described in Sections 5.6.1–5.6.3 are not directly integrated with the population balance. They can be used as stand-alone techniques but don't give detailed information about the full product size distribution and are complex to use if mill residence time distribution changes, internal or external classification is used, etc.

However, we can integrate the energy relationships into the population balance if we know the effect of specific energy input on  $S_i$  and  $\phi_{i,j}$ . There is no single, general

relationship for all types of mill and materials. However, models for such relationships are available for particular types of crushers and grinding mills.

$S_i$  is often found to be proportional to the rate of specific energy input in the mill:

$$S_i \propto \dot{E}_m \quad \text{5}$$

$\dot{E}_m$  is the power input to the mill per unit mass of material in the mill, i.e.,

$$\dot{E}_m = \frac{P}{M} = \frac{E_m}{t} \quad \text{5}$$

This suggests a transformation of Equation 5.12 as follows:

$$\frac{dm_i}{dE_m} = \frac{\dot{m}_{i,in} - \dot{m}_{i,ex}}{\dot{E}_m} + \sum_{j=1}^{i-1} \Phi_{i,j} S_j^E m_j - S_i^E m_i \quad \text{5}$$

where

$$S_i^E = \frac{S_i}{\dot{E}_m} \quad \text{5}$$

$S_i^E$  is relatively insensitive to changes in mill scale, grinding media size, and other process parameters.

The breakage distribution can also change with energy input as described in Section 5.6.2. We can correlate the effect of specific energy on the breakage function similar to Equation 5.42:

$$\phi'_{i-j} = A' [1 - \exp(-b' E_c)] \quad \text{5}$$

So if the energy a breakage event is known,  $\phi'_{i-j}$  can be taken from single particle breakage measurements or expressions such as Equation 5.54. This is particularly useful for crusher calculations.

In practice, both  $S_i$  and  $\phi_{i,j}$  will vary with energy input and it is often difficult to deconvolute these effects by simply looking at product size distributions. Typically, the effect of energy input is usually captured in one of other of the two key parameters.

---

### Example 5.5 Bond Work Index Calculation

- What is the required energy input for an impact mill to reduce copper ore from an 80% passing size of 10 mm to 0.5 mm at a rate of 5 tonne h<sup>-1</sup> using Bond Work Index and data from Table 5.2? What fraction of the product is passing 100  $\mu\text{m}$ ?
- For the copper ore in Figure 5.15a, how does the parameter  $t_{50}$  vary with energy input?

*Solution:*

(a) From Table 5.2, the Bond index is  $52.0 \text{ kJ kg}^{-1}$ . Substituting into Equation 5.41:

$$E_m = 52.0 \text{ kJ kg}^{-1} \left[ \frac{10}{\sqrt{500 \mu\text{m}}} - \frac{10}{\sqrt{10,000 \mu\text{m}}} \right] \mu\text{m}^{\frac{1}{2}} = 18.1 \text{ kJ kg}^{-1}$$

Therefore, the required mill power is:

$$P = E_m \dot{M}_F = 18.1 \text{ kJ kg}^{-1} * 5 \text{ tonne h}^{-1} \left[ \frac{1,000 \text{ kg}}{1 \text{ tonne}} \right] \left[ \frac{1 \text{ h}}{3600 \text{ s}} \right] = 25.1 \text{ kW}$$

The Bond Index approach does not give the complete size distribution information. Therefore, we cannot calculate the fraction passing  $100 \mu\text{m}$ .

(b)  $t_{50}$  is the fraction of fragments less than 1/50th of the original particle size ( $4.75 \text{ mm}$ ). Therefore, we read from the graph, the values of % passing ( $4.75 \text{ mm}/50$ ) =  $95 \mu\text{m}$ . From this information, we can construct the following table:

Energy input ( $\text{kJ kg}^{-1}$ )	379	623	1,773	5,814	51,837
$t_{50}$	0.011	0.019	0.065	0.15	0.2

Note that this  $t$  parameter approach does allow the full size distribution to be reconstructed.

**Example 5.6 Stirred Media Mill** I wish to grind a material with the characteristics given by Figure 5.17 to a median size of  $2 \mu\text{m}$  in a media mill where the media are  $1 \text{ mm}$ -diameter particles with a density of  $2,500 \text{ kg m}^{-3}$ . The tangential velocity in the mill is  $10 \text{ m s}^{-1}$ .

- (a) What is the specific energy requirement of the mill?  
 (b) If I double the media size, what is the new energy usage and median particle size?

*Solution:*

First calculate the stress energy for the media:

$$SE_{GM} = \rho_{GM} d_{GM}^3 V_t^2 = 2500 \text{ kg.m}^{-3} (10^{-3} \text{ m})^3 (10 \text{ m.s}^{-1})^2$$

$$\Rightarrow SE_{GM} = 2.5 * 10^{-4} \text{ N.m}$$

Reading from Figure 5.17, the specific energy input for  $x_{50} = 2 \mu\text{m}$  is  $250 \text{ kJ kg}^{-1}$ .

If we double the media size keeping the tangential velocity constant:

$$(SE_{GM})_2 = \frac{d_{GM,2}^3}{d_{GM,1}^3} (SE_{GM})_1 = 8(SE_{GM})_1 = 2.0 * 10^{-3} \text{ N.m}$$

However, the specific energy input will also change. From Equations 5.45, 5.47, and 5.48:

$$E_m \propto SE \cdot SN \propto \frac{d_{GM}^3}{d_{GM}^2} = d_{GM}$$

Therefore:

$$E_{m,2} = 2E_{m,1} = 500 \text{ kJ kg}^{-1}$$

Reading from Figure 5.17, at  $SE_{GM} = 2.0 \times 10^{-3} \text{ Nm}$ ;  $E_m = 500 \text{ kJ kg}^{-1}$ , we find that  $x_{50} = 1.8 \text{ }\mu\text{m}$ . Despite the fact that the specific energy has doubled, we only get a small decrease in the product particle size, as we have moved away from the optimum grinding conditions. By increasing the media size, we have reduced the number of stressing events which mostly counterbalances the increase in energy in each event.

## 5.7 Summary

Particle size reduction is a widely used and energy-intensive process in all industries producing particulate products. A huge variety of equipment designs are available and most can be broadly classified as:

- crushers which cleave individual particles or particle beds by slow compression between two surfaces;
- impact mills where particles break by impact at high speed against hard surfaces in the mill;
- tumbling mills where fine grinding takes place between grinding media (balls, rods) set in motion by the rotation of the mill;
- media mills where the grinding media is set in motion by high-speed discs or impellers; or
- fluid energy (jet) mills where high-speed fluid provides the energy for breakage by impact or shear.

Many crystalline materials break by semi-brittle failure via crack propagation under a tensile stress field. The fracture toughness of the material and the flaw distribution are important properties to determine its effective strength and its rate of breakage in a mill.

Population balance modeling is a strong tool for the design and optimization of milling circuits. For milling, the population balance is usually represented as a discrete mass–size balance (Equation 5.12). Equation 5.12 is generally applicable to any milling flowsheet. In this chapter, we derived simplified versions of the population balance for batch milling (Equations 5.15 and 5.16), continuous well-mixed mill in open circuit (Equation 5.25), and in a closed loop with a classifier (Example 5.4). You should be able to use the population balance models to predict product size

distributions for different mill configurations. With practice, you should be able to use these tools for design and optimization.

The key parameters in the population balance models for particle size reduction are the breakage rate constant  $S_i$ , the breakage function  $\phi_{i,j}$ , and the classifier grade efficiency  $Q_i$ . We discussed a variety of techniques for measuring these parameters from single particle breakage or laboratory-scale milling experiments (Section 5.4.2). We discussed how the parameters vary with particle size, mode of breakage, specific energy, and process parameters for some particular types of mill (Sections 5.4.2 and 5.6.4). You should be able to extract  $S_i$  and  $\phi_{i,j}$  from laboratory data using the techniques we have described, and make a reasonable stab at predicting how these parameters will change with energy input, scale, and process conditions.

We also described the relationship between energy input and product size using a range of empirical and semi-empirical correlations starting with the Bond Work Index. You should be able to use the approaches described in Section 5.6 for first-order estimates of the energy required for crushing or grinding, and for mill sizing.

## 5.8 Bibliography

- Austin, L.G., Klimpel, R.R., and Luckie, P.T., *Process Engineering of Size Reduction: Ball Milling*, Society of Mining Engineers of the AIME, Englewood, CO, USA, 1984, 561 pp.
- Diemer, R.B. and Olsen, J.H., 2002. A moment methodology for coagulation and breakage problems: Part 3 – Generalized daughter distribution functions. *Chemical Engineering Science*, 57, 4187.
- Green, D.W. and Perry, R.H. (eds.), *Perry's Chemical Engineers Handbook 8th edition*, chapter 20, McGraw-Hill, New York, 2008.
- Kelly, E.G. and Spottiswood, D.J., 1995. *Introduction to Mineral Processing*, chapters 7 and 8, Australian Mineral Foundation.
- Klimpel, R.R., 1997. *Introduction to the Principles of Size Reduction of Particles by Mechanical Means*, NSF Center for Particle Technology Instructional Series, University of Florida.
- Kwade, A. and Schwedes, J., 1997. Wet comminution in stirred media mills. *KONA*, 15, 91–101. Wet grinding in stirred media mills. In A.D. Salman, M. Ghadiri, M.J. Hounslow (eds.), *Handbook of Powder Technology Volume 12: Particle Breakage*, Elsevier, Amsterdam, 2007, chapter 6.
- Napier-Munn, T.J., 1996. *Mineral Comminution Circuits: Their Operation and Optimisation*, Napier-Munn, T.J. et al., JKMRRC monograph series, Julius Kruttschnitt Mineral Research Centre, University of Queensland, Australia, 413 pp.
- Rhodes, M.J., 2008. *Introduction to Particle Technology* (2nd ed.), John Wiley, Chichester; New York, Chapter 12.

Salman, A.D., Ghadiri, M. and Hounslow M.J. (eds), *Handbook of Powder Technology Volume 12: Particle Breakage*, A.D. Salman, M. Ghadiri, M.J. Hounslow (eds.), Elsevier, Amsterdam, 2007.

### 5.9 Problems

- 5.1. The energy required to break 150 catalyst beads is measured and fitted using a Weibull distribution with parameters  $W_m = 900 \text{ J kg}^{-1}$  and  $n = 1$ . What is the median breakage energy for these beads? Plot the breakage energy frequency distribution of (a)  $W$  and (b)  $\log(W)$ . How does the distribution change if  $n = 2$ ? How would you expect  $W_m$  to change if the bead size was doubled?
- 5.2. The grinding characteristics of an ore in a ball mill are given by:

$$S_i = 0.1x_i^{0.5}$$

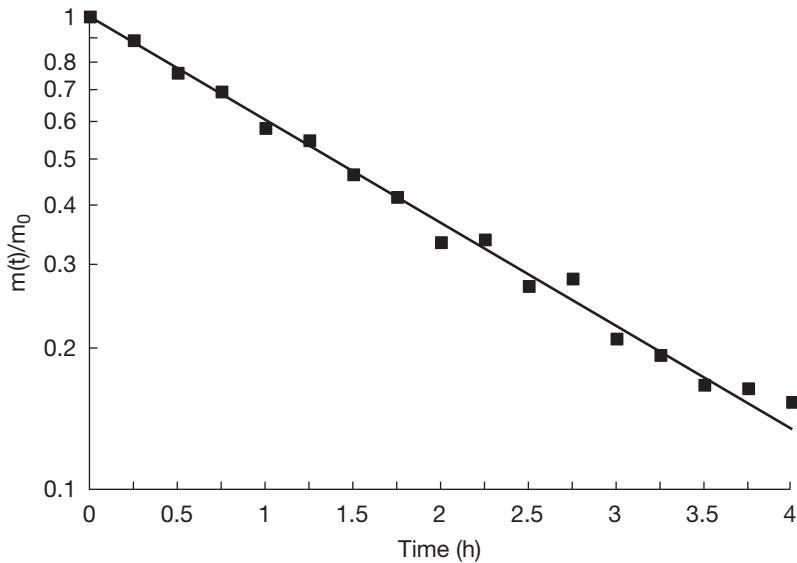
$$\Phi = \begin{bmatrix} 0 & 0 & 0 & 0 & 0 \\ 0.4 & 0 & 0 & 0 & 0 \\ 0.3 & 0.4 & 0 & 0 & 0 \\ 0.2 & 0.3 & 0.4 & 0 & 0 \\ 0.1 & 0.3 & 0.4 & 1.0 & 0 \end{bmatrix}$$

The mill has a 3 m diameter and is 3 m long. The flow rate to the mill is 8.4 tonne  $\text{h}^{-1}$  and the feed takes up 10% of the mill volume. The feed bulk density is 2,000  $\text{kg m}^{-3}$ . Assume the mill is well mixed. The size distribution of feed to the mill is:

Size interval	Top size $x_i$ (mm)	Mass fraction $y_{mi}$
1	2	0.1
2	1	0.3
3	0.5	0.3
4	0.25	0.2
5	0.125	0.1

What fraction of the ore remains above 0.25 mm in the product from the mill? Would this fraction be larger or smaller if the mill were plug flow?

- 5.3. A stirred media mill is used to grind cocoa solids during chocolate manufacturing.
  - (a) In an experiment, the size distribution of solids ( $4 - 8 \text{ }\mu\text{m}$ ) is used as the feed material. The mass fraction of solids remaining in the size fraction is shown as a function of time in the figure below. What is the breakage rate constant  $S_f$  of the  $4 - 8 \text{ }\mu\text{m}$  size fraction in this mill?



- (b) The same mill is reconfigured to run in continuous mode to grind 1 kg/h of cocoa solids feed with the following size distribution

Size interval ( $\mu\text{m}$ )	Mass fraction
45–63	0.4
37.5–45	0.3
22.5–37.5	0.2
<22.5	0.1

For this system, the breakage function is expressed as:

$$S_i = k \left[ \frac{x_i}{x_1} \right]^{0.5}$$

where  $x_i$  is the top size of size interval  $i$ , and the breakage function matrix is:

$$\Phi = \begin{bmatrix} 0 & 0 & 0 & 0 \\ 0.2 & 0 & 0 & 0 \\ 0.3 & 0.2 & 0 & 0 \\ 0.5 & 0.8 & 1.0 & 0 \end{bmatrix}$$

If the mill residence time is 1 h, what proportion of the cocoa solids leaving the mill are less than  $37.5 \mu\text{m}$ ? You may assume the mill is operating at steady state and is “well mixed.”

- 5.4. Consider a ball mill in an open circuit continuous process with the flow rate to the mill set so that the mill residence time is 5 min. The feed size distribution, selection function, and breakage function for the system are:

$$Y_{in} = \begin{bmatrix} 0.4 \\ 0.3 \\ 0.2 \\ 0.1 \end{bmatrix} \quad S = \begin{bmatrix} 0.5 \\ 0.3 \\ 0.1 \\ 0.1 \end{bmatrix} \quad \Phi = \begin{bmatrix} 0 & 0 & 0 & 0 \\ 0.35 & 0 & 0 & 0 \\ 0.4 & 0.35 & 0 & 0 \\ 0.25 & 0.65 & 1 & 0 \end{bmatrix}$$

where  $S$  has the units  $\text{min}^{-1}$ .

- a. Calculate the size distribution of the product. You can assume the mill is well mixed and operates at steady state.
- b. Now consider the same ball mill in batch operation. The batch grinding equation for the product is:

$$\frac{dm_i}{dt} = \sum_{j=1}^{i-1} \Phi_{i,j} S_j m_j - S_i m_i$$

Starting from this equation, derive the following expression for the mass of material in the top size fraction ( $i = 1$ ) at any time  $t$ :

$$m_1(t) = m_1(0) \exp(-S_1 t)$$

Assuming the selection function is the same as in part (a), what fraction of the original mass remains in the top size range after 5 min?

- c. In two different cases, explain why there is a much larger amount of broken material left in size range 1 for the mill in continuous operation than when it is run as a batch mill. How would you change your continuous flow sheet to get better efficiency from this mill?
- 5.5. Repeat question 5.4a for the mill operating in closed circuit if the classifier has the flowing characteristics:

$$Q = \begin{bmatrix} 1.0 \\ 0.7 \\ 0.3 \\ 0.1 \end{bmatrix}$$

Determine the particle size distributions and mass flow rates for all the streams in the grinding circuit if the feed flowrate is  $7 \text{ tonne h}^{-1}$ . What is the actual residence time in the mill in closed circuit?

- 5.6. A series of single-particle breakage tests and small-scale grinding experiments has been used to establish models for the breakage rate and breakage function for a mineral ore in a ball mill. The breakage rate is given by Equation 5.27



with  $a = 0.6 \text{ min}^{-1}$ ;  $\alpha = 0.8$ ;  $\mu = 1.9 \text{ mm}$ ;  $\Lambda = 3.7$ . The breakage function is given by Equation 5.30 with  $\gamma = 1.0$ ;  $\beta = 5.0$ ;  $\alpha = 0.55$ .

- a. Plot  $S_i$  and  $\phi'_{i,j}$  vs  $x_i$  on a log-log plot for a geometric size interval where  $x_1 = 2 \text{ mm}$  and  $x_{i+1} = 0.5x_i$ .
- b. Calculate the breakage rate vector  $\bar{S}$  and the breakage function matrix  $\bar{\Phi}$  for eight size intervals where the final size interval is the “pan.”
- 5.7. An ore is reduced from 80%–160 mm to 80%–20 mm at a rate of 100 tonne  $\text{h}^{-1}$  by a single cone crusher operating in open circuit. Estimate the power required for this process.

$$\rho_b = 2,000 \text{ kg m}^{-3}$$

$$W_i = 14 \text{ kWh t}^{-1}$$

- 5.8. You grind quartz down to 0.1  $\mu\text{m}$  diameter starting with 1 mm-diameter quartz glass beads for use in a special automotive coating. The beads cost \$10/kg. Your supplier offers you 5 mm quartz beads of similar purity and mechanical properties at a discount of 10% on the cost. Your mill can handle the feed. Would you recommend purchasing the larger feed at the reduced price? For purpose of calculation, the cost of electricity is \$0.1  $\text{kWh}^{-1}$ . For quartz,  $W_i = 12.7 \text{ kWh t}^{-1}$ .
- 5.9. A suspension of living cells is to be milled in a stirred media mill as a first step to recover a genetically engineered protein that will be used, ultimately, to make ultra-strong thread (with the trade name “SpideySilk”). Your job is to ultimately scale up the process. Lab-scale mill data are given below.

Time/trial	Mill speed (rpm)	Mass of cells (g)	Mass of protein in solution (g)	Energy (J)
0		300	0	10
Trial 1, 300 s	20	100	3.7	110
Trial 2, 300 s	30	95	1	235

Mill test parameters:

- grinding media: 1 mm-diameter glass beads
- grinding media density:  $\rho_{\text{gm}} = 2 \text{ g/cm}^3$
- mill speed: 20 rpm
- mill disk diameter: 5 cm
- media volume fraction:  $\phi_{\text{gm}} = 0.50$
- voidage:  $\varepsilon = 0.3$
- viscosity of slurry:  $\eta = 1 \text{ Pa s}$
- Concentration of slurry:  $C_v$ : 1  $\text{g/cm}^3$

- a. Derive a population balance model for the mill. Assume that there are only living cells in the feed (species “1”) and that they break up into two subspecies, desired protein “2” and other biological matter “3”, which is “junk.” The desired protein makes up 2% of the cell weight and this is released per breakage. Furthermore, take into account that milling will also slowly, but surely, destroy the protein (“2” → “3”).
- b. Using the data above, calculate the milling time required to break 90% of the cells if the mill is run at 20 rpm.
- c. Sketch what you expect for the concentration of cells, protein, and “junk” as a function of time for the 20 rpm mill run. Then explain how to determine the optimal time to run the batch at 20 rpm (“SpideySilk” is very, very expensive!). Identify all parameters used in the calculation. Using appropriate mathematical software, quantify your answer by solving the population balance equations from part (a).
- d. You have to scale up from the 100 g quantity to mill 3 kg. You have, at your disposal, a batch mill that can handle the total material; however, you have to decide how best to run it, and energy costs at this scale are important. Given the mill properties below, suggest a strategy for a first guess at the mill conditions.
- Grinding media: 3 mm and 1 mm glass beads
  - Rotational speed: 5–30 rpm
  - Disk diameter: 20 cm

5.10. The following scaling rules are suggested for a tumbling mill:

$$P \propto LD^{2.5}$$

where  $P$  is the power input,  $L$  is the length of the mill, and  $D$  is the mill diameter.

- (a) Assuming that the mill meets the specific energy scaling relationship described in Section 5.4, how does the breakage rate  $S_i$  change with mill diameter if (i) the mills are geometrically similar; or (ii) mill length  $L$  is held constant?
- (b) The required batch time for the milling operation is defined as the time for 95% of the top size particles to be broken. How does the batch time change if the mill diameter is increased five times?

# 6 Aerosol Processes

## 6.1 Consider a Case Study ...

*Perfect Particles Inc.*

Memo to: Technology Development Team  
Memo from: Manager Product Development  
August 24, 2014

### **re: Design of pipe line agglomerator**

#### **Background**

We have some problems with our plant producing our new fumed silica product, *Kitty Clean*<sup>®</sup>. Our new plant oxidizes silicon chloride  $\text{SiCl}_4$  in a flame reactor to produce an aerosol of very small  $\text{SiO}_2$  particles. By quenching the aerosol early in the process with a cooling gas we keep the primary particle size at  $0.25\ \mu\text{m}$ . The product is then a powder of highly porous agglomerates with extremely low bulk density and high surface area. It has very good moisture-carrying capacity and acts as an anticaking agent and there are great opportunities in the growing cat litter market.

Our problem is in the bag filters that collect the product particles. Our bag house is clearly overloaded (or under-designed). We are not meeting our emission guidelines and maintenance costs are very high due to the high frequency of cycling in the bag house. This means frequent replacement of bags due to fatigue.

We contracted a consultant, Dr. Bert Diemer from Diemer Solutions Inc., to troubleshoot the issue. Bert recommended we install a pipeline agglomerator and cyclone between the flame reactor and the bag house. Our fine aerosol particles naturally form loose agglomerates. By encouraging these to grow, they become large enough for a significant proportion to be removed in the cyclone. He recommends we remove 75% of the mass of particles in the cyclone to relieve the load on the bag house.

I've discussed the proposal with the plant manager and engineer. They are keen, but point out that we will still need to allow 8 psig for bag house operation. This leaves only 2 psig allowable pressure drop in the pipeline agglomerator.

Bert has offered to design the pipeline agglomerator and cyclone to reduce the mass load on the bag house by 75%. However, we have used up 95% of our consultant budget so we would like you to do the design. (It can't be that complicated. It's only a pipe after all.)

### Your Task

Your task is to design the pipeline agglomerator and cyclone specifying pipeline length and diameter and cyclone dimensions to achieve 75% reduction in bag house load within the pressure drop constraint discussed above.

This will involve an appropriate computer model to predict the development of the particle size distribution in the agglomerator and the performance of the cyclone with this particulate feed. As we roll out *Kitty Clean*<sup>®</sup> around the world we expect to need to do similar designs and troubleshooting so please make the model sufficiently flexible for more general use.

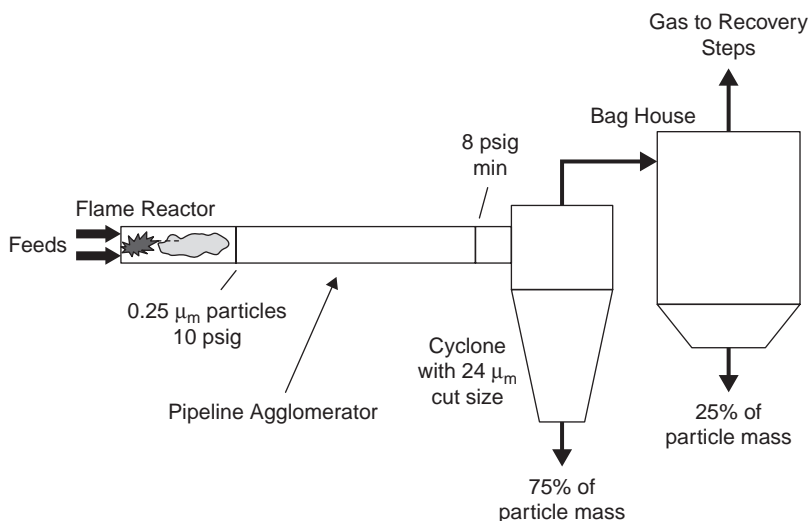
### Problem Specifications

Powder suspended in gas-leaving flame reactor:

Mass flow rate (gas + solid)	15,900 kg h <sup>-1</sup>
Temperature	200°C
Pressure	10 psig
Equivalent molecular mass*	44.5 g mol <sup>-1</sup>
Gas viscosity	0.0157 cP
Solids mass fraction	0.15
Solid density	2,200 kg m <sup>-3</sup>
Particle size	0.25 μm

\* Equivalent molecular mass = (mass gas + solid)/mole gas.

Allowable pressure drop in pipeline agglomerator and cyclone is 2 psig. Agglomerates leaving the pipe reactor are fractal with a fractal dimension 1.8. (See Diemer and Ehrman, 2007, for further details of this case study.)



Schematic of the flame reactor and proposed pipeline agglomerator and cyclone (Diemer and Ehrman, 2005).

Flame reactors are the most common form of an aerosol process where particles of controlled properties are formed from the vapor phase, in this case as the particulate product of a combustion reaction. There is an analogy to crystallization, where particles are formed from the liquid phase. Similar to crystallization, nucleation and growth are important particle-formation mechanisms. Aerosol processes are generally used to form submicron (nano-) primary particles. Due to their small size, a variety of agglomeration processes can occur so that the product particle is actually an agglomerate of many primary particles.

As an individual reflective exercise, or as a group discussion, discuss your approach to modeling the pipeline agglomerator in this case study:

- Can you write a population balance for the agglomerator? (Review Section 3.6.2.)
- What are the mechanisms by which agglomeration can occur in this gas-phase system?
- What sort of model can you use for the gas cyclone? (Review Section 5.4.3.)
- What is a fractal dimension? (Review Section 2.3.2.)
- What approaches might be available to you to change the primary particle size from 0.25  $\mu\text{m}$ ?

What learning goals related to aerosol processes does this case study inspire for you and how do they compare with the chapter learning goals listed below?

## 6.2 Learning Goals

At the completion of this chapter, the student should be able to:

1. Describe the different elements of a process plant based around aerosol particle synthesis and typical application areas for aerosol processes.
2. Describe the key mechanisms that control the particle size and morphology produced by aerosol synthesis and explain the mathematical expressions for these rate processes to a peer.
3. Use mass, energy, and population balances to address simple problems related to aerosol design and operation problems similar to those at the end of this chapter.
4. Critically analyze and interpret real aerosol reactor data sets from laboratory or plant trials using appropriate analysis tools.
5. Attack open-ended particle design or troubleshooting problems in aerosol processes of similar nature to the introductory case study for this chapter.

## 6.3 Aerosol Reactor Overview

Aerosol processes are analogous to crystallization processes in that discrete particles are formed from a continuous phase. Unlike crystallization, in this case the continuous phase is a gas. The particulate phase is often the product of a high-temperature

reaction. The thermodynamic driving force for condensation of the particles is often very high, resulting in very high nucleation rates and, therefore, very small particle size. Thus, aerosol processes are one of the main industrial processes for making submicron (nanosized) particles with primary particle size from 20 to 200 nm. Some of the advantages of the aerosol route to manufacturing fine particles are:

- there are no liquid byproducts;
- it is easier to separate very small particles from a gas phase than from a liquid phase;
- products have very high purity; and
- kinetics of the processes are fast and the process flowsheet is relatively simple.

Some of the application areas where such small particles are required are listed in Table 6.1. Although many of the products are modern (e.g., sunscreen), aerosol processes are not new. The process to produce submicron particles of carbon for making printing inks from oxygen-starved flames was first practiced in China at least 2,000 years ago!

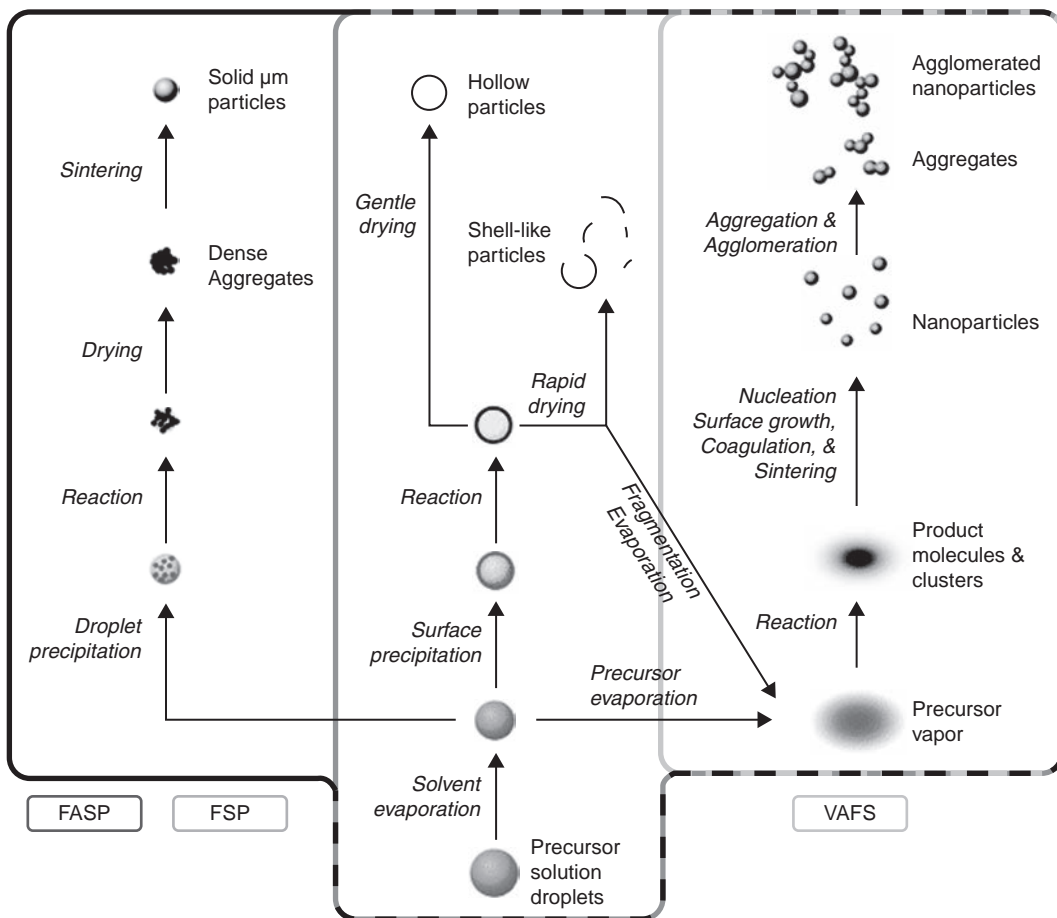
Flame reactors account for about 90% of fine particles made in aerosol reactors (Strobel and Pratsinis, 2007). Others are plasma, laser, and electrically heated wall reactors. Flame reactors can be divided into two types depending on the form of the precursor. Vapor-fed flame synthesis (VAFS) “burns” or hydrolyzes a vapor from a volatile precursor. Liquid-fed flame synthesis (LAFS) can handle non-volatile feeds. Particles are formed by a combination of solvent evaporation and reaction, where the flame provides the necessary energy source. LAFS is sometimes broken down into flame-assisted spray pyrolysis (FASP) and flame spray pyrolysis (FSP) depending on the enthalpic content of the feed liquid. Figure 6.1 shows these two routes to particle production.

A schematic of a general aerosol processing plant is shown in Figure 6.2. Preparation of the feed material is needed to give a volatile liquid precursor that can be heated and sent as a vapor to the reactor, or else atomized directly into the reactor. The aerosol reactor is responsible for both the reaction conditions and particle formation and growth. As for any chemical reactor, mixing conditions and residence time control are key. Heating and/or cooling are used to control the temperature profile. Regular wall scale removal may also be necessary. The base powder recovery involves separation of the particulate product (usually present in low-volume fractions) from the gas streams using standard techniques such as cyclones and bag filters. At this point, the particulate product is usually present as fluffy, loose agglomerates. Depending on the end use, a series of powder-refining processes such as degassing, desorption, and wet or dry grinding for deagglomeration are used to control the final powder properties. Products are formulated, often with additives to improve performance, as slurries, granules, or compacts using processes described in the later chapters of this book.

Aerosol synthesis chemistries include pyrolysis, oxidation, hydrolysis, and ammoniation. With the exception of carbon, the products are inorganic (metals, metal oxides, and nitrides). Table 6.2 gives examples of some of the more common chemistries used.

**Table 6.1** Application areas for submicron particles produced by aerosol reactors

Application	Key product attribute	Typical materials
Inks and pigments	Optical opacity, color	Titania, carbon black, lead oxide
Sunscreen	UV opacity	Titania, zinc oxide
Polymer fillers and composites	Enhanced mechanical properties	Carbon black
Flow aid	Improved powder flow	Fumed silica
Optical fibers	High purity, refractive index	Doped silica
Catalysts	Activity, photocatalytic performance	Titania, Pt/Al <sub>2</sub> O <sub>3</sub>

**Figure 6.1** Particle formation in different types of flame reactors (Strobel and Pratsinis, 2007).

Aerosol reactors can also be used to produce films if the reactor is designed to deposit particles on a surface. This is often achieved by thermophoresis, where the difference in temperature between the flame and the surface causes a diffusive flux

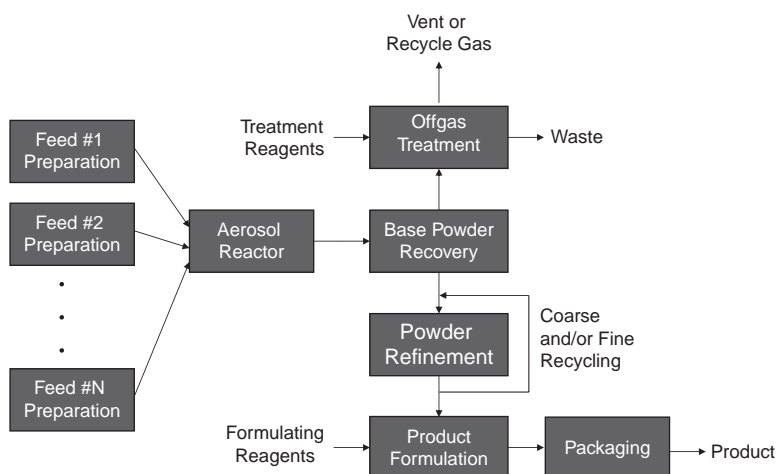


**Figure 6.2** Schematic of a typical aerosol processing plant.

**Table 6.2** Aerosol synthetic chemistries

Pyrolysis	$AL_y \rightarrow A + yL$	A = Si, C, Fe, ... L = H, CO, ...
Halide oxidation	$MX_y + (y/4)O_2 \rightarrow MO_{y/2} + (y/2)X_2$	M = Si, Ti, Al, Sn, ... X = Cl, Br, ...
Halide hydrolysis	$MX_y + (y/2)H_2O \rightarrow MO_{y/2} + yHX$	M = Si, Ti, Al, Sn, ... X = Cl, Br, ...
Alkoxide hydrolysis	$M(OR)_y + yH_2O \rightarrow MO_{y/2} + yROH$	M = Si, Ti, Al, Sn, ... R = CH <sub>3</sub> , C <sub>2</sub> H <sub>5</sub> , ...
Alkoxide pyrolysis	$M(OR)_y \rightarrow MO_{y/2} + (y/2)ROR$	M = Si, Ti, Al, Sn, ... R = CH <sub>3</sub> , C <sub>2</sub> H <sub>5</sub> , ...
Halide ammoniation	$MX_y + (y/3)NH_3 \rightarrow MN_{y/3} + yHX$	M = Si, Ti, Al, Sn, ... X = Cl, Br, ...

of particles that deposit on the wall (see Figure 6.3). Optical wave guide fibers are manufactured in this way.

## 6.4 The Rate Processes of Aerosol Reactors

The formation, growth, and transformation of particles within the aerosol reactor are complex (see Figure 6.4). Initially, particles nucleate and grow in a similar fashion to crystallization. As the particles are very small and the gas viscosity is very low, collisions between particles play a much larger role in changing the particle size and morphology than in liquid-phase crystallization. Particle collision leads to agglomeration, and the size of agglomerates may be set by a balance between agglomeration and breakage. Particularly when hot, agglomerates may coalesce via sintering



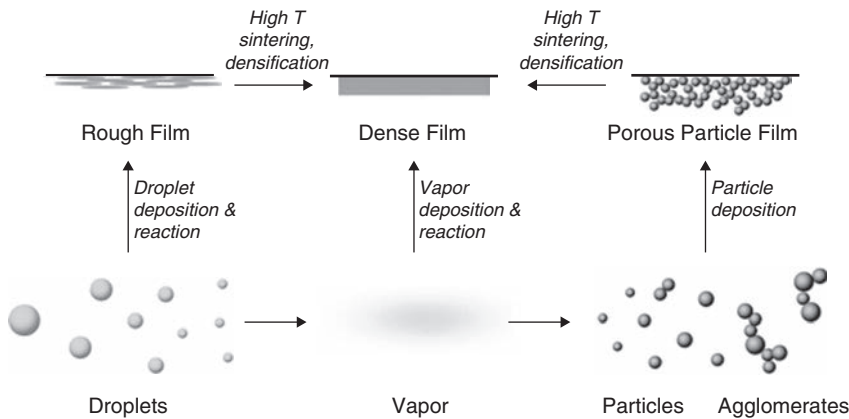


**Figure 6.3** Film formation using aerosol reactors (Strobel and Pratsinis, 2007).

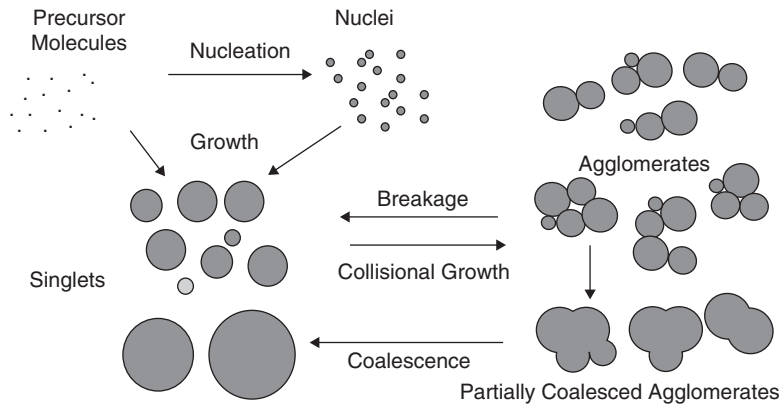


**Figure 6.4** Rate process map for particle formation, growth and transformation in aerosol processes.

to form a single, larger primary particle. When cooler, agglomerates may continue to grow and break, but will no longer coalesce. These agglomerates are held together by van der Waals forces and are relatively easy to break down in post-processing. Partially sintered agglomerates are often called aggregates. Held together by solid bridges, aggregates are relatively strong. The result of these competing processes gives a complex structured agglomerate or aggregate. The key properties we wish to control are the primary particle size, the agglomerate (aggregate) size, and the structure of the agglomerate (aggregate).

A typical aerosol reactor operates under near-plug flow conditions with small particles at relatively low concentration moving down the reactor with the gas streamlines. Once reaction is complete, heat is removed from the wall of the reactor to control the rate of coalescence. Figure 6.5 shows a typical temperature–axial distance profile along an aerosol reactor. Conceptually, we can break the reactor up into at least three different zones.

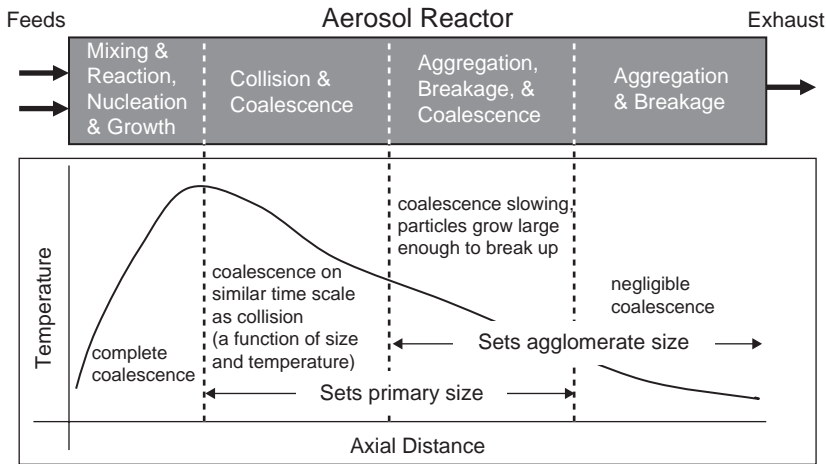


**Figure 6.5** Typical temperature profile and different mechanism zones within an aerosol reactor.

1. Reaction zone: In this zone the feed components mix rapidly and react. Nucleation and growth of primary particles of the reaction product occur.
2. Collision and coalescence zone: There is no more reaction, but agglomerates form by collision and coalescence transforms the agglomerates into single particles.
3. Aggregation and breakage: At cooler temperatures, no coalescence occurs, but aggregates are formed and may break within the flow field.

Figure 6.6 gives an example of differences in primary particle size and agglomerate structure as a function of (a) distance from the flame, and (b) temperature in an aerosol reactor. By controlling the mixing in the reactor and the temperature–time profile along the reactor length, the balance between the different rate processes is changed and very different primary particle and agglomerate properties are achieved.

### 6.4.1 Nucleation

For crystallization from the liquid phase, nuclei will form at a certain size  $v_0$  related to the critical cluster size (see Section 4.5.2). In aerosol systems,  $\Delta G_{crit}$  is generally very large so that the critical cluster size  $x_{nuc}$  is of the same order as the size of the molecule. Therefore, the nucleation rate is generally set by the reaction rate of the precursor in the gas phase, rather than by cluster formation.

### 6.4.2 Growth

The particle growth rate, sometimes called the accretion rate, is usually controlled by the chemical reaction rate:

$$\dot{m}_{rxn} = \rho_p \int_0^{\infty} V G_v(v) n(v) dv \quad 6.1$$

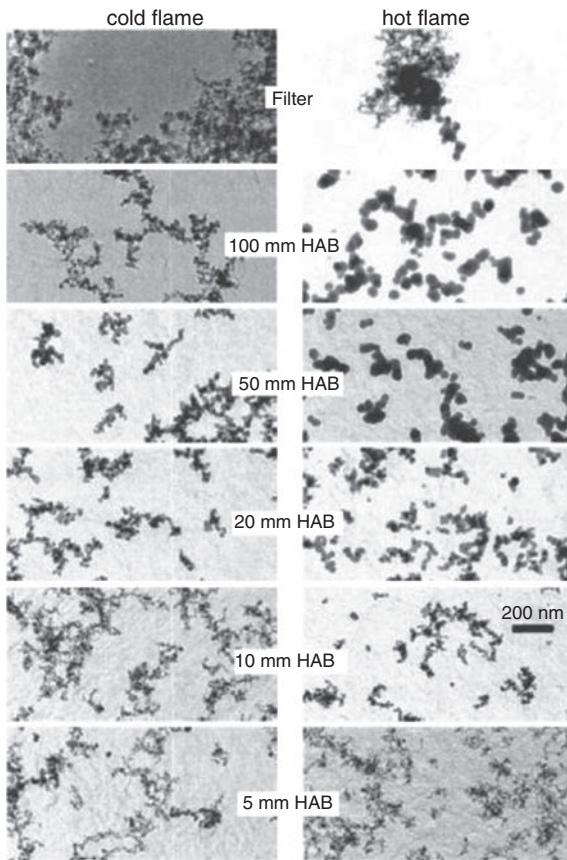


**Figure 6.6** Thermophoretically sampled TEM pictures of silica nanoparticles at different heights above the burner for a cold flame (left-hand side) and a hot flame (right-hand side) along with TEM pictures of the respective filter powders (Kammler *et al.*, 2005).

where  $\dot{m}_{rxn}$  is the rate of production of the particulate phase by reaction. The growth rate can be expressed as

$$G_v(v) = k_g v^n \quad 6.2$$

In the absence of other information, we normally assume the growth of granule volume is proportional to the surface area of the granule ( $n = 2/3$ ), or that the volume-based growth rate is size-independent ( $n = 0$ ).

### 6.4.3 Collision-based Agglomeration and Aggregation

The agglomeration and aggregation processes occur by collision between particles in the aerosol. In the aerosol literature, these processes are sometimes

called collisional growth processes. Agglomeration leads to fractal, relatively weak agglomerates. Aggregation involves collision and coalescence, leading to stronger sintered aggregates. As the particles are small and air has low viscosity, short- and long-range attractive forces between particles are strong compared to the stored energy during a collision. Hence most collisions lead to successful agglomeration and the rate of agglomeration is therefore set by the rate of collision.

We can model the binary collision process as described in Section 3.6.2, where the key parameter is the agglomeration kernel  $\beta(v, v')$ . Where the agglomeration kernel is equal to the rate of collisions, we can derive some first principles expressions for the kernel.

In the earliest stage of the process, when the particles are of the order of a few molecules, collisions occur in the free molecular regime. As particles grow into the 10–1000 nm range, collisions are mainly due to Brownian motion of the particles in the gas. In the continuum Brownian regime:

$$\beta_{Br}(v, v') = \frac{2kT}{3\mu_g} \left[ 2 + \left( \frac{v}{v'} \right)^{1/3} + \left( \frac{v'}{v} \right)^{1/3} \right] \quad 6.3$$

where  $k$  is Boltzmann's constant and  $\mu_g$  is gas viscosity. This kernel is relatively insensitive to the size of the particles in the collisions. For ease of calculation, we can often approximate  $\beta(v, v')$  for a relatively narrow particle size distribution as:

$$\beta_{Br}(v, v') \approx \beta_{Br}(v, v) = \frac{8kT}{3\mu_g} \quad 6.4$$

This simplified kernel is size-independent and only a function of temperature.

Downstream, where the particles are larger and the temperature lower, the rate of collision is controlled by turbulent shear in the flow field. The Saffman–Turner kernel for turbulent flow is:

$$\beta_{Tu}(v, v') = 0.31 \left( \frac{\epsilon \rho}{\mu_g} \right)^{1/2} \left[ v^{1/3} + v'^{1/3} \right]^3 \quad 6.5$$

where  $\epsilon$  is the turbulence intensity of the flowing gas stream which is directly related to the friction factor. This kernel increases with shear rate and is proportional to particle (agglomerate) volume, and so dominates the collision rate as the agglomerates grow.

Note that the agglomerates formed by these processes are fractal in nature, so we need to be careful about the definition of particle size. Here, the agglomerate volume  $v$  is the solid volume of the agglomerate, i.e.:

$$v = n_p \alpha_v d_p^3 \quad 6.6$$

where  $n_p$  and  $d_p$  are the number and size of the primary particles in the agglomerate. The linear size of the agglomerate is:

$$d_{agg} = d_p n_p^{1/D_f} \quad 6.7$$

It is important to note that the kernels in Equations 6.3–6.5 are all based on the rate of collision. We assume that all collisions lead to agglomeration – i.e., the agglomeration efficiency is 1. There is no general rule for calculating the agglomeration efficiency in aerosol processes.

#### 6.4.4 Coalescence

Coalescence is driven by the thermodynamic driving force to reduce the free energy of the agglomerate by reducing its surface area. Therefore, we can define the coalescence rate  $\sigma$  as:

$$\sigma = \frac{dA}{dt} = - \frac{A - A_\infty}{\tau_A} \quad 6.8$$

Here  $A$  is the total surface area of the agglomerate and  $A_\infty$  is the minimum surface area of the fully coalesced particle. If both the primary particles and the coalesced particle are considered as spheres, then:

$$A_0 = n_p \cdot 4\pi r_0^2 \quad 6.9$$

$$A_\infty = n_p^{2/3} \cdot 4\pi r_0^2 \quad 6.10$$

where  $n_p$  is the number of primary particles in the agglomerate, and  $\tau_A$  is the characteristic coalescence time.

If the aerosol particles are low viscosity liquid drops, coalescence is very fast: e.g., atmospheric processes such as raindrop formation and photochemical smog. For high-viscosity liquid and amorphous solids above the glass transition temperature, coalescence occurs by viscous flow. For amorphous solids below the glass transition temperature and crystalline solids, coalescence is much slower and occurs by a variety of different sintering mechanisms (see Table 6.3).

Figure 6.7 shows the geometry of the early stage of sintering of two spheres. As sintering proceeds, the sinter neck radius  $yr_0$  increases from the initial condition of a point contact ( $y = 0$ ). We can write an expression for the rate of change of the sinter neck radius as:

$$\frac{dy}{dt} = \frac{CY(T)}{r_0^m y^n} \quad 6.11$$

where the values of the parameters  $C$ ,  $Y(T)$ ,  $m$ , and  $n$  depend on the mechanism by which sintering occurs. Table 6.3 lists a number of different mechanisms with the corresponding expressions for the parameters in Equation 6.11.

**Table 6.3** Sintering mechanisms for coalescence of aerosol particles (Coblentz *et al.*, 1980)

Mechanism	$C$	$Y(T)$	$m$	$n$
Viscous flow	0.750	$\frac{\gamma^{lv}}{\mu}$	1	1
Evaporation–condensation	0.798	$\frac{\alpha_e P_0 \Omega}{\sqrt{MRT}} \frac{\gamma^{lv} \Omega}{RT}$	2	2
Surface diffusion	$4.157 \delta$	$D_s \frac{\gamma^{lv} \Omega}{RT}$	4	5
Grain boundary diffusion	$32b$	$D_b \frac{\gamma^{lv} \Omega}{RT}$	4	5
Lattice diffusion: grain boundary	24	$D_l \frac{\gamma^{lv} \Omega}{RT}$	3	4
Lattice diffusion: surface	5.945	$D_l \frac{\gamma^{lv} \Omega}{RT}$	3	3.33

$\Omega$  is the molar volume of the species,  $\alpha_e$  is the evaporation rate constant,  $\gamma^{lv}$  is the surface energy of the drop/particle,  $D_s$ ,  $D_b$ , and  $D_l$  are diffusion coefficients.

At extended sintering times, we can express the change in coalescence angle as a first-order expression:

$$\frac{d\lambda}{dt} = -\frac{\lambda}{2\tau_A} \quad 6.12$$

where  $\lambda$  is defined in Figure 6.7. Noting the  $\lambda(0) = 1$ , we can integrate Equation 6.12 to give:

$$\lambda(t) = \exp\left(-\frac{t}{2\tau_A}\right) \quad 6.13$$

Starting from Equations 6.11 and 6.12, it is possible to derive a general expression for calculating the characteristic coalescence time for all the mechanisms listed in Table 6.3 (Diemer, 2002):

$$\tau_A = \frac{(0.44)^{n-1}}{2} \left[ \frac{r_0^m}{CY(T)} \right] \quad 6.14$$

#### 6.4.5 Agglomerate Breakage

As agglomerates grow larger, turbulent shear in the gas stream may cause them to break, as well as to agglomerate. Using the analogy to breakage during milling

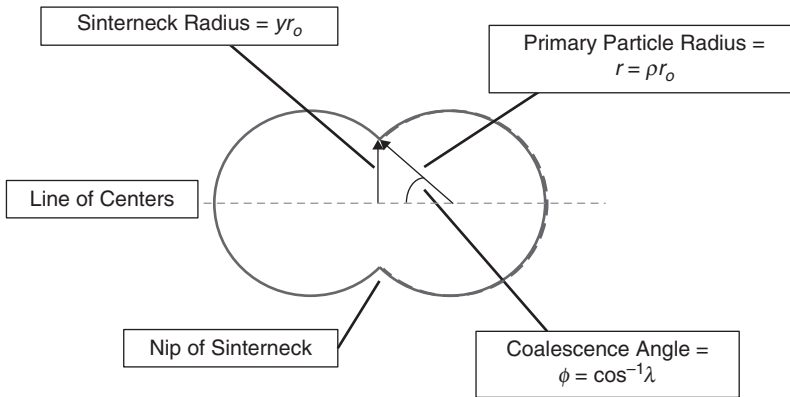


**Figure 6.7** Initial stage binary sintering and model.

operations (Chapter 5) and also borrowing from the breakage of flocs suspended in liquids, the rate of breakage can be represented as:

$$S_{br} = k_{br} \left( \frac{\epsilon \rho}{\mu_g} \right)^\kappa v^\eta \quad \text{with } 0 < \eta < 1 \quad 6.15$$

Recent work suggests that the breakage selection function may be linear in power input ( $\kappa = 1$ ), but this is not universal. Note the breakage rate can be a stronger function of the turbulence intensity than the collision rate for agglomeration (Equation 6.5). There is no clear model for the breakage fragment distribution. In the absence of such a model, one can assume the agglomerate breaks into fragments of equal volume:

$$\phi(v', v) = 2\delta(v - v'/2) \quad 6.16$$

**Example 6.1 Calculating the Agglomeration Rate** Aerosol particles are flowing in a gas stream at 700 K with a gas velocity of 20 m s<sup>-1</sup> in a smooth pipe of diameter 0.1 m. Assume the gas has the properties of nitrogen. The suspension has an equivalent molecular mass of 50 g mol<sup>-1</sup>. At what agglomerate size (measured by the volume  $v$ ) does the rate of agglomeration by turbulent shear exceed that by Brownian motion?

*Solution:*

At these conditions, the gas viscosity  $\mu_g = 3.2 \times 10^{-5}$  Pa.s and the suspension density is calculated as:

$$\rho = \frac{P}{RT} = \frac{1.01 \times 10^5 \text{ Pa.s}}{8.314 \text{ J mol}^{-1} \text{ K}^{-1} \times 700 \text{ K}} = 17.2 \text{ mol.m}^{-3} \left[ \frac{0.050 \text{ kg}}{\text{mol}} \right] = 0.86 \text{ kg.m}^{-3}$$

For simplicity, let us consider only equal-volume collisions ( $v' = v$ ). We can use Equation 6.4 to calculate the Brownian collision rate:

$$\beta_{Br}(v, v) = \frac{8kT}{3\mu_g} = \frac{8 \times 1.38 \times 10^{-23} \text{ J.K}^{-1} \times 700 \text{ K}}{3 \times 3.2 \times 10^{-5} \text{ Pa.s}} = 8.05 \times 10^{-16} \text{ m}^3 \text{ s}^{-1}$$

Note that the Brownian motion kernel is zero order: i.e., it is not a function of  $v$ .

The turbulent shear kernel is (Equation 6.5):

$$\beta_{Tu}(v, v') = 0.31 \left( \frac{\epsilon \rho}{\mu_g} \right)^{\frac{1}{2}} \left[ \frac{1}{v^3} + \frac{1}{v'^3} \right]^{\frac{3}{2}}$$

For equal size particles it reduces to:

$$\beta_{Tu}(v, v') = 2.48 \left( \frac{\epsilon \rho}{\mu_g} \right)^{1/2} v$$

To calculate  $\beta_{Tu}$  we first need to calculate the turbulence intensity  $\epsilon$ . This we can do using Equations 6.32–6.36 from Section 6.6 for turbulent fluid flow in a pipe:

$$Re = \frac{D_{pipe} \rho u_z}{\mu_g} = \frac{0.1 \text{ m} \times 0.86 \text{ kg.m}^{-3} \times 20 \text{ m.s}^{-1}}{3.2 \times 10^{-5} \text{ Pa.s}} = 54,000$$

$$f_F = \frac{0.04}{Re^{0.16}} = \frac{0.04}{54,000^{0.16}} = 0.007$$

$$\epsilon = \frac{2 f_F u_z^3}{D_{pipe}} = \frac{2 \times 0.007 \times (20 \text{ m.s}^{-1})^3}{0.1 \text{ m}} = 1.1 \times 10^6 \text{ m}^2 \text{ s}^{-3}$$

Substituting into the expression for  $\beta_{Tu}$ :

$$\beta_{Tu}(v, v') = 2.48 \left( \frac{1.1 \times 10^6 \text{ m}^2 \text{ s}^{-3} \times 0.86 \text{ kg.m}^{-3}}{3.2 \times 10^{-5} \text{ Pa.s}} \right)^{\frac{1}{2}} v = 4.3 \times 10^5 \text{ s}^{-1} \times v$$

Note the turbulent shear kernel is first-order in  $v$ , so increases as particle size increases.

Finally, we equate  $\beta_{Tu}$  and  $\beta_{Br}$ :

$$8.05 \times 10^{-16} \text{ m}^3 \text{ s}^{-1} = 4.3 \times 10^5 \text{ s}^{-1} \times v$$

$$\Rightarrow v = 1.9 \times 10^{-21} \text{ m}^3 = 1.9 \times 10^{-3} \text{ } \mu\text{m}^3$$

The turbulence intensity is very high in this small-diameter pipe with high gas velocity, and turbulent shear becomes the controlling agglomeration process at small particle size  $\sim 100 \text{ nm}$ .



**Example 6.2 Prediction of Coalescence Mechanism and Rate** In an effort to understand coalescence by sintering in an aerosol reactor, sintering experiments are conducted under similar environmental conditions for a powder compact. The rate of change in compact height  $\Delta L/L_0$  is analogous to the rate of change of sinter neck radius in binary particle coalescence given by Equation 6.11:

$$\frac{dL}{dt} = \frac{CY(T)}{r_0^m L^n}$$

Given the data below, identify the mechanism of sintering and find a value for the rate parameter  $K$  defined as:

$$K = \frac{CY(T)}{r_0^m}$$

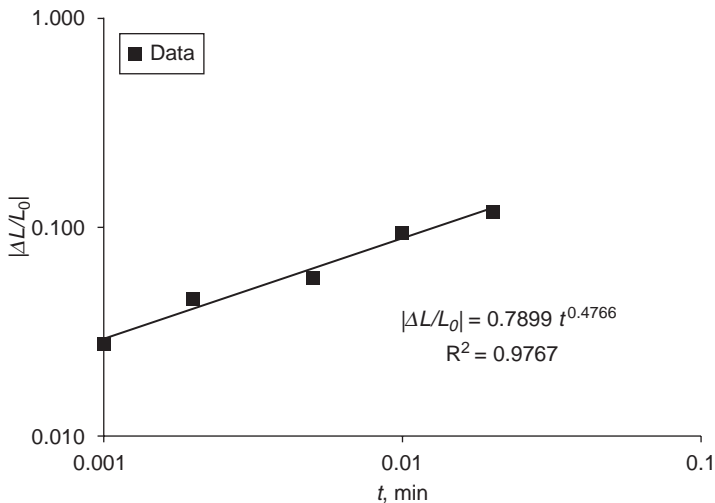
$t$ (min)	0.001	0.002	0.005	0.01	0.02
$\Delta L/L_0$	0.028	0.046	0.058	0.095	0.118

*Solution:*

A log–log plot of the data is expected to be a straight line that should yield a power-law relation:

$$\left| \frac{\Delta L}{L_0} \right| = A \left[ \frac{n+1}{2} \right] t^{\frac{2}{n+1}}$$

as shown in the plot below:



Based on the plot:

$$\text{exponent} = 0.4766 = \frac{2}{n+1} \Rightarrow n = 3.19$$

$$\text{Pre-factor} = 0.7899 \Rightarrow A = 0.376 \text{ min}^{-2/(n+1)}$$

Of the mechanisms listed in Table 6.3, the one with the nearest value of  $n$  is “lattice diffusion from the surface” for which  $n = 10/3 = 3.33$ .

Also note that given the definitions above:

$$A = \frac{K}{2[(n+1)K]^{n+1}}$$

Rearranging:

$$K = (2A)^{(n+1)/2}(n+1)^{(n-1)/2} = 2.66 \text{ min}^{-1}$$

## 6.5 The Population Balance for an Aerosol Reactor

### 6.5.1 General Expressions for Each Reactor Zone

The key attributes of particles from an aerosol reactor include the primary particle size, the agglomerate size, morphology, and surface area. Section 6.4 showed that a wide variety of rate processes can contribute to development of these particle attributes. The population balance is the ideal tool for following the generation of these attributes in the reactor.

Most aerosol reactors can be considered as approximately plug-flow reactors. In addition, there are different zones in the reactor where particular rate processes dominate. In the simplest case, we can divide the reactor into three zones (see Figure 6.5):

1. nucleation and growth;
2. agglomeration and coalescence; and
3. agglomeration and breakage.

Starting from Equation 3.6, we can write the population balance for the nucleation and growth zone as:

$$\frac{\partial n(v, l, t)}{\partial t} + \frac{\partial u_l n(v, l, t)}{\partial l} + \frac{\partial Gn(v, l, t)}{\partial v} = \dot{B}_{nuc} \delta(v - v_0) \quad 6.17$$

At steady state, Equation 6.17 reduces to:

$$u_l \frac{\partial n(v, l)}{\partial l} + \frac{\partial Gn(v, l)}{\partial v} = \dot{B}_{nuc} \delta(v - v_0) \quad 6.18$$

where  $u_l$  is the mean gas velocity in the pipe and we assume that the slip velocity between the particles and the gas is negligible. These equations are similar to those we developed in Chapter 4 for crystallizers (Equation 4.27). Here, however, the PFR rather than the MSMPR is the standard configuration. Also, we prefer to write the equations in terms of volume  $n(v)$  rather than linear size  $n(x)$  as this will make it easier mathematically for modeling the agglomeration, coalescence, and breakage terms below.

At the back end of the reactor, where the reaction is complete and the temperature is too low for coalescence via sintering, we can write the steady-state population balance for agglomeration and breakage as:

$$u_l \frac{\partial n(v, l)}{\partial l} = \frac{1}{2} \int_0^v \beta n(v', l) n(v - v', l) dv' - \int_0^\infty \beta n(v, l) n(v', l) dv' + \int_v^\infty \varphi(v', v) S_{br}(v') n(v', l) dv' - S_{br} n(v, l) \quad 6.19$$

Here we use the birth and death terms for agglomeration and breakage derived in Chapter 3 (Equations 3.28, 3.29, 3.38, and 3.39). Expressions for the agglomeration and breakage kernels are given by Equations 6.3–6.5, 6.15, and 6.16.

The model for the section of the aerosol reactor in which coalescence occurs requires a two-dimensional population balance. In this section of the reactor, agglomeration increases the volume of the particles  $v$  without changing their surface area while coalescence changes the surface area  $a$  without changing the agglomerate volume. The 2D population balance (plug-flow, steady-state) is:

$$u_l \frac{\partial n(v, l)}{\partial l} - \frac{\partial \sigma(a) n(v, a, l)}{\partial a} = \frac{1}{2} \int_0^v \beta n(v', a', l) n(v - v', a - a', l) dv' - \int_0^\infty \beta n(v, a, l) n(v', a', l) dv' \quad 6.20$$

Equations 6.18–6.20 can be solved sequentially to give the evolution of particle properties across the full length of the aerosol reactor. Inevitably, this is performed numerically if the full size distribution is required. However, some useful information can be extracted by solving the moments form of the equations, particularly for Equations 6.18 and 6.19.

### 6.5.2 Moments of the Population Balance

Often, Equations 6.18–6.20 are difficult to solve analytically and we rely on a variety of numerical approaches. However, the moments form of the population balance gives us a lot of useful information. Here, we write the moments in terms of particle volume:

$$\mu'_{vj} = \int_0^\infty v^j n(v) dv \quad 6.21$$

We can relate these volume-based moments to those in terms of particle size given in Equation 2.19–2.20:

$$\mu'_{vj} = \alpha'_v \mu'_{3j} \quad j \geq 1 \tag{6.22}$$

$$\mu'_{v0} = \mu'_0 \tag{6.23}$$

Note that the first moment of the distribution of particle volume is related to the third moment of the distribution of particle size and therefore to the total volume fraction of particles. From Equation 2.20 combined with Equation 6.22:

$$\mu'_{v1} = \alpha'_v \mu'_3 = V_T \tag{6.24}$$

Given Equations 6.23 and 6.24, we can use the information in Table 3.2 to garner information about  $\mu'_{v0}$  and  $\mu'_{v1}$  for the nucleation, growth agglomeration, and breakage terms.

For the growth term, to write:

$$\left( \frac{d\mu'_{vj}}{dt} \right)_{growth} = jVG'\mu'_{vj-1} \tag{6.25}$$

we must assume that  $G' \neq G'(v)$ . This is harder to justify physically than the assumption  $G \neq G(x)$  we used in Chapter 4 on crystallization. However, if the particle volume distribution is fairly narrow, it is reasonable.

The zeroth moment of the agglomeration terms is dependent on the controlling mechanism of agglomeration. For the agglomeration kernels given in Equations 6.3–6.5, rate of change of zeroth moments are:

$$\left( \frac{d\mu'_0}{dt} \right)_{Br} = -\frac{2kT}{3\mu} \left[ \mu_0'^2 + \mu'_{v,-1/3} \mu'_{v,-1/3} \right] \tag{6.26}$$

$$\left( \frac{d\mu'_0}{dt} \right)_{Br} \approx -\frac{4kT}{3\mu} \mu_0'^2 \tag{6.27}$$

$$\left( \frac{d\mu'_0}{dt} \right)_{Tu} = -0.31 \left( \frac{\epsilon\rho}{\mu} \right)^{1/2} \left[ \mu_0' \mu'_{v,1} + 3\mu'_{v,1/3} \mu'_{v,2/3} \right] \tag{6.28}$$

For any agglomeration kernel, we can write:

$$\left( \frac{d\mu'_1}{dt} \right)_{agg} = 0 \tag{6.29}$$

Can you explain why?

Similarly, we can write the zeroth and first volume-based moment for agglomerate breakage based on Equations 6.15 and 6.16 as:

$$\left( \frac{d\mu'_0}{dt} \right)_{break} = k_{br} \left( \frac{\epsilon \rho}{\mu_g} \right)^{3/2} \mu'_{v\eta/3} \quad 6.30$$

$$\left( \frac{d\mu'_{v,1}}{dt} \right)_{break} = 0 \quad 6.31$$

In some cases, depending on the expressions for growth, agglomeration, and breakage, the moments forms of Equations 6.18 or 6.19 can be solved analytically. Alternatively, the moments expressions provide one approach to numerical solution using Method of Moments approaches (Diemer and Olsen, 2012).

### Example 6.3 Modeling Collision-based Agglomeration and Coalescence Using the Population Balance

We are making 1,000 lb h<sup>-1</sup> (0.126 kg s<sup>-1</sup>) of a powder product formed by gas-to-powder conversion processes in an aerosol reactor. The initial aerosol is 50 nm-diameter spherical particles in a gas at 1,750 K. This must be cooled to 350 K before exhausting into gas–solid separation equipment. We are doing this in a jacketed pipe. We expect the particles to grow by collision and coalesce by solid-state sintering. At some temperature, the coalescence will be quenched by cooling. Up to that point, coalescence has been increasing the primary particle size. Beyond that point, continued collision will produce agglomerated particles.

Initial particle concentration is 0.009% by volume (i.e., this is the volume percent solids) and the solid density is 2,200 kg m<sup>-3</sup>. The reactor is at approximately 1 atm pressure and the gas has a molecular weight of 69.1 and may be treated as ideal. Gas viscosity is given by the following expressions:

$$\left[ \frac{\mu_g}{\text{Pa}\cdot\text{s}} \right] = 1.4 \times 10^{-6} \left[ \frac{T}{\text{K}} \right]$$

The overall heat transfer coefficient can be treated as approximately independent of temperature, but depends on the pipe diameter:

$$\left[ \frac{U}{\text{Wm}^{-2} \text{K}^{-1}} \right] = 2.22 \left[ \frac{D_{pipe}}{\text{m}} \right]^{-1.8}$$

The heat capacity of the flowing stream is 945 J kg<sup>-1</sup> K<sup>-1</sup>. The particles grow by collision in the continuum Brownian regime and coalesce by solid-state sintering. The characteristic sintering time is:

$$\tau_A = 3.33 \times 10^{-5} \exp \left[ \frac{12,000 \text{ K}}{T} \right]$$

Predict the product morphology from this aerosol reactor in terms of the equivalent spherical diameter of the agglomerates, the diameter of the primary particles, and the number of primary particles per agglomerate.

*Solution:*

We approximate the collisional growth kernel as size-independent (by assuming the colliding particles are the same size) but explicitly recognize its temperature-dependence. The result is:

$$\beta = \frac{8kT}{3\mu_g} = \frac{8kT_o(T/T_o)}{3\mu_g(T_o)(T/T_o)^{1/2}} = \left[ \frac{8kT_o^{1/2}}{3\mu_g(T_o)} \right] T^{1/2} = \beta_o T^{1/2}$$

$$\beta_o = 2.63 \times 10^{-17} \text{ m}^3 \text{ K}^{-1/2} \text{ s}^{-1}$$

One can show that the rate of change of the number mean particle volume  $V_n$  with axial distance  $z$  is expressed in terms of the particle volume fraction  $\phi_p$  and the axial velocity  $u$  as:

$$\frac{dV_n}{dz} = \frac{\beta \phi_p}{2u} = \frac{\beta_o \phi_p}{2u} T^{1/2}$$

where  $V_n = \frac{\mu'_{v1}}{\mu'_0}$  and  $\phi_p = \mu'_{v1} = V_T$ . As the flowing mass cools, the gas becomes more dense and the particle volume fraction increases in inverse proportion to temperature. Likewise, as the gas density increases, its velocity slows down in proportion to temperature. Therefore, the full temperature dependence of the particle volume equation is:

$$\frac{dV_n}{dz} = \left[ \frac{\beta_o \phi_p^o}{2u_o} T_o^2 \right] T^{-3/2}$$

The particle surface area is increased by collisional growth and decreased by coalescence. One can show that if we approximate the distribution as monodisperse, then the axial rate of change of the number mean area is given by in terms of the initial particle volume ( $v_o$ ) and area ( $a_o$ ) as:

$$\frac{dA_n}{dz} = \frac{A_n}{V_n} \frac{dV_n}{dz} - \frac{1}{u\tau_A} \left( A_n - a_o \left( \frac{V_n}{v_o} \right)^{2/3} \right)$$

In this equation, the velocity  $u$  and characteristic sintering time are both temperature-dependent.

The rate of cooling is given by:

$$\frac{dT}{dz} = - \frac{U}{W_\Sigma C_{p,\Sigma}} (\pi D_{pipe}) (T - T_c)$$

In this equation,  $W_\Sigma$  is the total mass flow rate,  $C_{p,\Sigma}$  is the heat capacity of the flowing stream and  $T_c$  is the coolant temperature. The total mass flow rate is:

$$W_\Sigma = \text{particle mass flow} \times \left( 1 + \frac{\text{volume gas}}{\text{volume particles}} \times \frac{\text{gas density}}{\text{solid density}} \right)$$

$$\text{gas density} = \frac{MP}{RT} = \frac{69.1 \text{ kg/kgmol} \times 1 \text{ atm}}{0.0821 \text{ m}^3 \cdot \text{atm/kgmol/K} \times 1,750 \text{ K}} = 0.481 \frac{\text{kg}}{\text{m}^3}$$

$$W_\Sigma = 0.126 \frac{\text{kg}}{\text{s}} \left( 1 + \frac{1 - 0.00009}{0.00009} \times \frac{0.481}{2,200} \right) = 0.431 \frac{\text{kg}}{\text{s}}$$

The initial temperature is 1,750 K. Given the initial particle diameter of 50 nm, one can calculate the initial particle volume and surface area. Thus, the initial conditions are known. What remains is to specify the design (the pipe diameter) and the operating conditions (the coolant temperature).

For a given pipe diameter, one can calculate the initial velocity from the volumetric flowrate (dominated by the gas flow) and the cross-sectional area. One can also calculate the heat transfer coefficient  $U$ . With the specification of the coolant temperature, one can then numerically integrate these three ODEs to find profiles of  $V_n$ ,  $A_n$ , and  $T$  versus axial distance  $z$ .

The calculation of the equivalent spherical diameter  $d_{sph}$  associated with the number mean is straightforward given the monodisperse assumption:

$$d_{sph} = \left( \frac{6V_n}{\pi} \right)^{1/3}$$

This is just one way to characterize the length dimension of the agglomerate and is maybe not the best way, because it does not take into account void spaces between primary particles, nor does it consider the likelihood that the agglomerates are fractal with a dimension less than 3. However, for the purposes of this problem, it is sufficient to give an idea of the agglomerate size that is more intuitive than the particle volume, especially when expressed in nanometers in comparison to the initial diameter of 50 nm.

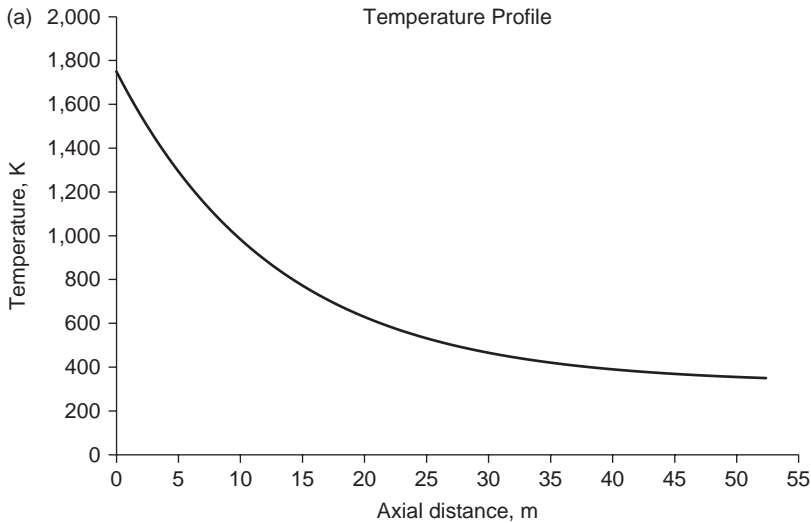
We calculate the primary particle diameter by assuming the primaries are all spheres and treating the joins as point contacts. In this approximation, one can relate both the number mean particle volume and surface area to the number of primaries per agglomerate ( $n_p$ ) and the primary particle diameter ( $d_p$ ):

$$V_n = n_p \frac{\pi}{6} d_p^3; \quad A_n = n_p \pi d_p^2$$

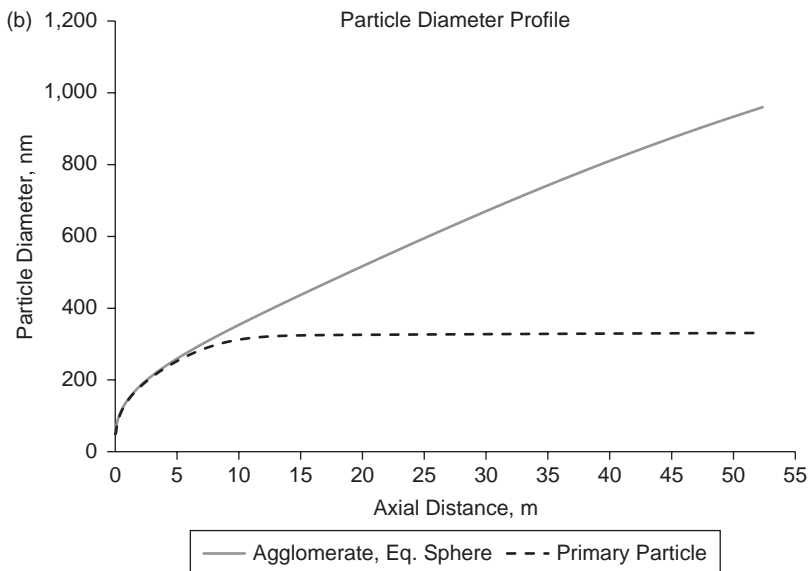
Therefore, we can estimate the primary particle diameter and number of primaries per agglomerate as:

$$d_p = \frac{6V_n}{A_n}; \quad n_p = \frac{6V_n}{\pi d_p^3} = \frac{6V_n}{\pi} \left( \frac{A_n}{6V_n} \right)^3 = \frac{A_n^3}{36\pi V_n^2}$$

For a 6'' pipe cooled with 325 K coolant, the following profiles result. The flowing mass reaches the target temperature at approximately 53 m or 172 ft.



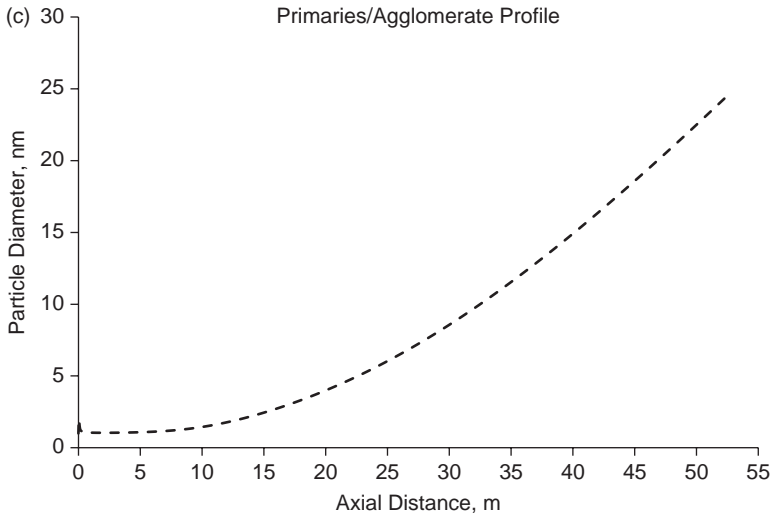
The agglomerate size continues to grow throughout the trajectory reaching an equivalent spherical diameter of nearly 1 micron (1,000 nm). On the other hand, the primary particles quit growing at about a distance of 10 m and only reach a diameter of 330 nm or about 1/3 of a micron. This indicates that coalescence is quenched at a temperature of approximately 1,000 K.





Initially, the coalescence process is rapid compared to collision. The particle population reaches a pseudo-steady state in which the coalescence is rapid enough to incorporate all collisional growth and maintain the particles as single spheres. This situation lasts until the flowing mass reaches the neighborhood of 1,000 K. Because the activation energy for solid-state sintering is so high, the coalescence rate is much more sensitive to temperature than is the collision rate. Over a fairly narrow temperature range, the coalescence rate goes from being much faster than collision to being much slower, at which point coalescence is effectively quenched and the primary particle size quits growing.

At lower temperatures, the agglomerate size continues to grow by collision, but the coalescence is too slow to alter the primary size further and the number of primary particles per agglomerate increases. By the time the flowing mass has reached the target temperature, the 1-micron agglomerates are comprised of approximately 25 primary particles each having a diameter of 1/3 micron. As we have calculated an equivalent spherical diameter for the agglomerate, we have tacitly treated the agglomerates as if they have a fractal dimension of 3. Therefore, we can estimate the number of primary particles spanning one agglomerate diameter in this hypothetical construction by taking the cube root of 25, which gives a value very close to 3. This is consistent with size estimates of primaries and agglomerates of 1/3 and 1 micron, respectively.



For growth by collision, it is likely that the agglomerates will have a fractal dimension less than 3, probably in the range 1.7–2.3. Taking 2 as an approximate fractal dimension, the actual agglomerate diameter for 25 primary particles each 1/3 micron in diameter would be more like 5/3 micron ( $d_{agg} = d_p n_p^{1/2}$ ).

The student should infer from this example that design and operating conditions can be used to control the product particle morphology. Different choices of pipe diameter and coolant temperature would be expected to produce a different

primary particle size, different agglomerate size, and a different number of primary particles per agglomerate.

## 6.6 Case Study Revisited

Now we understand more about aerosol processes, let us revisit the case study from Section 6.1.

### Tracking the Increase in Agglomerate Size in the Pipe

We are asked to design the downstream section of an aerosol reactor where agglomeration and breakage are occurring, so that Equation 6.19 represents the governing population balance for the system. Given the problem statement, we can make the following assumptions.

- No nucleation of new particles or coalescence of agglomerates occurs in the pipeline agglomerator.
- Primary particles enter the pipe as monosized 0.25  $\mu\text{m}$  particles.
- Agglomeration can be described by the sum of the kernel of Brownian motion (Equation 6.3) and the Saffman–Turner kernel for turbulent fluid flow (Equation 6.5).
- Agglomerate breakage is described by Equation 6.15 with  $\eta = 1/3$ ,  $\kappa = 3/2$ , and a binary fragment distribution described by Equation 6.16.

### Calculating the Pressure Drop Across the Pipe

To calculate the pressure drop across the pipeline agglomerator, we use standard expressions from fluid mechanics. The pressure drop across the pipeline agglomerator will be:

$$\Delta P = \frac{2f_F \rho u_z^2 L}{D_{\text{pipe}}} \quad 6.32$$

where  $f_F$  is the Fanning friction factor,  $u_z$  is the mean pipe velocity,  $L$  is the pipe length, and  $D_{\text{pipe}}$  is the pipe internal diameter. The following approximation gives the Fanning friction factor at high Reynolds number in a smooth pipe:

$$f_F = \frac{0.04}{Re^{0.16}} \quad 6.33$$

where the Reynolds number is defined as:

$$Re = \frac{D_{\text{pipe}} \rho u_z}{\mu_g} \quad 6.34$$

Note that  $\rho$  is the density of the suspension and is calculated from the ideal gas equation of state using the equivalent molecular mass for the suspension.

Finally, the mean velocity in the pipe, assuming no slip velocity between the agglomerates and the gas, is:

$$u_z = \frac{4\dot{Q}}{\pi D_{pipe}^2} \quad 6.35$$

Using Equations 6.33–6.35, we can calculate the pressure drop across the pipe as a function of pipe length. Note that the turbulence intensity required to calculate the agglomeration kernel and breakage rate constant is closely related to the pressure drop:

$$\epsilon = \frac{2f_F u_z^3}{D_{pipe}} \quad 6.36$$

Results are shown in Figure 6.6. Note that because the agglomeration and breakage process does not change the volume fraction of suspended powder, the pressure drop is independent of the agglomerate size.

### Cyclone Grade–Efficiency Curve

Our cyclone is an example of a classifier as described in Section 5.4.3. We use the following expression for the cyclone grade efficiency curve:

$$Q(x) = \frac{x^2}{x^2 + x_{50}^2} \quad 6.37$$

where  $x$  is the Stokes diameter of the particle. As our agglomerates are fractal in nature, based on Equation 6.7, we can approximately relate  $x$  to the agglomerate volume by:

$$x = d_0 \left( \frac{6v}{\pi d_0^3} \right)^{1/D_f} \quad 6.38$$

The total efficiency of the cyclone is:

$$E_T = \int_0^{\infty} Q(x) v n(v) dv \quad 6.39$$

Equations 6.37–6.39 allow us to calculate the cyclone efficiency for any given size distribution of agglomerates leaving the pipeline agglomerator.

### Problem Solution Strategy

This case study is open-ended and has more than one feasible solution. A possible solution strategy is:

1. Choose a pipe diameter.
2. Calculate the pipe length to give the 2 psi pressure drop constraint (Equations 6.32–6.35).

3. Calculate the agglomerate size distribution at the end of the pipe (Equations 6.19, 6.3, 6.5, 6.15, 6.16).
4. Calculate the cyclone efficiency (Equation 6.41).
5. Is  $E_T > 0.75$  (Equations 6.37–6.39)? If not, choose a new pipe size and repeat steps 2 to 4.

The population balance equations do not have an analytical solution. To solve the equations, we discretize the volume size distribution as follows:

$$v_i = 2v_{i-1} \tag{6.40}$$

$$v_1 = \frac{\pi d_0^3}{6} \tag{6.41}$$

With this discretization, Equation 6.19 becomes (Litster *et al.*, 1995; Wynn, 1996):

$$u_z \frac{dN_i}{dz} = N_{i-1} \sum_{j=1}^{i-2} \frac{\beta_{i-1,j}}{2^{i-j-1}} N_j + \frac{1}{2} \beta_{i-1,j} N_{i-1}^2 - N_i \left[ \sum_{j=1}^{i-1} \frac{\beta_{i,j}}{2^{i-j}} N_j + \sum_{j=1}^{\infty} \beta_{i,j} N_j \right] + 2S_{br,i+1} N_{i+1} - S_{br,i} N_i \tag{6.42}$$

where  $N_i$  is the number of particles per unit volume in size fraction  $i$ . The corresponding discrete forms of the coalescence kernel and breakage rate constant are:

$$\beta_{i,j} = \frac{2kT}{3\mu_g} \left[ 2 + 2^{(j-i)/3} + 2^{(i-j)/3} \right] + 0.31 \left( \frac{\epsilon \rho}{\mu_g} \right)^{0.5} \left( \frac{3v_1}{2} \right) \left[ 2^{i-1} + 3 \left( 2^{(2i+j)/3-1} + 2^{(i+2j)/3-1} \right) + 2^{j-1} \right] \tag{6.43}$$

$$S_{br,i} = \begin{cases} 10^6 s^2 m^{-1} \left( \frac{\epsilon \rho}{\mu} \right)^{3/2} \left( \frac{3v_1}{2} \right)^{1/3} 2^{(i-1)/3} & i > 1 \\ 0 & i = 1 \end{cases} \tag{6.44}$$

The discrete form of Equation 6.41 is:

$$E_T = \sum_{i=1}^{\infty} Q_i \bar{v}_i N_i \tag{6.45}$$

Equations 6.40–6.45 are a set of ordinary differential and algebraic equations that can be solved with a suitable software package. For example, Figure 6.8 shows the results for  $D_{pipe} = 14$  in. The pressure drop constraint is reached when the pipe length is approximately 2,000 ft (Figure 6.8a). However, the mean agglomerate size has asymptoted to a stable value after approximately 1,000 ft (Figure 6.8b), so there is little gain from having a longer pipeline agglomerator. The agglomerate size distributions

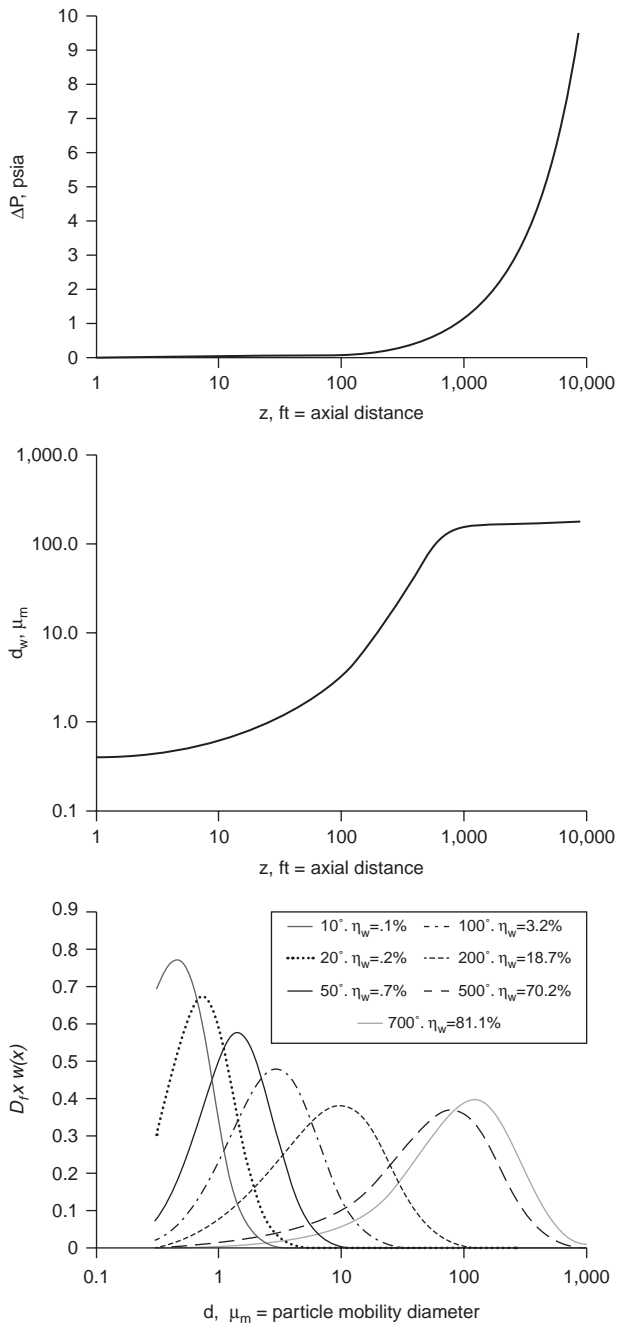


**Figure 6.8** Pipeline agglomerator results for  $D_{pipe} = 14$  in. (a) Pressure drop; (b) agglomerate mean particle size; (c) agglomerate size distributions and corresponding cyclone efficiencies (Diemer and Ehrman, 2005).

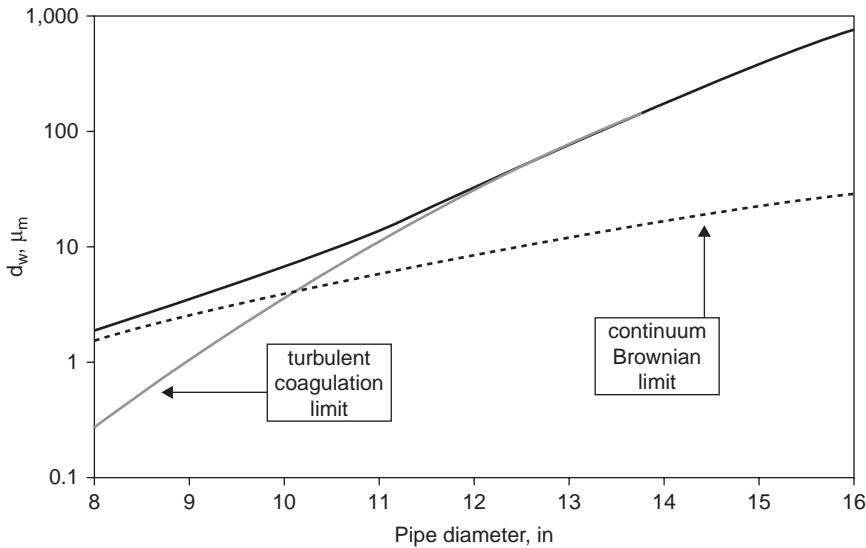


**Figure 6.9** Equilibrium mass mean agglomerate size as a function of pipe diameter (Diemer and Ehrman, 2005).

as a function of pipe length are shown in Figure 6.8c. By a pipe length of 700 ft,  $E_T > 0.75$  so that  $D_{pipe} = 14$  in and  $L = 700$  ft is one solution to the problem.

In this case study, an equilibrium agglomerate size distribution is reached. This is because as agglomerates grow, a balance is reached between agglomerate breakage and agglomeration. In fact, we could predict this from the problem formulation. The Vigil–Ziff criterion for agglomeration–breakage equilibrium stability is:

$$1 + \eta_{br} - \max(\eta_{agg}) > 0 \quad 6.47$$

In our problem,  $\eta_{br} = 1/3$ ,  $\eta_{agg,brownian} = 0$  and  $\eta_{agg,turb} = 1$ , so that the stability criterion is satisfied. Given that the total mass flow rate in the pipe is a given constraint, turbulence intensity increases as pipe diameter decreases. At small pipe diameter (high energy dissipation), breakage keeps the agglomerates small and in the Brownian agglomeration regime. At larger pipe diameter, turbulent agglomeration dominates. Figure 6.9 shows the equilibrium agglomerate mass mean size as a function of pipe diameter. For 75% cyclone efficiency, the mass mean diameter needs to be approximately three times the cyclone cut size (about 75  $\mu\text{m}$ ). Thus, for pipe diameters less than 13 in, 75% efficiency is impossible, no matter how long the pipe is.

## 6.7 Summary

Aerosol processes, where very small particles are produced directly from the gas phase, are important in nature, the environment, and industrially. Even if the

chemistry of the aerosol reaction is known, the physics of the formation and growth of the aerosol particles can be complex. Particles produced may be single dense particles, sintered aggregates, or loose agglomerates which are often fractal in structure.

Key processes occurring in aerosol reactors include nucleation, layered (accretion) growth, agglomeration, coalescence (sintering), and breakage. The rate of some of these processes can be predicted from fundamental rate expressions – e.g., agglomeration in the Brownian motion and turbulent shear regimes is well understood and quantified. Students should be familiar with these processes and how their rate is affected by environmental (process) conditions and material properties.

Despite the complexity of aerosol reactors, if we can identify the dominant rate process of interest of one part of the reactor, the analysis and modeling tools developed in this text can be used for design and troubleshooting. Most aerosol reactors are approximately plug-flow and can be divided into three sections: the reaction zone, the collision and coalescence zone, and the agglomeration and breakage zone. We have presented the population balance for each of these zones. Students should be able to track the evolution of particle volume in each of these zones using the population balance. The case study provides a good example of how such tools can be used for a complex open-ended problem.

## 6.8 Bibliography

- Coblentz, W.S., Dynys, J.M., Cannon, R.M., and Coble, R.L., 1980. Sintering Processes. In *Materials Science Research*, G.C. Kucunski (ed.), Plenum, New York, 13, 141–157.
- Diemer, R.B., 2002. *Moments Methods for Coagulation, Coalescence and Breakage Problems*. PhD thesis, University of Delaware.
- Diemer, R.B. and Ehrman, S.H. 2005. Pipeline agglomerator design as a model test case. *Powder Technology*, 156, 129–145.
- Diemer, R.B. and Olsen, J.H., 2002. A moment methodology for coagulation and breakage problems: Part 2 – Moment models and distribution reconstruction. *Chemical Engineering Science*, 57, 2229–2239.
- Ehrman, S.H., Castellanos, P., Dwivedi, V., Diemer, R.B., 2007. A population balance based design problem. *Chemical Engineering Education*, 41(2), 88–92.
- Freidlander, S.K., 2000. *Smoke, Dust and Haze: Fundamentals of Aerosol Behavior 2nd Edition*, Oxford University Press, Oxford.
- Green, D.W. and Perry, R.H. (eds.), *Perry's Chemical Engineers Handbook 8th edition*, chapter 20, McGraw-Hill, New York, 2008.
- Johnson, P.H. and Eberline, C.R., 1978. Carbon black, furnace black. In McKenna J.J., ed., *Encyclopedia of Chemical Processing and Design*, vol. 6, 187–257, Marcel Dekker, New York.
- Kammler, H.K., Beaucage, G., Kohls, D.J., Agashe, N., and Ilavsky, J., 2005. Monitoring simultaneously the growth of nanoparticles and aggregates by *in situ* ultra-small-angle x-ray scattering. *Journal of Applied Physics*, 97, 054309.
- Kodas, T.T. and Hampden-Smith, M.J., 1999. *Aerosol Processing of Materials*. Wiley-VCH, New York.

- Litster, J., Smit, D.J., and Hounslow, M.J., 1995. Adjustable discretized population balance for growth and aggregation. *AIChE Journal*, 41, 593.
- Ring, T.A., 1996. *Fundamentals of Ceramic Powder Processing and Synthesis*. Academic Press, New York.
- Strobel, R. and Pratsinis, S.E., 2007. Flame aerosol synthesis of smart nanostructured materials. *Journal of Materials Chemistry*, 17, 4743–4756.
- Wynn, E.J.W., 1996. Improved accuracy and convergence of discretized population balance of Lister *et al.* *AIChE Journal*, 42, 2084.

## 6.9 Problems

- 6.1. In the early stages of an aerosol pipe reactor, Brownian agglomeration dominates and breakage of the small agglomerates can be neglected. What distance along the reactor pipe will it take the mean agglomerate size to grow from 100 to 1,000 nm, if the temperature in the pipe is held constant at 1,000 K? Assume the gas has the properties of nitrogen and the structure of the agglomerate (fractal dimension) does not change.
- 6.2. Consider Example 6.2. Propose additional experiments that would allow you to determine the temperature-dependent group  $Y(T)$  including its temperature dependence. Besides the densification data, what other quantities do you need to measure or specify?
- 6.3. Consider the pipeline agglomerator in Example 6.1.
  - a. Do we expect an equilibrium size distribution to be reached if agglomerate breakage is described by Equation 6.15 with  $\kappa = \eta = 1$ ?
  - b. What is the value of  $k_{br}$  if the breakage rate matches the agglomeration rate at  $v = 70 \mu\text{m}$ ?
  - c. Write out the population balance for this system. Solve the equation to give the evolution of particle size distribution as a function of distance along the pipe. (A numerical solution to the population balance is required.)
- 6.4. In Example 6.3, one has both design, in the form of pipe diameter, and operating conditions, in the form of coolant temperature, to control the product characteristics. The practical lower limit to coolant temperature is 300 K.
  - a. Which of the product characteristics would you expect to respond to reducing the coolant temperature in this example from 325 K to 300 K? Please explain your reasoning.
  - b. If you wished to reduce primary particle size, would you increase or reduce the pipe diameter? What do you expect to happen to agglomerate size and primaries/agglomerate when you do this?
  - c. Find the pipe diameter that results in a primary particle size of 250 nm. Then find the coolant temperature that results in 35 primaries per agglomerate.
  - d. Derive a relationship for the rate of increase in number of primaries/agglomerate with axial distance in terms of only  $n_p$ ,  $V_n$ , and  $z$  under the condition that the rate of coalescence is zero.



- 6.5. I have a bright idea for a new aerosol reactor design based on a series of well-mixed tanks, each with different residence times and temperatures. In tank 1, only nucleation and layered growth occur. In the tank 2, which operates at lower temperature, only collision-based agglomeration occurs. Finally, the product is passed through a jet mill (tank 3) to break up oversize agglomerates. Derive the population balance model for each well-mixed tank. Clearly state any assumptions you make and define your nomenclature clearly.

# 7 Spray Drying and Spray Cooling

## 7.1 Consider a Case Study ...

### A Sticky Situation

*Litster Specialty Powders Inc.*

Memo to: Particle Products Team  
Memo from: Jim Litster  
September 9, 2015

### Finding a Solution for Sprayed Dried Fruit Juice

Our company has specialized in finding particulate product solutions in the specialty chemicals industry. We have a small pilot plant to test formulations and develop products. We have considerable expertise in producing spray-dried ceramic particles from high-solids fraction slurries of fine powders to make the dried pressbody which is pressed in dies to make ceramic tiles and other products. Our pressbodies are free-flowing, spherical particles of controlled size distribution which are ideal for pressing operations. We use a small bench-top spray drier (0.5 m diameter) to make product materials for testing.

To reduce risk in our business model, we have been actively seeking clients in other industry sectors and have a current project from a South East Asian company to develop a process to spray-dry locally produced fruit juice for the Chinese and European market. This material is causing us all manner of problems and we need your help.

When we try to spray-dry a range of fruit juices, some of them give almost no powder product with all the material ending up as a sticky mess on the wall of the spray drier. To counter this problem, we increased the inlet gas temperature to increase the drying rate. This slightly improved the situation for some juices but actually caused more build up in other cases.

Furthermore, when we transfer our more successful powders to the larger spray drier at the company site, we find the spray products have different product attributes to our laboratory powders (different caking propensity, shelf life, ability to redisperse when reconstituted). When we look at the powders under the microscope, they have both different size and morphology. They are certainly not nice spheres. When I asked my old colleague, Tony Howes, about this he said rather smugly that “spray-drying is unscalable.” Thanks a lot, Tony!

We view spray-dried organic materials such as foods and pharmaceuticals as a major growth area for our business, so we need to have a better understanding of this process.

Can you put together a team to answer the following questions and report to me within six weeks?

1. Why do some fruit juices produce sticky, high-moisture content particles that stick to the walls of the drier? Is there a property of the fruit juice we can measure in advance to predict if this behavior will occur?
2. What adjustments to the fruit juice (possible additives?) or the spray drier could avoid, or at least reduce, this problem?
3. Should we be investing in a larger-scale spray drier pilot plant, or in sophisticated single-drop drying experiments and CFD-based drier simulations, as we grow our business?

As a case study for testing your approaches, we have a particularly problematic pineapple–guava fruit juice mix available for characterization and spray-drying experiments.

Spray drying and spray cooling are two processes in which particles are formed from a liquid-phase feed stream via atomization of the liquid feed. Where the feed is a melt, the process is called spray cooling, solidification, or prilling. When the feed is a solution or suspension, the process is called spray drying. A very wide variety of particle morphologies can be achieved. The properties of the particles formed are controlled by the size distribution of drops formed and the rate at which they cool or dry, so a fundamental understanding of these rate processes is important to understanding and predicting the behavior of spray driers and coolers.

As an individual reflective exercise, or as a group brainstorming discussion, list possible reasons why fruit juice can often give sticky particles. What characterization test might be used to test these hypotheses? What size and structure of particle do you expect to get when you dry a drop of slurry or solution? Why do you think scaling-up a spray drier is so difficult? Your discussion will probably generate a lot more questions than answers!

Reflect on learning goals related to spray drying and spray cooling inspired by this case study. How do they compare with the chapter learning goals given below?

## 7.2 Learning Goals

At the completion of this chapter, the student should be able to:

1. Explain the difference between spray drying and spray cooling and describe the different types of particle formed by the two processes.
2. Calculate the drop size produced by single jet break up as a function of nozzle size, flow rate, and fluid properties.
3. Use empirical correlations to estimate drop size from rotating disc, pressure nozzle, and two fluid nozzle atomizers.
4. Calculate the solidification time for a drop (spray cooling) and drying time for a liquid drop (spray drying) as a function of gas velocity and temperature.

5. Explain the process of shell formation during spray drying and the impact on drying rate and particle morphology.
6. Calculate whether a shell will form given the properties of the drop, solute, or particle, and the gas temperature.
7. Design a spray-cooling tower given information about the atomizer and melt feed rates.
8. Perform mass and energy balance calculations around a spray drier.
9. Use population balance approaches to estimate particle size distributions and drying rates for a poly-disperse population of drops.
10. Attack open-ended particle design or troubleshooting problems in spray cooling and spray drying of similar nature to the introductory case study for the chapter.

### 7.3 Drop Formation and Atomization

In spraying drying and solidification, the final particle size distribution is often dominated by the drop size formed at the atomizer. Furthermore, the drop-drying kinetics which strongly influence the particle morphology are directly related to the drop size. Therefore, a consideration of atomization of the melt, solution, or suspension to be dried is essential. Drops are formed by the break up of unstable jets or sheets of liquid, so we begin with the classic analysis of jet break up by Rayleigh.

#### 7.3.1 Rayleigh Jet Break Up

At low flow rate of liquid through a simple orifice, the liquid will drip. As the flow rate is increased, a liquid jet forms at the orifice. At some point, the jet becomes unstable and breaks up into drops. You can observe these phenomenon at home from the tap in your kitchen sink. Let us see if we can analyze this phenomenon and predict the drop size formed from jet break up.

Consider a liquid jet that undergoes a sinusoidal disturbance at the free surface (Figure 7.1a). If the disturbance acts to increase the jet free surface area, it will dissipate. However, if the disturbance *decreases* the jet surface area, then the disturbance will grow and the jet will become unstable, ultimately leading to the jet breaking up into drops.

Geometry shows that the surface area is decreased (jet becomes unstable), when the disturbance wavelength  $\lambda$  exceeds the jet circumference:

$$\lambda > 2\pi r_j \quad 1$$

where  $r_j$  is the jet radius. We can rearrange Equation 7.1 to write it in terms of the dimensionless wave number  $k$ :

$$k = \frac{2\pi r_j}{\lambda} < 1 \quad 2$$

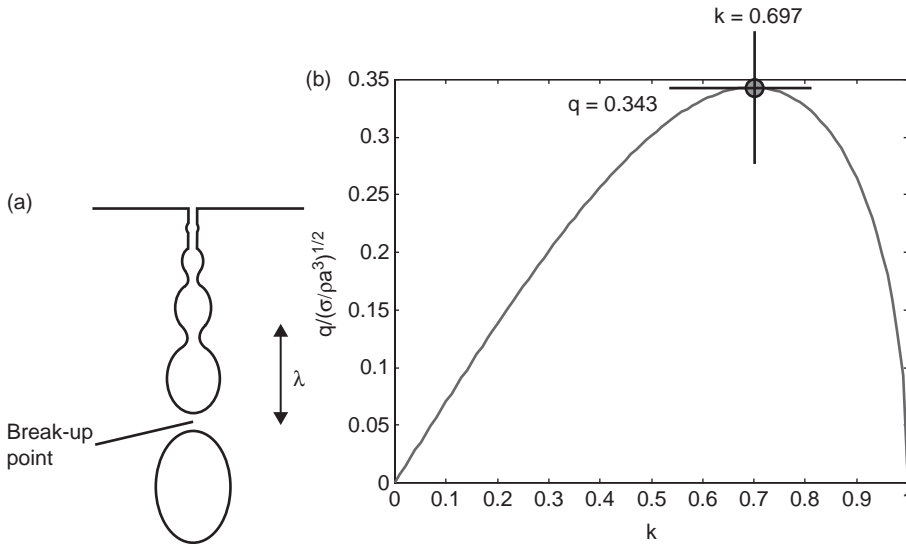


**Figure 7.1** Rayleigh jet break up of an inviscid jet. (a) Unstable disturbances of wavelength  $\lambda$  grow until drops form; (b) the disturbance growth rate is a function of the wave number  $k$ .

Thus, any disturbance with  $0 < k < 1$  will lead to jet break up, and the resultant drop size will be a function of disturbance wavelength. If the disturbances are random, the dominant disturbance will be the one that grows fastest. From basic fluid mechanics, Rayleigh derived the following expression for the disturbance growth rate  $G_d$ :

$$G_d \propto \exp(qt) \quad 3$$

where:

$$q^2 = \frac{\gamma^{lv}}{\rho_l r_j^3} k(1-k^2) \frac{I_1(k)}{I_0(k)} \quad 4$$

Here  $I_0(k)$  and  $I_1(k)$  are Bessel's functions. Figure 7.1b shows the predicted disturbance growth rate as a function of wave number. The growth rate is highest when  $k = 0.698$ . Thus, the typical drop size from jet break up is:

$$V_d = \frac{4}{3} \pi r_d^3 = \pi r_j^2 \lambda \quad 5$$

Substituting from Equation 7.2 and rearranging:

$$\begin{aligned} r_{d0}^3 &= \left( \frac{3\pi}{2 * 0.698} \right) r_j^3 \\ \Rightarrow r_{d0} &= 1.89 r_j \quad 6 \end{aligned}$$

where  $r_{d0}$  is the drop radius formed from an inviscid jet.

Rayleigh developed his theory in 1878 and it gives the basis for much modern work on atomization. His derivation is based on a number of simplifying assumptions:

- the fluid is inviscid ( $\mu = 0$ );
- there is no gravity;
- there is no external fluid; and
- the jet is subject to small disturbances so linear approximations can be used.

Rayleigh's theory predicts very uniform-sized drops are formed by jet break up. However, this is rarely the case. When a drop forms, a tail or ligament is generated which leads to the formation of small satellite drops, 5–10 times smaller than the main drop (Figure 7.2a). This often leads to bimodal particle size distributions from spray cooling and spray drying (Figure 7.2b). Satellite drops can be avoided by application of disturbances in the right frequency range (see Figure 7.3). In practice, disturbances can be applied acoustically, or by physical vibration of the nozzle.

### 7.3.2 Relaxing the Rayleigh Assumptions

If the jet is viscous, viscous resistance slows down the rate of disturbance growth. Jet break up is slower, so viscous jets are longer. Break up occurs at lower wave numbers ( $k < 0.697$ ) resulting in larger drops being formed. This effect can be quantified in terms of the dimensionless Ohnesage number  $Oh$ :

$$Oh = \frac{\mu}{(\rho_l \gamma^{lv} r_j)^{1/2}} \quad 7$$

$$r_d = (1 + 2.1Oh)^{1/6} r_{d0} \quad 8$$

where  $r_d$  is the drop radius of the viscous jet and  $r_{d0}$  is given by Equation 7.6.

Gravity acts to stretch a vertical jet so that the wave number changes with position along the jet as the jet radius decreases. Thus, the drop size formed is smaller than that predicted using the initial jet radius,  $r_0$  equal to the nozzle radius. Based on an approximate energy balance, the extent of jet stretching is given by:

$$\frac{r_{j,z}}{r_{j,0}} = \left( 1 + \frac{2gz}{u_o^2} \right)^{-1/4} \quad 9$$

where  $z$  is the distance from the orifice and  $u_o$  is the jet velocity at the orifice. Note that drop size increases as the velocity through the nozzle increases due to the decreasing importance of jet stretching.

The effect of jet stretching is most noticeable for atomization from a rotating bucket because the centripetal acceleration may be many times the standard gravitational acceleration. Equation 7.9 can be applied by replacing  $g$  with  $R\omega^2$  where  $R$  is the bucket radius and  $\omega$  is the angular velocity of the bucket.

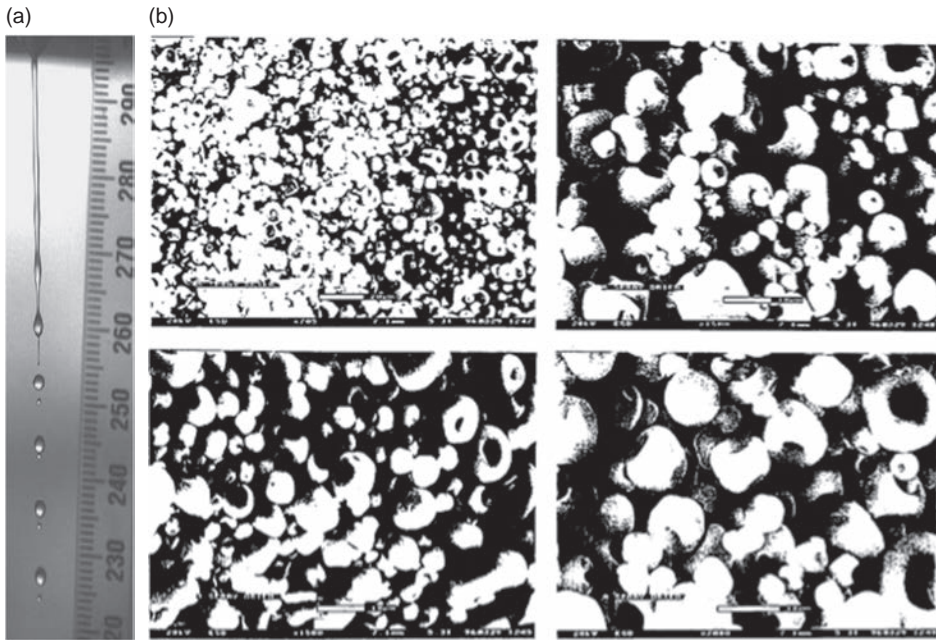


**Figure 7.2** Satellite drop formation during jet break up. (a) Satellites form from the ligaments between the main drops during jet break up; (b) example of a bimodal distribution of spray-dried particles resulting from satellite drop formation.

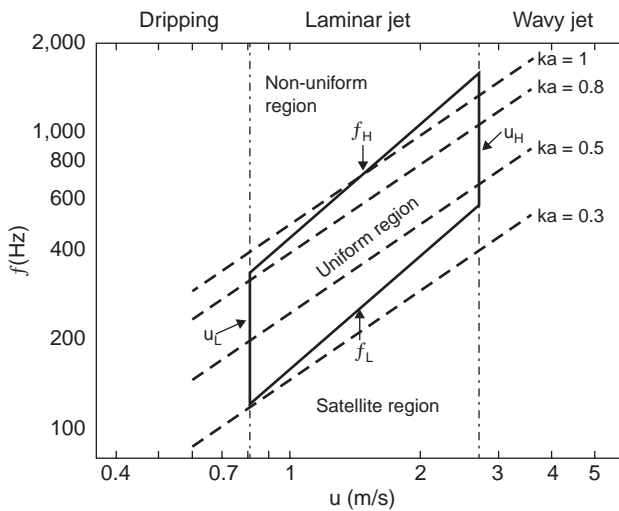


**Figure 7.3** Regime map for vibrated jet break up (Sakai and Hoshino, 1980).

**Example 7.1** A spray-cooling tower uses a shower head type array of 1 mm-diameter orifice nozzles. The jet velocity from the nozzles is  $2 \text{ m s}^{-1}$  and the estimated jet length is 0.1 m. Assume the fluid is inviscid ( $Oh = 0$ ). What is the expected drop size from the nozzle? If I replace the shower head arrangement with a rotating bucket of radius 0.15 m spinning at 120 rpm, how will the expected drop size change?

*Solution:*

First, let us calculate the extent of jet stretching. From Equation 7.9:

$$\frac{r_{j,z}}{r_{j,0}} = \left( 1 + \frac{2 \times 9.81 \text{ms}^{-2} \times 0.1 \text{m}}{(2 \text{ms}^{-1})^2} \right)^{-\frac{1}{4}} = 0.905$$

We then use Equation 7.6 to calculate the radius of the drop:

$$r_{j,0} = 05 \times 1 \text{ mm} = 05 \text{ mm}$$

$$r_{d,0} = 189 r_{j,z} = 189 \times 0905 \times 05 \text{ mm} = 085 \text{ mm}$$

When we use a bucket wheel, the impact of jet stretching will be higher.

$$\frac{r_{j,z}}{r_{j,0}} = \left( 1 + \frac{2R\omega^2 z}{u_o^2} \right)^{-\frac{1}{4}}$$

$$\frac{r_{j,z}}{r_{j,0}} = \left( 1 + \frac{2 \times 0.15 \text{m} \times (12.6 \text{s}^{-1})^2 \times 0.1 \text{m}}{(2 \text{ms}^{-1})^2} \right)^{-\frac{1}{4}} = 0.528$$

$$r_{d,0} = 189 r_{j,z} = 189 \times 0528 \times 05 \text{ mm} = 05 \text{ mm}$$

### 7.3.3 Atomization from Nozzles and Rotating Discs

In spray-drying applications, the geometry of the atomizing nozzles is much more complex than a series of orifices with single jets. Atomizer types can be classified by the source of energy used to induce atomization:

- rotating disc atomizers – centrifugal force;
- pressure nozzle atomizers (pressure);
- pneumatic (two-fluid) nozzle atomizers – kinetic energy; and
- vibrating (sonic) atomizers – vibrational energy.

In a rotating disc atomizer, liquid is pumped into the center of a horizontal disc rotating at very high speed, of order 10,000 rpm. The disc may be flat or etched with vanes to direct the liquid flow. There are three regimes of operation for rotating disc atomizers as disc speed is increased (Figure 7.4):



1. Direct droplet formation.
2. Ligament formation.
3. Sheet formation.

Although the geometry of the system is much more complex, drop formation by break up of a ligament or sheet is governed by similar growth of unstable disturbances as for the simpler geometry of a single jet. The drop size can be correlated to operating conditions and fluid properties. For example (Kapano and Kamiya, 1978):

$$r_d \propto \omega^{-0.79} Q^{0.32} R^{-0.69} \rho^{-0.29} \gamma^{0.26} \left( 1 + \left[ \frac{\mu}{\mu_w} \right]^{0.65} \right) \quad \text{10}$$

However, general correlations across a wide range of fluid properties and disc geometries cannot be used quantitatively with confidence and experimental testing is still the main basis for “predicting” drop size in industrial applications.

Droplet break formation from liquid sheets is due to a combination of sheet perforation, ligament formation and break up, and aerodynamic interaction.

Pressure nozzles use a swirling flow to generate conical liquid sheets that may be as thin as 0.5–5  $\mu\text{m}$ . The sheets break up due to Rayleigh-style instabilities and frictional interaction with the air stream. Pressure nozzles produce broad drop size distributions with mean sizes of the order 80–300  $\mu\text{m}$ . Drop size decreases as applied pressure increases.

Two fluid atomizers use kinetic energy in the gas stream to break up the liquid stream into drops. Gas velocities within the nozzle can be sonic or even supersonic. Two fluid nozzles are suitable for high-viscosity feeds and generate small drops in the range 10–30  $\mu\text{m}$ . However, they are limited in their throughput compared to rotating discs. The effect of operating conditions on drop size can be correlated as:

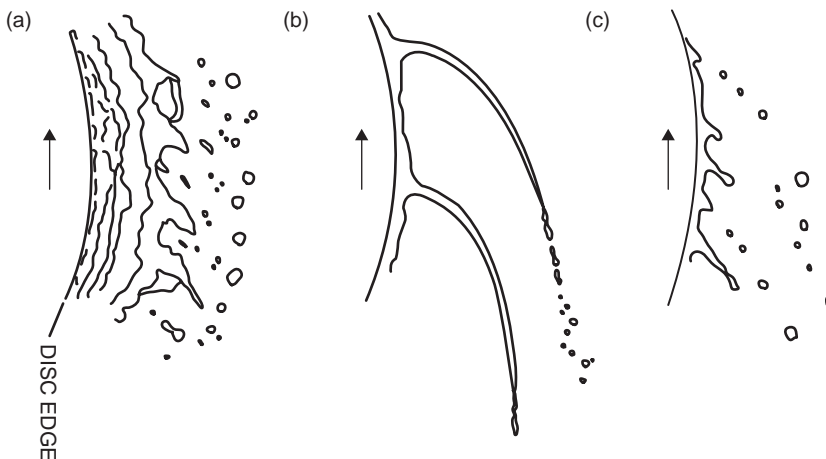


**Figure 7.4** Atomization regimes for a spinning disc atomizer as flow rate decreases (a) sheet formation, (b) ligament formation, (c) droplet formation (Masters, 1985).

$$r_d = \frac{A}{(\rho_g u_{rel}^2)^\alpha} + B \left( \frac{\dot{m}_g}{\dot{m}_l} \right)^{-\beta} \quad \text{I 1}$$

where  $u_{rel}$  is the relative velocity between the air and the liquid at the nozzle exit,  $\frac{\dot{m}_g}{\dot{m}_l}$  is the mass ratio of air to liquid, and  $A$  and  $B$  are constants that depend on

liquid properties. Typically,  $\beta \sim 1$  and  $\alpha \sim 1/3$  with  $\frac{\dot{m}_g}{\dot{m}_l}$  between 0.1 and 10.

## 7.4 Drop Drying and Solidification and Particle Formation

Once drops are formed by atomization, they must cool and solidify (spray cooling) or dry by evaporation (spray drying) to give a particulate product. The solidification or drying time for a single drop is an important parameter in spray drier/cooler design.

Drops in spray driers contain dissolved or suspended solids which complicate the drying profile. Also, the velocity, temperature, and humidity vary with position in the drier. Nevertheless, we can gain substantial insight to the cooling or drying process by starting with some ideal cases to which application of heat and mass transfer principles can be easily applied.

### 7.4.1 Cooling and Solidification of a Single Melt Drop

Figure 7.5 shows the temperature profile of a cooling melt drop (no evaporation) at some point within a spray-cooling tower. There are two resistances to heat transfer:

1. external resistance to convective heat transfer in the boundary layer around the particle; and
2. internal conductive resistance within the drop or particle.

When the drops are small, we can neglect the internal resistance and assume the temperature is uniform within the drop. Internal heat transfer resistance can be neglected when the Biot number  $Bi$  is small:

$$Bi < 0.1 \quad \text{I 1}$$

$$Bi = \frac{hd_p}{k_s} \quad \text{I2}$$

where  $h$  is the heat transfer coefficient in the gas phase surrounding the particle,  $d_p$  is the drop or particle diameter, and  $k_s$  is the thermal conductivity of the drop/particle.

The Ranz–Marshall correlation for heat transfer from a flowing fluid stream to a sphere is used to give the heat transfer coefficient for calculating the external resistance:

$$Nu = 2 + 0.6Re_p^{0.5}Pr^{0.33} \quad \text{I3}$$

where the Nusselt number  $Nu$ , the particle Reynold's number  $Re_p$ , and the Prandtl number  $Pr$  are dimensionless groups defined as follows:

$$Nu = \frac{hd_p}{k_g} \quad \text{I4}$$

$$Re_p = \frac{d_p u_{slip} \rho_g}{\mu_g} \quad \text{I5}$$

$$Pr = \frac{\mu_g C_{p,g}}{k_g} \quad \text{I6}$$

where  $k_g$  is the thermal conductivity of the gas,  $u_{slip}$  is the slip velocity between the drop/particle and the gas,  $\mu_g$  is the gas viscosity, and  $C_{p,g}$  is the specific heat of the gas.  $u_{slip}$  is often approximated by the terminal settling velocity of the drop/particle  $u_t$ . Droplets in spray driers are very small, so that  $u_t$  and therefore  $Re_p$  are very small. We can therefore simplify Equation 7.13 to that for a stationary drop:

$$Nu \approx 2 \Rightarrow h = \frac{2k_g}{d_p} \quad \text{I7}$$

For spray cooling (prilling), the drop size is of the order 1–2 mm and the heat transfer enhancement from forced convection cannot be neglected.

Now, we write the energy balance for drop as it (1) cools to its solidification temperature; and (2) solidifies. For cooling:

$$m_p C_{p,l} \frac{dT_p}{dt} = hS_p (T_g - T_p) \quad \text{I8}$$

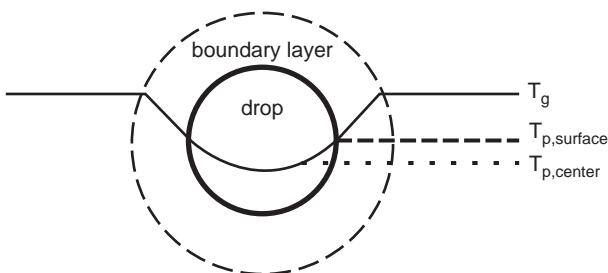


**Figure 7.5** Temperature profile for a melt drop during cooling and solidification.

where  $T_p$  and  $T_g$  are the temperature of the drop and the gas, respectively. As the drop is spherical, the mass and surface area of the drop are given by:

$$m_p = \frac{\pi d_p^3 \rho_p}{6} \quad 19$$

$$S_p = \pi d_p^2 \quad 20$$

Combining Equations 7.18 to 7.20:

$$\frac{dT_p}{dt} = \frac{6h(T_p - T_g)}{\rho_p d_p C_{p,l}} \quad 21$$

Integrating from the initial drop temperature  $T_{p,0}$  to the solidification temperature  $T_{solid}$  gives the cooling time:

$$t_1 = \frac{\rho_p d_p C_{p,l}}{6h} \ln \left[ \frac{T_{p,0} - T_g}{T_{solid} - T_g} \right] \quad 22$$

The energy balance for solidification is simpler because the drop temperature is constant at the solidification temperature:

$$m_p \lambda_s = h S_p (T_{solid} - T_g) t_2 \quad 23$$

where  $\lambda_s$  is the enthalpy of solidification of the drop. Combining with Equations 7.19 and 7.20 gives:

$$t_2 = \frac{\rho_p d_p \lambda_s}{6h(T_{solid} - T_g)} \quad 24$$

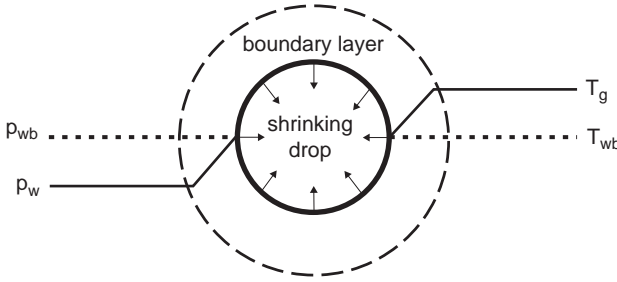
The total residence time for cooling and solidification is  $t_1 + t_2$ .

This derivation includes many assumptions:

1. the drops/particles are mono-dispersed spheres;
2. heat transfer is controlled by the external film resistance and the drop temperature is uniform;
3. there is no solvent evaporation;
4. there is no change to the drop/particle size during solidification; and
5. the gas temperature is constant.

## 7.4.2 Evaporation of a Single Drop

In spray drying, as distinct from spray cooling, the aim is to evaporate all the solvent from the drop to leave a dry particle. To start simply, let us consider evaporation of a liquid drop with no solid content (Figure 7.6).



$$\frac{h}{\lambda_l}(T_g - T_{wb}) = \frac{K_g MW_w}{RT}(p_{wb} - p_w)$$

Figure 7.6 Drop temperature and concentration profile during drying (pure solvent).

At the surface of the drop, there is simultaneous heat and mass transfer. As the drops are small, we can assume the external heat and mass transfer resistance dominates and the temperature is uniform throughout the drop. Heat arriving at the drop surface from the gas phase evaporates the liquid and reduces the drop temperature due to the enthalpy of evaporation,  $\lambda_l$ . The evaporated liquid is transferred away from the drop surface by diffusion and convection. Heat and mass transfer reach steady state. Thus, the gas boundary layer will be saturated with solvent (at equilibrium) at the drop surface and therefore at wet bulb conditions  $T_{wb}, p_{wb}$ . Thus the rate of mass transfer (rate of reduction in drop mass) is:

$$\dot{m}_p = K_g S_p (c_{wb} - c_w) = K_g S_p \frac{MW_w}{RT} (p_{wb} - p_w) \tag{25}$$

where  $K_g$  is the gas-phase mass-transfer coefficient,  $c_w$  and  $p_w$  are the mass concentration and vapor pressure of the solvent in the bulk gas phase and  $c_{wb}$  and  $p_{wb}$  are the equilibrium mass concentration and equilibrium vapor pressure of the solvent, and  $MW_w$  is the molecular mass of the solvent. The heat transfer rate is given by:

$$\dot{Q} = \dot{m}_p \lambda_l = h S_p (T_g - T_{wb}) \tag{26}$$

where  $\lambda_l$  is the enthalpy of evaporation and  $T_{wb}$  is the equilibrium (wet bulb) temperature at the drop surface.

We wish to find the time for the drop size to reduce to zero. Combining Equation 7.26 with Equations 7.19 and 7.20:

$$\begin{aligned} \dot{m}_p \lambda_l &= \lambda_l \rho_l \frac{d}{dt} \left( \frac{\pi d_p^3}{6} \right) = h \pi d_p^2 (T_g - T_{wb}) \\ \Rightarrow \int_0^t dt &= - \frac{\lambda_l \rho_l}{2(T_g - T_{wb})} \int_{d_{p,0}}^{d_p} \frac{d(d_p)}{h} \end{aligned} \tag{27}$$

As the drop size is small, Equation 7.17 applies and the heat transfer coefficient  $h$  is not constant as the drop shrinks. Substituting into Equation 7.22:

$$\begin{aligned} \Rightarrow t &= -\frac{\lambda_l \rho_l}{2(T_g - T_{wb})} \int_{d_{p,0}}^{d_p} \frac{d_p d(d_p)}{2k_g} \\ &= \frac{\lambda_l \rho_l (d_{p,0}^2 - d_p^2)}{8k_g (T_g - T_{wb})} \end{aligned} \tag{28}$$

Thus, the total drying time is:

$$t_D = \frac{\lambda_l \rho_l d_{p,0}^2}{8k_g (T_g - T_{wb})} \tag{29}$$

Again, it is important to record the assumptions in this simple derivation:

1. the drops/particles are mono-dispersed spheres;
2. heat transfer is controlled by the external film resistance and the drop temperature is uniform;
3. the heat transfer coefficient is that of a stagnant film; and
4. the gas temperature is constant.

It is easy to modify the equations to relax these assumptions, although in some cases numerical solutions may be required. If  $(T_g - T_{wb})$  is not constant during the drying process, Equation 7.29 can be used with the log mean temperature difference *LMTD* included:

$$LMTD = \frac{(T_g - T_{wb})_0 - (T_g - T_{wb})_1}{\ln \left[ \frac{(T_g - T_{wb})_0}{(T_g - T_{wb})_1} \right]} \tag{30}$$

### 7.4.3 Drying Drops with Dissolved or Suspended Solids

Drying of drops containing dissolved or suspended solids is much more complicated than drying a pure liquid. Figure 7.7 shows a typical temperature history for a drop containing suspended or dissolved solids and can be divided into several sections (Nesic and Vodnik, 1991; Handscomb *et al.*, 2009):

1. *Initial heating (AB)*: The initial period in which the drop reaches a steady state between mass and heat transfer.
2. *Constant rate drying (BC)*: This is very similar to the drying of a solvent drop (Section 7.3.4). The surface remains at wet bulb conditions. The drying rate is

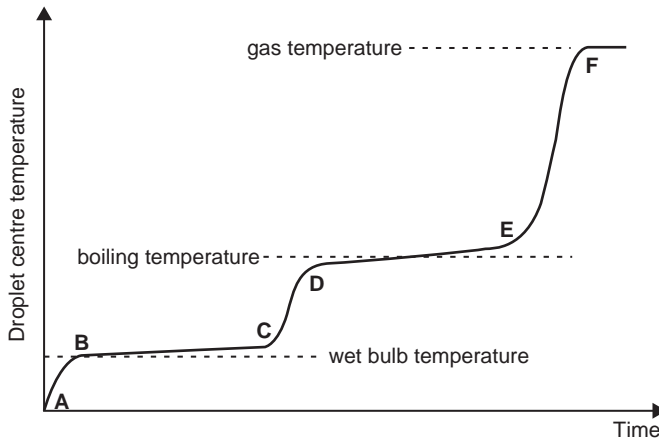


**Figure 7.7** The temperature history during spray drying of a liquid drop containing dissolved or suspended solids (Handscorn *et al.*, 2009).

almost constant. The temperature rises slightly during drying as the change in concentration of solute due to solvent evaporation changes the equilibrium vapor pressure  $p_{wb}$ .

3. *Crust (skin) formation (CD)*: This stage is also known as second-stage drying or falling rate drying. The solids concentration at the surface reaches a critical value at which a solid crust or skin forms. The crust has a high resistance to mass transfer. Thus, the drop surface is no longer wet and the assumptions of the constant rate period break down. The drop temperature rises rapidly and the crust thickens.
4. *Boiling (DE)*: If the surrounding gas temperature exceeds the boiling point of the solvent, the internal temperature rises to the boiling point. Once again, the drop temperature remains nearly constant during evaporation and the drying rate is controlled by external heat transfer to the drop.
5. *Porous particle drying (EF)*: All the free moisture is removed. Surface-bound moisture continues to be removed at a slow rate until the particle reaches the surrounding temperature.

When the gas temperature is below the boiling point of the solvent, there is no second temperature plateau and we normally considering the drying in the constant rate region and the crust formation/falling rate region only.

With such complex phenomena occurring, there is no single model to predict all situations. Within the constant rate period (*BC*), Equations 7.28 and 7.29 apply, noting that the equilibrium vapor pressure and temperature  $T_{wb}$ ,  $p_{wb}$  are not exactly constant, but increase as the concentration of solute in the drop increases due to solvent evaporation.

In the falling rate drying period (*CD*), the simplest models are semi-empirical fits to drying curve data for single drops of the solution/suspension of interest. These models are of the form:

$$\frac{N_V}{\widehat{N}_V} = f\left(\frac{X - X_e}{X_{cr} - X_e}\right) \tag{3}$$

where  $X$  is the volume-averaged moisture content of the drop(particle) on a dry basis (kg moisture/kg dry solid),  $X_e$  is the equilibrium moisture content at bulk gas temperature, and  $X_{cr}$  is the critical moisture content at which the constant drying rate period ends ( $B$ ).  $N_V$  is the drying flux (kg m<sup>-2</sup> s<sup>-1</sup>) and  $\widehat{N}_V$  is the drying flux in the constant rate regime given by Equation 7.25:

$$\widehat{N}_V = \frac{\dot{m}_p}{S_p} = K_g \frac{MW_w}{RT} (p_{wb} - p_w) = \frac{h}{\lambda_l} (T_g - T_{wb}) \tag{3}$$

A linear falling rate curve has been found to fit a range of data from single-drop drying studies:

$$N_V = \widehat{N}_V \left(\frac{X - X_e}{X_{cr} - X_e}\right) = \frac{h}{\lambda_l} (T_g - T_{wb}) \left(\frac{X - X_e}{X_{cr} - X_e}\right) \tag{3}$$

This simple, empirical approach to drying is practically useful, especially when the drop drying model is a submodel for an integrated CFD model of a spray drier. However, it does not contain direct mechanistic information. A number of drop-drying models have been developed which include more direct information about the structure of the drop/particle during drying. For example, consider a drop which forms a shell when the drop radius has reached  $r_{sh}$ . The mass transfer rate can then be shown to be (Nesic and Vodnik, 1991):

$$N_V = \frac{\widehat{N}_V}{1 + \left(\frac{D_g}{D_{sh}}\right)\left(\frac{\delta}{r_{sh} - \delta}\right)} \tag{3}$$

$$\dot{m}_p = \frac{4\pi r_{sh}^2 \frac{h}{\lambda_l} (T_g - T_{wb})}{1 + \left(\frac{D_g}{D_{sh}}\right)\left(\frac{\delta}{r_{sh} - \delta}\right)} \tag{3}$$

where  $\delta$  is the thickness of the shell,  $D_g$  is the diffusion coefficient of the solvent vapor through air, and  $D_{sh}$  is the diffusivity (permeability) of the shell to mass transfer. Once the shell has formed, the particle (shell) radius remains constant but  $\delta$  will increase with time as solvent is evaporated from the inside of the drop. Typically,  $D_{sh} < D_g$  so that the rate of drop drying is lower, the resistance increases, and the drying rate continues to fall as  $\delta$  increases with time.  $D_{sh}$  will depend on the structure of the shell and is more difficult to predict a priori.



More recent models take into account more phenomena and come closer to being truly predictive, but are beyond the scope of this chapter (e.g., see Adhikari *et al.*, 2004; Handscomb *et al.*, 2009).

**Example 7.2** Drops (180  $\mu\text{m}$ ) of a 30% by mass inorganic salt solution are spray-dried in air at a temperature of 90°C under conditions where the wet bulb temperature is 50°C. The drop undergoes 10% shrinkage before a shell starts to form and the critical moisture content is reached. The final moisture content of the particles is 5% on a dry basis. What is the expected drying time for these drops?

Data:

$$\rho_l = 1,000 \text{ kg m}^{-3}; \rho_s = 1,000 \text{ kg m}^{-3}; \lambda_l = 2,260 \text{ kJ kg}^{-1}; k_g = 3 \times 10^{-5} \text{ kW m}^{-1}\text{K}^{-1}; X_c = 0.01$$

*Solution:*

First, calculate the time for the drop to shrink 10% in the constant drying rate period from Equation 7.28:

$$t_1 = \frac{\lambda_l \rho_l (d_{p,0}^2 - d_p^2)}{8k_g (T_g - T_{wb})}$$

$$t_1 = \frac{2260 \text{ kJ kg}^{-1} \times 1000 \text{ kg m}^{-3} \left( (180 \times 10^{-6})^2 - (162 \times 10^{-6})^2 \right) \text{ m}^2}{8 \times 3 \times 10^{-5} \text{ kW m}^{-1}\text{s}^{-1}\text{K}^{-1} (90 - 50) \text{ K}} = 1.5 \text{ s}$$

Next, calculate the moisture content at the onset of the falling rate regime. When the drop size has shrunk by 10%, the amount of water evaporated is:

$$M_{\text{evap}} = \rho_w \frac{\pi}{6} (d_{p,0}^3 - d_p^3) = 1000 \text{ kg m}^{-3} \frac{\pi}{6} \left( (180 \times 10^{-6})^3 - (162 \times 10^{-6})^3 \right) \text{ m}^3 = 8.27 \times 10^{-10} \text{ kg}$$

The initial mass of water and solid are:

$$M_w = 0.7 \times 1000 \text{ kg m}^{-3} \times \frac{\pi}{6} \times (180 \times 10^{-6} \text{ m})^3 = 2.202 \times 10^{-9} \text{ kg}$$

$$M_s = 0.3 \times 1000 \text{ kg m}^{-3} \times \frac{\pi}{6} \times (180 \times 10^{-6} \text{ m})^3 = 9.34 \times 10^{-10} \text{ kg}$$

Therefore, the critical moisture content is:

$$X_{cr} = \frac{M_w - M_{evap}}{M_s} = \frac{2.202 \times 10^{-9} \text{ kg} - 8.27 \times 10^{-10} \text{ kg}}{9.34 \times 10^{-10} \text{ kg}} = 1.456$$

Assume we can use Equation 7.33 for the falling rate period:

$$N_V = \widehat{N}_V \left( \frac{X - X_e}{X_{cr} - X_e} \right) = \frac{2k_g}{\lambda_l d_p} (T_g - T_{wb}) \left( \frac{X - X_e}{X_{cr} - X_e} \right)$$

where

$$\widehat{N}_V = \frac{2k_g}{\lambda_l d_p} (T_g - T_{wb})$$

$\widehat{N}_V$  is a constant. We assume the particle does not shrink further during the falling rate period.

$$\begin{aligned} N_V &= \frac{M_s}{S_p} \frac{dX}{dt} = \widehat{N}_V \left( \frac{X - X_e}{X_{cr} - X_e} \right) \\ \Rightarrow \frac{dX}{dt} &= - \frac{\widehat{N}_V S_p}{M_s} \left( \frac{X - X_e}{X_{cr} - X_e} \right) \end{aligned}$$

Integrating gives:

$$t_2 = - \frac{M_s (X_{cr} - X_e)}{\widehat{N}_V S_p} \ln \left( \frac{X - X_e}{X_{cr} - X_e} \right)$$

Now we can substitute in numerical values:

$$\widehat{N}_V = \frac{2 \times 3 \times 10^{-5} \text{ kW m}^{-1} \text{ K}^{-1}}{2260 \text{ kJ kg}^{-1} \times 162 \times 10^{-6} \text{ m}} (90 - 50) \text{ K} = 6.56 \times 10^{-3} \text{ kg m}^{-2} \text{ s}^{-1}$$

$$S_p = \pi (162 \times 10^{-6} \text{ m})^2 = 8.24 \times 10^{-8} \text{ m}^2$$

$$t_2 = - \frac{9.34 \times 10^{-10} \text{ kg} \times (1.456 - 0.01)}{6.56 \times 10^{-3} \text{ kg m}^{-2} \text{ s}^{-1} \times 8.24 \times 10^{-8} \text{ m}^2} \ln \left( \frac{0.05 - 0.01}{1.456 - 0.01} \right) = 9.02 \text{ s}$$

Total drying time is therefore:

$$t = t_1 + t_2 = 1.5 \text{ s} + 9.0 \text{ s} = 10.5 \text{ s}$$

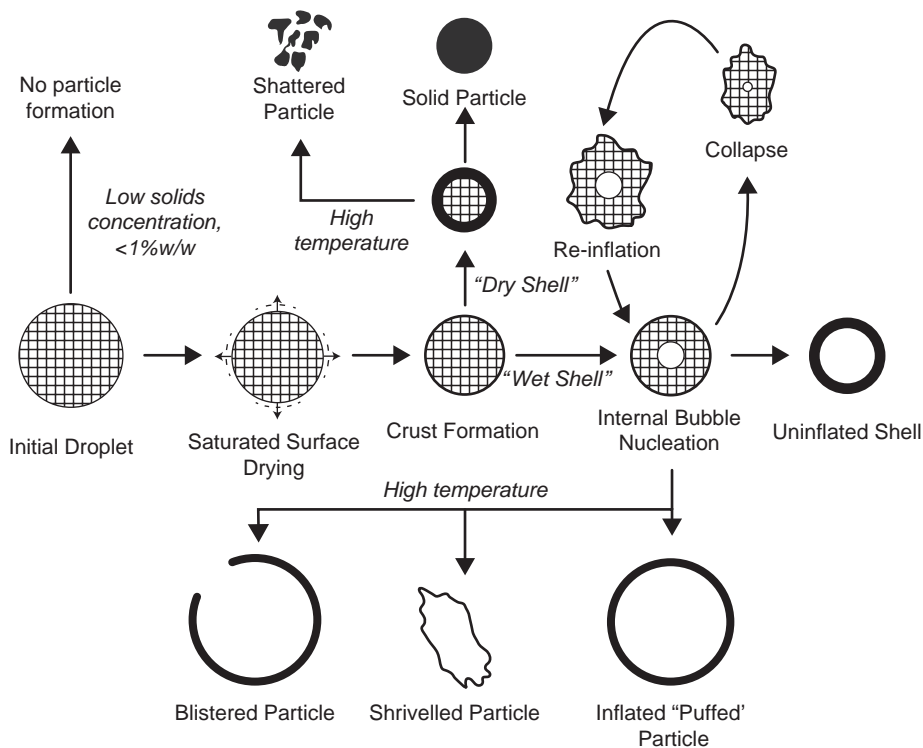


**Figure 7.8** Different particle morphologies resulting from spray-drying drops containing dissolved or suspended solids (Handscomb *et al.*, 2009).

## 7.5 Particle Morphology from Spray Drying and Spray Cooling

Spray cooling (prilling) gives dense, spherical particles of very similar size to the melt drops and with limited porosity. In contrast, spray drying yields a weird and wonderful array of particle morphologies. Many of these morphologies relate directly to the formation of a shell during the drying process. If a vapor bubble is nucleated at the center of the drying drop, then a variety of morphologies developed from hollow particles are possible. Figure 7.8 demonstrates a variety of the different morphologies and how they are produced. Some of the questions which determine the particle morphology are:

- Is a shell formed during drying?
- Does a bubble form at the center of the drop?
- Is the shell a hard crust or a soft skin?
- How permeable is the shell?
- Is the surrounding gas temperature above or below the solvent boiling point?

If no shell is formed, then a spherical, porous particle is produced. If a porous hard crust is formed, vapor escapes through pores in the crust and a solid particle or a hollow particle will form, depending on whether a bubble forms in the center

of the drop. Such crusts may result when suspended solids form crystals during drying, or for colloidal suspensions. If the crust has low permeability, there may be considerable pressure build up, especially if the liquid reaches boiling, causing fracture or shattering of the crust. A soft shell or skin can form when the dissolved solids precipitate as an amorphous phase above its glass transition temperature. Pressure build up can cause the particle to inflate or “puff” to later collapse when the particle cools. The inflated skin can burst to give a blistered particle.

For real systems, it is difficult to predict quantitatively the particle morphology without the aid of single-drop drying experiments. A key question is if and when a shell will form. This impacts both the drop drying time and the final morphology. We can do some useful calculations to estimate conditions under which a shell will form that take us a long way towards understanding these phenomena.

As the drop dries, the liquid–vapor interface recedes, causing a concentration of non-volatile solute or suspended solids at the drop surface (see Figure 7.9). At the same time, there will be a diffusional flux away from the surface driven by the concentration gradient formed. Concentration of solute or suspended particles at the receding drop surface can lead to the formation of a shell, skin, or crust at the drop surface, so it is important to be able to predict the extent of surface enrichment as the drop dries. We can rewrite Equation 7.29 as:

$$t_D = \frac{d_{p,0}^2}{\kappa} \tag{8}$$

where  $\kappa$  is the liquid evaporation flux given by:

$$\kappa = \frac{8k_g (T_g - T_{wb})}{\lambda_l \rho_l} \tag{9}$$

The concentration enrichment of the solute can then be derived from the diffusion equation as (Vehring *et al.*, 2007):

$$E = \frac{c_{su}}{c_m} = \frac{\exp(0.5Pe)}{3\beta} \tag{10}$$

where  $c_{su}$  is the surface concentration of solute and  $c_m$  is the average solute concentration in the drop. Here  $Pe$  is the dimensionless Peclet number, which gives the relative evaporation flux to the diffusional flux of solute away from the drop surface:

$$Pe = \frac{\kappa}{8D_l} \tag{11}$$

where  $D_l$  is the solute diffusion coefficient through the liquid.  $\beta = \int_0^1 R^2 \exp\left(\frac{R^2 Pe}{2}\right) dR$

and is a function that must be integrated numerically. For  $Pe < 20$ , Equation 7.38 can be approximated as:

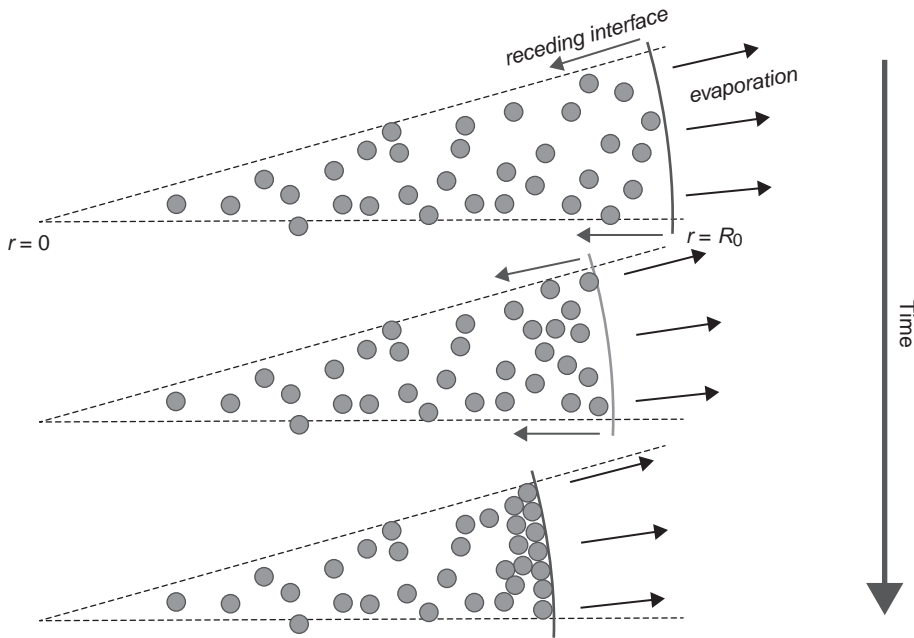


**Figure 7.9** Concentration of solute or suspended solids at the receding drop surface. If the surface recedes faster than the molecules or particles can diffuse to the drop interior, a shell will form (Andrew Bayley, used by permission).

$$E = \frac{c_s}{c_m} = 1 + \frac{Pe}{5} + \frac{Pe^2}{100} - \frac{Pe^3}{4000} \quad \mathbf{9}$$

The average concentration is calculated from the mass balance of the evaporating drop:

$$c_m = c_0 \left( 1 - \frac{t}{t_D} \right)^{\frac{3}{2}} \quad \mathbf{4}$$

where  $c_0$  is the initial solute concentration in the drop. The diffusion coefficient for the solute can be estimated from the Stokes–Einstein relationship:

$$D_l = \frac{kT}{6\pi\mu R} \quad \mathbf{4}$$

where  $k$  is Boltzmann's constant and  $R$  is the radius of the suspended particle or solute molecule.

Armed with this information about drying and diffusion rates, we can establish a lot of useful information about our drying system.

1. We can establish whether or not shell formation will occur. For  $Pe > 1$ , shell formation is likely because the concentration effect due to evaporation exceeds the diffusion rate away from the drop surface.
2. We can predict the time at which the surface concentration of solute becomes supersaturated, making crystallization of the solute possible:

$$t_{sat} = t_D \left[ 1 - \left( \frac{EC_0}{c_s} \right)^{2/3} \right] \tag{3}$$

We can then define the “precipitation window” available for crystallization:

$$t_p = t_D - t_{sat} = \frac{d_{p,0}^2}{\kappa} \left( \frac{EC_0}{c_s} \right)^{2/3} \tag{4}$$

If the induction time for crystal nucleation is longer than  $t_p$ , an amorphous particle will be formed.

3. For amorphous particle formation, an estimate of the time for an amorphous shell to form is the time it takes for the concentration at the surface to be similar to the true density of the amorphous solid:

$$t_a = t_D \left[ 1 - \left( \frac{EC_0}{\rho_s} \right)^{2/3} \right] \tag{5}$$

4. For a multicomponent system, by calculating the surface enrichment for each component, we can calculate which component(s) is likely to be in the shell and which component(s) will be in the core of the particle.

**Example 7.3** I am spray drying a suspension of 20 nm-diameter spheres as a 5% by volume suspension in water with drop size 100 μm. The drop temperature  $T_{wb} = 80^\circ\text{C}$  and the LMTD is  $30^\circ\text{C}$ . Do you expect to see concentration of particles at the drop surface? If so, at what drop diameter do you expect to see a shell begin to form?

*Solution:*

First, let us check the value of the Peclet number. We estimate the diffusion coefficient for the nanoparticles in water from the Stokes–Einstein equation (Equation 7.42):

$$D_l = \frac{kT}{6\pi\mu R} = \frac{1.38 \times 10^{-23} \text{ J K}^{-1} \times 353 \text{ K}}{6\pi \times 10^{-3} \text{ Pa}\cdot\text{s} \times 10 \times 10^{-9} \text{ m}} = 2.6 \times 10^{-11} \text{ m}^2 \text{ s}^{-1}$$

From Equation 7.37:

$$\kappa = \frac{8k_g (T_g - T_{wb})}{\lambda_l \rho_l} = \frac{8 \times 3 \times 10^{-5} \text{ kWm}^{-1} \text{ K}^{-1} \times 30 \text{ K}}{2260 \text{ kJ kg}^{-1} \times 1000 \text{ kg m}^{-3}} = 3.2 \times 10^{-9} \text{ m}^2 \text{ s}^{-1}$$

Therefore

$$Pe = \frac{\kappa}{8D_l} = \frac{3.2 \times 10^{-9} \text{ m}^2 \text{ s}^{-1}}{8 \times 2.6 \times 10^{-11} \text{ m}^2 \text{ s}^{-1}} = 15.4$$

As  $Pe > 1$ , we expect surface concentration of the nanoparticles.

Now, let us calculate the degree of surface concentration. From Equation 7.40:

$$E = \frac{c_s}{c_m} = 1 + \frac{15.4}{5} + \frac{15.4^2}{100} - \frac{15.4^3}{4000} = 5.54$$

From Equations 7.36 and 7.41:

$$c_s = Ec_m = Ec_0 \left( 1 - \frac{d_{sh}^2}{d_0^2} \right)^{-\frac{3}{2}}$$

The problem statement does not give the surface concentration at which a shell begins to form. Let us assume the shell has the solids fraction of a bed of randomly packed spheres, i.e.,  $c_s \approx 0.6$  (a bed with a voidage of 0.4):

$$0.4 = 5.54 \times 0.05 \left( 1 - \frac{d_{sh}^2}{(100 \mu\text{m})^2} \right)^{-\frac{3}{2}} \Rightarrow d_{sh} = 46.6 \mu\text{m}$$

Note that if attractive forces between the particles cause a shell to form at lower solids fraction (higher voidage), the shell diameter will be larger.

## 7.6 Spray-drier and Spray-cooler Design

### 7.6.1 Spray-cooling Towers (Prill Towers)

Spray-cooling towers are generally tall cylinders with countercurrent cooling gas flow (Figure 7.10). The melt enters the top of the tower from a series of simple nozzles where drops are formed by Rayleigh jet break up. As they fall, they cool and solidify, and must be fully solid at the bottom of the tower. If the melt enters the tower and we neglect subcooling of the solid particles, the overall energy balance for the tower is:

$$\dot{m}_p \lambda_s = \dot{m}_g c_{pg} (T_g(0) - T_g(L)) \quad \mathbf{3}$$

where  $\dot{m}_p$  and  $\dot{m}_g$  are the mass flow rates of the melt (particle) phase and gas phase, respectively.

Let us consider a simple, one-dimensional model for the spray-cooling tower. In a slice of the tower from length  $z$  to length  $z + dz$ , the rate of transfer of energy from the gas phase to the particulate phase is:

$$\dot{m}_g c_{pg} (T_g|_z - T_g|_{z+dz}) = \frac{6(1-\varepsilon)Adz}{d_p} h (T_{solid} - T_g|_z) \tag{7}$$

where  $\frac{6(1-\varepsilon)Adz}{d_p}$  is the total surface area of particles between  $z$  and  $z + dz$ ,  $A$  is the column cross-sectional area, and  $\varepsilon$  is the voidage in the column. The surface area of particles can be rewritten as:

$$\frac{6(1-\varepsilon)Adz}{d_p} = \frac{6\dot{m}_p dz}{U_p \rho_p d_p} \tag{8}$$

where  $U_p$  is the falling velocity of a particle in the tower. Rearranging and taking the limit as  $dz \rightarrow 0$ :

$$-\dot{m}_g c_{pg} \frac{dT_g(z)}{dz} = \frac{6\dot{m}_p h}{U_p \rho_p d_p} (T_{solid} - T_g(z)) \tag{9}$$

Integrating Equation 7.48 between the limits of  $z = 0$  and  $z = L$  gives us:

$$L = \frac{U_p \rho_p d_p \dot{m}_g c_{pg}}{6\dot{m}_p h} \ln \left[ \frac{T_{solid} - T_g(0)}{T_{solid} - T_g(L)} \right] \tag{10}$$

Combining Equations 7.46 and 7.50 gives:

$$L = \frac{U_p \rho_p d_p \lambda_s}{6h(T_g(0) - T_g(L))} \ln \left[ \frac{T_{solid} - T_g(0)}{T_{solid} - T_g(L)} \right] = \frac{U_p \rho_p d_p \lambda_s}{6h [LMTD(T_{solid} - T_g)]} \tag{11}$$

The column length is directly related to the residence time of the particle in the tower:

$$t = \frac{L}{U_p} \tag{12}$$

Substituting into Equation 7.51 gives:

$$t = \frac{\rho_p d_p \lambda_s}{6h [LMTD(T_{solid} - T_g)]} \tag{13}$$



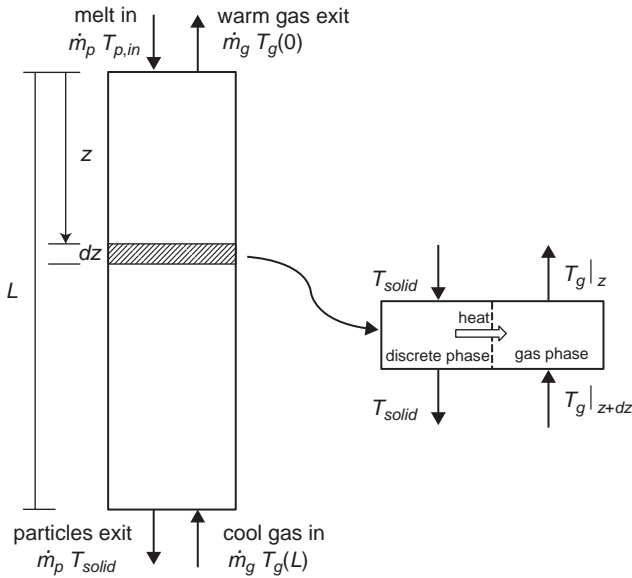


**Figure 7.10** Schematic of one-dimensional model for a spray-cooling tower.

Note that Equation 7.53 is very similar to Equation 7.22 using the LMTD in the column to represent the temperature difference for heat transfer.

To calculate the column height  $L$ , we need to know the falling velocity of the particles. In general:

$$U_p = U_{slip} - \frac{|U_g|}{\varepsilon} = U_{slip} - \frac{\dot{m}_g}{\varepsilon \rho_g A} \quad 3$$

where  $U_g$  is the superficial gas velocity in the column and the slip velocity is given by the Richardson–Zaki equation:

$$U_{slip} = U_t \varepsilon^{n-1} \quad 3$$

where  $U_t$  is the terminal settling velocity of the particle and  $n$  is the Richardson–Zaki exponent. As  $\varepsilon$  approaches 1, Equation 7.54 reduces to:

$$U_p = U_t - |U_g| = U_t - \frac{\dot{m}_g}{\rho_g A} \quad 3$$

The particle terminal settling velocity is likely to be outside the Stokes Law regime and the following correlation can be used to calculate  $U_t$ :

$$U_t^* = \left[ \frac{18}{(d^*)^2} + \frac{0.591}{(d^*)^{0.5}} \right]^{-1} \quad 3$$

where

$$U_t^* = U_t \left[ \frac{\rho_g^2}{\mu(\rho_p - \rho_g)g} \right]^{1/3}; d^* = \psi d_v \left[ \frac{\rho_g(\rho_p - \rho_g)g}{\mu^2} \right]^{1/3} \tag{8}$$

**Example 7.4** I want to design a spray-cooling tower to produce 1.5 mm-diameter lead shot. Molten lead enters the tower through a series of simple nozzles. The nozzle array can operate at a mass flux of 40 kg m<sup>-2</sup> s<sup>-1</sup>. Assume the melt enters the tower at its solidification temperature. The drops are solidified using a counter-current airflow. The air inlet temperature is 20°C and the air outlet temperature is limited to 200°C. How tall should my cooling tower be?

*Data:*

Average properties of air in this temperature range:

$$\rho_g = 1.2 \text{ kg m}^{-3}; C_{p,g} = 1 \text{ kJ kg}^{-1}\text{K}^{-1}; k_g = 3 \times 10^{-5} \text{ kW m}^{-1}\text{K}^{-1}; \mu_g = 2 \times 10^{-5} \text{ Pa s}; Pr = 0.7$$

Properties of lead:

$$\rho_{pb} = 11,300 \text{ kg m}^{-3}; \lambda_s = 2 \text{ W m}^{-1}\text{K}^{-1}; T_{solid} = 327 \text{ °C}$$

*Solution:*

First, complete the overall energy balance for the tower (Equation 7.46)

$$\begin{aligned} \dot{m}_p \lambda_s &= \dot{m}_g c_{pg} (T_g(0) - T_g(L)) \\ \Rightarrow \frac{\dot{m}_g}{\dot{m}_p} &= \frac{\rho_g U_g}{\left(\frac{\dot{m}_p}{A}\right)} = \frac{\lambda_s}{c_{pg} (T_g(0) - T_g(L))} \\ \Rightarrow U_g &= \frac{40 \text{ kg m}^{-2} \text{ s}^{-1} \times 24.7 \text{ kJ kg}^{-1}}{1 \text{ kg m}^{-3} \times 1 \text{ kJ kg}^{-1} \text{ K}^{-1} \times (200 - 20) \text{ K}} = 5.5 \text{ m s}^{-1} \end{aligned}$$

Next, calculate the particle falling velocity in the tower using Equations 7.56 to 7.58. We will assume here that the solids fraction in the tower is very low ( $\epsilon \rightarrow 1$ ) so the slip velocity is equal to the terminal settling velocity of the particle:

$$d^* = \psi d_v \left[ \frac{\rho_g(\rho_p - \rho_g)g}{\mu^2} \right]^{1/3} = 1.5 \times 10^{-3} \text{ m} \left[ \frac{1 \text{ kg m}^{-3} \times 11,340 \text{ kg m}^{-3} \times 9.81 \text{ m s}^{-2}}{(2 \times 10^{-5} \text{ Pa s})^2} \right]^{1/3} = 97.9$$

$$U_t^* = \left[ \frac{18}{(d^*)^2} + \frac{0.591}{(d^*)^{0.5}} \right]^{-1} = \left[ \frac{18}{(97.9)^2} + \frac{0.591}{(97.9)^{0.5}} \right]^{-1} = 16.2$$

$$U_t = U_t^* \left[ \frac{\rho_g^2}{\mu(\rho_p - \rho_g)g} \right]^{\frac{1}{3}} = 16.2 \left[ \frac{(1\text{kgm}^{-3})^2}{2 \times 10^{-5} \text{Pa s} \times 11,340\text{kgm}^{-3} \times 9.81\text{ms}^{-2}} \right]^{\frac{1}{3}} = 12.4\text{ms}^{-1}$$

From Equation 7.56

$$U_p = 12.4 \text{ m s}^{-1} \times 5.6 = 69 \text{ m s}^{-1}$$

The terminal settling velocity is very high because we have very dense, relatively large particles. We will need to use the full Ranz–Marshall equation (Equation 7.13) to calculate the heat transfer coefficient for the drop solidification time.

$$Re_p = \frac{d_p u_{\text{slip}} \rho_g}{\mu_g} = \frac{1.5 \times 10^{-3} \text{ m} \times 12.4 \text{ ms}^{-1} \times 1\text{kgm}^{-3}}{2 \times 10^{-5} \text{ Pa s}} = 930$$

$$Nu = 2 + 0.6 Re_p^{0.5} Pr^{0.33} = 2 + 0.6 \times 930^{0.5} \times 0.7^{0.33} = 18.3$$

$$h = \frac{Nu k_g}{d_p} = \frac{18.3 \times 3 \times 10^{-5} \text{ kWm}^{-1}\text{K}^{-1}}{1.5 \times 10^{-3} \text{ m}} = 0.36 \text{ kWm}^{-2}\text{K}^{-1}$$

Note that the heat transfer coefficient is an order of magnitude larger than that for stagnant conditions.

Now we can calculate the drop solidification time from Equation 7.53:

$$LMTD(T_{\text{solid}} - T_g) = \frac{(200 - 20)\text{K}}{\ln \left[ \frac{327.5 - 20}{327.5 - 200} \right]} = 204\text{K}$$

$$t = \frac{\rho_p d_p \lambda_s}{6h [LMTD(T_{\text{solid}} - T_g)]} = \frac{11,340\text{kgm}^{-3} \times 1.5 \times 10^{-3} \text{ m} \times 24.7\text{kJkg}^{-1}}{6 \times 0.36\text{kWm}^{-2}\text{K}^{-1} \times 204\text{K}} = 0.95\text{s}$$

The minimum tower height is that required to just solidify the drops with no subcooling:

$$L_{\text{min}} = t U_p = 0.95 \text{ s} \times 69 \text{ m s}^{-1} = 66 \text{ m}$$

The real design would be taller to allow the melt entering above the solidification temperature and for some subcooling of the lead shot.

### 7.6.2 Spray-drier Design

Spray can be configured in co-current flow, countercurrent flow, or somewhere in between (see Figure 7.11). Co-current driers can operate with rotary disc or nozzle atomizers. Driers using rotary atomizers have a larger diameter as the atomizer throws the drops radially towards the drier wall. Co-current driers have the advantage that the drop/particle is always at a relatively low temperature. Hot air entering the drier near the atomizer is quickly quenched by the rapid evaporation of solvent from the drops. In fact, the gas temperature within a co-current spray drier is fairly uniform and the driest particles are exposed to the coolest air. This is very important for temperature-sensitive materials.

Countercurrent driers usually operate with nozzle atomizers. Countercurrent driers have very large temperature gradients and dry particles are exposed to the highest temperature gas. However, they have better thermal efficiency.

The moisture mass balance for a spray drier is (with reference to Figure 7.11):

$$\dot{M}_{s,in}X_{in} + \dot{M}_{g,in}Y_{in} = \dot{M}_{s,ex}X_{ex} + \dot{M}_{g,ex}Y_{ex} \quad 9$$

where  $\dot{M}_s$  and  $\dot{M}_g$  are the dry basis mass flow rates of the slurry/particle stream and gas stream, respectively,  $X$  is the moisture content (kg water/kg dry solids) and  $Y$  is the absolute humidity of the air (kg water/kg dry air).

The overall energy balance for a spray-drier is:

$$\dot{M}_{s,in}h_{s,in} + \dot{M}_{g,in}h_{g,in} = \dot{M}_{s,ex}h_{g,ex} + \dot{M}_{g,ex}h_{g,ex} + \dot{Q}_L \quad 10$$

where  $h_s$  and  $h_g$  are the enthalpies of the solution/particle stream and the gas streams, respectively (J kg<sup>-1</sup> dry solids or J kg<sup>-1</sup> dry gas) and  $\dot{Q}_L$  is the rate of heat loss through the drier walls. Care needs to be taken to be consistent in defining the reference states for each of the components.

Spray driers are very energy-intensive as a large amount of energy is used to evaporate water and this energy is not usually recovered, so the true efficiency of spray-driers according to the 2nd Law of Thermodynamics is low. One practical measure of thermal efficiency is the evaporation efficiency:

$$\eta_{evap} = \frac{T_1 - T_2}{T_1 - T_{sat}} \quad 11$$

where  $T_{sat}$  is the adiabatic saturation temperature corresponding to the inlet air temperature  $T_1$ .

To complete a spray drier design, we need:

1. The overall mass and energy balance equations (Equations 7.59 and 7.60).
2. The spray drop distribution from the atomizer from experiment or correlations as given in Section 7.3.3.

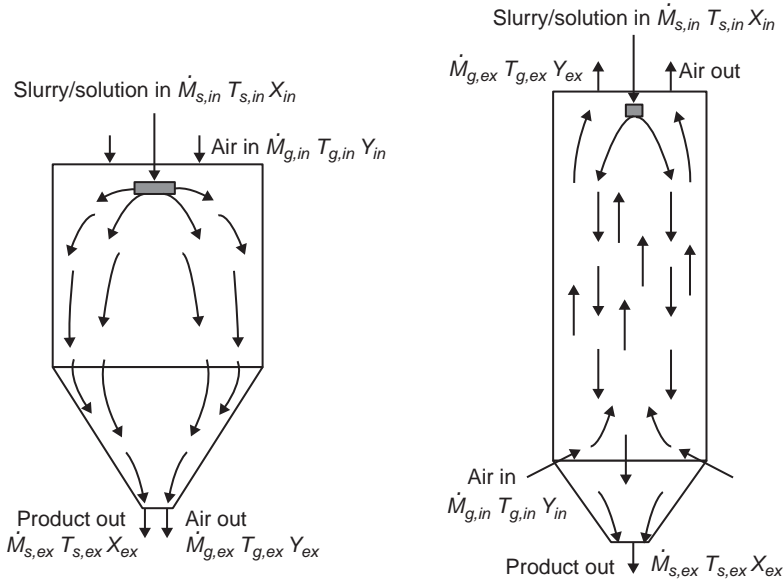


**Figure 7.11** Different spray-drying configurations. (a) Co-current with a rotary atomizer; (b) countercurrent with a nozzle atomizer.

3. A model for drying kinetics of single drops – e.g., Equations 7.32 or 7.33 – which may be incorporated into a population balance framework to account for the variation in drop size.
4. A mixing model for each of the gas phase and the drop/particle phase.

Mixing models are more complex for spray driers than for spray coolers. For a co-current drier, we can start from an assumption that the gas flow is plug flow and the drops travel with the gas with negligible slip velocity. However, this approach is usually insufficient for detailed design. Instead, computational fluid dynamics (CFD) approaches are used. A two-phase model is necessary consisting of the gas phase (using a Eulerian framework) and the drop/particle phase (using a Lagrangian framework incorporating a population balance to track the changing moisture content of the particles). The momentum, heat, and mass transfer equations are solved simultaneously. Description of this CFD approach is beyond the scope of this text, but is described in some detail in Tstosas and Mujumdar (2007).

It is important to recognize that spray drying is *inherently unscalable* – i.e., scaling rules based on a simple dimensionless group cannot predict the thermal efficiency and especially the product quality (moisture content, particle size, and morphology) of a large-scale drier from laboratory or even pilot-scale drier results. This is because small-scale and large-scale driers have different geometries and different types of atomizer, with different drop size distributions leading to large differences in drying rates, particle size, and morphology on scaling up. Instead we use a *multiscale* approach as described above:

1. Single-drop drying experiments under highly controlled conditions are used to develop or validate single-drop drying models and investigate particle morphology (skin or crust formation, etc.). (These experiments suspend a drop from a very thin filament or levitate it acoustically.)
2. Spray drop size distributions can be measured directly for new formulations using actual atomizers.
3. The drop-drying model and spray drop distributions can then be used as input for CFD simulations of large-scale driers for design.

Spray-drier designs can also include other features to control particle size distributions and other attributes including recycling of fines into the spray zone, or fluid bed agglomeration at the spray-drier exit.

**Example 7.5** Eight hundred kilograms per hour of dried product is produced at 6% moisture from a co-current flow spray-drier. Preheated air at 300°C and moisture content of 0.005 kg/(kg dry air) is used in the drier and the exit air temperature is 95°C. The feed solution contains 45% solids and enters at 20°C. The dried product leaves the drier at 80°C. How much air is required? What is the humidity of the exit air?

Data:

$$C_{p,wl} = 486 \text{ kJ kg}^{-1} \text{K}^{-1}; C_{p,ww} = 1900 \text{ kJ kg}^{-1} \text{K}^{-1}; C_{p,ds} = 16 \text{ kJ kg}^{-1} \text{K}^{-1};$$

$$C_{p,a} = 1 \text{ kJ kg}^{-1} \text{K}^{-1}; \lambda_{v0} = 2,600 \text{ kJ kg}^{-1}$$

Solution:

Calculate the parameters relevant for using in the overall mass (Equations 7.59 and 7.60):

$$X_{in} = \frac{(1-0.45) \text{ kg liquid}}{0.45 \text{ kg solid}} = \frac{1.22 \text{ kg}}{(\text{kg dry solid})}$$

$$X_{ex} = \frac{0.06 \text{ kg liquid}}{(1-0.06) \text{ kg solid}} = \frac{0.064 \text{ kg}}{(\text{kg dry solid})}$$

Note that at steady state, on a dry basis  $\dot{M}_{g,in} = \dot{M}_{g,ex} = \dot{M}_g$ , and substitute into Equation 7.59:

$$800 \text{ kg.hr}^{-1} \times 1.22 + \dot{M}_g \times 0.005 = 800 \text{ kg.hr}^{-1} \times 0.064 + \dot{M}_g Y_{ex}$$

$$\Rightarrow \dot{M}_g (Y_{ex} - 0.005) = 925 \text{ kg.hr}^{-1} \tag{A}$$

For the energy balance, we need expressions to calculate the enthalpy of all the streams. We take the reference temperature of all components as 0°C and standard state:

$$h_g = C_{p,a}(T - 0^\circ\text{C}) + Y(\lambda_{v,0} + C_{p,wv}(T - 0^\circ\text{C}))$$

$$h_s = C_{p,ds}(T - 0^\circ\text{C}) + XC_{p,wl}(T - 0^\circ\text{C})$$

For the conditions given in this problem, we can therefore write:

$$h_{g,in} = 1 \text{ kg}^{-1} \text{K}^{-1} \times 60 \text{ K} + 0.005 \times 2,600 \text{ kg}^{-1} + 1 \text{ kg}^{-1} (60 \text{ K}) = 3 \text{ kg}^{-1}$$

Similarly:

$$h_{g,ex} = (9 + 2,683 Y_{ex}) \text{ kg}^{-1}$$

$$h_{s,in} = 1 \text{ kg}^{-1} \text{ J kg}^{-1}$$

$$h_{s,ex} = 1 \text{ kg}^{-1} \text{ J kg}^{-1}$$

Substituting into Equation 7.60 (neglecting any heat loss) gives:

$$\begin{aligned} \dot{M}_g (95 + 2683 Y_{ex} - 315) \text{ kJ kg}^{-1} - 800 \text{ kg hr}^{-1} (149 - 134) \text{ kJ kg}^{-1} &= 0 \\ \Rightarrow \dot{M}_g (2683 Y_{ex} - 220) \text{ kJ kg}^{-1} &= 12000 \text{ kJ hr}^{-1} \end{aligned} \quad (\text{B})$$

We can now solve Equations A and B simultaneously to get  $\dot{M}_g$  and  $Y_{ex}$ :

$$Y_{ex} = 0.0824$$

$$\dot{M}_g = 12,000 \text{ kg.hr}^{-1}$$

### 7.6.3 Population Balance Models for Spray Drying and Spray Cooling

In Chapter 3 we presented the population balance for tracking the particle size distribution for particle formation processes. If we apply this approach to spray drying in its simplest form, then we need to consider only the rate process of nucleation. A continuous stream of liquid-phase nucleates new particles via atomization. Equation 3.3 reduces to:

$$\frac{dVn(r,t)}{dt} = -\dot{Q}_{ex}n(r) + V\dot{b}_{nuc} \quad \text{E2}$$

where  $r$  is the drop/particle radius. At steady state:

$$\dot{Q}_{ex}n(r) = V\dot{b}_{nuc} \Rightarrow n(r) = \dot{b}_{nuc} \tau \quad \text{E3}$$

In Chapter 4 (crystallization) and Chapter 6 (aerosol processes), nucleation was a molecular process. New nuclei were very small and assumed to be zero size or an arbitrarily small size and the Dirac delta function was used to describe this mathematically (Equations 3.19 or 3.25). However, for spray cooling and drying the nuclei size distribution is set by the drop size distribution from the nozzle or atomizer. If drop coalescence is neglected, then the expression of the nuclei distribution is:

$$V\dot{b}_{muc}(r) = \dot{Q}_{sp} n_d(r/k_{shr}) \quad 74$$

where  $n_d$  is the drop size distribution from the spray and  $k_{shr}$  is the shrinkage ratio, i.e., the ratio of the particle size to the drop size from which it is formed. Combining Equations 7.63 and 7.64:

$$n(r) = \frac{\dot{Q}_{sp}}{\dot{Q}_{ex}} n_d(r/k_{shr}) \quad 75$$

For spray cooling the shrinkage ratio is simply:

$$k_{shr} = \left( \frac{\rho_l}{\rho_p} \right)^{1/3} \quad 76$$

For spray drying, the shrinkage ratio depends on the morphology of the particle formed. For example, if a hard shell is formed during drying, then:

$$k_{shr} = \frac{r_{sh}}{r_0} \quad 77$$

Equation 7.65 emphasizes how critical control of drop formation is in determining the size distribution of the product (as well as the drying rate and particle morphology). For example, acoustically vibrated nozzles for spray coolers can produce essentially uniform drop sizes and therefore mono-sized particles. Note also that the product particle size distribution is the same, independent of the mixing on the spray drier (plug-flow or well-mixed).

For spray-dried product, the moisture content of the product particles is also an important property. The final moisture content of the particle will depend on both the initial drop size and the time–temperature history seen by the drop. To capture these effects completely, we need to track the two-dimensional particle distribution  $n(v_l, v_s)$  where  $v_l$  and  $v_s$  are the liquid and solid volume in the drop/particle, respectively. For a well-controlled volume at steady state, the two-dimensional population balance is:

$$\frac{dG_l n(v_l, v_s)}{dv_l} = \dot{Q}_{sp} n_d \left( v_l, \frac{v_l \rho_l}{X_{in} \rho_s} \right) - \frac{n(v_l, v_s)}{\tau} \quad 78$$



where  $X_{in}$  is the moisture content of the slurry/solution being sprayed into the tower, and  $G_l$  is the “growth rate” of the particle liquid volume. Note the “growth rate” of the particle solid volume is zero because no solid is evaporated during drying. The particle moisture content is then calculated as:

$$X = \frac{v_l \rho_l}{v_s \rho_s} \quad (7.69)$$

and the solid volume in the drops from the atomizer is:

$$v_s = \frac{v_l \rho_l}{X_{in} \rho_s} \quad (7.70)$$

$G_l$  must be negative of course and is derived from the single-drop drying models in Sections 7.3.4 and 7.3.5. For example, if a drop of a suspension is in the constant drying rate region ( $X > X_{cr}$ ), then from Equation 7.32 we can derive:

$$G_{l,1} = \frac{\dot{m}_p}{\rho_l} = -\frac{S_p h}{\rho_l \lambda_l} (T_g - T_{wb}) \quad (7.71)$$

where

$$S_p = \left[ 6\pi^{1/3} (v_l + v_s) \right]^{2/3} \quad (7.72)$$

In the falling rate regime ( $X < X_{cr}$ ), if the particle radius remains constant, then from Equation 7.33:

$$G_{l,2} = \frac{4\pi r_s^2 h}{\rho_l \lambda_l} (T_g - T_{wb}) \left( \frac{X - X_e}{X_{cr} - X_e} \right) \quad (7.73)$$

For a spray drier that can be considered as plug-flow, the two-dimensional population balance is:

$$\frac{dU_Z n(v_l, v_s, z)}{dz} + \frac{dG_v n(v_l, v_s, z)}{dv_l} = 0 \quad (7.74)$$

with the initial condition:

$$\dot{Q}_g n(v_l, v_s, 0) = \dot{Q}_{sp} n_d \left( v_l, \frac{v_l \rho_l}{X_{in} \rho_s} \right) \quad (7.75)$$

The population balance needs to be solved in conjunction with the heat and mass balance equations for the spray drier because the drying rates (Equation 7.71–7.73) are a function of the local air temperature. We have presented the equations

for the two ideal mixing cases: well-mixed and plug-flow. In reality, spray-drier analysis usually requires more detailed analysis of the flow field and temperature gradients. When written in its microscopic form, the two-dimensional population balance model can be linked with mass, energy, and momentum balance equations in CFD simulations to predict particle size and moisture distributions of product particles.

## 7.7 Summary

Spray cooling and spray drying are processes in which the formation of drops, and their subsequent cooling or drying, are critical in determining the attributes of the product particles.

Spray cooling is the simpler of the two processes to understand and model. Drops are formed from liquid jets from simple orifices by Rayleigh jet break up (Section 7.3.1). Very uniform-sized drops can be formed, especially if an external disturbance is applied to the jet. Drops then cool and solidify as they fall in the tower. External film resistance typically controls the rate of heat transfer, and the Ranz–Marshall equation can be used to calculate the heat transfer coefficient (Equation 7.13) for the gas film surrounding the falling drop. The spray cooling towers operate in countercurrent flow where plug flow can reasonably be assumed for both the gas and solid phases, leading to relatively straightforward design equations (Section 7.5.1).

Spray drying is more complex, has much broader application, and can yield a startling array of particle morphologies. Drops formed from different atomizers are not monosized, but the underlying physics of the break up of jet, ligaments, and films is similar so the impact of changes to liquid properties is also similar to simple jets, at least qualitatively (Section 7.3.3). Drop drying is similar to drop cooling, but the heat and mass transfer rates around the drop are balanced. Analysis of the drying of a pure solvent drop is well established, but drying of a solution or suspension is much more complicated due to the possible formation of a crust, shell, or skin as the particles dry. Section 7.3.5 gives models for drying drops containing solids, and Section 7.4 describes the mechanism for shell formation. You should be comfortable with using these approaches and be able to explain the many different particle morphologies that can be generated in terms of this framework. Thus, the drop size from the atomizer is the primary driver for product size distribution, and the structure formation during drying is the main driver for particle morphology.

Finally, integrated design of the spray-drying process and product is a multi-scale approach involving (1) choice and design of an atomizer; (2) modeling and/or experiments of drying and structure formation in single drops; and (3) CFD simulation of flow and temperature fields and particle trajectories in the full-scale drier (Sections 7.5.2 and 7.5.3). Scale-up based on primary parameters or dimensionless group is not possible!

## 7.8 Bibliography

- Adhikari, B., Howes, T., Bhandiri, B.R., and Troung, V., 2004. Effect of addition of maltodextrin on drying kinetics and stickiness of sugar and acid-rich foods during convective drying: experiments and modeling. *Journal of Food Engineering*, 62, 53–68.
- Genskow, L. and Hecht, J. (eds.), 2004. Special issue on spray drying, *Drying Technology*, 22(6).
- Handscomb, C.S., Kraft, M., and Bayly, A.E., 2009. A new model for the drying of droplets containing suspended solids after shell formation. *Chemical Engineering Science*, 64, 628–637.
- Kapano and Kamiya, 1978, *ICLSA 78*, p. 133.
- Masters, K., 1985. *Spray Drying Handbook 4th Ed.*, Wiley, New York.
- Masters, K., 1991. *Spray Drying Handbook 5th Ed.*, Wiley, New York.
- Nandiyanto, A.B.D. and Okuyama, K., 2011. Progress in spray drying methods for production of controlled particles, *Advanced Powder Technology*, 22, 1–19.
- Nesic, S., and Vodnik, J., 1991. Kinetics of drop evaporation. *Chemical Engineering Science*, 46, 527–537.
- Sakai, T. and Hoshino, N., 1980. Production of uniform droplets by longitudinal vibration of audio frequency. *Journal of Chemical Engineering of Japan*, 13, 263–268.
- Tsotsas, E. and Mujumdar, A.S. (eds.), (2007). *Modern Spray Drying Technology volumes 1 and 2*, Wiley-VCH, Weinheim.
- Vehring, R., 2008. Pharmaceutical particle engineering via spray drying, *Pharmaceutical Research*, 25(5), 999–1022.
- Vehring, R., Foss, W.R. and Lechuga-Ballesteros, D., 2007. Particle formation in spray drying, *Aerosol Science*, 38, 728–746.

## 7.9 Problems

- 7.1. Consider the shower head and rotating bucket nozzles in Example 7.1. In each case, what is the optimum frequency to vibrate the nozzle to avoid satellite drops? Repeat Example 7.1 if the fluid has a viscosity of 0.1 Pa s and a surface tension of 45 mPa s.
- 7.2. Atomization from a rotating plate is more complex than break up of a single jet. Nevertheless, break up of a sheet of liquid or a ligament via instabilities is a similar mechanism to that described in Sections 7.3.1 and 7.3.2. Consider the empirical correlation in Equation 7.10. Are the effects of the parameters consistent with those expected from the theory of the break up of a single jet? Consider each parameter in turn and be as quantitative as possible.
- 7.3. Consider drops of molten urea falling under gravity. Calculate the Biot number for drops of size 0.1, 1, and 10 mm. For which drops does the assumption that the drop temperature is uniform hold? Data:  $k_{s,urea} = 0.0265 \text{ W m}^{-1} \text{ K}^{-1}$ ;  $\rho_{urea,l} = 1,220 \text{ kg m}^{-3}$
- 7.4. A 1 mm-diameter urea melt drop at its solidification temperature (133°C) falls under gravity. How long does it take to solidify and subcool to 120°C if the air temperature is 55°C?

7.5. In Example 7.2, for the constant rate drying period calculations we assume:

- the heat transfer coefficient is that of a stagnant film; and
- the drop temperature is uniform.

Confirm that these assumptions are reasonable.

7.6. In a single-drop drying experiment, the initial rate of mass loss from a 300 μm water drop is  $2.5 \times 10^{-11}$  kg s<sup>-1</sup>. The air temperature is 80°C. What is the drop temperature and vapor composition at the drop surface?

7.7. Skim milk is approximately 9% total solids by mass (half of the solids is anhydrous lactose and about 8% is protein). A skin begins to form (denoting the end of the constant rate drying period) when the solids content of the drop is 30% by mass. A CFD simulation of a skim milk spray drier predicts the drop residence time to be 15 s and the LMTD to be 70°C. What is the largest drop size that can be dried to 4% moisture on a dry basis assuming Equation 7.33 can be used for the falling rate drying period?

$$\rho_l = 1,000 \text{ kg m}^{-3}; \lambda_l = 2,260 \text{ kJ kg}^{-1}; k_g = 3 \times 10^{-5} \text{ kW m}^{-1}\text{K}^{-1}; X_e = 0.01$$

7.8. Consider Example 7.3. How do you expect the particle structure to change if:

- a. The initial moisture content is 2% by mass.
- b. The particle radius is 5 μm.
- c. The particle radius is 60 μm.

Which particle is most likely to shatter from pressure build up during drying if the gas temperature exceeds 80°C?

7.9. 50 μm drops of different solutions are dried in a low-temperature environment  $T_g = 50^\circ\text{C}$ ;  $T_{wb} = 20^\circ\text{C}$ . Do you expect solid or hollow particles to form for the following solutes?

- a. trehalose: as calculated with  $D_l = 5 \times 10^{-10} \text{ m}^2 \text{ s}^{-1}$
- b. alginate: as calculated with  $D_l = 2 \times 10^{-11} \text{ m}^2 \text{ s}^{-1}$

The protein has an amorphous solid density of 1,400 kg m<sup>-3</sup>. If the initial protein concentration is 3 wt%, at what drop size do you expect a shell to begin to form?

7.10. I want to design a spray-cooling tower to produce 1.3 mm-diameter urea prills from a urea melt. The mass flux of urea is 0.3 kg m<sup>-2</sup> s<sup>-1</sup>. To avoid carry over of fine dust from satellite drops, the superficial air flow rate is limited to 2 m s<sup>-1</sup>. Assume the melt enters the tower at its solidification temperature (133°C) and should leave as subcooled particles at 115°C. The drops are solidified using a countercurrent airflow. The air inlet temperature is 20°C.

- a. What is the heat transfer rate to the air?
- b. How tall must the tower be?
- c. What is a suitable orifice diameter to produce prills of this size?

Physical property data for urea:

$$\rho_s = 1,335 \text{ kg m}^{-3}; \rho_l = 1,226 \text{ kg m}^{-3}; \lambda_l = 230 \text{ kJ kg}^{-1}; C_p = 1.3 \text{ kJ kg}^{-1} \text{ K}^{-1}$$

7.11. 500 kg h<sup>-1</sup> of dried product is produced at 1% moisture from a countercurrent flow spray drier. Preheated air at 300°C and moisture content of 0.007 kg/(kg

dry air) is used in the drier and the exit air temperature is 120°C. The feed solution contains 45% solids and enters at 20°C. The dried product leaves the drier at 150°C. How much air is required? What is the humidity of the exit air? What is the evaporative efficiency of this drier?

- 7.12. Consider the nanoparticle suspension from Example 7.3. The real drop size distribution can be considered a normal distribution with parameters in Equation 2.24 of  $\mu = 100 \mu\text{m}$ ;  $\sigma = 20 \mu\text{m}$  truncated between 60  $\mu\text{m}$  and 140  $\mu\text{m}$ . What is the frequency size distribution of the product particles?
- 7.13. A rotary atomizer produces a 50 kg h<sup>-1</sup> spray of water drops whose distribution is uniform between 200 and 300  $\mu\text{m}$ ; i.e.,

$$f(x) = \begin{cases} 0.01 \mu\text{m}^{-1} & \text{for } 100 \mu\text{m} < x < 200 \mu\text{m} \\ 0 & \text{for } x < 100 \mu\text{m} \text{ and } x > 200 \mu\text{m} \end{cases}$$

Near the nozzle, the local conditions are  $T_g = 120^\circ\text{C}$ ;  $T_{wb} = 65^\circ\text{C}$ . Derive an expression for evaporation growth rate  $G_{i,1}$  as a function of drop size. What is the total evaporation rate (kg s<sup>-1</sup>) near the nozzle?

# 8 Wet Granulation

## 8.1 Consider a Case Study ...

*3P Consulting Inc.*

Memo to: Purdue Powder Processing Team  
Memo from: Jim Litster  
October 22, 2015

### **Developing New QbD Approaches for Wet Granulation**

In the pharmaceutical industry, active drug is granulated with various excipients prior to tableting. The standard flowsheet commonly used at *Carefree Drugs* is similar to that shown for the case study in Chapter 2. The wet granulation process occurs in a vertical shaft mixer granulator not unlike a domestic food processor. New formulations are first granulated at the 6 liter-scale granulator. The process is then scaled to 60 liter-pilot scale before implementation at production scale – 300 liters. It is a batch process.

There are many difficulties in scaling new formulations but still retaining the product attributes within specification, and the problem is thought to be in the granulation process. Engineers in the technical services section are not confident on the “best” way to scale up the formulation and process provided for them by formulation design scientists. Some formulations are “easy” to scale and others are “hard,” but the reasons for this are not clearly known. Currently, the formulation design scientists choose the formulation to ensure the chemical stability of the active ingredient rather than as an aid to processing. They would love to have a standard set of characterization measurements to make, and some clear physical specifications for their excipients.

The FDA has recently introduced a new approach to registering solid dosage form processes – Quality by Design (QbD). If a company has good quantitative understanding of their processes (a good engineering model), they can register a process with reduced levels of expensive and time-consuming experimental validation at different scales of operation. Process optimization at manufacturing scale without having to file a process variation will also be easier. Importantly, there should be fewer lost batches due to the granulation not meeting specifications.

A senior manager at *Carefree Drugs* has recruited us to introduce some science into the scale-up process. You are required to set some “fool-proof” design and scale procedures for new formulations. The process will start from the formulation design stage – i.e., while binders and excipients are being chosen and when small amounts of active ingredient are available. You have an ideal formulation to practice on. Wonderdrug® was pulled by *Carefree Drugs* at the last minute due to some nasty side effects in the final stage of clinical

trials. (What's wrong with an extra ear?) This formulation is available for you to trial your new engineering scale-up approach.

Your team needs to:

1. Specify a set of standard characterization tests for the formulation.
2. Specify a set of scale-up rules to maintain the properties of the granulated material constant.
3. Demonstrate the approach using Wonderdrug® formulation as a case study.

Our lab has access to extensive characterization equipment and tests can be done at your request. You can also get data from the laboratory data from the 10-liter Diosna granulator in our laboratory.

This project is of the highest priority. We would like you to report to the Carefree Drugs Technical Manager when he visits on December 4, giving your recommendations on the scaling rules and characterization tests with appropriate justification.

This case study is typical of the challenge in many industries (e.g., pharmaceuticals, agricultural chemicals, detergents, catalysts, foods) where a new formulation involving fine powders is being developed, but the product needs to be delivered as well-behaved granules that have better properties for their transportation, further processing, or end use.

So where do you start? Some questions to think about include the following.

- What properties of the granules are critical and what are the specifications for these properties? (Indeed, why do we need to wet granulate the powder before later compacting the granules into a tablet anyway?)
- What properties of the formulation are likely to affect the wet granulation process?
- What process parameters can we control in the Diosna granulator? Or a more basic question: What types of equipment can we use for wet granulation?

In small groups, discuss the case study using the questions above to help initiate discussion. What further information would you request? Does anyone in the group have any experience in wet granulation? Identify your knowledge gaps, and use the discussion to identify learning goals that you can later compare with the ones listed in Section 8.2 below.

## 8.2 Learning Goals

At the completion of this chapter, the student should be able to:

1. Describe the three classes of processes that control granule attributes.
2. Name and describe the different classes of granulation equipment, their applications, advantages, and disadvantages.
3. For a given set of conditions, calculate the dimensionless groups that control wetting and nucleation, and use the nucleation regime map to predict good conditions for granule nucleation.

4. For a given set of conditions, calculate the dimensionless groups that control growth and consolidation, and use the appropriate growth regime map to predict good conditions for granule growth.
5. Model a granulation process with a population balance model including rate expressions for the important rate processes. Use the model to predict exit size distribution from a granulator.
6. Recommend process conditions for large-scale granulation given data from a smaller scale using appropriate dimensional analysis and regime maps.
7. Solve simple problems related to particle design in granulation.
8. Critically analyze and interpret real granulation data sets from laboratory or plant trials using appropriate analysis tools.
9. Attack open-ended particle design or troubleshooting problems in granulation of similar nature to the introductory case study for the chapter.

### 8.3 Overview

Wet granulation is a process that produces free-flowing granules by the addition of a liquid to either a fine powder or seed granules. The desired size of the granular product can vary widely from 100  $\mu\text{m}$  to 10 mm depending on the application. The granular product can be the final product (e.g., detergent granules, fertilizers) or an intermediate product (e.g., pharmaceutical granules to be tableted, iron ore granules to be sintered). Wet granulation is ubiquitous in any industry that handles fine powders. Fine powders are dusty, difficult to handle, and create safety and health issues. The reasons for granulation are many and varied and depend on the application area. Table 8.1 summarizes some of the main reasons for wet granulation of fine powders for different types of products.

In wet granulation, the liquid provides the bonds to form a granule from the fine powder. All wet granulation processes require a way to add liquid, usually as a spray from a nozzle, and a way to keep the wetted powder (wet mass) moving to distribute the liquid and allow the granules to consolidate and grow. There is a vast array of equipment that is used for wet granulation. Most equipment can be divided into three broad categories based on how the powder is agitated (Figure 8.1):

1. Mixer granulators, in which a rotating impeller is used to agitate the powder.
2. Tumbling granulators, in which the equipment rotates to agitate the powder.
3. Fluidized granulators, which have no moving parts but a gas is used to fluidize and agitate the powder bed.

Granulation processes can be batch or continuous and range in production rate from a few kilograms per hour to 100 tonnes per hour.

Given the very wide range of materials used as feed, the wide range of desired granule properties, and the wide range of equipment used, our challenge is to come up with general approaches that are useful for quantitative design, scale-up, and troubleshooting. To do this, we will:



**Table 8.1** Reasons for wet granulation of powders

Reason to wet granulate	Typical applications
Improve powder flow properties	All applications
Eliminate health and safety issues due to dust	All applications
Prevent caking during storage	Fertilizers, detergents
Improve bulk density for packaging	Detergents, food products
Control dispersion and dissolution	Food products
Prevent segregation of powder blends	Pharmaceuticals, agricultural chemicals, ore smelting
Control porosity and surface/volume ratio	Catalyst and absorbents
Improve permeability for future processing	Ore smelting
Provide useful structural forms	Powder metallurgy
Improve product appearance	Food products, consumer goods

1. Identify the key rate processes by which we control the product granule attributes.
2. Identify the formulation properties and process parameters which dictate these processes and use them to establish key dimensionless groups and create regime maps.
3. Provide the population balance framework from which design models can be tailored to specific products and processes.
4. Review scaling rules for different types of equipment that build on this fundamental knowledge.

## 8.4 Rate Processes and Regime Maps

We wish to control the generation of the distribution of product granule properties, particularly the size distribution, density, and morphology of the granules. However, wet granulation is a complex process in which a number of phenomena occur simultaneously which together control these properties. We can divide these rate processes into three classes (Figure 8.2).

1. Nucleation and binder dispersion, in which drops of liquid interact with powder in the bed to form new “nuclei” granules.
2. Consolidation and growth, in which granules collide with each other and the process equipment to consolidate (densify). Some of these collisions may lead to granule coalescence. Granules may also grow by layering of powder onto existing granules.
3. Breakage and attrition, in which wet granules break to form smaller granules due to impact with impellers and choppers or high shear in the powder bed.

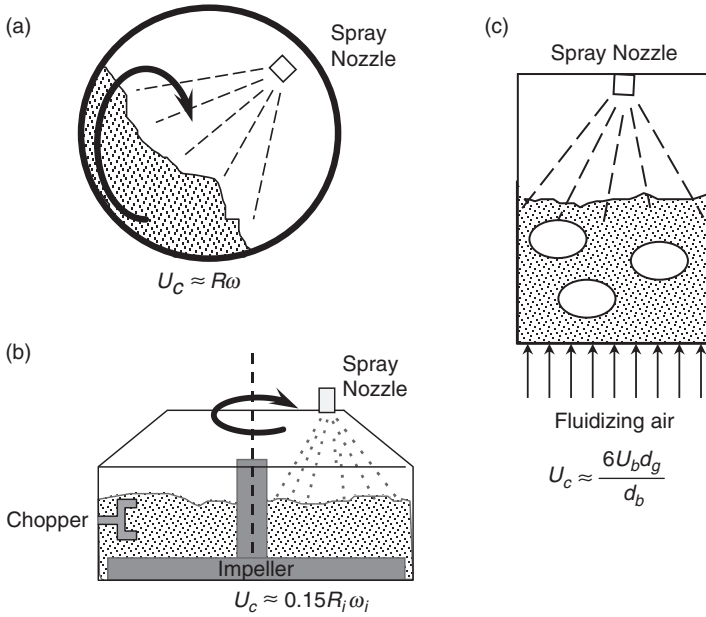


**Figure 8.1** Classes of equipment used for wet granulation. (a) Mixer granulators; (b) tumbling granulators; (c) fluidized granulators. (For definitions of symbols see Equations 8.20 to 8.22.)

The first step to predict granule properties is to understand each of these rate processes, and how formulation properties and equipment parameters influence the processes.

### 8.4.1 Nucleation

The first step in most wet granulation process is formation of new “nuclei” granules by the addition of liquid to the powder feed. If the liquid has a low to moderate viscosity, the liquid is atomized via a nozzle and contacts the surface of the powder bed in a spray zone. Figure 8.3 shows a schematic of the spray zone and the nucleation process that occurs in this zone. Drops are formed at the nozzle. When a drop impacts the powder bed, it wets into the bed via capillary action to form a nucleus granule. If the drop falls on top of another drop, they will coalesce to form a larger nucleus granule. In an extreme case, a wet cake will form across the width of the spray zone. If the drop does not quickly penetrate into the bed, it may roll and coalesce with other drops. In an extreme case, liquid may pool on the powder surface.

The nucleation processes that occur in the spray zone are extremely important to achieving good liquid distribution resulting in a well-behaved granulation with a relatively narrow granule size distribution. The best nucleation occurs when each drop forms a single nucleus granulation (*drop-controlled nucleation*). To achieve this we need:

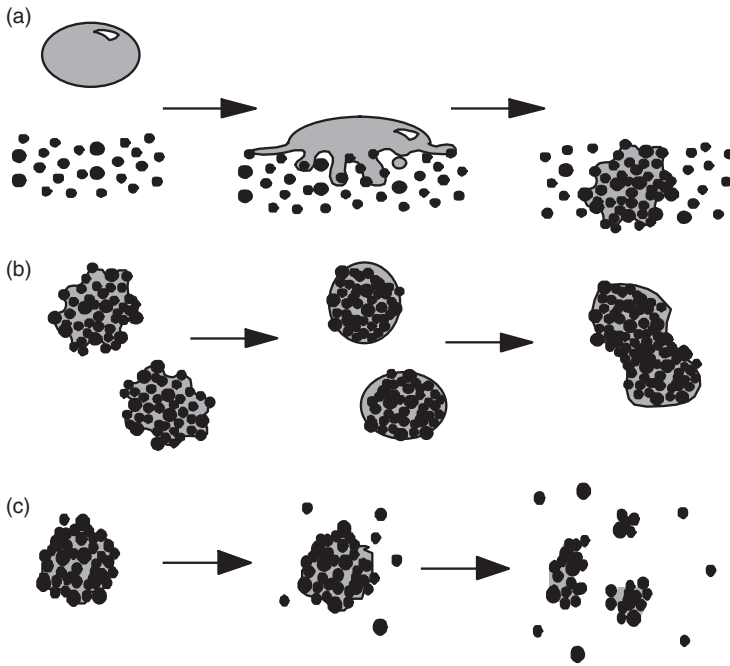


**Figure 8.2** Granulation rate processes. (a) Wetting and nucleation; (b) consolidation and growth; (c) breakage and attrition (Iveson *et al.*, 2001a)

1. fast drop penetration to prevent interaction with other slowly penetrating drops on the bed surface; and
2. minimal drop overall on the bed surface.

If these criteria are not achieved, large granules or clumps will form in the spray zone and mechanical action in the granulator is needed to break these lumps into smaller nuclei (*mechanical dispersion*).

Poor nucleation causes mal-distribution of liquid, formation of large lumps, a large amount of off-spec product, build up on granulator internals, segregation of active ingredients, and poor reproducibility of results. Drop-controlled nucleation is the best operating regime to avoid these problems. Let us now define as quantitatively as possible the requirements to achieve drop-controlled nucleation.

To understand drop penetration via capillary action, we need to first review the interaction between fluids and powders. When a drop is placed on a smooth, solid surface, there are three interfaces (liquid–solid, liquid–vapor, and solid–vapor). Each of these interfaces has a surface energy or tension associated with it:  $\gamma^{ls}$ ,  $\gamma^{lv}$ , and  $\gamma^{sv}$ . The balance of forces defines the contact angle of the drop with the surface  $\theta$  (Figure 8.4a) via the Young–Dupre equation:

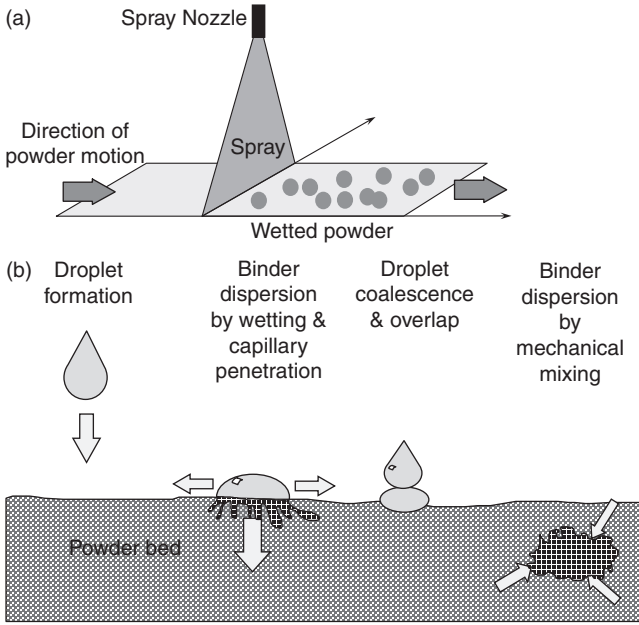


**Figure 8.3** The spray zone of a granulator. (a) An idealized view of the spray zone; (b) processes leading to nuclei formulation (Hapgood *et al.*, 2004).

$$\gamma^{sv} = \gamma^{ls} + \gamma^{lv} \cos \theta \tag{8.1}$$

Low values of  $\theta$  correspond to good wetting of the surface by the liquid. When  $\theta = 0$ , the liquid will form a film on the solid surface.

Imagine placing a cylindrical capillary in a pool of liquid (Figure 8.4b). If  $\theta < 90^\circ$ , the liquid will form a curved surface which is concave downwards. The tension on the curved surface causes a pressure difference across the surface and liquid will rise up the capillary until this pressure difference is balanced by gravity. This pressure difference is given by the Laplace–Young equation:

$$\Delta P = \frac{2\gamma^{lv} \cos \theta}{R} \tag{8.2}$$

where  $R$  is the capillary radius. This is the phenomenon observed when we place a straw into a glass of soft drink on a hot summer’s day. The same phenomenon causes drop penetration into a powder bed via capillary suction. The property grouping  $\gamma^{lv} \cos \theta$  appears in both Equation 8.1 and 8.2. We give this group its own name, the *adhesion tension*. Note that the liquid will only spontaneously penetrate into the powder bed if  $\theta < 90^\circ$ ; i.e.,  $\cos \theta > 0$ . If  $\cos \theta < 0$  – i.e.,  $\theta > 90^\circ$ , the drop will sit on the bed surface indefinitely. This is our first criterion for good drop penetration.

We also require the drop to penetrate into the powder bed quickly. Liquid will rise up the capillary in Figure 8.4b at a rate giving by the Washburn Equation:

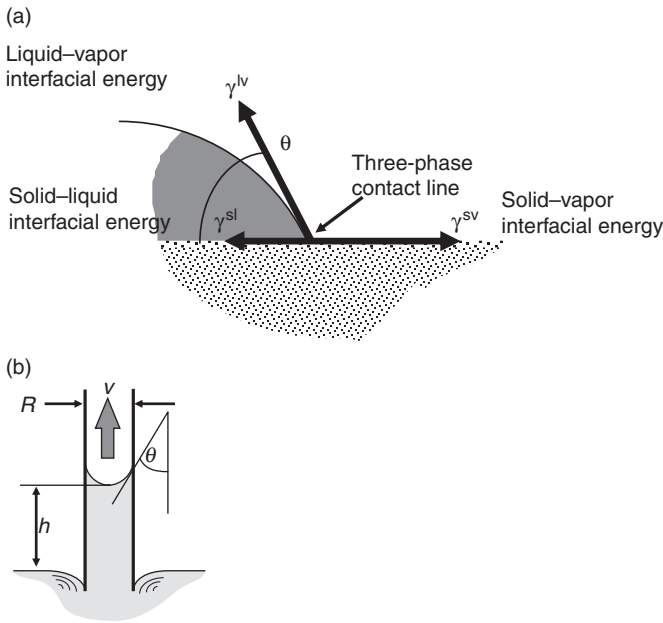


**Figure 8.4** The interaction between (a) a drop and a smooth solid surface, and (b) liquid in a solid capillary of radius  $R$  (Litster and Ennis, 2004).

$$h = \left[ \frac{R\gamma^{lv} \cos\theta}{2\mu} t \right]^{1/2} \quad 8.3$$

where  $h$  is the height in the capillary at time  $t$ . The Washburn equation is derived by considering the balance between the viscous resistance to flow and the driving force provided by capillary suction. The Washburn equation provides the basis for a method to measure contact angle of a powder. It also provides a way for us to calculate the time a drop will take to penetrate into a powder bed.

Consider a drop of volume  $V_d$  placed onto a powder bed where the effective capillary size is  $R_{eff}$  and the effective bed voidage is  $\epsilon_{eff}$ . The drop will cover a number of capillaries in the bed proportional to its projected area. Combining these geometric considerations with Equation 8.3, Hapgood *et al.* (2003) showed that the time for a drop to fully penetrate into the bed is:

$$t_p = 1.35 \frac{V_d^{2/3} \mu}{R_{eff}^2 \epsilon_{eff}^2 \gamma^{lv} \cos\theta} \quad 8.4$$

The expression for  $R_{eff}$  is that used in the Kozeny–Carmen equation for flow of a fluid through a packed bed:

$$R_{eff} = \frac{\phi \bar{x}_{32} \epsilon_{eff}}{3(1 - \epsilon_{eff})} \quad 8.5$$

For fine powders, the bed voidage is not uniform but consists of small capillaries and large holes or macrovoids. Liquid will not be drawn to the macrovoids by capillary suction. Hapgood showed the effective voidage available for drop penetration could be estimated as:

$$\varepsilon_{eff} = \varepsilon_{tap} (1 - \varepsilon + \varepsilon_{tap}) \quad 8.6$$

where  $\varepsilon$  is the bed voidage in a loose state and  $\varepsilon_{tap}$  is the voidage that corresponds to the tapped bulk density. Note that Equations 8.4 to 8.6 capture the important formulation properties that effect drop penetration (powder size distribution and packing, liquid viscosity, and adhesion tension). Thus, drop penetration time is largely controlled by the formulation.

On the other hand, drop overlap in the spray zone is controlled by process parameters. Consider the idealized spray zone shown in Figure 8.3a. The rate of generation of project area of drops from the nozzle is:

$$\dot{A}_d = \frac{3Q_{sp}}{2d_d} \quad 8.7$$

where  $Q_{sp}$  is the volumetric spray rate and  $d_d$  is the specific surface area mean drop size. The rate at which powder surface area passes through the spray zone is:

$$\dot{A}_p = v_{sp} W_{sp} \quad 8.8$$

where  $v_{sp}$  is the powder surface velocity in the spray zone and  $W_{sp}$  is the width of the spray zone perpendicular to the direction of powder flow. We call the ratio of these two area fluxes the dimensionless spray flux:

$$\Psi = \frac{3Q_{sp}}{2v_{sp} W_{sp} d_d} \quad 8.9$$

This single dimensionless group tells us everything we need to know about the spray zone. When the spray flux is low, there is a lot of powder flowing through the spray zone when compared to the generation of drops and each drop is likely to find a free area of powder on which to land. If the spray flux is high, drops are likely to overlap. Figure 8.5 shows simulations of drop footprint patterns on the powder surface for an arrangement of spray flux. Watering the garden is a good analogy. If the hose gives a controlled spray and is moved quickly over the garden bed, individual drops can be identified on the soil. If the hose gives a solid stream and is pointed at a single patch of soil, a mud pie is the result. The fraction of the powder surface wet by drops  $f_{wet}$  and the fraction of nuclei  $f_n$  formed from  $n$  drops are (Hapgood *et al.*, 2004):

$$f_{wet} = 1 - \exp(-\Psi) \quad 8.10$$

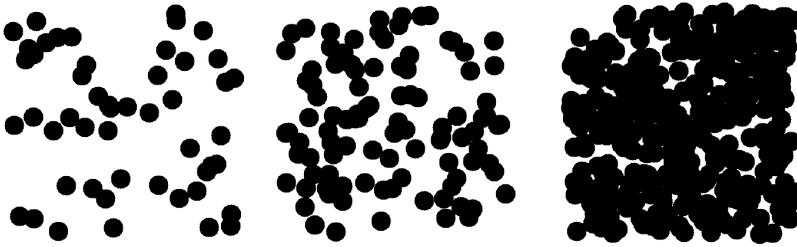


**Figure 8.5** Simulated drop patterns on a powder surface as a function of dimensionless spray flux  $\Psi$  (Hapgood *et al.*, 2004).

$$f_n = \exp(-4\Psi) \left[ \frac{(4\Psi)^{n-1}}{(n-1)!} \right] \quad 8.11$$

So for example, when  $\Psi = 0.1$ , 9.5% of the bed surface is wet, 67% of nuclei are formed from a single drop, and 94% of nuclei are formed from either one or two drops. When  $\Psi = 0.5$ , 39% of the bed surface is wet and only 13% of nuclei are formed from a single drop. At this point, we are close to the “mud pie” scenario. To get drop-controlled nucleation, low spray fluxes are required.

$\Psi = 0.3$	$\Psi = 0.6$	$\Psi = 2.4$
$f_{wet} = 0.26$	$f_{wet} = 0.45$	$f_{wet} = 0.91$
$f_1 = 0.35$	$f_1 = 0.1$	$f_1 = 0$

The operating regimes for nucleation can be presented in terms of a nucleation regime map where the two axes are the dimensionless drop penetration time (controlled by formulation properties) and the dimensionless spray flux (controlled by process parameters). This regime map is shown in Figure 8.6. There are three operating regimes.

1. Drop-controlled nucleation: requires both  $\tau_p$  and  $\Psi$  to be less than 0.1. There is a one to one correspondence between the drop size distribution and the nuclei size distribution. This is the most desirable regime for good nucleation.
2. Mechanical dispersion regime: either  $\tau_p$  or  $\Psi$  are greater than 1. In this case, the nuclei size and liquid distribution are independent of spray conditions. Shear or impact in the granulator controls the nuclei size distribution. Mechanical dispersion occurs in the impeller or chopper zone in a mixer granulator and is less effective than drop-controlled nucleation.
3. Intermediate regime: in this regime, small changes in process parameters or formulation properties will have a significant impact on the nuclei size and liquid distribution.

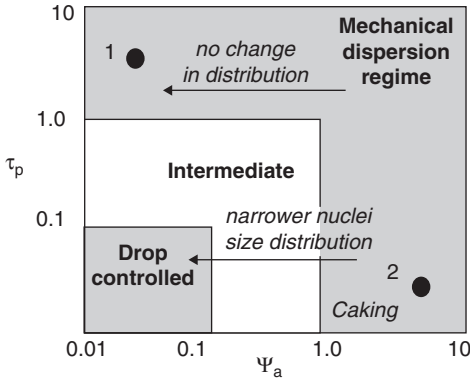


Figure 8.6 Nucleation regime map for wet granulation (Hapgood *et al.*, 2003).

The nucleation regime map is a useful tool for identifying potential problems, proposing potential solutions and developing appropriate scaling rules. As a thought exercise, consider operating points 1 and 2 as shown on the regime map in Figure 8.6. In each case, what changes to formulation properties or process parameters would you consider to bring the operation closer to drop-controlled nucleation? Why would reducing the spray rate be ineffective for improving operation if we currently operate at point 2?

**Example 8.1 Operating Conditions for Nucleation in a Vertical Axis Mixer Granulator** Some data for the granulation of a pharmaceutical formulation using water as the granulating liquid in a nominal 25 liter vertical axis, high-shear mixer granulator (0.4 m diameter, 6 kg powder batch, 300 rpm impeller speed) is given below. Estimate the penetration time and spray flux for the given system. What comments can you make about the nucleation regime in this case? We are considering replacing water with viscous HPC solution to given better granule dry strength. What effect will this have on the nucleation behavior?

Spray zone parameters:

$$v_{sp} = 0.82 \text{ m s}^{-1}; W_{sp} = 0.076 \text{ m}; Q_{sp} = 45 \text{ ml min}^{-1}; d_{d,w} = 100 \text{ }\mu\text{m}; d_{d,HPC} = 250 \text{ }\mu\text{m}$$

Liquid properties:

$$\mu_w = 10^{-3} \text{ Pa s}; \mu_{HPC} = 10^{-1} \text{ Pa s}; \theta_w = 50^\circ; \theta_{HPC} = 30^\circ;$$

$$\gamma_w^{lv} = 70 \text{ mN.m}^{-1}; \gamma_{HPC}^{lv} = 43 \text{ mN.m}^{-1}$$

Powder properties:

$$\phi_{x_{32}} = 17.9 \text{ }\mu\text{m}; \rho_p = 1540 \text{ kg.m}^{-3}; \rho_{ap} = 930 \text{ kg.m}^{-3}; \epsilon = 0.6$$



*Solution:*

Let us calculate  $t_p$  and  $\Psi$  for this system with water as the granulating fluid. From Equation 2.10:

$$\varepsilon_{tap} = 1 - \frac{\rho_{tap}}{\rho_p} = 1 - \frac{0.93}{1.54} = 0.4$$

Applying Equations 8.4 to 8.6:

$$\varepsilon_{eff} = \varepsilon_{tap} (1 - \varepsilon + \varepsilon_{tap}) = 0.4(1 - 0.6 + 0.4) = 0.315$$

$$R_{eff} = \frac{\varphi \bar{x}_{32} \varepsilon_{eff}}{3(1 - \varepsilon_{eff})} = \frac{17.9 * 10^{-6} \text{ m} * 0.315}{3(1 - 0.315)} = 2.7 * 10^{-6} \text{ m}$$

$$V_d = \frac{\pi d_d^3}{6} = \frac{\pi (10^{-4} \text{ m})^3}{6} = 5.2 * 10^{-13} \text{ m}^3$$

$$t_{p,w} = 1.35 \frac{V_d^{2/3} \mu}{R_{eff} \varepsilon_{eff}^2 \gamma^w \cos \theta} = 1.35 \frac{(5.2 * 10^{-13} \text{ m}^3)^{2/3} 10^{-3} \text{ Pa.s}}{2.7 * 10^{-6} \text{ m} * 0.315^2 * 70 \text{ mN.m}^{-1} * \cos 50^\circ}$$

$$= 7 * 10^{-4} \text{ s}$$

Applying Equation 8.9:

$$Q_{sp} = 45 \text{ ml.min}^{-1} \left[ \frac{1 \text{ m}^3}{10^6 \text{ ml}} \right] \left[ \frac{1 \text{ min}}{60 \text{ s}} \right] = 7.5 * 10^{-7} \text{ m}^3 \text{ s}^{-1}$$

$$\Psi_w = \frac{3Q_{sp}}{2v_{sp} W_{sp} d_d} = \frac{3 * 7.5 * 10^{-7} \text{ m}^3 \text{ s}^{-1}}{2 * 0.82 \text{ m.s}^{-1} * 0.076 \text{ m} * 10^{-4} \text{ m}} = 0.18$$

On the nucleation regime map (Figure 8.6), this places the operating point very close to the drop-controlled regime. Good liquid distribution is expected with 50% of granules formed from a single drop (Equation 8.11). However, any increase in  $\Psi$  will cause poorer liquid distribution.

A similar analysis for HPC solution as the granulating liquid gives:

$$t_{p,HPC} = 0.55 \text{ s}$$

$$\Psi_{HPC} = 0.072$$

As the HPC is more viscous, the mean drop size is larger than for water, slightly reducing the dimensionless spray flux. However, the high viscosity and larger drop size result in a much larger drop penetration time. Thus, the operating point is now well outside the drop penetration regime. We expect broader granule size distributions with the possibility of liquid pooling occurring in the granulator. Operating with a grade of HPC which gives less-viscous solutions will move the operating point towards the drop-controlled regime.

#### 8.4.2 Wet Granule Strength and Consolidation

Assuming the liquid is well distributed among granules within the granulator, we now need to determine how granules will densify (consolidate) and grow as a result of collisions with other granules, with impellers and choppers, and with the vessel walls.

The amount of deformation in these collisions controls the rate of consolidation and has a big effect of coalescence. Therefore, the *dynamic* strength of the granules during the collisions is an important property. Granules are a complex three-phase matrix with very complex mechanical properties. Consider a granule as an ideal elastic–plastic material with a strain rate-dependent yield stress  $Y$  ( $\text{Nm}^{-2}$ ) (Figure 8.7). If the yield stress is exceeded during a collision, the granule will deform until the collision energy is absorbed. Therefore, the ratio of the specific collision energy to the yield stress is an important dimensionless group, the Stokes Deformation number:

$$St_{def} = \frac{\rho_g U_c^2}{2Y} \quad 8.12$$

where  $U_c$  is the typical collision velocity of granules in the granulator.

The dynamic yield stress of a granule can be measured by unconfined compression of a pellet of the formulation with closely controlled porosity and liquid content (Figure 8.8a) (Iveson *et al.*, 2002). Capillary force within liquid bridges in the granule, viscous dissipation within the liquid bridges, and friction between particles all contribute to granule strength. In general, we can write:

$$Str^* = f(Ca, \varepsilon_g, \phi, S) \quad 8.13$$

Here,  $Ca$  is the capillary number which represents the ratio of viscous dissipation to capillary force in the granule:

$$Ca = \frac{\mu U_c}{\gamma^v \cos \theta} \frac{d_p}{d_g} \quad 8.14$$

and  $Str^*$  is the dimensionless strength which is the ratio of granule strength to the strength of a single liquid bridge within the granule:

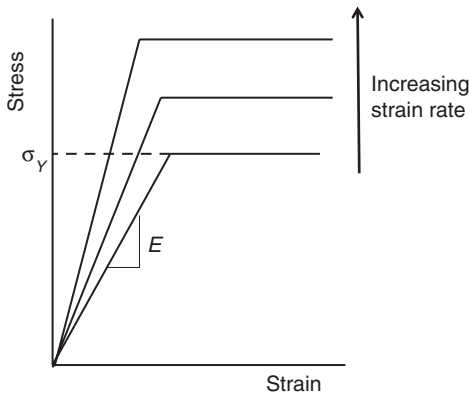


**Figure 8.7** Mechanical properties of a granule modeled as an elastic–plastic material.

$$Str^* = \frac{Yd_p}{\gamma^v \cos \theta} \quad 8.15$$

and  $S$  is the granule liquid content represented as the fractional liquid saturation of the granule pores:

$$S = \frac{(L/S) \rho_p (1 - \varepsilon_g)}{\rho_l \varepsilon_g} \quad 8.16$$

where  $L/S$  is the liquid to solid ratio in the granule (kg/kg).

The relationship in Equation 8.13 is complex. One empirical model for granule strength based on Equation 8.13 is (Smith, 2008):

$$Str^* = (7.0 + 221Ca^{0.58}) AR^{-4.3} \quad 8.17$$

where  $AR$  is the primary particle aspect ratio. While such empirical correlations should be used with caution, Figure 8.8b shows the granule strength of many different formulations that follow this trend. We can make several important observations.

1. At low  $Ca$ , the granule strength is independent of strain rate (collision velocity) and we can neglect the viscous contribution to granule strength.
2. For  $Ca > 10^{-4}$ , the granule strength is a strong function of strain rate and can be up to 50 times higher than the static strength. In this region, granule strength is a strong function of liquid viscosity.
3. The granule strength always increases as primary particle size decreases.
4. The granule strength is a very strong function of primary particle shape.
5. The granule strength is a strong function of granule porosity. We often evaluate the granule strength at the expected minimum granule porosity  $\varepsilon_{min}$ .

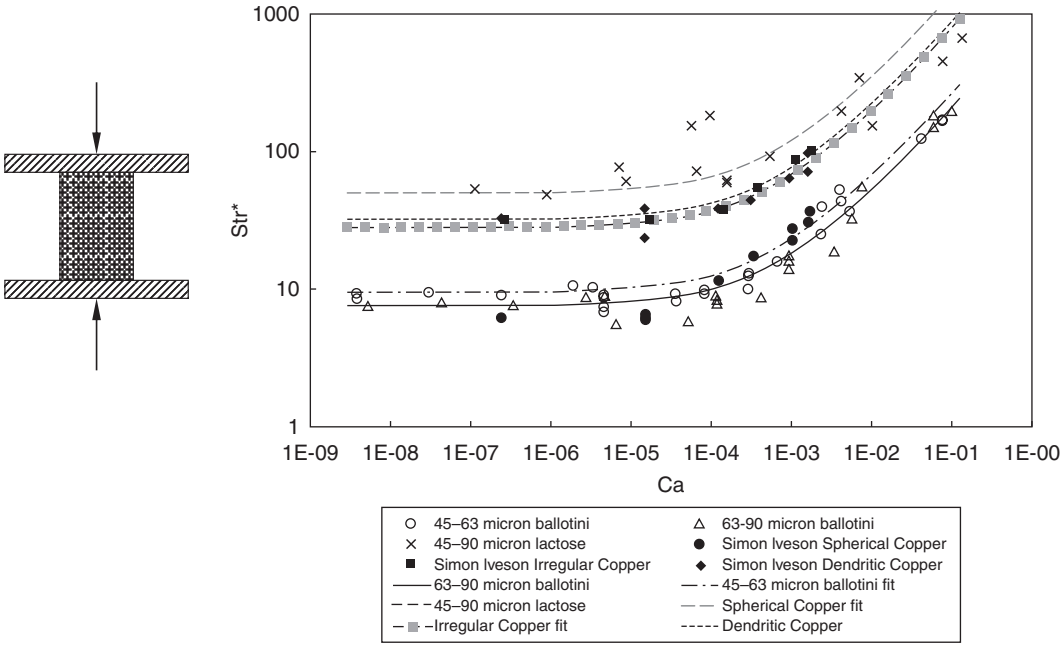


**Figure 8.8** Dynamic yield stress of granules. (a) Measurement using unconfined uniaxial compression; (b) correlation of  $Str^*$  with  $Ca$  and other granule properties (Smith, 2008).

In a batch granulation, granules will consolidate towards some stable minimum porosity over time (Figure 8.9). We can represent consolidation as a first-order process:

$$\frac{d\varepsilon}{dt} = -k_c (\varepsilon - \varepsilon_{min}) \tag{8.18}$$

Here, the consolidation rate constant  $k_c$  ( $s^{-1}$ ) is a function of  $St_{def}$  (Equation 8.12):

$$k_c = k_{c0} \exp(aSt_{def}) \tag{8.19}$$

where  $k_{c0}$  is the pre-exponential factor and  $a$  is a constant. There is an analogy here to the variation of a chemical reaction rate constant with temperature. The granule yield stress is a mechanical “activation energy” for consolidation to occur while increasing the energy in the collision is analogous to increasing temperature.

This analysis begs the question: “What is the correct choice of collision velocity?” In all granulators, there will be a range of collision velocities, but in the absence of any better information, good choices for this sort of lumped parameter approach are (Figure 8.1):

$$1. \text{ mixers: } U_c = 0.15R_i\omega_i \tag{8.20}$$

where  $R_i$  and  $\omega_i$  are the impeller radius (m) and angular velocity (rads/s), respectively;

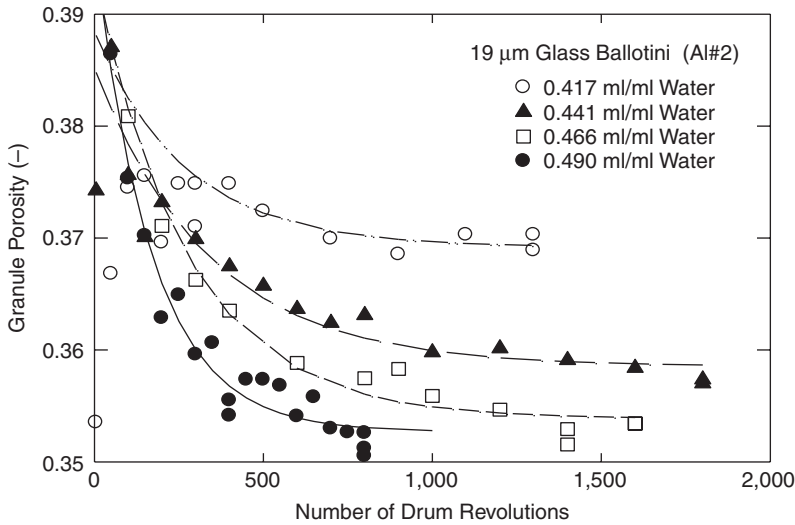


**Figure 8.9** Typical consolidation behavior of granules (Iveson *et al.*, 1996).

2. tumbling granulators:  $U_c = R\omega$  8.21

where  $R$  and  $\omega$  are the drum or disc radius (m) and angular velocity (rads/s), respectively; and

3. fluidized granulators:  $U_c = \frac{6U_b d_g}{d_b}$  8.22

where  $d_b$  and  $U_b$  are the size (m) and velocity ( $\text{ms}^{-1}$ ) of gas bubbles within the fluidized bed.

Given this analysis, individually reflect or discuss in a small group the formulation properties and process parameters you might change if you wished to increase the density of the product granules.

In a batch mixer or tumbling granulation, the time for consolidation is generally the total batch time that is of the order of minutes. However, in fluidized granulators there is simultaneous granulation and drying. The consolidation time corresponds to the time to dry a freshly wet granule in the fluid bed that is of the order of seconds. This is why fluidized granulators produce highly porous, fluffy granules. Anything that changes the drying time will therefore affect the granule density. Operating parameters that effect drying time include bed temperature, spray rate, and drop size from the spray.

**Example 8.2 Granule Consolidation Kinetics** During high-shear granulation of a cohesive material, the consolidation rate constant is measured to be  $0.0035 \text{ s}^{-1}$  and the minimum porosity  $\varepsilon_{min}$  is 0.25. If the nuclei porosity is 0.57, what is the required batch time to densify the granules to  $1.05\varepsilon_{min}$ ?

A system with similar granulation kinetics is granulated in a fluidized bed. The drying time for a newly wet granule is estimated to be 10 s. What is the product granule porosity?

*Solution:*

Beginning with Equation 8.18:

$$\begin{aligned} \frac{d\varepsilon}{dt} &= -k_c (\varepsilon - \varepsilon_{min}) \\ \Rightarrow \frac{d\varepsilon}{(\varepsilon - \varepsilon_{min})} &= -k_c dt \\ \Rightarrow \ln(\varepsilon - \varepsilon_{min}) \Big|_{\varepsilon_0}^{1.05\varepsilon_{min}} &= -kt \\ \Rightarrow t &= -\frac{\ln\left[\frac{0.05\varepsilon_{min}}{\varepsilon_{nuc} - \varepsilon_{min}}\right]}{k} = -\frac{\ln\left[\frac{0.05*0.25}{0.57 - 0.25}\right]}{0.0035\text{s}^{-1}} = 926\text{s} \end{aligned}$$

Over 15 min granulation time is needed to reach the desired granule porosity.

For the fluid bed granulator, no matter how long the batch time, the granules only have the drying time in which to consolidate:

$$\begin{aligned} \Rightarrow \ln(\varepsilon - \varepsilon_{min}) \Big|_{\varepsilon_0}^{\varepsilon} &= -kt_{dry} \\ \Rightarrow kt_{dry} &= -\ln\left[\frac{\varepsilon - \varepsilon_{min}}{\varepsilon_{nuc} - \varepsilon_{min}}\right] \\ \Rightarrow \frac{\varepsilon - \varepsilon_{min}}{\varepsilon_{nuc} - \varepsilon_{min}} &= \exp(-kt_{dry}) \\ \Rightarrow \frac{\varepsilon - 0.25}{0.57 - 0.25} &= \exp(-0.0035\text{s}^{-1} * 10\text{s}) \\ \Rightarrow \varepsilon &= 0.56 \end{aligned}$$

Within the fluid bed granulator, consolidation is negligible with the granule porosity nearly equal to that of the nuclei.

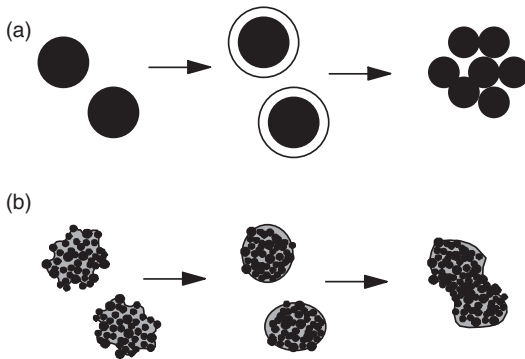


**Figure 8.10** Two different models for considering granule growth. (a) Large particles with small drops – relatively elastic particles with a sticky liquid layer collide and possibly coalesce. (b) Fine powder with large drops – surface-dry nuclei deform on collision and liquid must be squeezed to the surface for coalescence to occur.

### 8.4.3 Growth by Coalescence or Powder Layering

When two granules collide within the granulator, they may coalesce or rebound. There are two scenarios to consider depending on the way liquid is distributed in the granulator (Figure 8.10).

If the drop size is small compared to the size of primary particle traversing the spray zone, each particle will attract multiple drops to form a layer around the particle. These surface-wet granules will coalesce if viscous dissipation in the liquid layer surrounding the granule is sufficient to absorb the kinetic energy of the collision (Figure 8.10a). This scenario is common for fluidized granulators. If the drop size is large compared to the primary particle size, nuclei granules form in the spray zone (Section 8.4.1). These nuclei are deformable but surface-dry because of capillary action. If granules deform or consolidate sufficiently to make the granules surface-wet, coalescence can occur (Figure 8.10b). This scenario is common in mixer granulators. We have different models for these two different scenarios.

#### Small Drops and Large Particles

To answer the question “Will collision lead to coalescence?” we need to establish if viscous dissipation in the liquid surface layer is sufficient to reduce the relative velocity of the granules to zero. This is very similar to the lubrication problem in fluid mechanics. Ennis *et al.* (1991) defined the follow coalescence/rebound criterion:

$$St_v < St^* \text{ coalescence}$$

$$St_v > St^* \text{ rebound} \quad 8.23$$

where  $St_v$  is the viscous Stokes number defined as:

$$St_v = \frac{4\rho_g U_c d_g}{9\mu} \quad 8.24$$

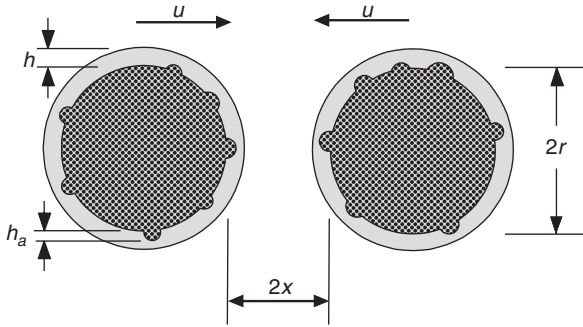


**Figure 8.11** Schematic of the collision between two surface-wet, rough particles for the Ennis and Tardos collision model (Ennis *et al.*, 1991).

and  $St^*$  is the critical Stokes number:

$$St^* = \left[ 1 + \frac{1}{e_r} \right] \ln \left( \frac{h_l}{h_a} \right) \tag{8.25}$$

The collision is shown schematically in Figure 8.11. Here,  $h_l$  is the thickness of the liquid film on the granule surface,  $h_a$  is the height of the surface roughness (asperities), and  $e_r$  is the coefficient of restitution of the dry granule.

$St_v$  is the ratio of viscous dissipation of energy as the liquid film is squeezed during collision to the initial kinetic energy of the collision. It is relatively easy to calculate and can vary over several orders of magnitude for different formulations.  $St^*$  is more difficult to calculate, but will not vary greatly and is typically between 2 and 8. Not all collisions in the granulator have the same energy. We can therefore divide the growth behavior into three regimes:

1. *The non-inertial regime*  $St_v \ll St^*$ : All collisions between wet granules will lead to coalescence and the rate of growth will be high.
2. *The inertial regime*  $St_v \approx St^*$ : Some collisions will lead to coalescence. The rate of granule growth will be moderate and sensitive to formulation or process parameters that change  $St_v$ .
3. *The layering regime*  $St_v \gg St^*$ : No collisions lead to coalescence. Granules grow very slowly by layering (coating) only.

This model is particularly useful to analyzing fluidized granulators where dried particles or granules are re-wet as they pass through the spray zone. Fluidized beds are used to produce fluffy agglomerates by operating in the non-inertial regime (instant foods, pharmaceutical granules) or to produce round, dense granules in the layering regime (fertilizers, explosives, particle coating). We can use Equations 8.23 to 8.25 to predict which type of granule will be produced. Note that  $St_v$  increases as the particle size increases, so that if we start in the non-inertial regime, the granules will



eventually grow to some maximum size when  $St_v \approx St^*$ , at which time the granule growth rate will slow dramatically.

**Example 8.3 Analyzing Granule Growth Behavior in a Fluidized Bed** I would like to use my fluid bed granulator to make coated microspheres. In this process, I want to spray a polymer solution onto the outside of the spheres from a single-spray nozzle in the fluidized bed. The solvent evaporates to leave a uniform polymer coating on each sphere. The following data are available:

$d_p = 100 \mu\text{m}$	$\mu = 1 \text{ Pa s}$	$\rho_p = 1,500 \text{ kg m}^{-3}$
$d_b = 0.03 \text{ m}$	$U_b = 0.08 \text{ m s}^{-1}$	$St^* = 4$

Are single-coated particles possible? Justify your answer quantitatively using an appropriate regime analysis.

*Solution:*

For fluid bed granulation, the Ennis regime analysis based on  $St_v$  is appropriate. First, we estimate the average collision velocity (Equation 8.22):

$$U_c = \frac{6U_b d_g}{d_b} = \frac{6 \times 0.08 \text{ m.s}^{-1} \times 10^{-4} \text{ m}}{0.03 \text{ m}} = 1.6 \times 10^{-3} \text{ m.s}^{-1}$$

The viscous Stokes number is (Equation 8.24):

$$St_v = \frac{4\rho_g U_c d_g}{9\mu} = \frac{4 \times 1500 \text{ kg.m}^{-3} \times 1.6 \times 10^{-3} \text{ m.s}^{-1} \times 10^{-4} \text{ m}}{9 \times 1 \text{ Pa.s}} = 10^{-4}$$

$$St_v \ll St^*$$

There is a four-order of magnitude difference between the viscous and critical Stokes number, so coalescence will always occur between wet particles. Individually coated microspheres are definitely not possible.

How could we achieve coated microspheres? Simply changing the fluidization velocity will make only small differences to  $St_v$  and mainly act to increase attrition and elutriation of fines. Changing the spray rate will change  $St^*$  by changing the liquid layer thickness, but again only by a small amount. Spout fluid beds, such as the Wurster coater, apply the coating layer at high velocity in a central spout. This will increase the collision velocity by about two orders of magnitude, not enough to be in the coating regime still, but getting closer. If, in addition, the formulation could be changed so that the liquid coating viscosity was nearer to that of water, we are getting even closer to the target regime. In practice, Wurster coaters are used successfully in coating applications for particles as small as 500  $\mu\text{m}$  diameter with low-viscosity coating liquids.

### Large Drops and Small Particles

This is the common scenario for the granulation of fine powders in tumbling and mixer granulators. Nuclei granules are formed as described in Section 8.4.1. Generally, the nuclei are surface-dry due to capillary suction. However, we need liquid to be available at the surface of the granule for coalescence to occur. If the granule is very deformable, liquid can be squeezed to the contact point during collision and coalescence takes place. Granules generally reach their minimum porosity very quickly and granule growth happens at a steady pace. This type of behavior is termed *steady growth* (Figure 8.12a).

If the granules are strong (low deformation in collision), then initially collisions will not lead to coalescence as they are surface-dry. However, as granules slowly consolidate, liquid is eventually squeezed to the granule surface and coalescence may take place. We term this behavior *induction growth* because there is a period of time where consolidation and powder layering occurs without coalescence (Figure 8.12b). After a certain time (the induction time), denser surface-wet granules begin to coalesce and the granule growth rate suddenly becomes rapid.

The two different growth behaviors present different challenges for controlling granule attributes. For *steady growth*:

- Granules quickly reach a minimum porosity.
- There is lots of deformation on collision.
- The granule growth rate is very sensitive to liquid content and changes to the granule collision velocity.

For *induction growth*:

- Consolidation kinetics are important and granule density will vary with collision velocity.
- There is little deformation on collision.
- There is the potential to control granule growth by a combination of nucleation and fines layering.

It is important to be able to predict which type of behavior will be observed. As the difference between steady growth and induction behavior depends on granule deformation, the criterion for distinguishing between the two types of behavior is given by the Stokes deformation number:

$$St_{def} < 2 \times 10^{-3} \quad \text{Induction growth}$$

$$St_{def} > 2 \times 10^{-3} \quad \text{Steady growth} \quad 8.26$$

When the granules are very weak ( $St_{def} > 0.2$ ), they fall apart due to collisions and no granule growth occurs. This is the *crumb* regime.

However, no coalescence can be achieved in either growth regime unless the granules are surface-wet. When the average liquid content is low, we have some partially

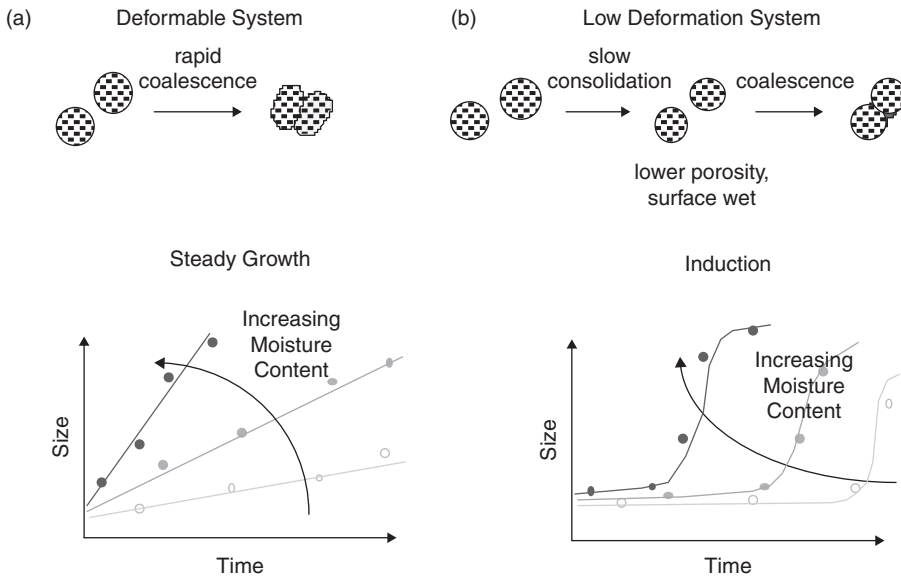


**Figure 8.12** Contrasting growth behavior for deformable granules. (a) Steady growth, (b) induction growth.

saturated nuclei granules and a lot of unwet powder. Even if the nuclei consolidate, the unwet powder layers to the surface of the granule to keep it surface-dry. We call this the *nucleation-only* regime. Only when many granules are surface-wet will granule coalescence occur. Thus, granule coalescence requires the liquid saturation of the granules  $S$  to exceed some critical value of the order 0.7–0.85. When  $S > 1$ , granule growth may become very rapid, leading to the formation of a single “dough ball” or even a slurry. Thus, granule growth behavior is very sensitive to liquid content in the range  $0.7 < S < 1.0$  and will be a strongly non-linear function of liquid content in this range.

All of these regimes can be summarized in the Iveson growth regime map (Figure 8.13). The operating regime is defined by the two dimensionless groups,  $St_{def}$  and  $S$ . Typically, a batch granulation begins in the nucleation-only regime and finishes in either the steady growth, or induction growth regime. The regime map gives a powerful tool for understanding complex granule growth behavior. It is useful to consider how changing process parameters or formulation properties will change the position of the operating point on the regime map. For example, doubling the impeller speed on a mixer granulator will increase the Stokes deformation number because the collision velocity is increased (Equations 8.12 and 8.20), although the granule strength may also increase as the capillary number for the collision increases (Equation 8.17). How do you expect the operating point to change if the liquid viscosity is substantially increased?

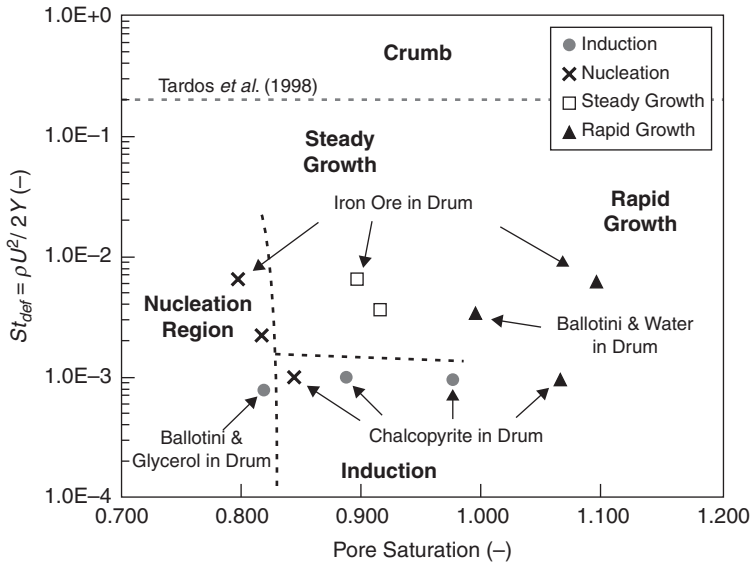


**Figure 8.13** The Iveson growth regime map for deformable granules with example data for tumbling granulators (Iveson *et al.*, 2001b).

**Example 8.4 Growth Regimes in a Drum Granulator** I am performing granulation of a fine powder in a drum granulator and have estimated the values of the key dimensionless groups to be  $St_{def} = 10^{-3}$  and  $S = 0.95$ .

- (a) What type of growth behaviour is expected?
- (b) How will  $St_{def}$  change if the liquid binder viscosity is increased by a factor of 10?
- (c) Will it be easy to scale up this process keeping granule density constant?

*Solution:*

- (a) Reading from the Iveson regime map (Figure 8.11), we expect to see induction growth behavior; i.e., initially, the granule size distribution will not change markedly while granule densification is occurring. Once the granules become surface-wet, rapid coalescence will occur.
- (b) From Equation 8.12, we know that:

$$St_{def} = \frac{\rho_g U_c^2}{2Y}$$

Thus  $St_{def}$  is not a direct function of viscosity. However, the yield stress  $Y$  may be a function of  $\mu$  from Equation 8.17 and Figure 8.8. Without more information on the formulation properties and process conditions, we cannot quantify the effect, but we can look at the limiting cases. For  $Ca < 10^{-5}$ ,  $Str \neq f(Ca)$ . Therefore, the yield stress  $Y$  will not vary with viscosity and  $St_{def}$  will be unchanged. For  $Ca > 10^{-5}$ :

$$Str \propto Ca^{0.58}$$

$$\Rightarrow Y \propto \mu^{0.58}$$

$$\Rightarrow Y_2 = 10^{0.58} Y_1 = 3.8 Y_1$$

$$\Rightarrow St_{def,2} = \frac{St_{def,1}}{3.8} = \frac{10^{-3}}{3.8} = 2.63 \times 10^{-4}$$

(c) No, it will not be easy. In the induction growth regime, the granule density will be controlled by consolidation kinetics. These kinetics may change with scale, so the granule density may vary if the batch time is held constant.

#### 8.4.4 Wet Granule Breakage

Within the granulator, in regions of high shear or high impact velocity, the wet granules may break. Breakage may occur near the impeller or chopper of a high-shear mixer granulator. We write the breakage criterion as:

$$St_{def,max} > St_{def}^* \quad 8.27$$

In the absence of any other information, we expect  $St_{def}^* \approx 0.2$ ; i.e., the criterion for the crumb region in Figure 8.13. Note that  $St_{def,max}$  refers to the maximum collision velocity, typically equal to the impeller or chopper tip speed. In mixer granulators, depending on equipment design:

$$St_{def,max} \sim 20 St_{def,av} \text{ to } 1,000 St_{def,av} \quad 8.28$$

This explains why granule coalescence, based on  $St_{def,av}$  and granule breakage, based on  $St_{def,max}$  can occur simultaneously in different regions of the same mixer granulator. Mixers therefore allow the options to use breakage for nucleation by mechanical dispersion, or to limit the maximum granule size. However, the balance will be difficult to predict without a detailed knowledge of the powder flow field and mixing patterns in the granulator.

Breakage and coalescence do not occur together in fluid bed granulators and tumbling granulators, where the difference between the average and maximum  $St_{def}$  is much smaller. Therefore, breakage can usually be neglected in these granulators.

Equation 8.27 should be used with caution. We know empirically that (a) large granules are more likely to break than small granules, and (b) the probability of breakage is a strong function of impeller and granulator geometry. Neither of these factors is directly accounted for in Equation 8.27.

The strength and resistance to attrition of the dried product granules is often a key quality attribute. Chapter 9 describes how to measure and predict the strength of dry product granules and compacts.

## 8.5 The Population Balance for Granulation

Wet granulation gives a population of product granules with a distribution of properties via a series of rate processes. Therefore, we should be able to track the evolution of the granule property distributions using the population balance expressions developed in Chapter 3. The processes we wish to describe are:

- drop-based nucleation of new granules;
- coating/layering of liquid and powder onto the outside of granules;
- consolidation of granules;
- coalescence of granules; and
- breakage of granules (including mechanical dispersion nucleation).

The population balance based on a well-mixed granulator can therefore be written based on Equation 3.3 as:

$$\frac{\partial Vn(v,t)}{\partial t} + \frac{\partial V[G_v - G_c]n(v,t)}{\partial v} = \dot{Q}_{in}n_{in}(v) - \dot{Q}_{ex}n_{ex}(v) + V[\dot{b}_{muc}(v) + \dot{b}_{coat}(v) - \dot{d}_{coal}(v) + \dot{b}_{br}(v) - \dot{d}_{br}(v)] \quad 8.29$$

The expressions for the birth and death terms for coalescence and breakage are given by Equations 3.28 and 3.29, and Equations 3.38 and 3.40, respectively.  $G_v$  and  $G_c$  are the rate of increase of granule volume due to layered growth, and the rate of decrease of granule volume due to consolidation, respectively. Equation 8.29 is written in terms of the granule volume  $v$  in order to simplify the birth and death terms for coalescence and breakage. The equation is written for the discrete granule phase. The liquid and fine powder feeds are treated as separate continuous phases. Powder and liquid are converted to the granule phase via a combination of nucleation of new granules and the layered growth of existing granules.

A single, well-mixed tank is often a poor representation of a granulator. To properly capture most of the physics of the system and the heterogeneous flows, we can consider a granulator consisting of three zones (see Figure 8.14):

1. a spray zone where liquid is added and some combination of nucleation and layered growth occurs;
2. a bed zone where consolidation, coalescence and layered growth occurs; and
3. an impeller zone where breakage occurs.

Often, the spray zone and impeller zone are small and can be considered to operate at steady state. If we apply Equation 8.29 to each zone we derive:

$$\frac{\partial V_s G_v n_s(v,t)}{\partial v} = \dot{Q}_{s-b} n_b(v) - \dot{Q}_{b-s} n_s(v) + V_s \dot{b}_{muc} \quad 8.30a$$

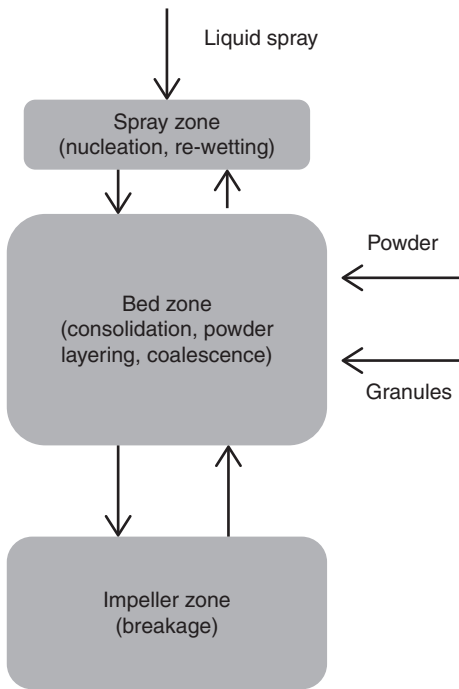


**Figure 8.14** Representation of a mixer granulator as three compartments for population balance modeling.

$$\frac{\partial V_b n_b(v, t)}{\partial t} + \frac{\partial V [G_v - G_c] n_b(v, t)}{\partial v} = \dot{Q}_{s-b} n_s(v) + \dot{Q}_{i-b} n_i(v) - [\dot{Q}_{b-s} + \dot{Q}_{b-i}] n_b(v) + V_b [\dot{b}_{coal}(v) - \dot{d}_{coal}(v)] \quad 8.30b$$

$$0 = \dot{Q}_{b-i} n_b(v) - \dot{Q}_{i-b} n_i(v) + V_i [\dot{b}_{br}(v) - \dot{d}_{br}(v)] \quad 8.30c$$

where the subscripts  $s$ ,  $i$ , and  $b$  refer to the spray zone, the impeller zone, and the bed zone, respectively. Other ways to break up the granulator into suitable compartments can be imagined depending on the type and geometry of the granulator – e.g., for a fluidized bed granulator we may use a spray zone and a bed zone but no impeller zone and assume granule breakage can be neglected.

A one-dimensionless population balance such as Equations 8.29 or 8.30 does not allow us to track changes in the distribution liquid content or density of the granule. These may be tracked by separate equations. For example, Equation 8.18 can be used to track the change in density of granules if we are happy to assume all granules have the same density. To allow for granules of the same size to have different liquid content or porosity, we need to write a population balance in two or three

dimensions  $[n(v_s, v_l) \text{ or } n(v_s, v_l, v_g)]$ . However, multidimensional population balances are beyond the scope of this text.

To effectively use the models described by Equations 8.29 and 8.30, we need good estimates of the rate constants for nucleation, layered growth, coalescence, and breakage. New granules are not nucleated as zero size as we often assume in crystallization and condensation processes (as in Equation 3.29). Instead, a nucleus granule is formed when a drop interacts with the powder bed to form a nucleus of finite size. In the drop-controlled nucleation regime, each drop is responsible for one nucleus:

$$V\dot{b}_{muc}(v) = (1 - \phi_g)\dot{Q}_{sp}n_d(v_d) \tag{8.31}$$

where  $v = \frac{v_d}{\varepsilon_{muc}S_{muc}}$  and  $\phi_g$  is the volume fraction of already formed granules entering the spray zone. If the spray flux  $\psi$  is high, some nuclei are formed from a combination of more than one drop and the nuclei size distribution will be broader and skewed. From a consideration of the properties of the Poisson distribution (Equations 8.10 and 8.11) we can give the mean nuclei size as:

$$\bar{v}_{10}(\psi) = 4\psi\bar{v}_{10}(\psi \rightarrow 0) \tag{8.32}$$

When the drop penetration time is high, nucleation by mechanical dispersion can be considered as a breakage process.

Layered growth can result from spraying of new liquid onto existing granules or large primary particles. If the liquid is a melt, solution, or suspension, then the solid phase is added as well and remains after solidification or drying. Alternatively, new wet granules may pick up a layer of fine powder in the granulator. For these processes, the growth rate is directly linked to the mass balance:

$$\dot{Q}_{feed} = \phi_g(1 - \varepsilon_g)\int_0^\infty VG_v(v)n(v)dv \tag{8.33}$$

Equation 8.33 can be used for either the whole granulator, or for the spray zone in a compartment model. For the layered growth law, in general, we may write:

$$G_v(v) = k_g v^n \tag{8.34}$$

In the absence of other information, we normally assume the growth of granule volume is proportional to the surface area of the granule ( $n = 2/3$ ). Combining Equations 8.33 and 8.34 and rearranging gives:

$$\dot{Q}_{feed} = \phi_g(1 - \varepsilon_g)Vk_g\alpha_v^{2/3}\int_0^\infty x^2n(x)dx = \phi_g(1 - \varepsilon_g)V\alpha_v^{2/3}k_g\mu_2' \tag{8.35}$$



Thus, Equation 8.35 is the same as the (linear) size-independent growth expression given in Equations 3.16 to 3.18 and is used extensively in crystallization (Chapter 4).

Coalescence is an important rate process in wet granulation. We need an appropriate expression for the coalescence kernel  $\beta$  for Equations 3.28 and 3.29. A wide variety of expressions for the coalescence kernel have been proposed (Abinger, 2008). Let us examine one expression based on the physics developed in Section 8.4.2. Starting from Equation 3.31, we can suggest a kernel of the form:

$$\beta(v, v'; p_i, e_i) = \eta(v, v'; p_i, e_i) \cdot \xi(v, v'; p_i, e_i) \quad 8.36$$

where  $\eta$  is the frequency of collision between granules of volumes  $v$  and  $v'$ , and  $\xi$  is the probability of a collision leading to coalescence. If the granules behave as described by the Ennis and Tardos model (Equations 8.23 to 8.25), then coalescence will be successful if  $St_v < St^*$ :

$$\xi = \begin{cases} 1 & \text{if } St_v < St^* \\ 0 & \text{if } St_v \geq St^* \end{cases} \quad 8.37$$

At the transition point between coalescence and rebound:

$$St^* = St_v = \frac{4\rho_g U_c d_g^*}{9\mu} \quad 8.38$$

Rearranging:

$$d_g^* = \frac{9\mu St^*}{4\rho_g U_c} \quad 8.39$$

Converting to granule volume:

$$w^* = \frac{\pi d_g^{*3}}{6} = \frac{\pi}{6} \left[ \frac{9\mu St^*}{4\rho_g U_c} \right]^3 \quad 8.40$$

Thus, Equation 8.37 becomes:

$$\xi = \begin{cases} 1 & \text{if } w < w^* \\ 0 & \text{if } w \geq w^* \end{cases} \quad 8.41$$

where:

$$w = \frac{v \cdot v'}{v + v'} \quad 8.42$$

Other similar kernels can be derived based on other models of the physics of granule collisions (e.g., Liu *et al.*, 2002).

We also need an expression for the collision frequency  $\eta$ . It is common to assume size-independent collision frequency:

$$\eta(v, v'; p_i, e_i) = \eta(p_i, e_i) \text{ only} \tag{8.43}$$

and then use  $\eta$  as a fitting parameter. If granules in the granulator are well separated, such as in a well-fluidized bed, the collision frequency can be modeled based on considering the granule movement and using the kinetic theory of granular flow. This leads to the equikinetic energy (EKE) kernel:

$$\eta = k_\eta \left( v^{1/3} + v'^{1/3} \right)^2 \left( \frac{1}{v} + \frac{1}{v'} \right)^{1/2} \tag{8.44}$$

In general, physically based kernels lead to complex expressions that require numerical solution of the population balance. However, sometimes a simplified approach may still be valuable. For example, if (1) conditions in the granulator are such that we can assume  $St_v \ll St^*$  for all collisions, and (2) we assume size-independent collision velocity, Equations 8.36, 8.37 and 8.43 give:

$$\beta = \eta(p_i, e_i) \text{ only} \tag{8.43}$$

This size-independent kernel is amenable to analytical solution of the population balance in some circumstances (see Section 3.6.2).

Expressions for the breakage selection function and fragment size distribution are similar to those used for crushing and grinding (see Chapter 5). We would expect the breakage selection function to increase with (1) increasing granule size, and (2) decreasing Stokes deformation number  $St_{def}$ .

**Example 8.5** Consider a well-mixed batch granulator. Initially, liquid is sprayed into the granulator to form nuclei granules. After the liquid spray is turned off, granules grow by agglomeration only (no layering, no further nucleation). Assume that the coalescence process is size-independent. Starting with the general moments form of the population balance, derive an expression which gives the total number density  $N_T$  and mean size of granules as a function of the nuclei granule size distribution and the wet massing time after the spray is stopped. State clearly all assumptions you make.

*Solution:*

For the special case of size-independent coalescence, we can use Equation 3.37 to describe the zeroth moments of birth and death terms for coalescence:

$$\dot{B}_{coal} = \frac{1}{2} \beta N_T^2; \dot{D}_{coal} = \beta N_T^2$$

Applying the zeroth moments form of Equation 8.29 without layering, nucleation or breakage gives:

$$\frac{dVN_T}{dt} = \frac{1}{2}V\beta N_T^2 - V\beta N_T^2 = -\frac{1}{2}V\beta N_T^2$$

Rearranging:

$$\frac{dN_T}{N_T^2} = -\frac{\beta}{2}dt$$

Taking  $t = 0$  when the spray is turned off and integrating:

$$\left[ -\frac{1}{N_T} \right]_{N_T(0)}^{N_T} = -\frac{\beta}{2}(t-0)$$

$$-\frac{1}{N_T} + \frac{1}{N_T(0)} = -\frac{\beta t}{2}$$

Rearranging:

$$N_T = \frac{N_T(0)}{1 + \frac{1}{2}\beta t N_T(0)}$$

In this process, only coalescence is occurring and the total volume of granules is preserved:

$$\frac{d\mu'_{1v}}{dt} = 0$$

Integrating:

$$\mu'_{1v} = V_T = V_T(0)$$

The change in mean granule volume with time is:

$$\bar{v}_{10} = \frac{\mu'_{1v}}{\mu'_0} = \frac{V_T}{N_T} = \bar{v}_{10}(0) \left[ 1 + \frac{1}{2}\beta t N_T(0) \right]$$

This analysis predicts that the mean granule volume increases linearly with time and has no upper limit. Granules will continue to grow until there is a single granule the size of the granulation equipment. Indeed, this is sometimes observed, particularly when the liquid to solid ratio is set too high (rapid growth in Figure 8.13)! From our definition of mean size, if the granules are considered spherical we can write:

$$\bar{v}_{10} = \frac{\pi \bar{x}_{3,0}^3}{6}$$

Therefore:

$$\bar{x}_{3,0} = \bar{x}_{3,0} \left[ 1 + \frac{1}{2} \beta t N_T(0) \right]^{1/3}$$

Example 3.2 in Chapter 3 is a good example for granulation with layered growth.

## 8.6 Equipment Design and Scaling Rules

It is not the aim of this book to give detailed qualitative descriptions of processing equipment (see the bibliography for this chapter for books which do this). However, the equipment used for wet granulation is so diverse it is important for the student to have some idea of the different types of equipment in order that the engineering science described in Sections 8.4 and 8.5 can be effectively applied.

Granulation equipment is often broken down into three broad categories by the way in which the powder is set in motion (Figure 8.1):

- tumbling granulators;
- mixer granulators; and
- fluidized granulators.

Let us briefly describe some key elements of the different types of granulator, their range of application, and engineering science-based scaling rules.

### 8.6.1 Tumbling Granulators

Tumbling granulators cover rotating drums and discs in which powder is set in motion by rotating the whole equipment. Tumbling granulators typically produce round, medium-density granules in the range 1–20 mm. They generally operate in continuous mode and very large throughputs are possible, up to 100 tonne h<sup>-1</sup>. For this reason, they are often used in the mineral industry and for commodity chemicals such as fertilizers.

Figure 8.15 shows a typical disc granulator. The disc rotates in a plane of angle  $\beta$  to the horizontal. As the disc rotates, granules rise up the disc by a combination of centripetal and frictional forces that are opposed by gravity. Small granules are drawn higher up the disc, creating segregation of the granules. This is used to obtain an inherent product classification as the granules discharge from the lower part of the disc where larger granules have preferentially collected. The location of the fresh powder feed and the liquid spray can also be adjusted to vary the balance between nucleation and powder layering in order to control the granule size distribution.

A drum granulator (Figure 8.1a) is a nearly horizontal rotating cylinder, with just a small angle from the horizontal to encourage flow of the granules from the inlet towards the outlet. Rotating drums do not have the same inherent product

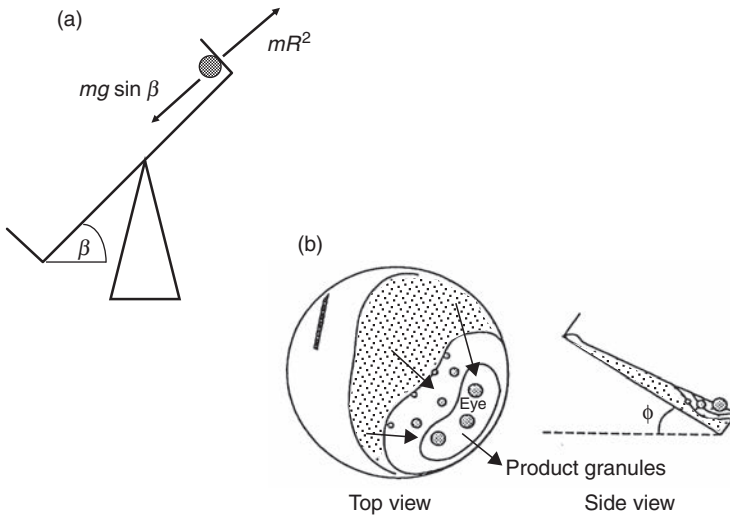


**Figure 8.15** Schematic of the operation of tumbling granulators. (a) Balance of forces for calculating the critical speed on a disc granulator; (b) granule segregation on the disc (Litster and Ennis, 2004).

classification properties of rotating discs. Therefore, if a tight control of granule size is required, drum granulators often operate with very high recycle rates (2:1 to 5:1), especially if coalescence is the dominant granule growth mechanism. However, drum granulators can be scaled to at least 4 m in diameter and 20 m long, and are therefore used for very high throughput applications.

The rotational speed of a tumbling granulator is set to keep the granules in the cascading flow regime, where granules cascade down the face of the moving granule bed. If the speed is too high, granules are thrown across the drum or disc (cataracting regime). If the speed is too low, the granule bed slides in the base of the drum as a solid body (sliding regime). The criteria for good solids flow can be expressed in terms of the Froude number  $Fr$ , the ratio of centripetal force to gravitational force acting on a granule traveling with the wall of the granulator:

$$Fr_{drum} = \frac{R\omega^2}{g} \quad 8.45a$$

$$Fr_{disc} = \frac{R\omega^2}{g \sin \beta} \quad 8.45b$$

where  $R$  is the drum or disc radius,  $\omega$  is the angular velocity (rad/s),  $g$  is gravitational acceleration, and  $\beta$  is the angle of the disc from the horizontal plane. For drums and discs, the typical operating ranges for  $Fr$  are 0.3–0.5 and 0.5–0.75, respectively.  $Fr = 1$  denotes the *critical speed* at which a single granule would be held against the

rim of the drum or disc by centripetal forces alone. If the critical speed is defined in terms of revolutions per second, rather than radians per second, it follows that:

$$N_{c,drum} = \frac{1}{2\pi} \sqrt{\frac{g}{R}} \quad 8.46a$$

$$N_{c,disc} = \frac{1}{2\pi} \sqrt{\frac{g \sin \beta}{R}} \quad 8.46b$$

### 8.6.2 Mixer Granulators

In mixer granulators, the rotation of an impeller imparts motion to the powder bed. There are dozens of different mixer geometries, often borrowed directly from blending applications. Some resemble kitchen food processors. The rotating shaft can be vertical or horizontal, the impeller can be a blade, a pin or a ploughshear, additional high-speed “choppers” may be employed, and operation can be either batch or continuous. The agitation intensities seen by the granules can vary widely between granulators, and also within granulators. Figure 8.16 gives examples of just two designs that are available.

The wide variety of geometries makes general statements about mixer granulators dangerous. However, mixer granulators tend to give small granules (0.2–2 mm) with moderate density that are often non-spherical. Mixers are quite robust with a wide range of formulation properties. They can disperse very viscous liquids and pastes and handle very fine powders. However, mixers are the most mechanically complex of granulators with the most variable powder flow fields. This makes prediction of product properties and scale up a challenge.

The powder flow field in a mixer granulator is also set by the balance of centripetal and gravitational forces. We need to define the Froude number in terms of the impeller rotational speed:

$$Fr_{mixer} = \frac{R_i \omega^2}{g} \quad 8.46$$

and criteria for good powder flow can then be written in terms of  $Fr_{mixer}$ , but the exact criteria will be mixer and impeller geometry-dependent. The impeller does not perfectly impart its momentum to the powder bed. For order of magnitude calculations, it is reasonable to assume:

$$U_{c,av} \approx v_{sp} \approx 0.15 R_i \omega_i \quad 8.47$$

In other words, the powder velocity is approximately 15% of the impeller tip speed. This means the flow transitions happen at higher values of  $Fr$  than are typical for rotating granulators.

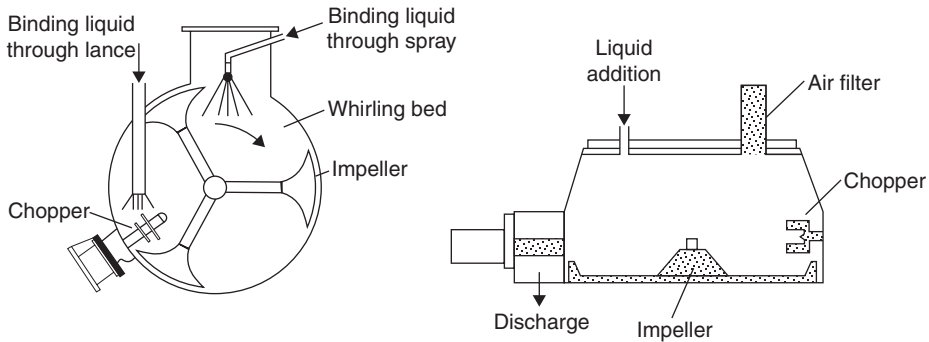


**Figure 8.16** Examples of the geometry of (a) horizontal, and (b) vertical axis mixer granulators (Litster and Ennis, 2004).

As an example, in vertical axis mixers, flow will transition from undesirable *bumping* flow to desirable *roping* flow when the Froude number exceeds some critical value (see Figure 8.17). This value is approximately  $Fr_{mixer} = 20$ . The high value is because the powder is moving more slowly than the impeller. Based on Equation 8.47, the corresponding particle Froude number would be approximately 0.5.

Drop-based nucleation, granule consolidation, coalescence, and powder layering occur in the moving powder bed of a mixer granulator in a similar fashion to those processes in a tumbling granulator. However, the high-stress region near the impeller and chopper in a mixer granulator may also cause breakage of large granules as well as mechanical dispersion of large lumps. The extent of breakage depends on both the intensity of the flow field in this region, and the circulation rate of powder through this region. Thus, this rate process is especially dependent on equipment geometry and impeller/chopper speed and is particularly difficult to generalize across different equipment designs.

### 8.6.3 Fluidized Granulators

Fluidized granulators use air to set the powder bed in motion, rather than mechanical moving parts. In a traditional fluid bed, air is distributed uniformly at the bottom of the bed (Figure 8.18). Rising bubbles in the fluid bed create chaotic mixing of the powder. Top spray of the liquid is common, but the spray zone can be located anywhere in the bed. In Wurster coaters and spouted beds, air is preferentially channeled through a central spout giving a more controlled recirculation pattern for the solids and high velocities in the spout. In these designs, the spray is usually introduced at the bottom of the spout. All fluidized designs incorporate simultaneous drying as a sticky, wet powder cannot be fluidized. This gives the advantage of removing a separate drying unit operation from the powder processing train.

Fluidized granulators can give two distinctly different types of granule. For batch granulation of a fine powder, highly porous agglomerates in the size range

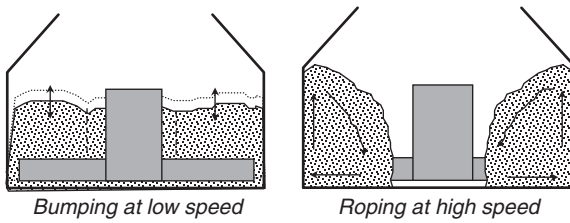


**Figure 8.17** Flow regimes in vertical axis mixer granulators: (a) bumping, (b) roping.

0.2–1 mm are produced. When seed granules, or larger primary particles, are used, layered “onion skin” granules are produced if the liquid phase is a melt, solution, or suspension of the desired phase. Fluidized beds are generally used for agglomerate production, while Wurster coaters and spouted beds are used for layered granulation and coating applications. The Ennis coalescence model can be used to establish whether agglomerate or layering will dominate under a given set of conditions (see Section 8.4.3).

Fluidized beds are so named because the drag force of the fluid (air) rising through the particle bed is sufficient to balance the weight of the particles in the bed leading to the bed behaving similarly to a fluid. This gives many advantages over other powder-processing regimes, including easier transfer of powder and excellent heat and mass transfer. The simpler flow behavior also leads to more reliable scale up than tumbling and mixer granulators. However, the high gas velocities may lead to attrition and fines loss. There are limitations on the formulations that can be used. Fluidized beds cannot handle very fine, cohesive powders (because they will not fluidize uniformly) or viscous liquids (because they cannot be atomized).

A brief description of the fluid dynamics on fluidized beds is needed to understand their use as granulators. (For a more detailed introduction to fluidized beds, see Rhodes, 2008, chapter 7.) Consider a packed bed of powder into which we introduce a uniform air flow from the bottom of the bed and gradually increase the air flow rate. The superficial velocity of the air is defined as:

$$U = \frac{Q_{air}}{A} \quad 8.48$$

where  $Q_{air}$  is the volumetric air flow rate and  $A$  is the cross-sectional area of the fluidized bed. As the air flow is increased, a point is reached at which the drag force from the gas equals the weight of the bed. This is denoted as the point of minimum fluidization where  $U = U_{mf}$ . As we further increase velocity, the bed expands while maintaining constant pressure drop. This expansion may be accompanied by the presence of rising gas bubbles in the bed. As  $U$  continues to increase, fluidization becomes more violent. When the fluidizing velocity of is a similar order to the terminal settling velocity of a single particle  $U_t$ , particles will be elutriated from the bed.



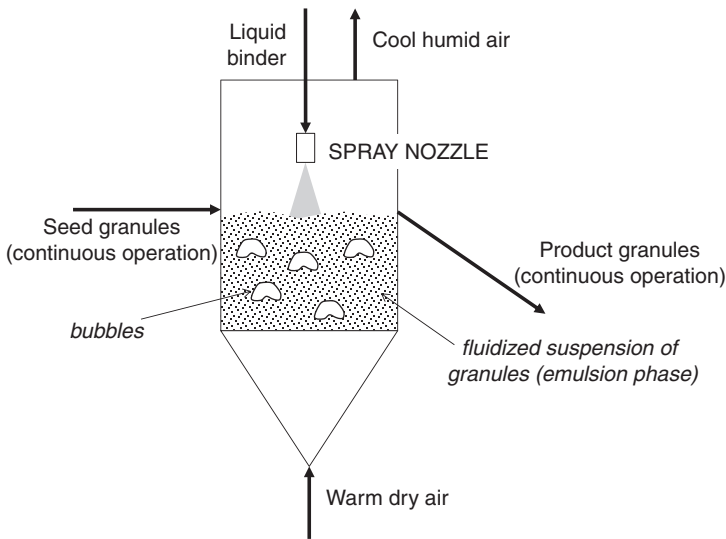


**Figure 8.18** Typical configuration for a fluid bed granulator.

Uniform fluidized bed granulators usually operate in the bubbling fluidized bed regime. The required superficial gas velocity to achieve this regime is given by the Wen and Yu equation:

$$\frac{d_v U_{mf} \rho_f}{\mu} = \left[ 33.7^2 + \frac{0.0408 d_v^3 \rho_f (\rho_g - \rho_f) g}{\mu^2} \right]^{-33.7} \quad 8.49$$

Typically, the bed is operated with  $1.5U_{mf} < U < 5U_{mf}$  to ensure good mixing while minimizing attrition of the granules and elutriation of feed powder. However, remember  $U_{mf}$  will change with time in batch granulation as the granule size increases (Equation 8.49). In the bubbling regime, the bed pressure drop is given by:

$$\Delta P = \rho_g (1 - \varepsilon) gH \quad 8.50$$

where  $H$  is the fluidized bed height. In spouted and spout-fluid beds, the spout will often be in the pneumatic conveying regime.

Different types of powders behave differently in fluidized beds. Geldart classified these powders into four types (see Figure 8.19):

- Type A: Easily fluidized powders in which the bed first expands uniformly before the onset of bubbling.
- Type B: Easily fluidized powders in which bubbling begins immediately the bed fluidizes and bubbles grow as they rise through the bed.
- Type C: Fine, cohesive powders that do not fluidize uniformly.
- Type D: Large particles suitable for processing in a spouted bed.

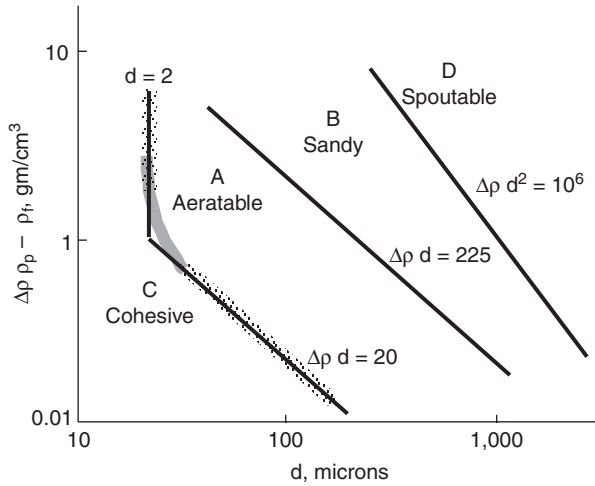


Figure 8.19 Geldart classification of powders for fluidization (Litster and Ennis, 2004).

Many of the powders we wish to granulate are type C, and this is a limitation on the use of fluidized beds. However, type A powders are suitable for fluid bed granulation to give type B agglomerates. Type B and D seed particles are suitable for layered granulation or coating in fluidized and spouted beds.

Bubbles in gas fluidized beds play a very important role in particle mixing, heat and mass transfer, attrition, and elutriation. Therefore, most correlations for the performance of fluidized bed driers and granulators contain reference to the bubble size  $d_b$ , the bubble rise velocity in the bed  $U_b$ , and the volumetric flow rate of bubbles  $Q_b$ . For example, an estimate of the particle collision velocity in a fluidized bed is written in terms of  $d_b$  and  $U_b$  (Equation 8.22). The simplest “two-phase” model for a fluidized bed states that all the gas flow rate above that required for minimum fluidization goes into the generation of bubbles:

$$Q_b \approx A(U - U_{mf}) \tag{8.51}$$

Thus,  $U - U_{mf}$  appears in many correlations. For example, we can estimate  $d_b$  and  $U_b$  from the following equations (Rhodes, 2008, chapter 7):

$$d_b = 0.54g^{-0.2} (U - U_{mf})^{0.4} (L + 4N^{-0.5})^{0.8} \tag{8.52}$$

$$U_b = 1.6D^{0.4} (gd_b)^{0.5} \tag{8.53}$$

where  $L$  is the height above the distributor,  $D$  is the diameter of the bed, and  $N$  is the orifice density of the distributor.

### 8.6.4 Scaling Rules

Table 8.2 gives a summary of suggested scaling rules for different types of granulators. Where possible, the scaling rules are given in terms of dimensionless groups, based on an understanding of (a) maintaining geometric similarity during scaling, (b) the kinematics of the powder flow (Sections 8.6.1–8.6.3), and (c) the controlling granulation rate processes (Section 8.4). This dimensional analysis approach to scaling is an established engineering tool. Nevertheless, we need to give some warnings about scaling wet granulation processes.

- It is surprisingly common for granulation equipment of different scales not to preserve geometric similarity, even from the same manufacturer.
- The scaling rules are based on lumped parameters such as  $U_c$ , whereas in reality, the velocity and stresses seen by the powder bed may vary significantly in different parts of a granulator.
- It is usually not possible to keep all the relevant dimensionless groups constant when scaling up.

Thus, the scaling rules should be considered a guide, not an inalienable truth.

For bubbling fluidized beds, the bed height and superficial gas velocity should be kept constant on scale up because bubble size and frequency, and therefore powder mixing, collision velocity, and attrition vary with bed height and gas velocity. Therefore, the batch size and required gas flowrate will scale with the area of the fluidized bed. Narrow fluidized beds may operate in the slugging regime, which gives different mixing behavior. Therefore, it is dangerous to directly scale from beds less than 0.3 m diameter, where slugging is more likely. Following the scaling rules in Table 8.1 should keep both  $\Psi$  and  $St_v$  constant.

Mixer granulators should be scaled using similar fill fraction (relative fill height) and with impeller and chopper size that scale with the vessel diameter. Scaling the impeller speed gives a difficult choice. Scaling with the constant Froude number (kinematic similarity) ensures similar powder flow fields and gives the following scaling rule:

$$\frac{N_2}{N_1} = \left( \frac{D_1}{D_2} \right)^{0.5} \quad 8.54$$

However, this results in an increase in impeller tip speed, and thus increased  $St_{def}$ . Sometimes, a constant tip speed scaling rule is recommended:

$$\frac{N_2}{N_1} = \left( \frac{D_1}{D_2} \right) \quad 8.55$$

provided that  $Fr$  remains above some critical value to give the desired flow regime; e.g., roping flow in a vertical axis mixer or annular flow in a horizontal axis mixer. The scaling rule suggested by Michaels *et al.* (2009) is intermediate between

**Table 8.2.** Summary of recommended scaling rules for wet granulation processes

<i>Fluidized beds</i>		
Parameter	Scaling rule	Comment
Bed height	$H_1 = H_2$	Fluid bed capacity scales with bed area
Gas flowrate	$\frac{Q_2}{Q_1} = \frac{U_2}{U_1} = \frac{D_2^2}{D_1^2}$	Constant bed height and superficial velocity should keep $St_v$ nearly constant.
Spray conditions	$\frac{A_{p,2}}{A_{p,1}} = \frac{D_2^2}{D_1^2}$ $\frac{Q_{sp,2}}{Q_{sp,1}} = \frac{D_2^2}{D_1^2}$	These rules will keep $\Psi$ constant and are usually achieved by using multiple nozzles in larger-diameter beds
<i>High-shear mixers</i>		
Parameter	Scaling rule	Comment
Geometry	$\left(\frac{H}{R_i}\right)_1 = \left(\frac{H}{R_i}\right)_2$ $\left(\frac{R_c}{R_i}\right)_1 = \left(\frac{R_c}{R_i}\right)_2$	Keep mixers geometrically similar if possible
Capacity	$\frac{M_2}{M_1} = \frac{H_2 R_{i2}^2}{H_1 R_{i1}^2}$	Batch size scales with mixer volume
Spray conditions	$\Psi_2 = \Psi_1$	Can be achieved by using multiple nozzles in larger mixers
Impeller speed	$\frac{\omega_2}{\omega_1} = \left(\frac{R_{i,1}}{R_{i,2}}\right)^n$	$n = \begin{cases} 0.5 \text{ constant } Fr \\ 0.8 \text{ constant shear} \\ 1 \text{ constant } St_{def} \end{cases}$

Equations 8.54 and 8.55. For tumbling granulators, the rotational speed is usually scaled to keep  $Fr$  constant, as shown in Equations 8.45 and 8.46.

For all granulator designs, the dimensionless spray flux should be held constant to ensure good liquid distribution when operating in, or near, the drop-controlled regime. If the batch time (residence time) is held constant, this can only be achieved by using multiple spray nozzles in large-scale granulators.

These dimensionless group-based scaling rules are consistent with the regime map approaches described in Section 8.4. It may not be possible to keep all relevant dimensionless groups constant when scaling, but great care should be taken not to move into a different operating regime when scaling up.

## 8.7 Summary

Wet granulation is key process in the manufacturing of particulate delivery forms. It is both ubiquitous and complex. The process is carried out in a wide variety of equipment using a huge range of feed formulations. Nevertheless, we have identified in this chapter a number of engineering and scientific approaches that can be generally used.

Designing and scaling wet granulation involves both product and process design. It is important that you understand the three key rate processes that occur during granulation:

- wetting and nucleation;
- consolidation and growth; and
- breakage and attrition.

For each rate process, there are important formulation properties, process parameters, and controlling dimensionless groups including  $\psi$ ,  $\tau_p$ ,  $S$ ,  $St_v$ ,  $St_{def}$ ,  $Ca$ , and  $Fr$ .

You should know the definitions of these dimensionless groups, and be able to calculate them from formulation properties and process parameters. These dimensionless groups can be used with the Iveson, Hapgood, and Ennis regime maps (Figures 8.6, 8.11, and 8.13, respectively) for understanding granulation processes, process and product design, and troubleshooting. The dimensionless groups also give a basis for process scale up (Table 8.2).

Population balance approaches can be used for quantitative design provided that the controlling rate processes are clearly defined and the rate constants are known or can be predicted. This is more challenging for granulation than for crystallization (Chapter 4) or particle size reduction (Chapter 5). Section 8.5 outlines the approaches to using the population balance for granulation and gives some solutions for limiting cases (drop-controlled nucleation, size-independent coalescence/agglomeration).

Finally, students should have at least a general understanding of different types of granulation equipment and the likely product attributes of granules produced from tumbling granulators, mixer granulators, and fluidized beds (Section 8.6).

## 8.8 Bibliography

- Abinger, T., 2008. Population Balance Modeling of Granulation. In Salman A.J. (ed.). *Granulation Handbook*, chapter 24.
- Ennis, B.J., Tardos, G., and Pfeffer, R., 1991. A microlevel-based characterization of granulation phenomena. *Powder Technology*, 65, 257–272.
- Hapgood K., Litster, J.D., and Smith, R., 2003. Nucleation regime map for liquid bound granules. *AIChE Journal*, 49(2), 350–361.
- Hapgood, K., Litster, J.D., White, E.T., Mort, P.R., and Jones, D.G., 2004. Dimensionless

- spray flux in wet granulation: Monte-Carlo simulations and experimental validation. *Powder Technology*, 141, 20–30.
- Iveson, S.M., Litster, J.D., and Ennis, B.J., 1996. Fundamental studies of granule consolidation Part 1: Effects of binder content and binder viscosity. *Powder Technology*, 88, 15–21.
- Iveson, S.M., Litster, J.D., Hapgood, K., and Ennis, B.J., 2001a. Nucleation, growth and breakage phenomena in agitated wet granulation processes: A review. *Powder Technology*, 117, 3–39.
- Iveson, S.M., Wauters, P.A.L., Forrest, S., *et al.*, 2001b. Growth regime map for liquid-bound granules: Further development and experimental validation. *Powder Technology*, 117, 83–87.
- Iveson, S.J., Beathe, J.A., and Page, N.W., 2002. The dynamic strength of partially saturated powder compacts: the effect of liquid properties. *Powder Technology*, 127, 149–161.
- Litster, J.D. and Ennis, 2004. *The Science and Engineering of Granulation Processes*, chapters 3 to 6, Kluwer, Dordrecht.
- Liu, L.X. and Litster, J.D., 2002. Population balance modelling of granulation with a physically based coalescence kernel. *Chemical Engineering Science*, 57, 2183–2191.
- Michaels, J.N., Farber, L., Wong, G.S., *et al.*, 2009. Steady states in granulation of pharmaceutical powders with application to scale-up. *Powder Technology*, 189, 295–303.
- Parihk, D.M. (ed.), 2005. *Handbook of Pharmaceutical Granulation Technology 2nd edition*, Taylor and Francis, New York.
- Perry, R.H., and Green, D.W. (eds.), 2008. *Perry's Chemical Engineers Handbook 8th edition*, chapter 20, McGraw-Hill, New York.
- Rhodes, M.J., 2008. *Introduction to Particle Technology* (2nd ed.), John Wiley, Chichester, chapter 11.
- Salman, A.L., Hounslow, M.J., and Seville, J.P.K. (eds.), 2007. *Handbook of Powder Technology v.11: Granulation*, Elsevier, Amsterdam.
- Smith, 2008. *Wet granule breakage in high shear mixer granulators*. PhD thesis, The University of Queensland.

## 8.9 Problems

- 8.1. The Rainbow Paint Company is having problems dispersing a new pigment “extra dark black” into water. A highly paid consultant engineer has recommended that a Washburn test be performed to assess the wetting properties of the powdered pigment in water. Given below are the results for the tests for rise of water into a bed of the powder. For comparison, results for dodecane (which is assumed to perfectly wet the powder) are shown as well.
- What is the effective pore size of the powdered bed?
  - What is the contact angle of water on the powder?
  - What advice would you give RPC to solve their problem?

Time (s)	Water height (cm)	Dodecane height (cm)
200	3.6	5.0
400	5.0	7.1
600	6.1	8.7
800	7.2	10.2
1,000	7.9	11.3
1,500	9.6	13.6
2,000	11.1	16.0
2,500	12.4	18.0
3,000	13.7	19.5

$$\begin{aligned} \gamma_{water}^h &= 72.7 \text{ mN m}^{-1} & \mu_{water} &= 0.001 \text{ Pa s} \\ \gamma_{dodec}^h &= 25.4 \text{ mN m}^{-1} & \mu_{water} &= 0.0008 \text{ Pa s} \end{aligned}$$

- 8.2. During batch granulation, induction time behavior is sometimes observed; i.e., there is little or no change in granule size for a long time followed by a sudden sharp increase in granule size. Explain why this phenomenon occurs in terms of your understanding of granule consolidation and growth. If the feed powder size is decreased, how will induction time change? Why?
- 8.3. Two powders are being considered for granulation in a drum granulator using a binding fluid with properties similar to water. Your company wishes to do laboratory scale tests in their 0.3 m-diameter drum granulator and then transfer results to their existing 2 m-diameter production facility. The drums both run at 40% of their critical speed. The product granules need to be in the range 1–3 mm and control of granule density is also important. The desired range of granule porosity is 0.3–0.32. As a good particle technologist, you have done some characterization tests on your feed formulation that yield the information given below:

$$\text{Powder A: } \bar{x}_{32} = 60 \mu\text{m} \quad \rho_p = 2500 \text{ kg m}^{-3}$$

$$\text{Powder B: } \bar{x}_{32} = 0.8 \mu\text{m} \quad \rho_p = 1400 \text{ kg m}^{-3}$$

- What range of moisture contents (kg water per kg dry powder) would you recommend to study at the bench scale for each powder?
- What sort of densification and growth behavior do you expect for each powder? Justify as quantitatively as possible.
- Comment on the suitability of drum granulation for these materials and any issues in scaling up the process. What other formulation characterization tests would you recommend?

- 8.4. Consider Example 8.2 with water as the liquid. An engineer proposes to scale up the process keeping spray time and total batch time constant and scaling impeller speed to keep Froude number constant. You can assume powder surface velocity is proportional to impeller tip speed. What are the implications for wetting/nucleation when scaling up this formulation from a 25-liter granulator to a 300-liter granulator? Assume the granulators are geometrically similar.
- 8.5. A pharmaceutical product is produced in a 300-liter vertical shaft high-shear mixer granulator. The product leaving the granulator has a very wide size distribution with some large high-liquid content granules and lumps, and some fine dry powder. A troubleshooting team is put together to analyze the problem. They establish that the problem is due to poor powder wetting and nucleation, but disagree on how to solve the problem. The formulation scientist proposes to add surfactant to the liquid binder to make it wet the powder better by reducing the contact angle from 70° to 10°. The process engineer proposes increasing the number of nozzles from one to four to better distribute the liquid spray.

The values of  $t_p$  and  $\Psi$  for this system are 1.5 s and 0.6, respectively. Using a sketch of the nucleation regime map, locate the current operating regime for the mixer granulator. Calculate the expected change to  $t_p$  and  $\Psi$  for each proposed change to conditions. Comment critically on whether either (or both) of the changes will achieve better nucleation and liquid distribution.

- 8.6. Consider ammonium nitrate melt granulation. Ammonium nitrate melt is sprayed into a “fluidized drum” granulator fed with recycled granules. The process is continuous and can be assumed to be at a steady state. A sampling trial gives the following data:

melt flow rate = 5 tonne per hour  
 recycle flow rate = 8.5 tonne per hour

Size distributions:

Size range	Mass fraction (recycle)	Mass fraction (ex-granulator)
> 4 mm	0.073	0.4
-4 + 2.8 mm	0.291	0.34
-2.8 + 1.7 mm	0.475	0.25
-1.7 + 1.2 mm	0.161	0.01
-1.2 mm	0	0

For the given recycle and melt flows:

- (i) show that fewer granules are leaving the granulator than enter it; and
- (ii) calculate the size distribution leaving the granulator if size enlargement is by layering only (no coalescence, nucleation, breakage).



For the above calculation, assume that the granulation drum is a plug-flow vessel. Sketch how the exit size distribution is likely to vary if the drum behaved as a well-mixed vessel.

- 8.7. A pharmaceutical company is testing a new drug. The drug is carried on 200  $\mu\text{m}$  lactose particles. They want to use a fluid bed to coat the lactose with a polymer coating to protect the particles from attrition during handling and to provide controlled release of the active agent on delivery. There is a problem, however. Early pilot tests show the particles are agglomerating in the fluid bed. At a developing team meeting, Joe Brightspark is supremely confident the problem is easily overcome by increasing the gas velocity in the fluidized bed? Is he right? If not, what other measures could be taken.

Data for initial pilot plant tests:

$$U = 2U_{mf}$$

$$T_b = 50^\circ\text{C} \text{ (any higher will damage the drug)}$$

$$T_{air,in} = 15^\circ\text{C} \text{ (dry air)}$$

Polymer solution added as 5% polymer in water at a rate equivalent to 20% of that required to saturate the exit air.

$$\mu_p = 0.1 \text{ Pa}\cdot\text{s}$$

$$h = 25 \mu\text{m} \text{ (an estimate based on the size of the spray zone and the circulation rate in the fluidized bed)}$$

- 8.8. Consider the following process for “fattening” urea prills. Urea prills (1.5 mm diameter; assume monosized) are fed to a continuous fluid bed granulator where urea melt is added such that the mean size of the exit stream is 2 mm. The feed rate of urea prill is 1 tonne  $\text{h}^{-1}$ . The mean residence time for a prill in the bed is 3 h. Size enlargement is by layering only. Derive the population balance equation for the bed and (if possible) solve the moments form of the equation to give the standard deviation of the fattened prills leaving the bed if the bed is well mixed with particles growing at constant linear growth rate while in the bed.
- 8.9. A fluidized bed is to be used to granulate urea from solution. Some proposed design variables are given below. Do you see any problems with the design? Note that a quick check with sensible assumptions is required, rather than a detailed analysis.

Bed diameter: 1.5 m

Fluidized height: 5 m

Mean particle size in the bed: 2 mm

Fluidizing air flowrate: 0.38 kg/s

Fluidizing air temperature: 200°C

Bed temperature: 50°C

Fluidizing air humidity: saturated at 20°C

Liquid flow rate: 0.15  $\text{kg s}^{-1}$  of 80% w/w urea solution.

- 8.10. Consider the powder B in Question 8.3. We propose to scale up a disc pelletizer for this material. In a 1.5 m-diameter disc,  $0.5 \text{ m}^3 \text{ h}^{-1}$  of material is successfully processed with the disc operating at 55% of critical speed with an angle to the horizontal of  $50^\circ$ . A residence time of 10 min gave pellets of the required size and density.
- If the full-scale disc is required to treat  $20 \text{ m}^3 \text{ h}^{-1}$ , specify the disc diameter, speed, and power requirements for the large disc assuming the same residence time.
  - Is the same residence time a good assumption for scale up? Will granule density and size change on scale up?
- 8.11. Consider a batch granulator in which coalescence is the primary mechanism of growth. By very careful control of the nucleation process, we produce nuclei granules that are essentially uniform in size at 0.2 mm. These then grow by coalescence.
- Assuming a size-independent and constant kernel, write down the population balance in terms of the number size distribution with respect to volume  $n(v)$  and the moments form of the size distribution. Solve the moments form of the population balance and sketch how the following parameters of the distribution vary with time:  $N(t), V(t), \bar{v}, n(v)$  vs  $v$ . Be as quantitative as possible.
  - Repeat this analysis for a well-mixed continuous granulator operating at steady state.
  - Now a size-independent, constant kernel is probably not a really good model. Consider this alternative model. There is no successful coalescence until liquid is squeezed to the surface of the granules. There is a finite time (say 2 min after nucleation) for this to happen. After this time, our “ball bearing and honey” model is true; i.e., granule collision events are successful provided the mean size of granules in the collision is less than some critical size (2 mm for this system). Now reconsider the batch granulator. Sketch the way you expect  $N(t), V(t), \bar{v}, n(v)$  vs  $v$  to vary with time. (This can be a qualitative analysis.)
  - If I make the binder viscosity 10 times as large, how do your expectations change?

# 9 Strength, Breakage, and Attrition of Particulate Delivery Forms

## 9.1 Consider a Case Study ...

*3P Consulting Inc.*

Memo to: Purdue Powder Processing Team  
Memo from: Jim Litster  
March 6, 2014

### **Dust Generation in a Water-dispersible Granule Plant**

Our client manufactures water-dispersible granules (WDG) of agricultural chemicals for use on corn and soybean crops in Indiana, USA. These granules are made from primary particles of the active ingredient (90%–95%) combined with surfactants, binders, and disintegrants (5%–10%). The granules are easy and safe to meter and transport. At the farm, they are redispersed and dissolved to form a solution that is sprayed onto the crops.

There is a problem with dust formation in the back end of the processing and bagging plant. This is a serious issue due to health issues associated with inhaling the active ingredient, as well as creating a risk of dust explosion. The fines generated are likely responsible for reduction in the flowability of the powder and caking during storage.

We have visited the plant and interviewed engineers and operators. The processing train has pneumatic conveying, vibrating feeders, hoppers, and drops off conveyor belts that have been identified as possible sources of dust generation by attrition. Some formulations behave better than others. However, often the operators can't predict which products will be the bad players. As new formulations are regularly introduced into the plant, this is a significant problem.

We are looking to the 3P team to give advice on how to identify and address the problem. Specifically, can you advise on the following questions.

- How do we characterize granules for their strength or potential to attrit?
- How do we improve strength by formulation changes?
- How do we reduce attrition by process optimization?

We have access to batches of a number of different products, some of which are relatively dust-free and some of which caused major problems. Ungranulated formulations of these products are also available. You will need to demonstrate your proposed approach using these formulations and products.

We would like you to report to our client's Product Quality Manager when she visits on April 20 giving your recommendations on characterization tests and process optimization with appropriate justification.

As an individual exercise, or as a group brainstorming session, reflect on the questions presented by this case study.

- What aspect of the handling in the plant is most likely to cause attrition?
- Is it possible to estimate the stress on the granules under these conditions?
- Can we handle the granules more gently to avoid dust generation?
- What properties of the granule are most likely to impact the granule attrition resistance?
- Are these properties most easily controlled by formulation changes or changes to process conditions?

Most of this book has described *process models* to understand and predict the properties and property distributions of particles and particulate delivery forms – size and size distribution, density and porosity, shape and so on – given the process conditions and formulation parameters. This approach implicitly assumes that we know what the desired properties of the product are! However, the true product attributes of interest may be more complicated and difficult to define: strength, non-dustiness, caking resistance, dispersibility, dissolution rate, chemical stability, shelf life, mouth feel, etc. Product design often requires *reverse engineering* – i.e., given a set of product attributes, what structure and properties of the product are required? To answer this question, we need good *product models*. The last two chapters of this book address product modeling. It is a complicated area. Perhaps the easiest to understand and the best-developed models are those for attributes related to the physical strength of the product, which is the topic discussed in this chapter.

## 9.2 Learning Goals

At the completion of this chapter, the student should be able to:

1. Describe the different mechanisms by which particles in an agglomerate are bonded and calculate bond strengths between particles using models presented in this chapter.
2. Explain the Rumpf and Kendall models for granule strength to a peer and estimate granule strength from these models.
3. Describe the strengths and weaknesses of different approaches to measuring granule strength.
4. Estimate rates of agglomerate breakage due to either impact or attrition in industrial environments such as pneumatic conveying, fluidized beds, and bins.
5. Attack open-ended particle design and troubleshooting problems related to particle delivery form strength, attrition, and breakage of a similar nature to the introductory case study for this chapter.

### 9.3 Micromechanical Models for Agglomerate Strength

Many particulate products are in the form of agglomerates of smaller primary particles – granules, compacts, tablets, aggregates, etc. For the purposes of product design, we would like to be able to predict the strength of an agglomerate based on:

1. the size of the primary particles and the strength of bonds between the particles (largely given by the design of the formulation); and
2. the structure of the granule/agglomerate/compact (largely given by the process choice and conditions).

This turns out to be quite difficult to do quantitatively. However, there are two separate micromechanical models available which give us a great starting point, the models of Rumpf and Kendall. These models are based on different mechanisms by which the agglomerate fails.

#### 9.3.1 The Rumpf Model for Agglomerate Tensile Strength

Rumpf developed his model by assuming that for the granule to fail in tension, all the bonds between particles in the fracture plane in the agglomerate need to be broken simultaneously (Figure 9.1a). For monosized, spherical primary particles of diameter  $d_p$ , the number of particles that are cut but the theoretical fracture plane are:

$$n_p = \frac{6A(1-\varepsilon_g)}{\pi d_p^2} \quad 9.1$$

If the coordination number for each primary particle is  $Q$  and the fraction of those bonds that needs to break for fracture is  $f$ , then the force required to break all the bonds is:

$$F_{br} = A\sigma_T = \frac{4A(1-\varepsilon_g)}{\pi d_p^2} \frac{fQF_b}{2} \quad 9.2$$

Rearranging:

$$\sigma_T = \frac{6(1-\varepsilon_g)QfF_b}{\pi d_p^2} \quad 9.3$$

where  $F_b$  is the tensile strength of the bond between particles, sometimes described as the pull-off force required to separate the particles.  $Q$  is a function of the particle packing. Rumpf approximated  $Q$  and  $f$  by:

$$Q \approx \frac{\pi}{\varepsilon_g} \quad 9.4a$$

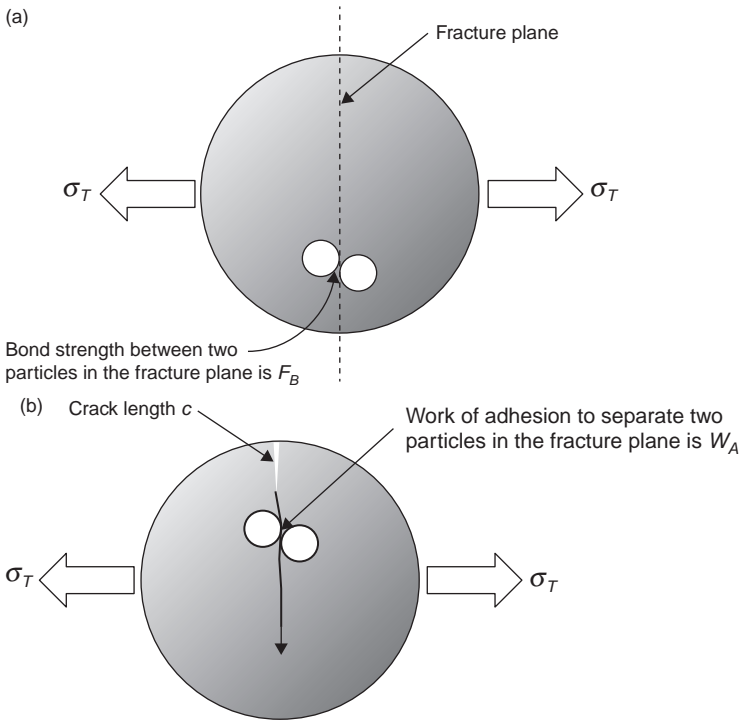


**Figure 9.1** Granule failure in tension according to two different models. (a) Rumpf model, where all bonds in the failure plane fail simultaneously; (b) Kendall model, where failure is by crack propagation.

$$f = \frac{3}{16} \tag{9.4b}$$

Combining Equations 9.3 and 9.4 gives:

$$\sigma_T = \frac{9(1 - \epsilon_g) F_b}{8\epsilon_g d_p^2} \tag{9.5}$$

The bonding force between particles has been proposed for a number of different types of bond and these are summarized in Table 9.1.

In principle, the Rumpf model gives an a priori prediction of agglomerate strength. His work in the 1950s and 1960s put this area of particle technology on a scientific footing for the first time. However, there are many limitations of the model, including:

- The agglomerate structure may not be uniform; i.e., the particle packing and binder distribution may not be uniform.

**Table 9.1** Expressions for bond strength between particles for use in the Rumpf or Kendall models

van der Waals adhesion <sup>1</sup>	$F_b = \frac{A_H d_p}{24z^2}$	$A_H$ is the Hamaker constant $z$ is the separation distance between particles
Capillary liquid bridge <sup>1</sup>	$F_b = C d_p \gamma^v \cos\theta$	$C$ is a constant that depends on liquid saturation. $C = 2$ for pendular bridges; $C = 8$ for saturated capillaries; $C = 8S$ for $0.3 < S < 1.0$ funicular state
JKR adhesion <sup>2</sup>	$F_b = \frac{3\pi d_p W_A}{8}$	$W_A$ is the work of adhesion between the particles
Viscous liquid bridge <sup>2</sup>	$F_b = \frac{3\pi\mu v d_p^2}{2h_0}$	$v$ is the separation velocity in the normal direction $h_0$ is roughness or asperity height
Solid bridge <sup>2</sup>	$F_b = \pi r_{sb}^2 \sigma_{sb}$ $\frac{r_{sb}}{d_p} = 0.82 \left[ \frac{C_{solid} V_b}{\rho_p d_p^3} \right]^{1/3}$	$\sigma_{sb}$ is the solid bridge strength $r_{sb}$ is the radius of the solid bridge $V_b$ is the initial liquid bridge volume $C_{solid}$ is the concentration of solid dissolved in the liquid

<sup>1</sup> Rumpf (1962).<sup>2</sup> Cheong *et al.* (2007).

- The primary particles may not be spherical or mono-dispersed.
- The real bond force between particles is often difficult to know accurately; e.g., the van der Waals adhesion force is very sensitive to separation distance between particles, which is in turn highly sensitive to particle roughness.
- If agglomerate failure is by brittle or semi-brittle fracture, then the stress at the tip of the propagating crack is much higher than the average stress across the whole fracture plane.

In most cases, the Rumpf model overpredicts granule strength.

### 9.3.2 The Kendall Model

This model is based on brittle fracture of agglomerates by crack propagation – i.e., the same mechanism we described for single particles in Section 5.3. When brittle fracture occurs, the local stress distribution is highly non-uniform across the fracture plane, with the highest stress intensity ahead of the propagating crack (see Figure 9.1b). Therefore, instead of summing the *total force* for fracture like the Rumpf model, the Kendall model sums the *total fracture energy* required for failure

(Kendall *et al.*, 1988). For brittle fracture, Equations 5.3 and 5.4 apply. Thus we can write:

$$\sigma_T \propto \left[ \frac{E_g U_g}{c} \right]^{1/2} \quad 9.6$$

where  $U_g$  is the energy absorbed during fracture of the granule or compact,  $E_g$  is granule or compact elastic modulus, and  $c$  is the characteristic flaw size. Our challenge, then, is to relate  $U_g$  and  $E_g$  to the agglomerate structure and primary particle properties.

We start by considering two spheres held together by an adhesive force, e.g., van der Waals attraction. This attractive force will cause the two spheres to deform at the contact point to give a circular contact area of radius  $a_0$  (see Figure 9.2).  $a_0$  is set by the balance between the adhesive force and the elastic resistance to deformation of the particle. When the particles are separated, new particle surfaces are created. The increase in surface energy per unit area is called the work of adhesion:

$$W_A = 2\gamma^{sv} \quad 9.7$$

The JKR theory from contact mechanics (Johnson *et al.*, 1971) gives the net energy required to separate the two spheres as the energy required to create new surface less the elastic energy released:

$$u_f = u_a - u_e = \pi a_0^2 W_A - \frac{1}{10} \pi a_0^2 W_A = \frac{9}{10} \pi a_0^2 W_A \quad 9.8$$

The corresponding pull-off force is:

$$F_b = \frac{3\pi d_p W_A}{8} \quad 9.9$$

and the contact area is related to the work of adhesion and the elastic properties of the particle by:

$$a_0 = \left[ \frac{9\pi W_A d_p^2 (1-\nu^2)}{16E} \right]^{1/3} \quad 9.10$$

where  $E$  and  $\nu$  are the Young's modulus and Poisson's ratio for the primary particles.

Based on a consideration of regular cubic packings, Kendall proposed that the number of contacts in the fracture plane was proportional to the 4th power of the solid fraction:

$$n_c \propto \frac{4(1-\varepsilon_g)^4}{\pi d_p^2} \quad 9.11$$



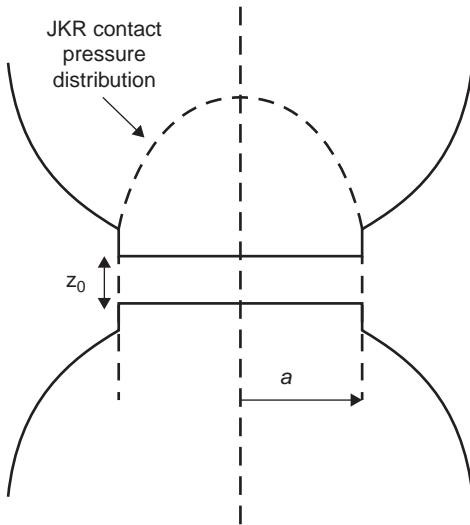


**Figure 9.2** Deformation of two elastic spheres in contact due to adhesive force (Cheong *et al.*, 2007).

The total energy required for fracture is:

$$U_g = n_c u_f \tag{9.12}$$

Combining Equations 9.8, 9.10, 9.11, and 9.12 gives:

$$U_g = 59.7(1 - \epsilon_g)^4 \left[ \frac{W_A^5 (1 - \nu^2)^2}{E^2 d_p^2} \right]^{1/3} \tag{9.13}$$

An analogous expression for the agglomerate elastic modulus can also be derived:

$$E_g = 13.1(1 - \epsilon_g)^4 \left[ \frac{9\pi W_A E^2}{16d_p^2 (1 - \nu^2)^2} \right]^{1/3} \tag{9.14}$$

Combining Equations 9.6, 9.13, and 9.14 gives an expression for the tensile strength of the agglomerate:

$$\sigma_T = 8.75(1 - \epsilon_g)^4 \frac{W_A}{d_p^{1/2} c^{1/2}} \tag{9.15}$$

To compare this model with the Rumpf model, it is useful to write the tensile strength in terms of the pull-off force (bond strength) between two particles. Combining Equations 9.13 and 9.9 gives:

$$\sigma_T = 3.75(1 - \epsilon_g)^4 \frac{F_B}{d_p^{3/2} c^{1/2}} \tag{9.16}$$

Although originally derived for adhesive bonds between elastic particles, in the form of Equation 9.16, Kendall's model can be used for any of the bonding mechanisms described in Table 9.1, provided failure by crack propagation is expected.

**Example 9.1** During a granulation process, a fully saturated liquid granule is formed from a 2% by volume solution of a polymer. The primary particle size is 25  $\mu\text{m}$  and the liquid has a viscosity of 0.05 Pa s and a surface tension of 30 mN  $\text{m}^{-1}$  with good wetting of the powder ( $\theta = 0^\circ$ ). The granule porosity is 0.33. Estimate the strength of this granule (a) during slow compression, and (b) during an impact at 10  $\text{m s}^{-1}$  using the Rumpf model.

*Solution:*

(a) Under slow compression, we can assume pseudo-static conditions with the granule strength provided by capillary suction. From Equation 9.5 and Table 9.1, we have:

$$\sigma_T = \frac{9(1 - \varepsilon_g)F_b}{8\varepsilon_g d_p^2}$$

$$F_b = C d_p \gamma^{lv} \cos\theta$$

where  $C = 8$  for a fully saturated granule. Thus:

$$\sigma_T = \frac{9(1 - \varepsilon_g)}{8\varepsilon_g d_p^2} 8 d_p \gamma^{lv} \cos\theta$$

$$\Rightarrow \sigma_T = \frac{9(1 - 0.33)}{0.33 \times 25 \times 10^{-6} \text{m}} \times 30 \times 10^{-3} \text{Nm}^{-1} \times 1 = 21.9 \text{kPa}$$

(b) Under dynamic conditions, the viscous resistance to motion will be important. We are not told the primary particle roughness, which can be difficult to measure. Let us assume that  $(h_0/d_p) = 0.1$ , i.e.,  $h_0 = 2.5 \mu\text{m}$ . Thus:

$$F_b = \frac{3\pi\mu v d_p^2}{2h_0} = 30\pi\mu v d_p$$

Substituting into Equation 9.5:

$$\sigma_T = \frac{9(1 - \varepsilon_g)}{8\varepsilon_g d_p^2} 30\pi\mu v d_p$$

$$\Rightarrow \sigma_T = \frac{9(1-0.33)}{8 \times 0.33 \times 25 \times 10^{-6} \text{ m}} \times 30\pi \times 0.05 \text{ Pa.s} \times 10 \text{ ms}^{-1} = 4.3 \text{ MPa}$$

The dynamic strength of the granule is 200 times higher than the static strength under the conditions given.

**Example 9.2** A ceramic compact has been formed by compression. The primary particle size is 2  $\mu\text{m}$  and compact solid fraction is 0.8. The surface energy of the ceramic is 200  $\text{mN m}^{-1}$ .

- (a) Predict the compact strength using the Rumpf and Kendall models, assuming the compact has a very uniform structure. By how much do their predicted strengths differ?  
 (b) Our measured compact strength is less than predicted in part (a). X-ray microtomography of sample compacts shows the presence of a small number of air bubbles of diameter 100  $\mu\text{m}$  in the compacts. What is your new estimate of the compact strength under these circumstances?

*Solution:*

- (a) Let us use the JKR theory to predict the bond strength using Equations 9.9 and 9.7:

$$F_b = \frac{3\pi d_p W_A}{8} = \frac{6\pi d_p \gamma^{sv}}{8} = \frac{6\pi \times 200 \times 10^{-3} \text{ Nm}^{-1}}{8} = 9.4 \times 10^{-7} \text{ N}$$

If the compact is uniformly structured,  $c \sim d_p$ . Thus the Kendall model becomes (Equation 9.16):

$$\sigma_T = 3.75(1-\varepsilon_g)^4 \frac{F_b}{d_p^2} = 3.75 \times 0.2 \times \frac{9.4 \times 10^{-7} \text{ N}}{(2 \times 10^{-6} \text{ m})^2} = 176 \text{ kPa}$$

The Rumpf model gives:

$$\sigma_T = \frac{9(1-\varepsilon_g)F_b}{8\varepsilon_g d_p^2}$$

Therefore:

$$\frac{\sigma_{T,Rumpf}}{\sigma_{T,Kendall}} = \frac{9(1-\varepsilon_g)}{8\varepsilon_g \times 3.75(1-\varepsilon_g)^4} = \frac{9(1-0.2)}{8 \times 0.2 \times 3.75(1-0.2)^4} = 2.93$$

The two models predict the same effect of primary particle size. Although the effect of porosity has very different functional form, the predicted strengths are of a similar order.

(b) In this case  $c = 100 \mu\text{m}$ , which is much larger than the primary particle size. The Kendall model gives:

$$\sigma_T = 3.75(1 - \varepsilon_g)^4 \frac{F_B}{d_p^{3/2} c^{1/2}} = 27.8 \text{ kPa}$$

$$\frac{\sigma_{T,Rumpf}}{\sigma_{T,Kendall}} = 2.93 \times \left( \frac{100}{2} \right)^{0.5} = 20.7$$

For these ceramic compacts, we expect brittle, or at least semi-brittle, failure by crack propagation. The presence of the air bubble (a flaw) reduces the granule strength sevenfold. Rumpf's model cannot account for this change and substantially over predicts the compact strength.

## 9.4 Macroscopic Strength of Particles and Particulate Products

Macroscopically, we often consider a compact or agglomerate as a continuum solid phase with defined macroscopic properties. With this world view, granule porosity represents the cracks or flaws within the continuum matrix. Thus, we can define macroscopic properties in a similar way to that we used for single particles in Chapter 5, namely the agglomerate tensile strength  $\sigma_T$ , fracture toughness  $K_c$ , Young's modulus  $E$ , and Poisson's ratio  $\nu$ .

The tensile strength of an agglomerate is difficult to measure by applying a direct tensile force. Instead, tensile strength is measured indirectly in unconfined uniaxial compression (Figure 5.2a). Equation 5.2 can be used for estimating the tensile strength from the crush strength of granules:

$$\sigma_{c,g} = \frac{kF_c}{d_g^2} \tag{9.17}$$

where  $k \sim 0.4\text{--}0.7$  depending on the size of the contact area between the agglomerate and the platen. If the agglomerate fails in brittle or semi-brittle failure, the tensile strength measured in this fashion will be highly variable as the flaw size distribution will relate directly to the non-uniform packing of primary particles in the agglomerate. Typically, 100–200 agglomerates need to be tested to get an accurate measure for the mean tensile strength and tensile strength distribution, making the test very tedious.

The Weibull distribution can be used to correlate data on the crush strength distribution (Section 5.3):

$$P_s(\sigma) = \exp \left[ - \left( \frac{\sigma}{\sigma_{37}} \right)^m \right] \quad 9.18$$

where  $P_s(\sigma)$  is the probability of survival at the stress level  $\sigma$ ,  $\sigma_{37}$  is the Weibull constant or characteristic strength of the material at which 37% of the agglomerates remain unbroken, and  $m$  is the Weibull modulus.  $m$  measures the variability in failure properties between samples and is therefore related to the flaw size distribution in the granules. The larger the value of  $m$ , the narrower the crush strength distribution.

Due to the number of particles to be tested, using individual particle crush strength to measure granule strength distributions is tedious and time-consuming. A simpler test is to compact a bed of particles in confined, uniaxial compression. The first inflection point in the compaction curve is assumed to be the point at which granules are crushed into their primary particles and is therefore a measure of average granule crush strength (see Adams and McKeon, 1998). However, not all the granules undergo the same stress in this test, so it is not a true measurement of the granule property distribution.

Traditionally, fracture toughness of materials is measured from the energy absorbed when a bar with a crack of known geometry is fractured in tension via a three-point bend test (Figure 9.3a). For purely brittle fracture, the fracture toughness is given by:

$$K_c = Y\sigma_f (\pi c)^{1/2} \quad 9.19$$

where  $c$  is the crack length,  $\sigma_f$  is the applied stress at fracture, and  $Y$  is a geometric constant. Agglomerates and compacts rarely give completely brittle failure. Instead, there is microcracking (equivalent to plastic deformation) in the process zone at the crack tip (Figure 9.4). In this case, Equation 9.19 is modified to:

$$K_c = Y\sigma_f (\pi(c + \delta_c))^{1/2} \quad 9.20$$

where  $\delta_c$  is the process zone size.

The challenge with using this approach is to reproducibly form a bar with uniform packing density and interparticle bonding that are similar to the real agglomerates of interest. An alternative approach is using micro- or nano-indentation (Figure 9.3b). In this approach, the force–displacement curve for indentation is measured using an indenter of well-defined geometry which gives the elastic modulus  $E$  and the yield strength  $\sigma_y$ . The hardness of the agglomerate  $H$  is calculated as:

$$H = \frac{F}{A} \quad 9.21$$

where  $F$  is the applied force and  $A$  is the area of indentation.

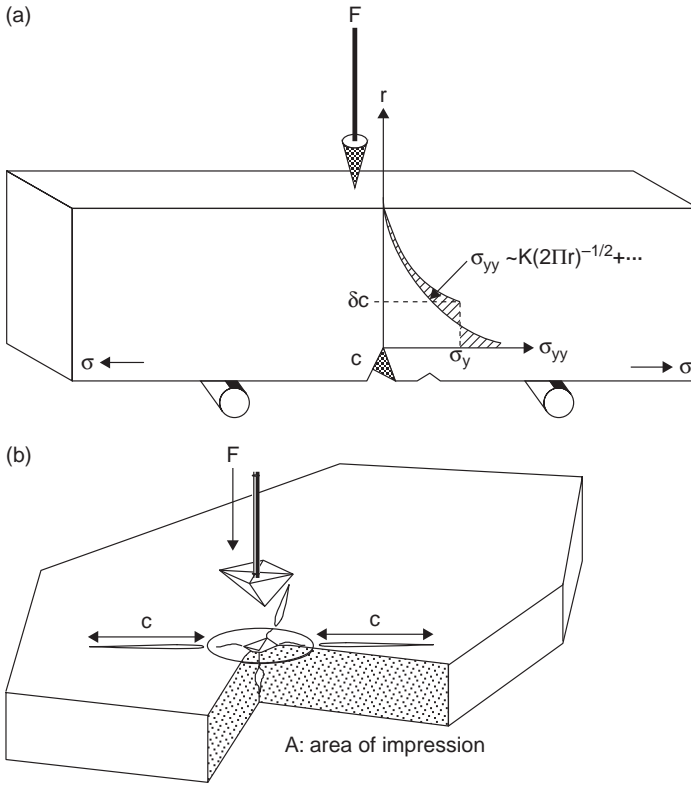


**Figure 9.3** Measurement of agglomerate fracture properties using (a) three-point bend test on a manufactured agglomerate bar; and (b) indentation of a compact or agglomerate (Litster and Ennis, 2004).

If radial cracks form from the corners of the indentation, indicating brittle failure, the fracture toughness can be calculated as:

$$K_c = \beta \left( \frac{E}{H} \right)^{1/2} \frac{F}{c^{3/2}} \tag{9.22}$$

where  $c$  is the crack length and  $\beta$  is a geometry-dependent constant. This approach has been used to measure  $K_c$  for regular particles such as single crystals. The fracture toughness of an agglomerate is a physically sensible concept when the agglomerate is large compared to the primary particle size. When  $d_g < 9d_p$ , treating the agglomerate as a continuous solid matrix is less reasonable. When the indentation method is used, the indent needs to be large compared to the primary particle size but small compared to the size of an agglomerate.

Breakage of granules during impact can also be used to measure fracture properties, provided that the equipment is designed so that the impact velocity of the

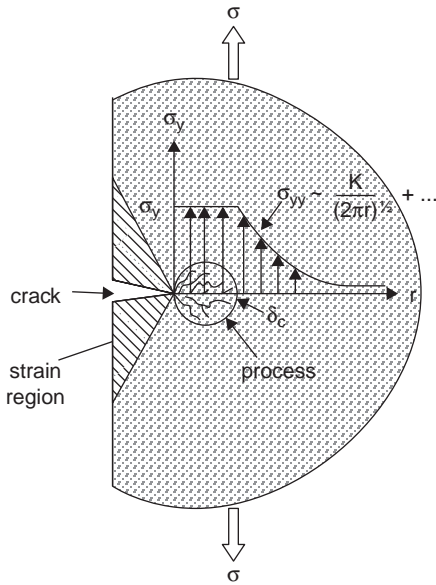


**Figure 9.4** Fracture of a brittle material via crack propagation (Litster and Ennis, 2004).

particle or agglomerates is well known. A good design for single-impact tests at high velocity is given by Papadopoulos and Ghadiri (1997). A novel resonant cantilever shaker that can measure fatigue cracking from multiple impacts is given by Beekman *et al.* (1998).

There are a wide variety of empirical tests used to measure granule strength indices. Often, the size distribution of granules, particularly the fraction of fines, after a particular type of handling is used as a measure of strength or attrition resistance. These empirical tests include drop tests, pneumatic conveying loops, fluidized beds, and vibrating screens. In all cases, the stress history of the particles is not well defined, so it is difficult to extract particle properties from the results. The mode of failure may vary in different tests, and the ranking of different materials in the different tests is therefore not always the same. Such empirical tests should be used with great caution, if at all. A good question to ask when critically examining a breakage test is: *Is the impact velocity or applied stress to the agglomerate well defined and measured?* If the answer is “no,” this is not a good test. Remember our motto from Chapter 2: *Measure properties, do not perform rituals.*

Typical values of the mechanical properties of agglomerates lie in the range (Bika *et al.*, 2001):

Yield strength: 20–300 MPa

Fracture toughness: 0.03–5 MPa m<sup>-0.5</sup>

Process zone size: 0.1–1 mm

Elastic modulus: 0.1–10 GPa

Agglomerates are generally weaker, and have larger process zone size, than single crystals or metals. As we would expect from our micromechanical models, yield strength and fracture toughness are higher for low-porosity compacts than for high-porosity granules.

## 9.5 Agglomerate Attrition and Breakage

The type and extent of breakage of an agglomerate under stress depend on the material properties and the mode of application of stress. If the agglomerate has a relatively small process zone size, then the agglomerate will break by brittle fracture into a relatively small number of fragments (*fracture mechanism*). If the process zone size is large, elastic energy is dissipated by microcracking near the point of stress application. This leads to the generation of a large amount of fines (*wear, erosion, attrition*) – see Figure 9.5. Agglomerates can have significant process zone size. Therefore, attrition and erosion are the main modes of failure for agglomerates during handling.

During processing and handling, agglomerates typically break in one of three stress modes: wear and attrition, impact, or compaction. The rate of attrition due to impact for single particles is given by Ghadiri *et al.* (1991):

$$\dot{V} \propto \frac{\rho_p U_c^2 d_p H}{K_c^2} \quad 9.23$$

where  $U_c$  is the impact velocity and  $\dot{V}$  is the volumetric attrition rate. The attrition rate is a strong function of fracture toughness. Tough materials resist attrition by impact. In contrast, the attrition is proportional to hardness. Hard materials concentrate stress at the impact point and increase the probability of fracture by stress concentration.

Agglomerates give more variable results with the type of damage depending on the distribution of porosity (flaw size distribution). Two breakage regimes are observable: wear (localized breakage) and fragmentation. Subero and Ghadiri (2001) developed a regime map for agglomerate breakage where the likelihood of fragmentation increases with both impact velocity and non-uniformity of granule structure; i.e., the presence for macrovoids in the agglomerate (Figure 9.6). In general, single-impact material loss scales with  $v_i^m$  over seven orders of magnitude, although other researchers find varying values of  $m \neq 2$  (Figure 9.7). Equation 9.23 and similar relationships are useful for estimating agglomerate damage and attrition where high-velocity impacts are important – e.g., during pneumatic conveying.

For abrasive wear of agglomerates when an indenter is dragged across the agglomerate surface, we can write (Evans and Wiltshire, 1976):

$$\dot{V} \propto \frac{d_l^{0.5} P^{1.25} l}{A^{0.25} K_c^{0.75} H^{0.5}} \quad 9.24$$



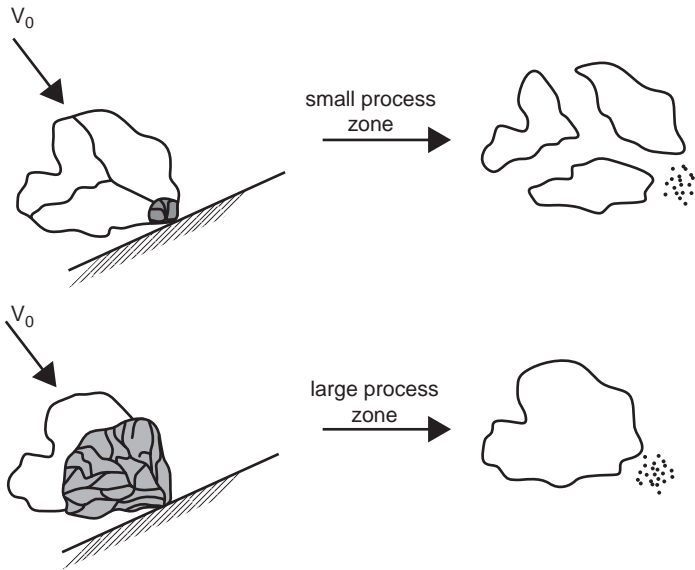


**Figure 9.5** Failure by (a) fracture, and (b) erosion/attrition depending on process zone size (Litster and Ennis, 2004).

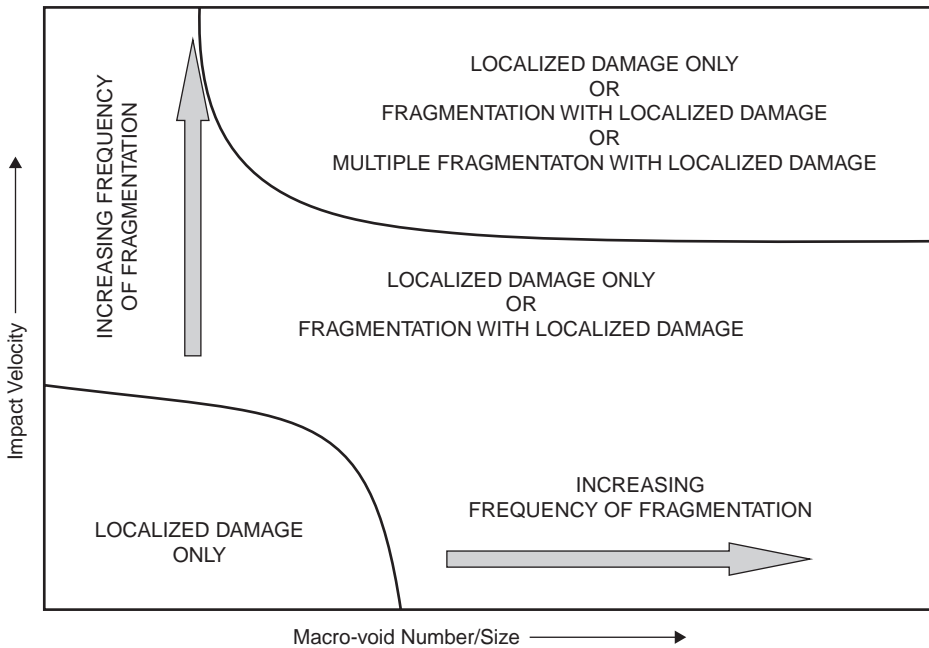


**Figure 9.6** Regime map for agglomerate breakage on impact (Subero and Ghadiri, 2001).

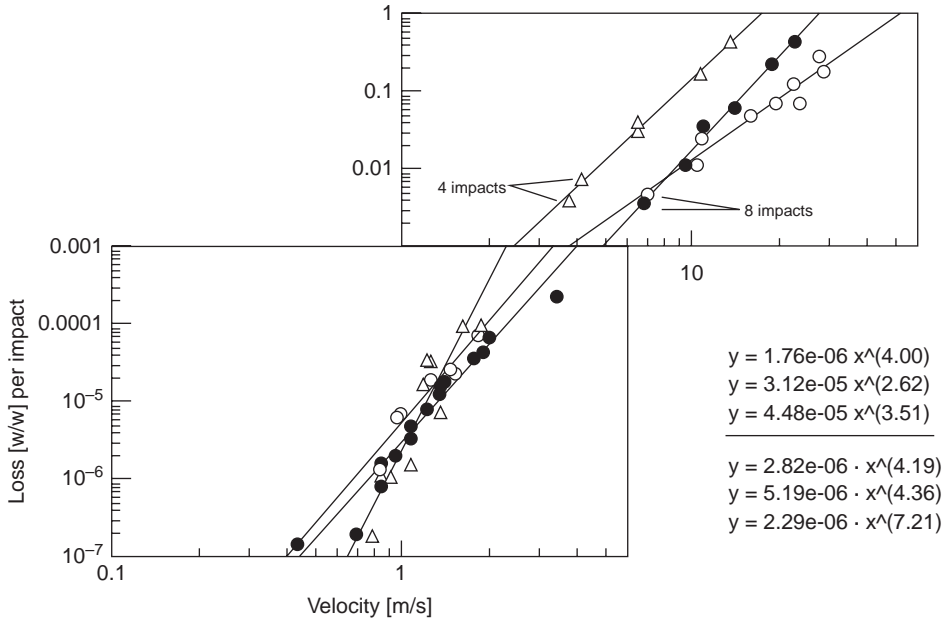


**Figure 9.7** Fractional mass loss of agglomerates showing power law dependence on velocity (Gentzler and Michaels, 2004).

where  $d_i$  is the indenter diameter,  $P$  is the applied normal load,  $l$  is the indenter displacement, and  $A$  is the apparent contact area of the indenter with the surface. Note that there is a different dependence of attrition rate on material properties when compared to impact attrition. Hard materials are more resistant to wear; i.e.,  $H$  appears in the denominator of Equation 9.24. Qualitatively, increasing fracture toughness reduces attrition rate by either impact or wear. However, quantitatively, impact attrition is more sensitive to changes in fracture toughness.

### 9.5.1 A Case Study – Fluid Bed Attrition of Agglomerates

Consider the attrition of agglomerates in a fluidized bed that could occur during agglomerate drying or other processing. What type of attrition mechanism do we expect to see?

Fluidized beds have complex flow patterns where bubbles play an important role (see Section 8.6.3). More than one mechanism of attrition is possible. There is likely to be some impact attrition where particles are thrown up from the bed and hit walls or internals. However, the majority of contacts with the vessel and other particles occur at low velocity where particles are shearing against each other. This mechanism is closer to wear, rather than impact. The number of collisions will depend on the excess gas velocity  $U - U_{mf}$  because this is directly related to the amount of bubbles in the bed, and the bed height  $H_b$  because this is proportional to

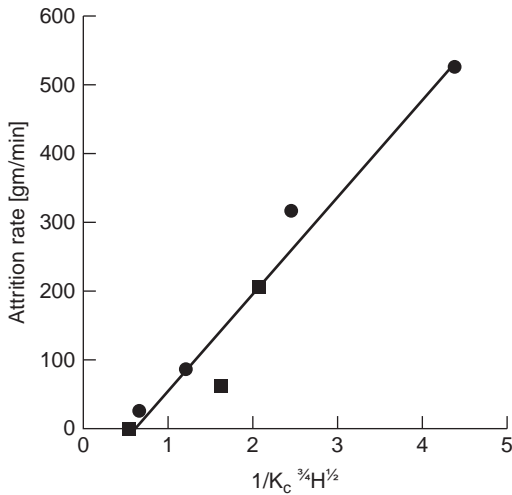


**Figure 9.8** Attrition rate of agglomerates in a fluidized bed as a function of their material properties (Ennis and Sunshine, 1993).

the pressure in the bed. By analogy to Equation 9.24, Ennis and co-workers (Ennis and Sunshine, 1993; Litster and Ennis, 2004) suggested the following equation for attrition in the fluidized bed:

$$\dot{V}_{fb} \propto \frac{d_o^{0.5} H_b^{1.25} (U - U_{mf})}{K_c^{0.75} H^{0.5}} \quad 9.25$$

where  $d_o$  is the gas distributor orifice diameter.

A variety of herbicide materials and model systems were formed into bars and their fracture properties measured. The measured erosion rates in the fluid bed are plotted as a function of  $1/(K_c^{0.75} H^{0.5})$  in Figure 9.8. There is a strong linear relationship between the property grouping for erosion by wear and the erosion rate in the fluidized bed, confirming we can accurately predict the relative erosion rate in the fluid bed for different formulations.

How do we control the agglomerate properties to control the attrition rate? This is a classic *reverse engineering* problem. From our micro-mechanical understanding of agglomerate strength (Section 9.3), we might conclude the agglomerate strength is a strong function of:

1. the strength of the bonds between particles in the agglomerate ( $F_b$  in Equation 9.16); and
2. the agglomerate porosity  $\epsilon_g$  and any macrovoids or flaws  $c$ .

The bond strength is essentially a formulation issue. For example, it may depend on the yield strength of the polymer binder, the amount of binder added, and how well

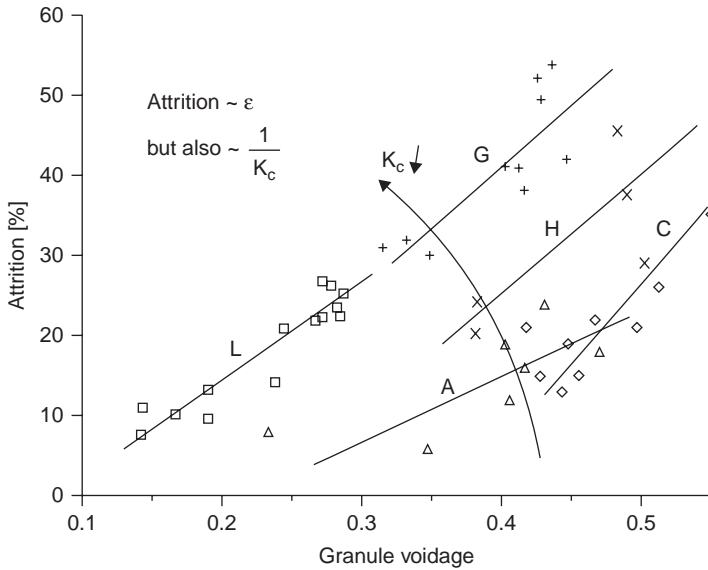


**Figure 9.9** Effect of granule porosity on fluidized bed attrition of five agricultural formulations (Litster and Ennis, 2004).

the binder bonds to the particle. Agglomerate porosity is mainly set by the process conditions at which you make the agglomerate, such as the residence time for wet granulation (Chapter 8) or the roll pressure for roll compaction (Chapter 9).

Figure 9.9 shows the attrition rate in a fluidized bed for several different herbicide formulations as a function of granule porosity (voidage). Clearly, both the formulation type and agglomerate porosity have a major effect on the amount of attrition. Reverse engineering problems do not generally have one unique solution because we have a number of degrees of freedom in choosing both process parameters and formulation properties.

## 9.6 Summary

Resistance to attrition and fracture during processing, handling, and transportation is an important attribute of particulate products, especially agglomerates, granules, compacts, and tablets. We don't have perfect models to predict these processes, but the models we do have are useful for quantitative engineering.

At a macroscopic level, we can define agglomerate properties based on material science for more uniform materials – yield strength, Young's modulus, hardness and fracture toughness (see Section 9.4). Agglomerates often behave as semi-brittle materials during attrition and fracture. Porosity can be viewed as “flaws” and the flaw size distribution, especially the size of the largest flaw, and fracture toughness of the agglomerate and key properties to predict behavior. Agglomerates have large

process zone sizes when compared to more uniform materials, making failure by attrition more common than failure by fracture.

Measuring the properties is tricky. Three-point bend tests, indentation, and single agglomerate crush tests, and well-designed impact tests can all be used. Tests are easiest, and results make most sense, when the agglomerate is much larger than the primary particle size. Empirical tests where the stress state of the agglomerate or particle is not known should be avoided.

When these key properties are known, relationships such as Equations 9.20 to 9.22 can be used to predict relative rates of attrition or fracture and to design handling systems. These relationships also let us rank the attrition resistance of different products. If we want to change (*reverse engineer*) the product attributes, we need micro-mechanical models that relate the agglomerate properties to agglomerate structure (often controlled by the agglomeration process) and the bond strength between primary particles (often controlled by the formulation properties). The models of Rumpf and Kendall (Section 9.3) are very useful in this regard. While both models have some fairly significant assumptions, they are very useful for predicting quantitative trends and making decisions on process or formulation changes.

## 9.7 Bibliography

- Adams, M.J. and McKeon, R., 1998. Micromechanical analyses of the pressure–volume relationship for powders under confined uniaxial compression. *Powder Technology*, 88, 155.
- Beekman, W.J., Meesters, G.M.H., and Scarlett, B., 2002. Measurement of granule attrition and fatigue in a vibrating box. *Particle and Particle System Characterisation*, 19, 5–11.
- Bika, D.G., Gentzler, M., and Michaels, J.M., 2001. Mechanical properties of agglomerates. *Powder Technology*, 117, 98–112.
- Cheong, Y.S., Mangwandi, C., Fu, J., *et al.*, 2007. A mechanistic description of granule deformation and breakage. In Salman, A.D., Hounslow, M.J., and Seville, J.P.K. (eds.), *Handbook of Powder Technology vol. 11 – Granulation*, chapter 26, Elsevier, Amsterdam.
- Ennis, B.J. and Sunshine, G., 1993. On wear as a mechanism of granule attrition. *Tribology International*, 26, 319.
- Evans, A.G. and Wiltshire, T.R., 1976. Quasi-static solid particle damage in brittle solids – I. Observations analysis and implications. *Acta Metallurgica*, 24, 939–959.
- Gentzler, M. and Michaels, J.N., 2004. Impact attrition of brittle structured particles at low velocities: Rigorous use of a laboratory vibrational impact tester. *Chemical Engineering Science*, 59, 5949–5958.
- Ghadiri, M., Moreno-Atanasio, R., Hassanpour, A., and Antony, S.J., 2007. Analysis of agglomerate breakage. In Salman, A.D., Ghadiri, M., and Hounslow, M.J. (eds.), *Handbook of Powder Technology vol. 12 – Breakage*, chapter 19, Elsevier, Amsterdam.
- Ghadiri, M., Yuregir, K.R., Pollock, H.M., Ross, J.D.J., and Rolfe, N., 1991. Influence of processing conditions on attrition of NaCl crystals. *Powder Technology*, 65, 311–320.
- Johnson, K.L., Kendall, K., and Roberts, A.D., 1971. Surface energy and the contact of elastic solids. *Proceedings of the Royal Society of London. Series A*, 324, 301–313.

- Kendall, K., Alford, N., and Birchall, J.D., 1986. The strength of green bodies. *Ceram. Proc.*, 8, 255–265.
- Litster, J.D. and Ennis, B.J., 2004. *The Science and Engineering of Granulation Processes*, chapter 5, Kluwer Academic Publishers, Dordrecht.
- Papadopoulos, D.G. and Ghadiri, M., 1996. Impact breakage of poly-methylmethacrylate (PMMA) extrudates: I. Chipping mechanism. *Advanced Powder Technology*, 7, 183.
- Rumpf, H., 1962. The strength of granules and agglomerates. In Knepper, W.A. (ed.), *Agglomeration*, Interscience, New York, 378–418.
- Subero, J. and Ghadiri, M., 2001. Breakage patterns of agglomerates. *Powder Technology*, 120, 232–243.

## 9.8 Problems

- 9.1. For each of the Rumpf and Kendall models, produce a graph of how agglomerate strength varies with porosity over the range 0.25 to 0.5. What do you conclude about the importance of granule structure in determining granule strength? (You may assume the porosity is very uniform within the agglomerate.)
- 9.2. A ceramic compact is formed from 5  $\mu\text{m}$  particles. The compact porosity is 0.27 and we have measured the yield strength to be 200 kPa. One batch of primary particles is contaminated with 1% by volume of sand grit (250  $\mu\text{m}$ ). Our production engineer is not too concerned: “The grit is only 1% by volume so it will not affect the compact strength substantially.” Do you agree? Justify your answer as quantitatively as possible.
- 9.3. I have formed a granulated product by high-shear wet granulation using a 2% polymer binder in the liquid phase. During fluid bed drying of this material, the attrition rate of the dried granules is too high. Our formulation scientist has suggested increasing the amount of polymer binder to 4% to increase the bond strength between primary particles in the dry granules while keeping the overall liquid to solid ratio during granulation on constant. However, the higher binder content increases the liquid viscosity during granulation and results in a higher porosity in the dried granules (0.45 compared to 0.35 for the original formulation). Use Rumpf’s model to decide if adding additional polymer has increased the granule strength.
- 9.4. In a crush test for dried granules, the three quartiles for cumulative yield strength distribution are:  $\sigma_{75} = 315$  kPa;  $\sigma_{50} = 405$  kPa;  $\sigma_{25} = 494$  kPa. If the strength follows a Weibull distribution:
  - a. What are the Weibull parameters for this material?
  - b. My product quality specification is that no more than 1 in 1,000 granules fail if they are stressed at  $\sigma = 100$  kPa. Do these granules meet this specification?
- 9.5. My product handling facility involves the pneumatic conveying line. CFD simulations indicate the maximum impact velocity of 150  $\mu\text{m}$  crystals in the line is 12  $\text{m s}^{-1}$  and a vertical to horizontal corner. When used for glutamic acid crystals, the level of crystal damage is acceptable. We now wish to use the system for lysozyme crystals which seem to be more fragile.

- a. Estimate how much greater attrition/crystal damage you expect to see.
- b. We are considering moving to dense-phase pneumatic conveying, in which attrition is likely caused by wear (many low-velocity impacts). How do the relative resistances of glutamic acid and lysozyme crystals compare in this scenario?

Mechanical properties measured by indentation:

	$H$ (MPa)	$E$ (GPa)	$K_c$ (MPa m <sup>1/2</sup> )
Glutamic acid	2100	32	$68 \times 10^{-3}$
Lysozyme	15	0.49	$1.6 \times 10^{-3}$

- 9.6. I am producing a granulated product in a fluid bed granulator using a solution of polymer binder to spray onto inert particles. One of the requirements is to minimize dust formation during handling in the bagging plant, which involves pneumatic conveying to a hopper above a bagging station. Design a helpful troubleshooting guide for operators, engineers, and formulators on ways to minimize attrition through:
- a. improved design and operation of the handling system;
  - b. improved granule properties through operation of the fluid bed granulator; and
  - c. improved granule properties through formulation changes.

Present your guide as a table with a row for each process parameter or formulation property you are considering. Give the effect of each variable. Be quantitative if possible. Reference the equations/sections in this book you use to justify your advice.

# 10 Dispersion, Disintegration, and Dissolution

## 10.1 Consider a Case Study ...

*3P Consulting Inc.*

Memo to: Purdue Powder Processing Team  
Memo from: Jim Litster  
March 6, 2014

### **Dissolving Water-dispersible Granules**

3P Team, you did such a good job reducing the dust problems at the water-dispersible granule plant (see Chapter 9 case study) that our client has retained us to look at another problem with the product.

The granules need to quickly (ideally instantaneously) disperse and dissolve when the farmer adds them to his herbicide mixing tank on the farm. However, customers are frequently reporting a sludge at the bottom of the tank, and spray nozzles on the farm equipment are frequently being blocked by grit from undissolved granule fragments. Sometimes granules float on top of the water in the tank and form a muddy clump.

We have been asked to review the standard design for the mixing tanks and develop a series of operating instructions for farmers to ensure complete dispersion and dissolution. Once again, the problem is more prevalent in some formulations than in others. There are conflicting reports from company representatives in the field as to whether the problem correlates with the primary particle size of the active ingredient in the granules. Although our client has not suggested this, I am concerned that the process and formulation changes we suggested to make the granules stronger may now be contributing to the dispersion problem.

I can supply you with details of the standard mixing tank specifications as well as samples of granules for testing and analysis. Please give this your urgent attention. Can you report back within one month?

As an individual reflection, or in a group discussion, review the case study above. How do you design a mixing tank for dissolution? Are you concerned with the size of the primary particles or with the size of the granules? Why might the granules “float” when added to the tank? Is it possible to make strong granules that also disperse easily? Are granules harder to disperse if they are old?

Engineers and technologists spend large amounts of time and money building up complex structured particulate products. In many cases, however, their key performance criteria relate to how these structures are deliberately broken down.



Product performance is dominated by the three Ds: *Dispersion*, *Disintegration*, and *Dissolution*. There are many examples of such products:

- pharmaceuticals and agricultural chemicals for which ultimate delivery of active ingredients where and when you want them is essential;
- “instant” food products such as dried milk, coffee, and juice;
- powdered and granular detergents; and
- paint, pigments, and fillers for polymers where the ultimate product is a fine particle suspension in a fluid.

In the first three cases, the product is supplied as a purposely constructed agglomerate of smaller primary particles. In the case of dispersing powders, the agglomerates form naturally, due to the cohesivity of the primary particles. In either case, the agglomerates must be dispersed into smaller particles. In the ideal situation, agglomerates are dispersed into their constituent primary particles.

This chapter gives you tools to help understand and predict the dispersion and dissolution of powders and particulate delivery forms such as granules and tablets. Product modeling in this area is complex as many different processes may be controlling the dispersion and dissolution rate. Nevertheless, quantitative analysis of limiting cases is possible and is a powerful tool for product design and analysis.

## 10.2 Learning Goals

At the completion of this chapter, the student should be able to:

1. Describe the different mechanisms by which agglomerates disperse in both gases and liquids.
2. Estimate the dispersion rate of an agglomerate in a gas for a known, simplified flow field.
3. Explain the similarity between agglomerate dispersion and particle breakage.
4. Estimate the agglomeration filling time and dispersion rate of an agglomerate in a liquid due to liquid imbibition.
5. Calculate the dissolution time for a single particle within a stirred tank for (a) stagnant conditions, and (b) non-zero slip velocity.
6. Use the population balance to calculate the dissolution rate of a size distribution of particles.
7. Attack open-ended particle design and troubleshooting problems related to particle dispersion and dissolution of a similar nature to the introductory case study for this chapter.

## 10.3 Overview of Agglomerate Dispersion

Figure 10.1 shows schematically the possible steps for the case of dispersing a single large agglomerate, like a pharmaceutical tablet, and dissolving one or more of the

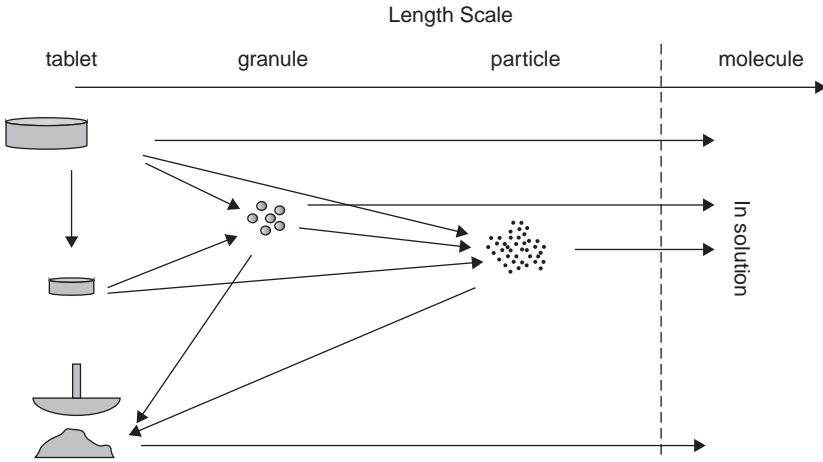


Figure 10.1 Agglomerate dispersion and dissolution pathways.

constituents into a liquid in an agitated tank. There are many pathways to dispersion and dissolution. The agglomerate can disintegrate into many smaller agglomerates (granules), which subsequently disperse into particles. Alternately, the large agglomerate can erode to form small particles directly. If the small particles are soluble, they will dissolve by molecular diffusion into the liquid. If they are small aggregates of soluble and insoluble compounds, the soluble compound can leach out of the particle and then diffuse into the bulk liquid. Finally, if the agitation rate is insufficient to fluidize the small agglomerates, they will form a pile at the bottom of tank. Further dispersion will cease, and dissolution will be very slow and irreproducible.

Dispersion is the process of breaking down an agglomerate into primary particles. It has a lot in common with milling – arguably, it is a type of milling. Dispersion is differentiated by:

- Strength of particles: Agglomerates are typically much weaker than monolithic particles.
- Ultimate state: Dispersion ends when the agglomerate is fully dispersed into primary particles. Primary particles ideally remain unbroken.

Because agglomerates are relatively weak, dispersion generally requires lower mechanical stresses than particle fracture. The mechanical stress can be applied through collisions as in milling (interparticle or particle–surface), and by exposure to shear in a liquid or gas, including simple shear and extensional flow. In each case, an agglomerate will start to break into primary particles when the applied stress exceeds a fracture strength that scales with the interparticle forces that hold the agglomerate together. Agglomerates may *rupture* into large daughters or *erode* by slow removal of primary particles from a shrinking parent agglomerate. They can also shatter if the daughter agglomerates are weaker than the parent, although this is less common.

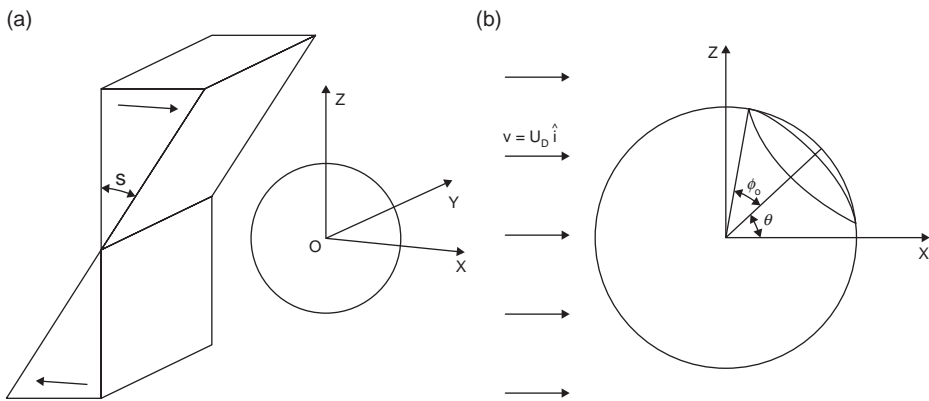


**Figure 10.2** Sphere in a simple shear field (a), and accelerated by a uniform flow field (b) (Bagster and Tomi, 1974).

In all cases, break up of agglomerates may be characterized by a dimensionless *fragmentation number*,  $Fa$ , which is the ratio of the applied stress to the intrinsic cohesive strength of the agglomerate:

$$Fa = \frac{\sigma_{app}}{\sigma_c} \quad 10.1$$

The applied stress can be a tensile or shear stress resulting from the relative motion of the particle in a fluid or collisions between particles or with the walls of a container or dispersing device. The agglomerate strength is determined by its structure and the strength of bonds holding the primary particles together as described in Section 9.3 (see Equations 9.5, 9.16 and Table 9.1). Depending on the nature of the agglomerate and the stresses that it encounters, it can fail by tension or by shear.

Clearly, the agglomerate will not disperse when the fragmentation number is less than unity. When  $Fa \geq 1$ , the agglomerate will begin to erode. At higher values of  $Fa$ , the probability of rupture increases.

In general, the applied stress cannot be calculated a priori. In both shear- and collision-induced dispersion, this stress depends on both the flow fields and agglomerate size and shape, which in systems of practical importance are highly complex. However, there are a small number of ideal systems that provide useful insight into the magnitude of the applied stress and how it varies with system properties. For example, Bagster and Tomi (1974) calculated tensile and shear stresses on an impermeable spherical particle in a simple shear field with shear rate  $\dot{\gamma}$  and accelerated by a uniform flow field with velocity  $U_o$ .

The analysis yields both the maximum shear and tensile stresses applied by the fluid on the particle and the location of the maximum stress. These are summarized in Table 10.1.

**Table 10.1** Applied stresses on a sphere in fluid flow (Bagster and Tomi, 1974)

Shear field	Maximum shear stress	Maximum tensile stress
Agglomerate in steady simple shear, shear rate $\dot{\gamma}$	$8.5\mu\dot{\gamma}$ On $y$ - $z$ plane through origin through center of agglomerate	$5\mu\dot{\gamma}$ On $y$ - $z$ planes through origin inclined $\pm 45^\circ$ from vertical
Agglomerate accelerated by uniform flow, velocity $U_o$	$3\mu U_o/d_{agg}$ On circumference of agglomerate on plane through $y$ -axis inclined $45^\circ$ to $x$ -axis	$3\mu U_o/2d_{agg}$ On circumference of agglomerate on $x$ - $y$ plane

An interesting result of this analysis is that the applied stresses on an agglomerate in a simple shear field are independent of the agglomerate size. The shear and tensile strength of the particle is also independent of its size. This implies that the fragmentation number is size-independent; i.e., there is a critical shear rate above which all agglomerates begin to fracture and will continue to erode and or rupture until they are fully dispersed into primary particles. Similarly, the stresses on an agglomerate accelerated by a uniform flow field scale with  $1/d_{agg}$ , implying that at a given fluid velocity, there's a critical agglomerate size below which all agglomerates will be fully dispersed.

Reality is more complicated. Large agglomerates typically don't disperse into primary particles; rather, they break down into smaller agglomerates. The rate and extent of dispersion typically increase with fragmentation number. The dependence on agglomerate size arises from size-dependence of the agglomerate strength. Agglomerates are intrinsically heterogeneous, which means that their tensile and shear strength is not uniform. When stressed, they break at their weakest points (flaws); the daughter particles will tend to be stronger, because the weakest flaws are eliminated as the parent breaks.

Finally, if particles collide, either with each other or with a process boundary such as an impeller or wall, the collision imparts a tensile stress through the middle of the particle along the axis of collision (Calvert *et al.*, 2009):

$$\sigma_T = \frac{2}{3} \rho_p d_p \left( \frac{v_i}{\Delta t} \right) \tag{10.2}$$

where  $v_i$  is the impact velocity and  $\Delta t$  is the impact time. In this case, the applied stress scales with the aggregate particle size. Assuming that impact velocity doesn't vary with agglomerate size (which is probably not a great assumption!), the fragmentation number also scales with the aggregate size. This implies that in collisional dispersion, there is critical agglomerate size below which dispersion stops. Large agglomerates will disperse into smaller agglomerates, but they won't necessarily be dispersed to primary particles.

**Example 10.1** Estimate the relative magnitudes of the shear and impact stresses in a powder disperser using air to disperse the agglomerates with the following flow field and particle properties:

$$\mu = 2 \times 10^{-5} \text{ Pa s}; v = 1 \frac{\text{m}}{\text{s}}; d_p = 10^{-4} \text{ m}; \dot{\gamma} = 100 \text{ s}^{-1}; \rho_p = 1000 \text{ kg m}^{-3}; \Delta t = 10^{-3} \text{ s}$$

*Solution:*

We will use the simple Bagster and Tomi expressions from Table 10.1. The sudden acceleration stress is:

$$\sigma_T = \frac{3\mu v}{d_p} = \frac{3 \cdot 2 \times 10^{-5} \text{ Pa s} \cdot 1 \frac{\text{m}}{\text{s}}}{10^{-4} \text{ m}} = 0.6 \text{ Pa}$$

The stress due to constant shear stress is:

$$\sigma_T = 8.5\mu\dot{\gamma} = 8.5 \cdot 2 \times 10^{-5} \text{ Pa s} \cdot 100 \text{ s}^{-1} = 1.7 \times 10^{-2} \text{ Pa}$$

Equation 10.2 gives the stress due to impact:

$$\sigma_T = \frac{2}{3} \rho_p d_p \left( \frac{v_i}{\Delta t} \right) = \frac{2}{3} \cdot 1000 \text{ kg m}^{-3} \cdot 10^{-4} \text{ m} \cdot \left( \frac{1 \text{ ms}^{-1}}{10^{-3} \text{ s}} \right) = 66 \text{ Pa}$$

Clearly, the stresses imparted by impact are greater than by shearing in the gas phase. The former will be sufficient to disperse very weak agglomerates (i.e., low-density cohesive agglomerates) but insufficient to break stronger ones. Also, if a device promotes collisions, impact breakage is likely to dominate the dispersion kinetics. In a generic sense, aerodynamic dispersion is no different than aerodynamic milling – i.e., an air-jet mill.

Because dispersion to primary particles is typically incomplete, it is useful to have a metric that describes the extent of dispersion. A *dispersion efficiency*,  $\eta_T$ , can be defined by comparing the particle size distributions of the dispersed agglomerates and their constituent primary particles (Masuda and Gotoh, 1995):

$$\eta_T = \int_0^{d_p^*} f_D(x) dx + \int_{d_p^*}^{\infty} f_o(x) dx \quad 10.3$$

where  $f_o$  and  $f_D$  are the size distributions of primary particles and agglomerates, respectively, and  $d_p^*$  is the particle size at which the two distributions intersect (see Figure 10.3).  $\eta_T$  is the shaded area where the two distributions overlap. Complete dispersion yields  $\eta_T = 1$ . Note that  $\eta_T$  is not a perfect metric, as it is not necessarily zero when there is no dispersion.

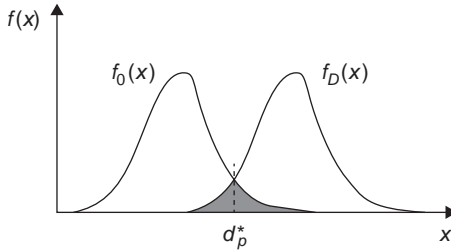


**Figure 10.3** Illustration of the definition of dispersion efficiency,  $\eta_T$ .

## 10.4 Dispersion by Gases

In applications that require dry dispersed particles, agglomerates must be dispersed in gases. This is called aerodynamic dispersion. Examples include dry powder inhalers for administering pulmonary drugs and dry powder dispersers for particle size analyzers. Dry dispersion can occur by accident rather than design: in this case, it is called attrition. An example of this is particle attrition in pneumatic conveying systems.

In aerodynamic dispersion, agglomerates are entrained in a gas flow. There are many geometries designed to establish different flow fields, with or without impact (see Figure 10.4). Some are turbulent, others laminar. Mechanical stress is applied to the particles by the fluid directly or by impact with other particles or solid surfaces in the dispersing device.

As noted in Example 10.1, the tensile stress induced by impact is much larger than the viscous stresses impressed on an agglomerate by a flowing gas. For this reason, aerodynamic dispersion is dominated by collisions. Shear stresses in the gas phase (even in turbulent systems) are capable of dispersing only very weak agglomerates.

The discussion so far has dealt only with the stresses that agglomerates experience in aerodynamic dispersion. How do we turn this into kinetics? One approach is to develop rate expressions that are explicit in velocity or shear rate. In fact, we have already done this in Chapter 9 when we considered agglomerate strength and attrition. The relationships developed in Section 9.5 (especially Equations 9.20 and 9.21, and Figures 9.6 and 9.7) are useful in developing such rate expressions for aerodynamic dispersion.

We have seen in earlier chapters that particle collisions can also result in agglomeration. Aerodynamic dispersion actually involves a balance between dispersion and reagglomeration. This is similar to the balance between agglomeration and breakage in aerosol reactors (see Equation 6.47 in Section 6.7). If the order of the breakage rate is greater than zero order with respect to particle size, then an equilibrium distribution with a balance between breakage and agglomeration is achieved. For impact breakage, we know from Equation 10.3 that  $\eta_{br} = 1$ . The

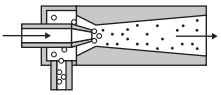
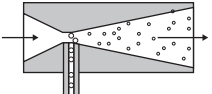
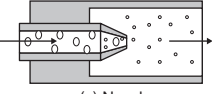
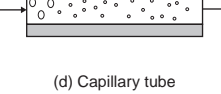
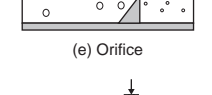
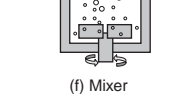
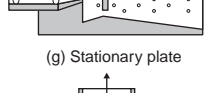
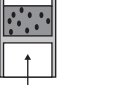
Disperser type	Dispersion mechanisms	Comments
 <p>(a) Eductor</p>	<ul style="list-style-type: none"> <li>• Acceleration and/or shear flow</li> <li>• Collisions with other particle clusters and device walls</li> </ul>	Powders are dispersed reasonably well due to large relative velocity. May find fine, extremely cohesive materials difficult to disperse
 <p>(b) Venturi</p>	<ul style="list-style-type: none"> <li>• Acceleration and/or shear flow</li> <li>• Collisions with other particle clusters and device walls</li> </ul>	The relative velocity difference is possibly not great enough for dispersing fine cohesive materials
 <p>(c) Nozzle</p>	<ul style="list-style-type: none"> <li>• Acceleration and/or shear flow</li> <li>• Collisions with other particle cluster and device walls</li> </ul>	The powder is already entrained in a pressurized air stream. Therefore, the nozzle may not generate sufficient separating forces
 <p>(d) Capillary tube</p>	<ul style="list-style-type: none"> <li>• Acceleration and/or shear flow</li> <li>• Impaction as the powder enters the tube</li> </ul>	It is shown that dispersion occurs at the instant the powder enters the tube and that changing the length does not enhance performance
 <p>(e) Orifice</p>	<ul style="list-style-type: none"> <li>• Acceleration and/or shear flow</li> <li>• Impaction on the orifice plate</li> </ul>	This device may disperse a wide range of materials due to impaction with rapid acceleration and deceleration. However, impaction may break fragile particles
 <p>(f) Mixer</p>	<ul style="list-style-type: none"> <li>• Acceleration and/or shear flow</li> <li>• Impaction impeller blades</li> </ul>	The mixer disperser has been shown to have good concentration control of exiting particles
 <p>(g) Stationary plate</p>	<ul style="list-style-type: none"> <li>• Acceleration and/or shear flow through the nozzle</li> <li>• Impaction on the stationary plate</li> </ul>	An addition to the nozzle disperser is to include an impaction plate. This may disperse extremely cohesive materials but is likely to also break particles
 <p>(h) Fluidized bed</p>	<ul style="list-style-type: none"> <li>• Acceleration from the fluidizing air</li> <li>• Impaction between the powder and the dispersing aids</li> </ul>	The fluidized bed disperser has been shown to disperse powder well, although collisions with dense dispersing aids may break particles and the air flow rate is limited to the point when dispersing aids are entrained

Figure 10.4 Typical powder dispersers (Calvert *et al.*, 2009).

balance then depends on the relative magnitude of the two competing rate processes. Agglomeration will be favored by lower dispersing force (lower gas velocity) and higher particle loading. Note that increasing the dispersion force above the point where breakage to primary particles dominates just wastes energy.

## 10.5 Dispersion and Disintegration of Agglomerates and Powders in Liquids

Dispersion of an agglomerate in a liquid involves a number of overlapping processes: wetting of the particles, imbibition of the fluid by the particle, and dispersion of the agglomerate. The strength of an agglomerate can be highly sensitive to the properties and amount of fluid imbibed, thus the kinetics of dispersion depend not only on the stresses applied to agglomerates by the flow field, but also to the physical properties of the fluid – i.e., viscosity and interfacial tension.

In contrast to aerodynamic dispersion, the viscous stresses on agglomerates are always significant. This is due to the large difference between gas and liquid viscosities. Higher liquid viscosities directly affect the applied shear and tensile stresses on particles, as shown in Table 10.1. In addition, the higher viscosity increases drag on particles, which causes them to remain in the streamlines of the flow. Particle Reynolds numbers are low; i.e., inertial forces are small compared to viscous forces. As a result, collisions with other particles and with boundaries are less likely than in aerodynamic dispersion. Together, this means that fragmentation induced by shear is more important in liquid-phase dispersion.

Agitation is therefore necessary for good dispersion. Most dispersion equipment consists of stirred tanks with specialized impellers, such as high-shear rotor-stators and high-speed dispersers. Dispersion of very small particles, such as pigments, may require higher stresses, such as those generated by stirred bead mills. All of this equipment is also used for wet milling, demonstrating again the similarity between dispersion and milling.

Dispersion in liquids is not fundamentally different than in gases. However, the situation is more complex, because the dispersing liquid (dispersant) can modify interparticle adhesion. There are four basic mechanisms for this.

1. *Dissolution of solid bridges or primary particles.* This is probably the primary mechanism by which granules made by wet granulation disperse. Dissolution of primary particles also reduces the contact area between particles, and this will reduce the adhesive force even in the absence of solid bridges.
2. *Modification of van der Waals and electrostatic forces.* Immersing particles in a liquid will reduce the van der Waals adhesive force relative to its value in a gas; i.e., the Hamaker constant between the solid and the liquid is smaller than that between the solid and the gas (see Table 9.1). If the particles are charged, a liquid can moderate the electrostatic interaction. If the dispersant is water, any ions in solution (they are always there) will adsorb to neutralize charge on the particle as well as form diffuse double layers – both will act to reduce the electrostatic attraction. It is possible to choose a dispersant composition to create a net repulsive electrostatic force between particles in order to facilitate and maintain dispersion.
3. *Creation or modification of capillary force.* In order for a dispersant to work, it has to penetrate into the agglomerate. This requires that it wets the particles. As the liquid penetrates and displaces the gas, it will form capillary bridges around



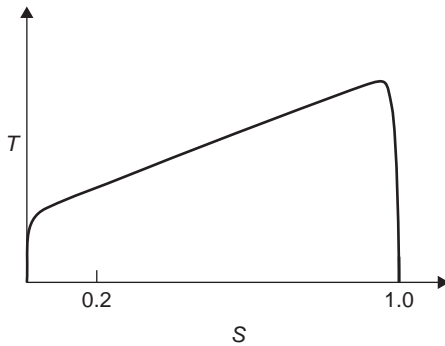


**Figure 10.5** Strength of a liquid-bound agglomerate as a function of liquid saturation.

particle contacts. These *add* strength to the contacts (Table 9.1). As the liquid saturation increases, the number and volume of capillary bonds increases, as does the agglomerate yield strength. Eventually, as pores fill, the curvature of individual bridges decreases and the tensile strength decreases. This is shown schematically in Figure 10.5. The ultimate strength of the fully saturated agglomerate may be less than the dry agglomerate if the fluid also significantly reduces the other forces holding it together. If the original agglomerate contains liquid bridges that are immiscible in the dispersant, they will remain in place as air is displaced and will continue to contribute to the tensile strength of the agglomerate. The strength of the bonds will change, however, because the controlling interfacial tension is  $\gamma^{ll}$  rather than  $\gamma^{lv}$ .

4. *Generation of internal mechanical stress:* If particles in an agglomerate can absorb the fluid, they will expand. If the agglomerate is rigid, this will generate an internal mechanical stress that can facilitate fracture of the agglomerate. In many applications, swelling materials are purposely added to agglomerates to speed disintegration. These materials are called *disintegrants*.

In order to be dispersed, initially dry particles must be able to imbibe the fluid and be imbibed by it. Poorly wetted solids will float on the fluid–air interface, and if they can be mechanically mixed into the fluid, the fluid will not be able to penetrate even low-density cohesive agglomerates. In this case, dispersion kinetics will either be controlled by the rate of engulfment into the fluid or by shear-induced agglomerate fracture. The latter can be analyzed with the same types of models as dry dispersion.

By selecting a dispersant that wets the agglomerates, engulfment of agglomerates from air into the liquid and imbibition of liquid into the pores of the agglomerates can become spontaneous. Spherical agglomerates will be spontaneously engulfed at the air–fluid interface when the contact angle is less than (Diao and Fuerstenau, 1991):

$$\cos\theta_{max} = 1 - \frac{d_p^2}{3\gamma_{LV}} g(\rho_S - \rho_L) \quad 10.4$$

Note that for neutrally buoyant agglomerates,  $\theta_{max} = 0$ . As the contact angle approaches this value, it becomes easier to engulf the particles by mechanical agitation.

Imbibition into an agglomerate is less stringent in terms of contact angle. If we model the pore structure of an agglomerate as an assembly of straight cylindrical pores, the maximum contact angle for spontaneous imbibition is  $\theta_{max} = 90^\circ$ . Real agglomerates don't have smooth pores, and the maximum contact angle for spontaneous imbibition is typically smaller (Yang and Xi, 1995).

Imbibition of liquid into an agglomerate is the same process as drop-imbibition into a dry powder (Chapter 8, Section 8.4.1), and it is described in the same way. The driving force is the capillary pressure difference across the advancing menisci in the agglomerate. The rate is controlled by the viscous drag of fluid in the pores as they fill. The only difference is that the liquid surrounds the initially dry agglomerate, and its volume is infinite compared to the pore space in the agglomerate. A Washburn-type analysis, which assumes that a channel exists for air inside the agglomerate to escape so it creates no back pressure on the advancing fluid front, yields the following expression for the imbibition rate into a spherical agglomerate of diameter  $d_{agg}$  (Bohin *et al.*, 1994):

$$16 \left( \frac{r}{d_{agg}} \right)^3 - 12 \left( \frac{r}{d_{agg}} \right)^2 + 1 = \Gamma t \quad 10.5$$

where  $r$  is the radius of the uninfiltrated core and  $\Gamma$  is the infiltration rate constant. Assuming the Blake–Kozeny relationship for drag in the pores of an agglomerate of monodisperse spheres of diameter,  $d_p$ :

$$\Gamma = \frac{7d_p \varepsilon^2 \gamma^{lv} \cos \theta}{75\mu d_{agg}^2 (1 - \varepsilon)} \quad 10.6$$

Note that the time to completely fill the agglomerate is:

$$t_{fill} = 1 / \Gamma \quad 10.7$$

It is useful to compare Equations 10.5 and 10.6 to the equation for drop penetration time given in Chapter 8 (Equation 8.4).

The extent of fluid infiltration into an agglomerate affects the agglomerate breakage rate and the size of fragments that are produced (Boyle *et al.*, 2005). Agglomerates can break by cohesive or adhesive failure (Figure 10.6). Cohesive failure occurs in agglomerates in which fluid infiltration doesn't change the packing structure of the agglomerate. In a partially infiltrated agglomerate, this means that the particles on the dry side of the infiltration boundary remain bound to those on the wet side. The tensile stress applied to the agglomerate by the shear field is transmitted to both the infiltrated and dry regions. The particle breaks at a fracture plane that goes through both regions: failure is by cohesive failure of both infiltrated and dry regions.

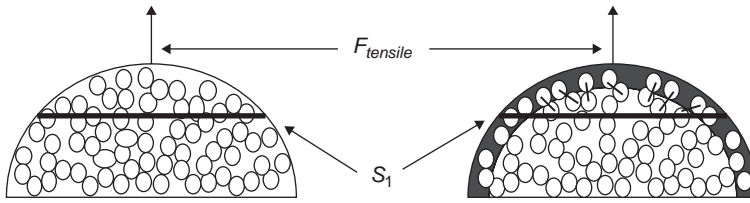


**Figure 10.6** Cohesive and adhesive failure of agglomerates depending on liquid imbibition (Boyle *et al.*, 2005).

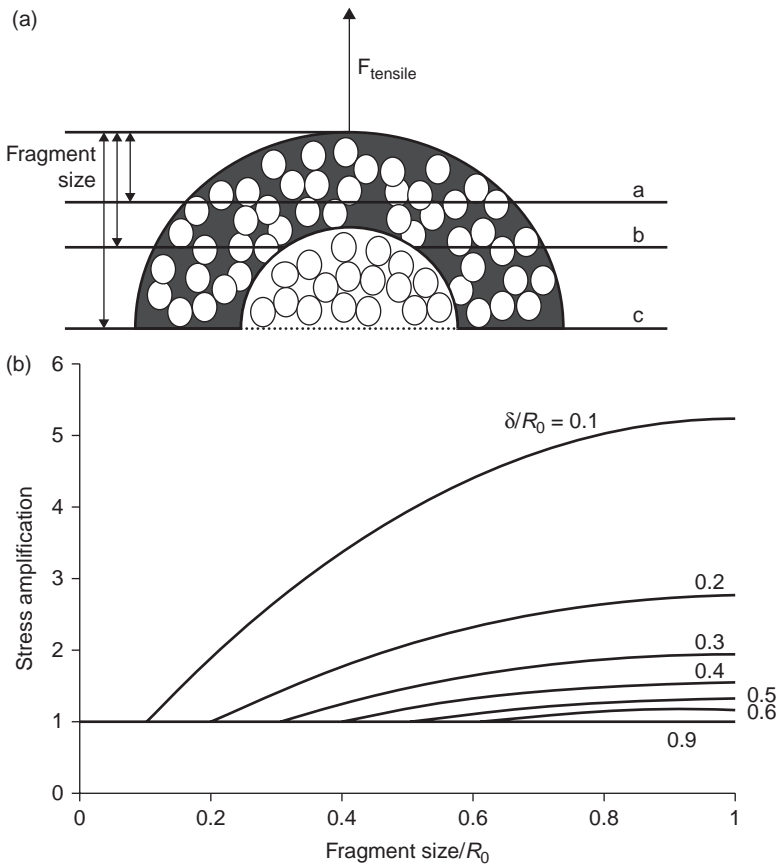


**Figure 10.7** Stress distribution in liquid-infiltrated agglomerate that fails by adhesive failure (Boyle *et al.*, 2005).

If the packing of primary particles is changed by fluid infiltration (as would be expected when the fluid overcomes the adhesive force between dry primary particles), the interparticle force at the boundary between infiltrated and dry areas of the agglomerate is diminished. In this case, the tensile stress on the agglomerate is transmitted only in the infiltrated region. Depending on the strength of the infiltrated region, the agglomerate may break in different ways. If the wet region is

relatively weak, it can break along a fracture surface fully in the wet region – i.e., a small fragment will be formed by cohesive failure. If the wet region is stronger, failure may occur deeper into the agglomerate. This is counterintuitive, but it happens because if adhesion between wet and dry regions is weak, the tensile stress gets distributed over a smaller area of infiltrated agglomerate, as shown in Figure 10.7.

**Example 10.2** You have been asked to measure the primary particle size distribution of a fine Teflon powder (Hamaker constant =  $3.8 \times 10^{-20}$  J, mean particle size ca. 5  $\mu\text{m}$ ). You can choose between water, ethanol, or hexane as dispersants. Your dispersing equipment consists of a relatively low-shear agitator in a small beaker. Which of the dispersants will you use? Provide quantitative justification for your answer.

Solvent	Viscosity	Surface tension	Contact angle	Hamaker constant
	mPa s	mN m <sup>-1</sup>	degrees	J $\times 10^{20}$
Water	0.894	72	107	4.4
Ethanol	1.07	22	28	4.2
Pentane	0.24	16	15	3.9

*Solution:*

A good dispersing fluid must be able to engulf agglomerates, penetrate their pore space quickly, and reduce van der Waals forces between particles. Water can be eliminated immediately, because its contact angle with Teflon is greater than 90°, therefore it will not spontaneously engulf the particles. They will tend to float on the air–water surface.

Ethanol and pentane both wet Teflon, so we should compare how quickly they penetrate agglomerates and how much they reduce the interparticle attraction:

Imbibition rate from Equations 10.7 and 10.8:

$$\frac{1}{t} = \Gamma = \frac{7d\epsilon^2\gamma_{LV}\cos\theta}{75\mu D_p^2(1-\epsilon)}$$

The relative imbibition rate of ethanol and pentane is:

$$\frac{\Gamma_{\text{ethanol}}}{\Gamma_{\text{pentane}}} = \frac{[\gamma_{LV}\cos\theta]_{\text{ethanol}} \mu_{\text{pentane}}}{[\gamma_{LV}\cos\theta]_{\text{pentane}} \mu_{\text{ethanol}}} = \frac{22 \times \cos(28)}{16 \times \cos(15)} \times \frac{0.24}{1.07} = 0.28$$

Adhesion force:

$$F \sim A_{13} = (\sqrt{A_{11}} - \sqrt{A_{33}})^2$$

$$\text{Ethanol: } A_{13} = (\sqrt{3.8} - \sqrt{4.2})^2 \times 10^{-20} \text{ J} = 0.0678 \times 10^{-20} \text{ J}$$

$$\text{Pentane: } A_{13} = (\sqrt{3.8} - \sqrt{3.9})^2 \times 10^{-20} \text{ J} = 0.000649 \times 10^{-20} \text{ J}$$

The agglomerates will be 100 times weaker in pentane, and pentane imbibes ca. 3 times faster. Therefore, pentane is the preferred dispersant.

### 10.5.1 Wet Dispersion Kinetics

Scurati *et al.* (2005) also developed an expression for the rate of dispersion in simple shear. In order to detach a fragment of a parent agglomerate, the hydrodynamic force has to exceed either the tensile or shear strength of the agglomerate. In general, the tensile strength is less than the shear strength, so failure was assumed to occur under tensile loading. In simple shear, particles rotate, so different regions of the agglomerate experience time-varying tensile and compressive stresses. The model assumes that small fragments are created when the tensile stress exceeds the tensile strength of the agglomerate, and the rate of fragment formation depends on the frequency of the stressing and compression. Finally, they assumed that the agglomerate remains spherical as it loses fragments (erodes). Thus:

$$-\frac{dr}{dt} = K(F_N - F_c) \left( \frac{\dot{\gamma}}{2} \right) \quad 10.8$$

where  $K$  is a rate constant that depends on granule structure.  $\dot{\gamma}/2$  is included because it characterizes the rotation rate of the particle in the shear field – this is the frequency of tensile stressing of the particle. The tensile force  $F_N$  can be expressed as a function of the fragment size using the model of Bagster and Tomi (Table 10.1). The fragment is modeled as a spherical cap described by a solid angle  $\Psi_o$  (Figure 10.8). Combining this description with Equations 10.1 and 10.9 and integrating yields an expression for the rate of erosion of a homogeneous (non-fractal) agglomerate:

$$1 - \frac{r}{r_o} = \frac{\pi K r_o \sin^2 \Psi_o \sigma_c [Fa - 1] \dot{\gamma} t}{(2 + K r_o \sin^2 \Psi_o \sigma_c [Fa - 1] \dot{\gamma} t)} \quad 10.9$$

where  $\sigma_c$  is the cohesive strength of the agglomerate and  $Fa$  is the fragmentation number,

$$Fa = 5\mu\dot{\gamma} / \sigma_c \quad 10.10$$

Note that this expression indicates that  $r$  becomes zero in a finite time – a compact agglomerate can disperse completely.

Dispersion of fractal agglomerates, for example loose flocs of colloidal particles, is also described by Equation 10.8; however, no general closed-form solution exists for the agglomerate radius as a function of time. The normal force on the agglomerate and the cohesive force scale differently with particle radius:  $F_N \sim r^2$

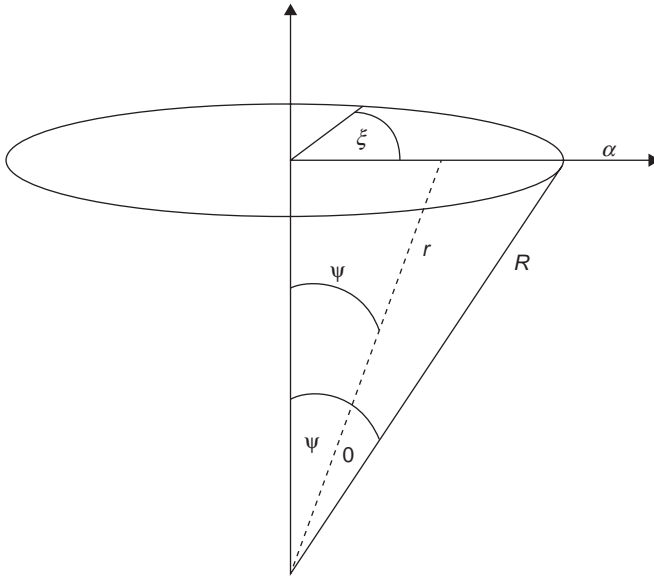


**Figure 10.8** Representation of the fracture plane of a fragment identified by solid angle  $\Psi_0$  (Scurati *et al.*, 2005).

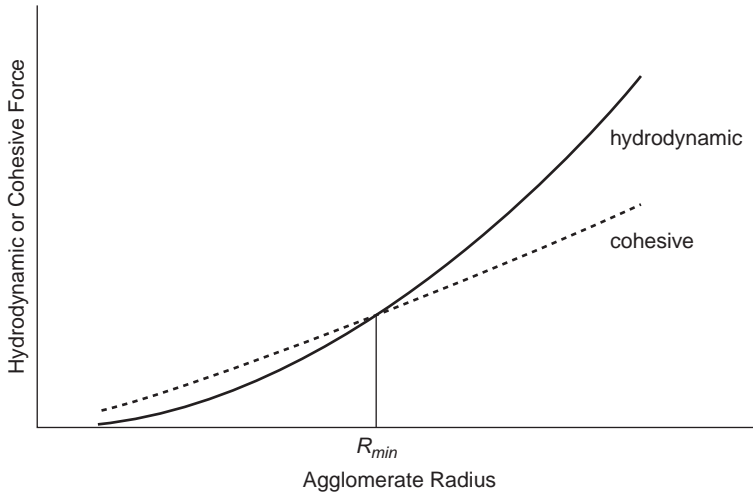


**Figure 10.9** Schematic diagram showing scaling of hydrodynamic and cohesive forces for fractal agglomerate,  $D^f = 2.3$ . Agglomerate will disperse until its radius equals  $r_{min}$ .

and  $F_c \sim r^{(D^f - 1)}$ , where  $D^f$  is the fractal dimension of the agglomerate. Because  $D^f < 3$ , the cohesive force decreases more slowly with radius than the hydrodynamic force, as shown schematically in Figure 10.9. This means that dispersion

stops before the agglomerate is fully dispersed. The minimum agglomerate radius is given by:

$$\frac{r_{min}}{r_0} = \left[ \left( \frac{D^f - 1}{2} \right) Fa \frac{\sin^2 \Psi_o}{1 - (\cos \Psi_o)^{D^f - 1}} \right]^{\frac{1}{D^f - 1}} \quad 10.11$$

## 10.6 Agglomerate and Powder Dissolution

Dissolution of powder in liquid in an agitated tank is a very basic unit operation in particle technology. Despite its apparent simplicity, the process is often not designed properly and fails to operate efficiently, particularly when scaled up. The basic process involves putting a powder into a tank with a liquid, agitating the mixture for a specified time at a specified temperature, and then discharging the (hopefully) clear solution to the next step in the process.

For example, think of the case study that introduced this chapter. We need to design a process to dissolve a granular pesticide in water for spraying onto a field. The pesticide has a broad size distribution, ranging from dust (10  $\mu\text{m}$ ) to 1 mm. How do we approach this? The key considerations designing for powder dissolution are:

- There are three steps that occur during the process: dispersion, suspension, dissolution. Our dissolution equipment must be designed for each.
- Dispersion is a critical first step in dissolution. If dispersion is poor, dissolution will be slow (see Section 10.5).
- Good agitation design is necessary to disperse the particles as completely as possible and to keep them suspended. If the particles settle in the tank, dissolution will occur by leaching out of a large pile at the bottom of the tank. This is both slow and erratic.
- We need to understand the particle trajectories in the tank, which requires knowledge of the flow regime (laminar or turbulent) and calculation of the streamlines and particle slip velocity.

### 10.6.1 Single Particle Dissolution

If we've designed our solids addition and agitation systems correctly, the particles in the powder are all separated in the liquid, moving with the fluid. The rate at which the powder dissolves is the sum of the rates at which each particle dissolves. If we can compute the single-particle dissolution rate, we can compute the rate of the whole collection of particles – i.e., the dissolution profile of the powder in the tank. We will do this by assuming the particles are spherical, and use mass-transfer coefficients to compute mass-transfer rates. We can make a priori estimates of the mass-transfer coefficients using engineering correlations.

Note that dissolution and crystal growth are mirror images of each other. In Chapter 4 (Section 4.5.1) we have already discussed the transition from intrinsic

to mass-transfer limited crystal growth. Dissolution rates tend to be larger than crystallization rates under comparable conditions. This indicates that the intrinsic dissolution rate – the rate of pulling molecules out of the lattice – is faster than the intrinsic crystallization rate. For this reason, dissolution is more likely to be mass-transfer-controlled than intrinsic rate-controlled. From here on, we'll assume that dissolution is mass-transfer-controlled.

To start, we'll assume that the particles are sufficiently small that they move with the fluid streamlines. This is valid for small particles, for which inertia is small compared to viscous drag. This can be characterized by a particle relaxation time,  $\tau_p$ :

$$\tau_p = \frac{(\rho_p - \rho)d_p^2}{18\mu_f} \quad 10.12$$

If this relaxation time is short, particles respond rapidly to changes in fluid velocity and move at the local fluid velocity.

Consider a particle dissolving at a rate controlled by external diffusion of the solute away from the particle (Figure 10.10). If the particles are sufficiently small, they will move with the fluid streamlines. From the viewpoint of the particle (the Lagrangian view), the fluid is not moving. Therefore, dissolution is happening in a stagnant medium. The mass-transfer rate away from a particle is:

$$\dot{m} = k_l (4\pi r_p^2) (C_s - C_b) \quad 10.13$$

where  $r_p$  is the particle radius,  $k_l$  is the mass-transfer coefficient, and  $C_b$  is the “bulk” concentration of the solution far from the particle. We assume that the concentration at the surface is the saturation concentration – i.e., intrinsic dissolution is fast. Note that as the particle dissolves the radius decreases – this is what makes the problem interesting. It is an example of the classic “shrinking core model” that appears in many different applications, including drop-drying as described in Chapter 7.

Also assume that  $C_s \gg C_b$ , i.e., dissolution occurs under “sink” conditions. Qualitatively, this doesn't change the problem, but it makes it possible to derive a closed-form solution for the rate at which the particle dissolves. Note that the mass of the particle is:

$$m_p = \frac{4}{3}\pi r_p^3 \rho_p \quad 10.14$$

The rate of dissolution is the first derivative of Equation 10.14:

$$\frac{dm_p}{dt} = \dot{m}_p = -4\pi r_p^2 \rho_p \frac{dr_p}{dt} \quad 10.15$$



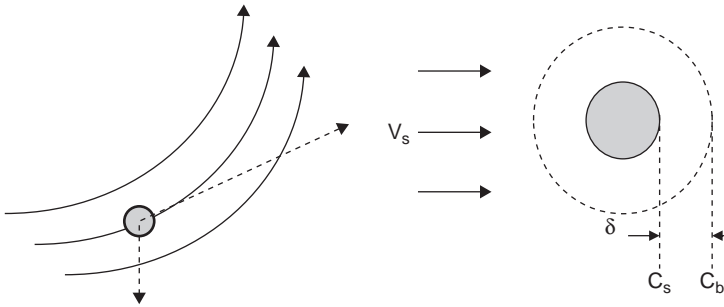


**Figure 10.10** Dissolution of a particle in a flow field. (a) Forces acting on the particle; (b) dissolution of the particle controlled by diffusion through a boundary layer.

Combining Equations 10.13 and 10.15 gives:

$$-\frac{dr_p}{dt} = \frac{k_l C_s}{\rho_p} \quad 10.16$$

The boundary condition for Equation 10.16 is  $r_p = r_{p0}$  at  $t = 0$ . We are typically less interested in the evolution of the particle size than we are with the mass that dissolves. It is useful to express this in dimensionless form:

$$\theta(r_o, t) = \frac{r_p^3(t) - r_{p0}^3}{r_{p0}^3} \quad 10.17$$

where  $\theta$  is the dimensionless dissolution profile of a particle of initial radius  $r_{p0}$ .

Equations 10.16 and 10.17 are valid whether or not the particle is moving relative to the fluid. In the limiting case where it is not, the concentration profile in the boundary layer and resulting diffusion flux (dissolution rate) can be computed analytically. This is manifested by a very simple relationship for the mass-transfer coefficient. It is convenient to express this as a Sherwood number:

$$Sh = \frac{k_l d_p}{D_l} = 2 \quad 10.18$$

where  $d_p = 2r_p$  is the particle diameter and  $D_l$  is the mass diffusivity of the solute in the solvent. Note that this implies that the mass-transfer coefficient varies as  $1/d_p$ , i.e., it increases as the particle dissolves. Substituting Equation 10.18 into Equation 10.16:

$$-\frac{dr_p}{dt} = \frac{D_l C_s}{\rho_p} \frac{1}{r_p} \quad 10.19$$

Remembering that the boundary condition is  $r_p = r_{p0}$  at  $t = 0$ , Equation 10.19 can be integrated to give:

$$r_p^2 = r_{p0}^2 - \frac{2\mathcal{D}_l C_s}{\rho_p} t \quad 10.20$$

Note the similarity of Equation 10.21 to that for the shrinking of a drop during drying in the constant rate regime given by Equation 7.29. It is essentially the same problem. The total dissolution time is:

$$t_D = \frac{r_{p0}^2 \rho_p}{2\mathcal{D}_l C_s} \quad 10.21$$

Note that the dissolution time is proportional to the particle surface area. Equation 10.21 gives no dependence on the flow field and implies the dissolution rate is independent of stirrer speed. This is because of our assumption that the particles are small and travel with the streamlines with no slip velocity.

As particles get larger and/or more dense, the assumption that they stay in a streamline breaks down. In relatively laminar flows, they develop a slip velocity that can be approximated as their terminal settling velocity (Harriott, 1962). This can be calculated from the drag coefficient  $C_D$ :

$$u_t = \sqrt{\frac{8gr_p(\rho_p - \rho)}{3\rho C_D}} \quad 10.22$$

which is for a sphere:

$$C_D = \left( \frac{24}{Re_t} \right) \left( 1 + 0.14Re_t^{0.7} \right) \quad 10.23$$

and the particle Reynolds number is:

$$Re_t = \frac{\rho_p u_t d_p}{\mu} \quad 10.24$$

[Note that in Chapter 7, a different correlation was suggested for terminal settling velocity (Equation 7.57). Either Equation 7.57 or Equation 10.23 can be used.]

As the slip velocity increases, so does convection of mass away from the particle. The mass-transfer coefficient begins to increase. This can be accounted for by using an appropriate mass-transfer correlation. The most common is the Ranz and Marshall correlation (Ranz and Marshall, 1952), which is reasonably accurate for agitated dispersions that are not highly turbulent and is consistent with the theoretical value of the Sherwood number for zero slip velocity:

$$Sh = 2 + 0.6Re^{\frac{1}{2}} Sc^{\frac{1}{3}} \quad 10.25$$

$Sc$  is the Schmidt number:

$$Sc = \frac{\mu}{\rho D_i} \quad 10.26$$

Note that Equation 10.27 has exactly the same form as the Ranz–Marshall correlation for heat transfer (Equation 7.13).

Note an interesting result of this analysis: dissolution rate is independent of agitation! This is a result of assuming that the slip velocity equals the terminal velocity. We need to explore this further. The assumption that the particle slip velocity equals the terminal settling velocity breaks down in turbulent flows – e.g., well-agitated and baffled tanks commonly used to disperse and dissolve powders. In the vicinity of the agitator, particles get accelerated by the motion of the fluid close to the agitator, and it may be more accurate to use the centripetal acceleration rather than  $g$  in calculating the slip velocity, at least for particles close to the agitator:

$$a = \frac{v_t^2}{R} \quad 10.27$$

where  $R$  is distance from the impeller shaft and  $v_t$  is the tangential velocity (tip speed) of the agitator. Under this assumption,  $g$  would be replaced by  $a$  in Equation 10.22, and the slip velocity (and through it, the dissolution rate) becomes an explicit function of agitation rate.

Turbulence also increases the mass-transfer coefficient by carrying fluid eddies to and from the particle surface (e.g., adding an eddy diffusivity to the molecular diffusivity) and by continuously accelerating the particle by subjecting it to a fluctuating velocity field.

There are numerous approaches to including turbulence in the correlations (Pangarkar and Yawalkar, 2002):

1. Use the terminal velocity in the Reynolds number and augment the Sherwood number correlation with a term that includes turbulent intensity:

$$Sh = 2 + A'' Re_t^{\frac{1}{2}} Sc^{\frac{1}{3}}, \quad A'' = f(\text{turbulent intensity}) \quad 10.28$$

2. Direct correlations with impeller speed:

$$k_l = A \left( \frac{N}{N_S} \right)^a Sc^b \quad 10.29$$

where  $N_S$  is minimum impeller speed at which all particles are suspended.

3. Use a Reynolds number based on Kolgamaroff's theory of turbulence

$$Re_\epsilon = \left( \frac{\epsilon d^4}{\nu^3} \right)^{\frac{1}{3}} \quad 10.30$$

where  $\epsilon$  is the agitation power per unit mass. Sherwood number correlations look similar to those based on slip velocity:

$$Sh = A + BRe_\epsilon^a Sc^b \tag{10.31}$$

There is no single best correlation. Ultimately, mass-transfer coefficients depend on the design of the agitator and the tank. Correlations either ignore this (i.e., argue that power to weight ratio predicts turbulent intensity and length scale regardless of agitator design) or are specific to one type of agitator (i.e., turbine, pitched blade, etc.).

### 10.6.2 Dissolution of a Powder (Multiparticle System)

Of course, most real powders cannot be assumed to be monosized. From Equations 10.20 to 10.22, it is clear that particles of different size dissolve at different rates and have different total dissolution times. To predict the generation of a batch dissolution curve for a powder, or to predict the amount dissolved in a continuous dissolver, we can use the population balance approach we developed in Chapter 3 and used extensively throughout this book.

Consider the population balance for a well-mixed system given in Equation 3.3. Where dissolution is the only process occurring (no nucleation, agglomeration, or breakage), for a batch dissolver, Equation 3.3 reduces to:

$$\frac{\partial Vn(x,t)}{\partial t} + \frac{\partial VG_d n(x,t)}{\partial x} + V\dot{d}_d(x,t) = 0 \tag{10.33}$$

Similarly for a continuous, well-mixed dissolver at steady state, Equation 3.3 reduces to:

$$\frac{dG_d n(x)}{dx} = \frac{n_m(x) - n(x)}{\tau} - \dot{d}_d(x) \tag{10.34}$$

Here the two key parameters, are the dissolution rate  $G_d$  and the dissolution death rate  $\dot{d}_d$ . By definition:

$$G_d = \left( \frac{dx}{dt} \right)_n \tag{10.35}$$

To be consistent with previous chapters, we take  $x$  to be the particle diameter ( $x = 2r_p$ ). Therefore, from Equation 10.19, we can write:

$$G_d = - \frac{4D_l C_s}{\rho_p} \frac{1}{x} \tag{10.36}$$

Note that Equation 10.36 contains two important assumptions:

1. stagnant conditions (particles traveling with the streamlines); and
2.  $C_s \gg C_b$ .

More generally, we can write:

$$G_d = -\frac{2k_l}{\rho_p}(C_s - C_b) \tag{10.37}$$

Note that the dissolution rate  $G_d$  is always numerically negative because the particles are shrinking.

The death term due to dissolution accounts for particles that disappear completely when they shrink to zero size. Thus we can write:

$$\dot{d}_d(x) = \dot{D}_d \delta(x) \tag{10.38}$$

The death rate must equal the rate at flux at which particles are shrinking to zero size:

$$\dot{D}_d = -G_d n|_{x=0} \tag{10.39}$$

Thus, although dissolution appears in both the growth term and the death term of the population balance, there is only one parameter we need to know,  $G_d$ , along with the initial or boundary conditions of the particle size distribution:  $n(x,0)$  or  $n_{in}(x)$ .

Let us look more closely at the batch dissolution case. In the domain  $x > 0$  we write from Equation 10.33:

$$\frac{\partial Vn(x,t)}{\partial t} = -\frac{\partial VG_d n(x,t)}{\partial x} \tag{10.40}$$

Substituting from Equation 10.36:

$$\frac{\partial Vn(x,t)}{\partial t} = \frac{4\mathcal{D}_l C_s}{\rho_p} \frac{\partial x^{-1} Vn(x,t)}{\partial x} = \frac{4\mathcal{D}_l C_s}{\rho_p} \left[ \frac{1}{x} \frac{\partial Vn(x,t)}{\partial x} - \frac{Vn(x,t)}{x^2} \right] \tag{10.41}$$

In general, Equation 10.41 needs to be solved numerically, usually by first discretizing the size distribution and then solving the resulting set of ODEs:

$$\frac{dVN_i}{dt} = \frac{4DC_s}{\rho_p} \left[ \frac{1}{\bar{x}_i} \frac{V(N_i - N_{i-1})}{\Delta x_i} - \frac{VN_i}{\bar{x}_i^2} \right] \tag{10.42}$$

where  $N_i$  is the number concentration in size interval  $i$ . The mass dissolved at any time is calculated from the third moment of the distribution:

$$M_d = \frac{\pi}{6} \rho_p V (\mu_3'(0) - \mu_3'(t)) \tag{10.43}$$

Starting from the general form of the moments form of the population balance (Equation 3.7), we can derive an expression directly for the rate of change of the third moment for a batch dissolver:

$$\frac{d\mu_3'}{dt} = -\int_0^\infty x^3 \frac{\partial V G_d n(x,t)}{\partial x} dx \tag{10.44}$$

Note that  $G_d$  is *not* size-independent. However, substituting for  $G_d$  from Equation 10.36 and after some manipulation, we can show that:

$$\frac{d\mu_3'}{dt} = -\frac{12\mathcal{D}_l C_s \mu_1'}{\rho_p} \tag{10.45}$$

$$\dot{M}_d = -\frac{\pi}{6} \rho_p V \frac{d\mu_3'}{dt} = 2\pi V \mathcal{D}_l C_s \mu_1' \tag{10.46}$$

Unfortunately, we do not have a closed form of the moments expressions so there is not an analytical solution. However, it is interesting to note that dissolution rate is proportional to  $\mu_1'$  not  $\mu_2'$ ; i.e., the dissolution rate is not proportional to the particle surface area.

Another approach to tracking the dissolution curve is to track the dissolution rate and profile for each initial size class based on Equation 10.20:

$$-\frac{dr_i}{dt} = \frac{\mathcal{D}_l C_s}{\rho_p} \frac{1}{r_i}, r_i = r_i^o \text{ at } t = 0 \tag{10.47}$$

which can be solved to give a series of equations similar to 10.21 and 10.22:

$$r_i^2 = (r_i^o)^2 - \frac{2\mathcal{D}_l C_s}{\rho_p} t \text{ for } t < t_{Di} \tag{10.48}$$

where

$$t_{Di} = \frac{(r_i^o)^2 \rho_p}{2\mathcal{D}_l C_s} \tag{10.49}$$

The volume fraction of particles in this size class that dissolves in time  $t$  is:

$$\theta_i(t) = 1 - \frac{r_i^3}{(r_i^o)^3} \tag{10.50}$$

To get the total fraction of powder dissolved, we sum the fraction of each size class dissolved multiplied by their initial volume fraction  $V_i$ :

$$\Theta(t) = \sum_{i=1}^n V_i \theta_i(t) \tag{10.51}$$

One major simplification we have in Equations 10.48–10.51 is that the bulk concentration is small compared to the saturation concentration. This is rarely true, and it adds a mathematical complication in that the driving force for mass transfer becomes time-dependent:

$$-\frac{dr_i}{dt} = \frac{D}{\rho_p} \frac{1}{r_i} (C_{sat} - C_b(t)) \quad 10.52$$

where

$$C_B(t) = C_{B0} + \Theta(t) \frac{M_0}{V} \quad 10.53$$

and  $M_0$  is the initial mass of powder. Equations 10.50–10.53 can be solved numerically.

With this, we have a complete model for dissolution of fully suspended particles in a batch agitated tank. Note that you won't do this operation in a continuous stirred tank, as your product would always contain undissolved particles. If a continuous process is needed, it can be done in a tubular geometry by using a static mixer.

---

**Example 10.3** A poorly soluble pharmaceutical drug needs to dissolve quickly in the GI tract for an immediate release formulation. The drug has a bi-modal size distribution. We test the dissolution of the drug in an in vitro dissolution experiment in water in a stirred tank. Compute and plot the dissolution profile of the fully dispersed bimodal powder in water under “sink” conditions (e.g., bulk concentration always  $\ll$  saturation concentration). Assume  $Sh = 2$ . The regulatory agency requires that for an immediate-release formulation, 80% of the drug must dissolve within 20 minutes. Will this specification be met?

*Data:*

Particle size distribution: 30 wt% 1  $\mu\text{m}$  (diameter), 70% 10  $\mu\text{m}$

Solubility: 0.01  $\text{g l}^{-1}$

Diffusivity:  $8 \times 10^{-6} \text{ cm}^2 \text{ s}^{-1}$

Particle density: 1.4  $\text{g ml}^{-1}$

*Solution:*

First, it is useful to calculate the dissolution time for each type of particle using Equation 10.22:

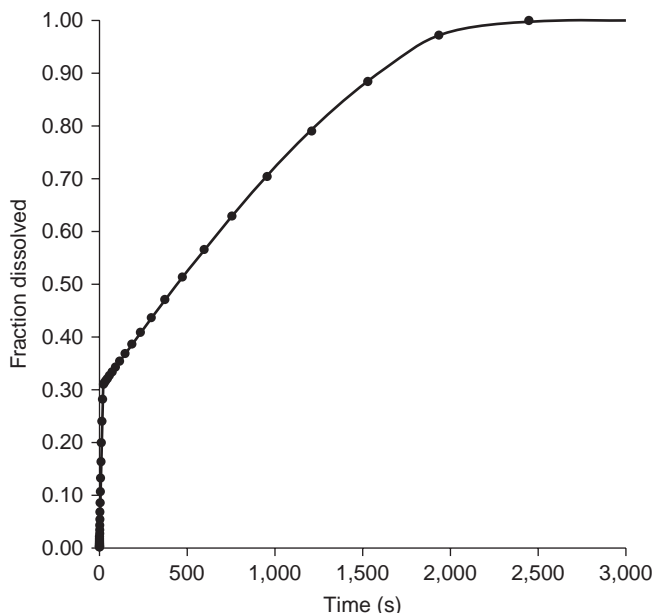
$$t_{D,1} = \frac{r_{p0,1}^2 \rho_p}{2D_l C_s} = \frac{(0.5 \times 10^{-6} \text{ m})^2 \times 1400 \text{ kg m}^{-3}}{2 \times 8 \times 10^{-10} \text{ m}^2 \text{ s}^{-1} \times 0.01 \text{ kg m}^{-3}} = 21.9 \text{ s}$$

Similarly

$$t_{D,2} = 2,190 \text{ s}$$

So we expect dissolution to be complete in 2,190 s.

To calculate the dissolution profile, we use Equations 10.48 to 10.51. These are solved in an Excel spreadsheet to yield the dissolution profile given below:



From this profile, we see that 80% of the drug will be dissolved in just over 1,200 s (20 min), so we are very close to meeting the specification but have no margin for error. Note how much faster the 1  $\mu\text{m}$  particles dissolve. Dissolution time is proportional to  $r_{p0}^2$  so the 10  $\mu\text{m}$  particles take 100 times longer to dissolve.

These results show that the dissolution time, calculated assuming  $Sh = 2$ , is conservative. They are nevertheless useful: If the time that it takes to dissolve a powder is larger than the simple estimate for the largest size class in the powder, it indicates that there is something wrong with powder dispersion and suspension in the process. The dissolution time and dissolution profile are useful troubleshooting and design tools.

## 10.7 Summary

Dispersion and dissolution are important product attributes for many particulate products. There are many pathways to achieve the product in solution at the rate required (Figure 10.1). Nevertheless, we can use some established understanding of the physics of dispersion and dissolution to get useful information about limiting cases and therefore get useful information about controlling processes and relative time scales.



In aerodynamic dispersion, agglomerates disperse by impact rather than by shear. The process can be considered a special case of impact breakage and the relationships developed in Section 9.5 are all applicable. For dispersion in the liquid phase, the higher viscosity of liquids means that dispersion by shear is more important. In addition, we must consider the rate at which liquids imbibe into the agglomerate, as this process destroys the bonds between primary particles in the agglomerate (Equations 10.5 to 10.7). In determining the probability that an agglomerate will disperse, the fragmentation number  $Fa$  is very useful for defining the dispersion regime.

Assuming the agglomerate is dispersed into primary particles, the dissolution of these particles is a classic application of mass transfer theory. The dissolution time for a particle of any size can be calculated for stagnant conditions (Equation 10.21), and extended to non-stagnant conditions using the Ranz–Marshall correlation for mass-transfer coefficient (Equation 10.25). For a distribution of particle size, we can calculate the dissolution profile using Equations 10.47–10.53. Where dissolution occurs in conjunction with other rate processes, the formulation of the population balance terms for dissolution is also given in Section 10.6.2.

## 10.8 Bibliography

- Bagster, D.F. and Tomi, D., 1974. The stresses within a sphere in simple flow fields. *Chemical Engineering Science*, 29, 1773–1783.
- Bohin, F., Manas-Zloczower, I., and Feke, D.L., 1994. Penetration of silicone polymers into silica agglomerates and its influence on dispersion mechanism. *Rubber Chemistry and Technology*, 67(4), 602–609.
- Boyle, J.F., Manas-Zloczower, I., and Feke, D.L., 2005. Hydrodynamic analysis of the mechanisms of agglomerate dispersion. *Powder Technology*, 153, 127–133.
- Calvert, G., Ghadiri, M., and Tweedie, R., 2009. Aerodynamic dispersion of cohesive powders: A review of understanding and technology. *Advanced Powder Technology*, 20(1), 4–16.
- Diao, J. and Fuerstenau, D.W., 1991. Characterization of the wettability of solid particles by film flotation 2. Theoretical analysis. *Colloids and Surfaces*, 60, 145–160.
- Evans, A.G. and Wilshaw, T.R., 1976. Quasi-static solid particle damage in brittle solids – I. Observations analysis and implications. *Acta Metallurgica*, 24(10), 939–956.
- Gentzler, M. and Michaels, J.N., 2004. Impact attrition of brittle structured particles at low velocities: Rigorous use of a laboratory vibrational impact tester. *Chemical Engineering Science*, 59(24), 5949–5958.
- Harriott, P., 1962. Mass transfer to particles: Part I. Suspended in agitated tanks. *AIChE Journal*, 8(1), 93–101.
- Masuda, H. and Gotoh, K., 1995. Performance evaluation of dry dispersers. *Advanced Powder Technology*, 6(4), 305–315.
- Pangarkar, V. and Yawalkar, A., 2002. Particle–liquid mass transfer coefficient in two-/three-phase stirred tank reactors. *Industrial & Engineering Chemistry Research*, 41(17), 4141–4167.

- Ranz, W. and Marshall, W., 1952. Evaporation from drops. 2. *Chemical Engineering Progress*, 48(4), 173–180.
- Scurati, A., Feke, D.L. and Manas-Zloczower, I., 2005. Analysis of the kinetics of agglomerate erosion in simple shear flows. *Chemical Engineering Science*, 60, 6564–6573.
- Subero, J. and Ghadiri, M., 2001. Breakage patterns of agglomerates. *Powder Technology*, 120, 232–243.
- Yang, X.F. and Xi, X.M., 1995. Critical wetting angle for spontaneous liquid infiltration into orderly packed fibres or spheres. *Journal of Materials Science*, 30(20), 5099–5102.

## 10.9 Problems

- 10.1. A new design for a dry powder inhaler has been developed. In this design, 1 mm-diameter agglomerates are accelerated in an air stream from rest to a velocity of  $10 \text{ m s}^{-1}$  where they impact a hard surface at a  $90^\circ$  angle bend. We estimate the impact time to be  $10^{-3} \text{ s}$ . The aim is for the agglomerates to disperse into  $5 \text{ }\mu\text{m}$  primary particles to be captured in the lungs. Larger particles are captured in the nasal passages, which is undesirable. These agglomerates behave as “Kendall agglomerates” (Section 9.3.2) with the following properties:  $W_A = 0.2 \text{ N m}^{-1}$ ;  $\epsilon_g = 0.35$ ;  $c \sim d_p$ . Calculate the fragmentation number for these agglomerates in this system. Are they likely to disperse well? How might you change the design of the agglomerate or the inhaler to improve dispersion?
- 10.2. Estimate the agglomerate filling time for a 1 mm agglomerate made from  $10 \text{ }\mu\text{m}$  inert particles in water if the agglomerate is easily wet. Produce a plot of the proportion of the agglomerate dispersed as a function of time.
- 10.3. Prove that  $Sh = 2$  for a sphere dissolving into a stagnant liquid:
- Set up the differential equation for the steady-state concentration profile around the sphere, assuming constant diffusivity and boundary conditions of concentration  $C_s$  at the particle surface and bulk concentration  $C_b$  infinitely far from the particle.
  - Solve the differential equation and determine the mass transfer flux at the particle surface.
  - Equate this flux to that expressed in terms of a mass transfer coefficient and solve for the Sherwood number.
- 10.4. Equation 10.21 gives an expression for the radius of a dissolving particle in sink conditions ( $C_{bulk} \ll C_s$ ) as a function of time that is valid for small spherical particles with small slip velocities. This expression will underestimate the rate at which larger particles dissolve. In this problem, develop an analogous expression for the particle radius as a function of time valid for large particles with large slip velocities.
- Show that at large Reynolds number, the Reynolds number dependence of the drag coefficient in the expression for particle terminal velocity is weak, therefore the drag coefficient can be treated as a constant.

- b. Assuming that the drag coefficient is constant, show that the settling velocity of large particles scales with the square-root of particle radius.
- c. Assuming the result of part (b), derive an expression for particle radius as a function of time.
- 10.5. You are working in a materials science laboratory for a pharmaceutical company. You get a phone call requesting support for a problem that has arisen during scale-up of a process for preparing growth media for fermentation of a new biologics product. The process consists of adding a number of salts and sugars to pure water in a 1000-liter stainless steel tank and agitating it until the solids have disappeared. The process was initially developed in a 10-liter stirred glass tank, and the dissolution time was always less than 10 minutes. In the larger tank, it's taking more than an hour. The salts that were used in development came from the same source as those used in the factory, although different lots were used. The solution composition did not change on scale-up.
- a. The plant engineer is asking you to help diagnose this problem. She has asked specifically that you characterize the powders that were used in the development lab and factory. What do you propose, and what's your rationale?
- b. The least-soluble component in the growth medium is a polysaccharide with solubility  $10 \text{ g l}^{-1}$ . In order to save money, Purchasing is proposing to buy the cheaper coarse grade, which has a particle size specification of no more than 5% of particles larger than 1 mm (diameter). It is essential that the preparation time for the growth medium does not exceed 15 minutes (not including filling and discharge time). Using good engineering judgment, do you approve the switch to a coarse grade of this material?
- 10.6. A new artificial sweetener, Supersweet<sup>®</sup>, is dispensed as "minitabs" that can be assumed a 3 mm-diameter spheres with a porosity of 0.2 made up of  $10 \mu\text{m}$  crystals. When the minitab is wetted, it is very weak and falls apart. In consumer tests, consumers complain that their cups of tea do not taste as sweet as they like. We believe the issue is slow release of Supersweet<sup>®</sup> into solution. Our new hot-shot chemical engineer has used his mass transfer textbook to calculate the dissolution rate. He estimated the diffusivity of Supersweet<sup>®</sup> in hot water as  $5 \times 10^{-6} \text{ cm}^2 \text{ s}^{-1}$ . The solubility in hot water is  $50 \text{ g l}^{-1}$  and the crystal density is  $1,500 \text{ kg m}^{-3}$ . He claims we should decrease the primary particle size of the crystals because "dissolution rate is inversely proportional to particle size." Do you agree with him? If not, what do you suggest we do? (Hint: How do the timescales for agglomerate wetting and dissolution compare?)



# Index

- 3-point bend test, 284 f9.3
- active pharmaceutical ingredient, 1
- adhesion, 277 t9.1
- aerodynamic dispersion, 300
- aerosol processes, 161
- aerosol reactor, 163, 176
- aerosol synthesis, 164
- agglomerate, 15, 164
- agglomerate attrition, 286
- agglomerate breakage, 286
- agglomerate dispersion, 295
- agglomerate dissolution, 309
- agglomerate structure, 276
- agglomerate tensile strength, 282
- agglomeration, 64, 65, 169
- aggregates, 167
- aggregation, 65, 169
- amorphous particle formation, 212
- atomization, 194
- attrition, 59, 122, 131, 231, 262, 273, 286
- attrition rate, 286
- autogenous mills, 142
- ball mill, 131, 142
- batch crystallizers, 98
- batch grinding, 126
- batch grinding tests, 133
- bead mills, 144
- bed zone, 252
- binder dispersion, 231
- Biot number, 200
- birth and death terms, 64, 65, 123, 177
- Bond Work Index, 146
- breakage, 64, 70, 172, 231, 251, 273
- breakage distribution, 152
- breakage function, 71, 125, 130
- breakage kernel, 130
- breakage mechanisms, 119
- breakage rate constant, 71, 130
- breakage selection function, 71, 124, 173
- brittle, 119
- Brownian motion, 170
- bulk density, 17, 31
- bumping, 261
- capillary liquid bridge, 1, 277 t9.1
- capillary number, 240
- CFD simulations, 220
- classification, 136
- classifier, 106
- cleavage, 122, 131
- coalescence, 65, 171, 245
- coalescence kernel, 65, 67, 68, 255
- coating, 59
- co-current driers, 218
- collision and coalescence zone, 168
- collision velocity, 242
- comminution, 118
- concentration enrichment, 210
- condensation, 59
- consolidation, 240
- consolidation and growth, 231
- consolidation rate constant, 242
- constant drying rate, 223
- constant rate drying, 204
- contact angle, 233
- continuous crystallizer, 81
- cooling, 200
- counter-current driers, 218
- crack propagation, 121
- critical cluster size, 93
- critical speed, 259
- critical Stokes number, 246
- crumb regime, 248
- crush strength, 119
- crushers, 141
- crushing and grinding, 70, 118
- crust (skin) formation, 205
- crystal engineering, 107
- crystal face growth rates, 109
- crystal growth, 59, 88
- crystal growth kinetics, 88
- crystal nucleation kinetics, 93

- crystal shape, 109  
 crystal size distribution, 88  
 crystal systems, 108 t4.2  
 crystallization, 80  
 crystallization rate processes, 88  
 crystallizer design, 86, 98  
 crystallizer mass balance, 107  
 cumulative distribution, 19  
 cyclone, 162, 185
- dendritic growth, 110  
 designer particles, 4  
 diffusion flux, 311  
 dimensionless spray flux, 234, 236  
 Dirac delta function, 56, 64  
 disc granulator, 258  
 discrete distributions, 20  
 disintegration, 294  
 dispersion, 294, 309  
 dispersion by gases, 300  
 dispersion efficiency, 299  
 dispersion in liquids, 302  
 dissolution, 59, 294, 309  
 dissolution rate, 315  
 dissolution time, 312  
 drag coefficient, 312  
 drop-controlled nucleation, 232, 237, 254  
 drop drying, 200  
 drop-drying model, 206, 220  
 drop-drying time, 204  
 drop formation, 194  
 drop penetration time, 235  
 drop size distributions, 220  
 drum granulator, 250, 258  
 dry powder inhalation, 6  
 drying drops with dissolved or suspended solids, 204  
 dynamic yield strength, 240  
 dynamic yield stress, 242 f8.8
- effective voidage, 236  
 elastic–plastic, 122 f5.3  
 emulsion, 72  
 energy balance, 201  
 energy relationships for grinding, 145  
 energy–size relationships, 147  
 Ennis coalescence criterion, 245, 262  
 envelope density, 17  
 equikinet energy (EKE) kernel, 69  
 equivalent diameters, 13, 256  
 erosion, 59, 286, 307  
 Eulerian framework, 219  
 evaporation of a single drop, 202
- Fanning friction factor, 184  
 Feret’s diameter, 16 t2.2
- film formation, 167 f6.3  
 fines dissolution, 106  
 flame reactor, 162, 164  
 flocculation, 65  
 fluid bed attrition, 288  
 fluid energy mills, 144  
 fluidized beds, 288  
 fluidized granulators, 230, 243, 246, 261  
 formulated products, 1  
 fractal dimension, 15, 308  
 fracture energy, 278  
 fracture mechanics, 119  
 fracture toughness, 121, 282  
 fragmentation, 286  
 fragmentation number, 297, 307  
 frequency distribution, 19, 24  
 Froude number, 144, 259, 260
- Gaussian (normal) distribution, 29  
 Geldart powder classification, 263  
 geometric discretization, 126  
 geometric size intervals, 25  
 Ghadiri, 285  
 grade efficiency, 137  
 grade efficiency curve, 137, 185  
 granulation, 9  
 granulation rate processes, 233 f8.2  
 Griffith criterion, 121  
 grinding media, 131  
 growth processes, 50, 59  
 growth rate, 90, 168  
 growth rate dispersion, 92  
 growth regime map, 249, 250 f8.13
- hammer mill, 136, 142  
 Hapgood, 238 f8.6  
 heat and mass transfer, 200, 203  
 heat transfer coefficient, 200  
 heterogeneous primary nucleation, 93
- imbibition into an agglomerate, 304  
 impact, 119  
 impact mills, 142  
 impact testing, 284  
 impact velocity, 120  
 impeller tip speed, 260  
 impeller zone, 252  
 indentation, 283  
 induction growth, 248  
 inertial regime, 246  
 Iveson, 249
- jaw crusher, 142 f5.11  
 jet mill, 136, 144  
 jet stretching, 196  
 JKR model, 277 t9.1

- Kendall Model, 277  
 Kozeny–Carmen equation, 235
- Lagrangian framework, 219  
 Laplace–Young equation, 234  
 laser light diffraction, 30  
 layered growth, 254  
 layering regime, 246  
 liquid evaporation flux, 210  
 liquid saturation, 241, 249  
 liquid-fed flame synthesis, 164  
 log mean temperature difference, 204  
 logarithmic frequency distribution, 25  
 log-normal distribution, 29
- macroscopic population balance, 50, 51  
 macroscopic strength of particles and particulate products, 282  
 mass–balance, 126  
 mass–moment mean, 27  
 mass–size balance, 123, 127 f5.5  
 mass transfer, 59  
 mass-transfer coefficient, 59, 203, 310, 314  
 mass-transfer controlled, 310  
 mass-transfer-controlled growth, 90  
 McCabe  $\Delta L$  law, 89  
 mean of the distribution, 27  
 measuring properties, 30  
 mechanical dispersion, 233, 237  
 median size, 27  
 mercury porosimetry, 33  
 metastable, 83  
 metastable region, 83  
 metastable zone, 86  
 micromechanical models for agglomerate strength, 275  
 microscopic population balance, 52  
 microscopy, 30  
 Miller Indices, 108  
 minimum fluidization velocity, 27, 262  
 mixer granulator, 230, 238, 242, 253 f8.14, 260  
 moment of the frequency size distribution, 26  
 moments, 177  
 moments form of the population balance, 53  
 MSMPR continuous crystallizer, 101, 105  
 multiscale model, 219
- non-inertial regime, 246  
 normalized moments, 26  
 nozzles, 198  
 nucleation, 64, 168, 222, 231, 232  
 nucleation kinetics, 93  
 nucleation-only regime, 249  
 nucleation regime map, 238 f8.6  
 Nusselt number, 201
- Ohnesage number, 196
- packed bed, 262  
 paint pigments, 3  
 parameter estimation, 135  
 particle bed crushing, 119  
 particle characterization, 9  
 particle density, 17, 32  
 particle design, 82  
 particle formation, 200  
 particle morphology, 209  
 particle property distributions, 9  
 particle relaxation time, 310  
 particle Reynolds number, 201, 312  
 particle shape, 14  
 particle size, 12, 30  
 particle size distribution, 21 t2.3  
 particle size measurement, 31  
 particle size reduction, 117  
 particle size reduction equipment, 141  
 particle size reduction equipment selection, 146 t5.1  
 particulate delivery forms, 273  
 particulate products, 2 t1.1  
 Peclet number, 210  
 phase diagram, 83  
 phase-space, 52  
 pin mill, 142  
 pipeline agglomerator, 162, 184  
 plug flow, 52  
 plug flow grinding, 126  
 pneumatic (two-fluid) nozzle atomizers, 198  
 poisoning, 90, 109  
 polymorphism, 109  
 population balance, 5, 7, 46, 47, 48, 49, 50, 51, 52, 53, 54, 55, 58, 59, 63, 65, 66, 68 t3.1, 71, 72, 74, 75, 75t3.2, 79, 88, 89, 98, 101, 102, 103, 107, 108f4.12, 111, 116, 118, 123, 127f5.5, 137, 151, 160, 163, 176, 177, 184, 186, 189, 190, 191, 194, 219, 221, 222, 230, 231, 252, 253, 256, 271, 272, 295, 314, 315, 319  
 pore size distribution, 33  
 porosity, 17, 18, 33  
 porous particle drying, 205  
 powder dispersers, 301 f10.4  
 powder dissolution, 309, 314  
 powder layering, 245  
 Prandtl number, 201  
 pressure drop, 184  
 pressure nozzle atomizers, 198  
 primary nucleation, 83  
 primary nucleation region, 83  
 process design, 82  
 process model, 4  
 process zone size, 283  
 product design, 82

- product engineering, 4  
 product model, 5, 274  
 projected area diameter, 16t2.2  
 properties of a single particle, 11  
 property distributions, 19
- quality by design, 228
- range of the distribution, 27  
 Ranz–Marshall equation, 97, 201, 313  
 rate processes, 75 t3.2, 88, 166, 231  
 Rayleigh jet break up, 194  
 reaction zone, 168  
 regime maps, 231  
 relative supersaturation, 83  
 reverse engineering, 5, 274, 289  
 Richardson–Zaki equation, 215  
 Rittinger, 146  
 rod mills, 142  
 roll crusher, 141  
 roping, 261  
 Rosin–Rammler distribution, 29  
 rotating disc atomizers, 198  
 Rumpf model for Agglomerate Tensile Strength, 275, 276
- Saffman–Turner kernel, 170  
 salting out, 85  
 scattering diameter, 16t2.2  
 Schmidt number, 313  
 secondary nucleation, 84, 95  
 secondary nucleation region, 84  
 seeded crystallizers, 86  
 semi-brittle, 119  
 shape factors, 14  
 shell formation, 209, 212  
 Sherwood number, 98, 311  
 shrinkage ratio, 222  
 shrinking core, 59  
 sieve size, 14  
 single drop drying, 220  
 single particle breakage, 134f5.7  
 single particle crushing, 119  
 single particle dissolution, 309  
 single particle testing, 133  
 sintering, 171  
 size-independent growth, 53, 59, 255  
 size-independent kernel, 67  
 skeletal (true) density, 17, 32  
 slip velocity, 215, 313  
 Smoluchowski shear kernel, 69  
 solid bridge, 277 t9.1  
 solidification, 200  
 solubility, 83  
 special distributions, 28  
 specific energy, 151, 151 f5.17  
 specific surface diameter, 16 t2.2  
 specific surface mean, 27  
 sphericity, 15  
 spray cooler design, 213  
 spray cooling, 65, 192  
 spray drier design, 218  
 spray drying, 65, 192  
 spray-drying configurations, 219 f7.11  
 spray pyrolysis, 164  
 spray zone, 232, 252  
 steady growth, 248  
 stirred media mills, 144, 149  
 Stokes deformation number, 240, 248  
 Stokes diameter, 14  
 stress energy, 149  
 stress intensity factor, 121  
 superficial gas velocity, 215, 265  
 superficial velocity, 262  
 supersaturation, 83, 85 t4.1  
 supersaturation ratio, 83  
 surface integration, 90
- t* curves, 148  
 tableting, 9  
 terminal settling velocity, 262, 312  
 total numbers balance, 54  
 toughness, 121  
 tumbling granulators, 230, 243, 258  
 tumbling mills, 142  
 twinning, 110  
 two-dimensional population balance, 222
- uniaxial compression, 120f5.2
- van der Waals adhesion, 277 t9.1  
 vapor-fed flame synthesis, 164  
 vibrating (sonic) atomizers, 198  
 Vigil–Ziff criterion, 188  
 viscous liquid bridge, 277 t9.1  
 viscous Stokes number, 245  
 voidage, 18  
 volume equivalent number, 13  
 volume (mass) size distribution, 24
- Washburn equation, 235  
 water-dispersible granules, 273, 294  
 wear, 286  
 Weibull distribution, 121, 282  
 well-mixed granulator, 64  
 well-mixed grinding mill, 124, 127  
 Wen and Yu equation, 263  
 wet dispersion kinetics, 307



- 
- wet granulation, 228, 230
  - wet granulation equipment design, 258
  - wet granulation scaling rules, 258, 265
  - wet granule breakage, 251
  - wet granule strength, 240
  - wetting, 234
  - work of adhesion, 278
  - X-ray microtomography, 34
  - Young–Dupre equation, 233